N81-71812

Prediction of Millimeter Wave Propagation Effects on Earth-Space Paths(10-100GHz)

ORI, Inc.
Silver Spring, MD

Prepared for

National Aeronautics and Space Administration
Greenbelt, MD

Dec 78

Technical Report Documentation Page

1. Report No.	2. Government Accession No.	3. Recipient's Catalog No.
NASA-CR-163843		N81-71812

4. Title and Subtitle	5. Report Date
Prediction of Millimeter Wave Propagation Effects on Earth-Space Paths	December 1978
	6. Performing Organization Code: Code 760.1
7. Author(s): Dr. R. Kaul, D.B. Hodge and D.M. Theobold	8. Performing Organization Report No.: Technical Report 1418
	10. Work Unit No. (TRAIS)
9. Performing Organization Name and Address: ORI, Inc. 1400 Spring St. Silver Spring, MD 20910	11. Contract or Grant No.: NAS5-23438, Mod 68
	13. Type of Report and Period Covered: Final Report July 1978 - January 1979
12. Sponsoring Agency Name and Address: NASA/Goddard Space Flight Center Greenbelt, MD 20771 Technical Officer: Dr. Louis J. Ippolito	14. Sponsoring Agency Code

15. Supplementary Notes

Dr. R. Kaul is at ORI, Inc. Dr. D.B. Hodge is at Ohio State Univ. Dr. D.M. Theobold is at Lockheed Missile and Space Co. The authors gratefully acknowledge the contributions of Dr. Ippolito and Mr. Hirschmann of NASA/GSFC.

16. Abstract

This report summarizes recent prediction techniques and results obtained by U.S. propagation researchers and system engineers. The results are written for satellite system engineers working in the 10 to 100 GHz frequency range in the US and Canada.

The seven sections of this report present prediction techniques for attenuation, path diversity, signal fluctuations and low angle fading, depolarization, bandwidth coherence and sky noise.

Each section may be utilized individually and example calculations have been included as a guide for the system engineer.

DIS

17. Key Words	18. Distribution Statement
Propagation Prediction Millimeter Wave Propagation Earth-Space Path Design	Unlimited

19. Security Classif. (of this report)	20. Security Classif. (of this page)	21. No. of Pages	
Unclassified	Unclassified	236	

SQ1

Technical Report 1418

PREDICTION OF MILLIMETER WAVE PROPAGATION EFFECTS ON EARTH-SPACE PATHS (10-100 GHz)

Final Report

December 1978

Goddard Space Flight Center
Greenbelt, Maryland 20771

ATTENTION

AS NOTED IN THE NTIS ANNOUNCEMENT,
PORTIONS OF THIS REPORT ARE NOT LEGIBLE.
HOWEVER, IT IS THE BEST REPRODUCTION
AVAILABLE FROM THE COPY SENT TO NTIS.

TECHNICAL REPORT 1418

ORI
Silver Spring, Maryland 20910

PREDICTION OF MILLIMETER WAVE PROPAGATION EFFECTS ON EARTH-SPACE PATHS

(10-100 GHz)

FINAL REPORT

DECEMBER 1978

1-b

PREFACE

The seven sections in this report summarize recent prediction techniques and results obtained by U.S. propagation researchers and system engineers. The results are written for use by satellite system engineers working in the 10 to 100 GHz frequency range.

The key subjects covered in these sections are:

- Attenuation, Section II
- Path Diversity, Section III
- Signal Fluctuations and Low Angle Fading, Section IV
- Depolarization Effects, Section V
- Bandwidth Coherence, Section VI
- Sky Noise, Section VII

Each section may be utilized individually and example calculations have been included as a guide for the system engineer.

PREDICTION OF MILLIMETER WAVE PROPAGATION EFFECTS ON EARTH-SPACE PATHS

TABLE OF CONTENTS

SECTION I. INTRODUCTION

SECTION II. ATTENUATION ON EARTH-SPACE PATHS

SECTION III. PATH DIVERSITY ON EARTH-SPACE PATHS

TABLE OF CONTENTS (CONT.)

SECTION IV. SIGNAL FLUCTUATIONS AND LOW ANGLE FADING ON EARTH-SPACE PATHS

TABLE OF CONTENTS (CONT.)

SECTION V. DEPOLARIZATION ON EARTH-SPACE PATHS

SECTION VI. BANDWIDTH COHERENCE ON EARTH-SPACE PATHS

SECTION VII. SKY NOISE

ACKNOWLEDGEMENT

ORI gratefully acknowledges the reviews of an earlier partial version of this report entitled "Prediction of Attenuation, Diversity and Scintillation Effects on Earth-Space Paths," ORI Technical Report No. 1400. The reviews, comments and corrections have been incorporated wherever practicable.

In addition, the authors must credit Dr. Louis Ippolito and Mr. Erwin Hirschmann, NASA/GSFC for the many hours of discussions and reviews of this report. At ORI, Eugene Feinberg and Ronald Wallace made many suggestions which have been included for additional clarity.

SECTION I

ORI
Silver Spring, Maryland 20910

INTRODUCTION

DR. ROGER KAUL

DECEMBER 1978

ORI, INC.
1400 SPRING STREET
SILVER SPRING, MD 20910
CONTRACT NAS5-23438, MOD. 68

TABLE OF CONTENTS

LIST OF ILLUSTRATIONS

TABLES

FIGURES

1.0 PURPOSE

This report provides a compilation of prediction methods and related propagation studies for the evaluation of earth-space paths operating above 10 GHz. The topics covered in this report are:

Attenuation
Path Diversity
Signal Fluctuations and Low Angle Fading
Depolarization Effects
Bandwidth Coherence
Sky Noise

The techniques described here have been developed from recent ongoing NASA supported studies and from the relevant published literature. These techniques represent the state of knowledge of the adverse effects of the earth's atmosphere on reliable earth-space transmissions above 10 GHZ.

This report provides propagation data in a format suitable for use by earth-space link system designers operating in the frequency range from 10 to 100 GHz in the United States and Canada. In this frequency range the troposphere can have a significant effect on the carrier to noise ratio of a propagating wave. Typically, the troposphere attenuates and depolarizes the carrier signal and adds broadband amplitude and phase noise to the signal. The resulting carrier-to-noise ratio reduction reduces the allowable data rate for a given bit error rate (digital systems) and the quality to transmission (analog systems). In the most severe cases the medium will significantly attenuate the carrier and destroy the transmission capabilities of the link (termed a link outage). The frequency of occurrence and average outage time per year are usually of most interest to system designers. Propagation studies to date now allow the predictions to be made with a high degree of certainty and have developed means to reduce the frequency and length of these outages.

2.0 ORGANIZATION OF THIS REPORT

This report is arranged in seven relatively independent sections covering the key topics related to the interaction of the troposphere and earth-space propagation paths. Each section attempts to present a description of the effect(s) and an example calculation related to a typical communication system. Because these examples provide a concise guide to the calculations required, an index to the examples is given in Table 1.

An attempt has been made to keep the style and format consistent, however, this has not always been possible. Three authors were involved and this document has evolved over a 6 month period. Thus, some inconsistencies are inevitable and surely some arithmetic mistakes are still present.

TABLE 1

GUIDE TO PROPAGATION EXAMPLES

Subject	Location of Example
Clear Air Attenuation	Sect. II, Par. 2.0
Rain Attenuation Statistics (Global, Rice-Holmberg, Lin, Dutton-Dougherty models)	Sect. II, Para. 3.5.2.1
Rain Attenuation Statistics (given various statistical inputs)	Sect. II, Para. 3.5.3 and 3.5.4
Path Diversity	Sect. III, Para. 2.2
Amplitude Fluctuations	Sect. IV, Para. 6.1
Phase and Angle-of-Arrival Variations	Sect. IV, Para. 6.2
Average Signal Gain Reduction	Sect. IV, Para. 6.3
Depolarization Statistics	Sect. V, Para. 3.0
Amplitude Coherence (rain induced)	Sect. VI, Para. 2.1.1
Phase Coherence (ionospheric induced)	Sect. VI, Para. 3.1
Sky Noise Statistics	Sect. VII, Para. 2.1.2

3.0 FREQUENCY BANDS FOR EARTH-SPACE COMMUNICATION

Within the guidelines established by the International Telecommunications Union (ITU) for Region 2, the Federal Communications Commission (FCC) in the U.S. and the Department of Communications (DOC) in Canada regulate the earth-space frequency allocations. In most cases, the FCC and DOC regulations are more restrictive than the ITU regulations for Region 2. Therefore, the FCC and DOC earth-space frequency bands are considered in this report.

The services which operate via an earth--space link are listed in Table 2 along with their ITU index number. The definitions of each of these services are given in Ref. 1. The specific frequency allocations for these services are listed in Table 3. These frequency allocations are taken from the FCC's Eight Notice of Inquiry and represent an estimate of the Region 2 frequency allocations beyond 1981 (two years following the 1979 World Administrative Radio Conference). The Canadian frequency proposals are similar and are not included here. Both frequency proposals are given in detail in References 2 and 3.

TABLE 2

TELECOMMUNICATION SERVICES UTILIZING

EARTH-SPACE PROPAGATION LINKS

Fixed Satellite (84AG)
Mobile Satellite (military satellite) (8AAGB)
Aeronautical Mobile Satellite (8AAGB)
Maritime Mobile Satellite (84AGD)
Land Mobile Satellite (84AGD)
Broadcasting Satellite (84AP)
Radionavigation Satellite (84AQ)
Earth Exploration Satellite (84ASA)
Meteorological Satellite (84AT)
Amateur Satellite (84ATA)
Standard Frequency Satellite (84ATB)
Space Research (84ATD)
Space Operation (84ATE)
Radio Astronomy (75A)

TABLE 3

PROPOSED UNITED STATES EARTH-SPACE FREQUENCY ALLOCATIONS

FREQUENCY (GHz)	SERVICES
10.6 - 10.7	RADIO ASTRONOMY
10.7 - 12.2	FIXED SATELLITE (Downlink)
11.7 - 12.5	BROADCASTING SATELLITE
12.5 - 13.25	FIXED SATELLITE (Uplink)
12.75 - 14.2	SPACE RESEARCH (Downlink)
13.4 - 14.0	EARTH-EXPLORATION SATELLITE (Active Sensors)
	STANDARD FREQUENCY SATELLITE (Uplink)
14.0 - 14.5	FIXED SATELLITE (Uplink)
14.4 - 14.5	SPACE RESEARCH (Space-Space)
14.5 - 15.35	SPACE RESEARCH
15.2 - 15.4	EARTH-EXPLORATION SATELLITE (Passive)
15.35 - 15.4	SPACE RESEARCH (Passive)
16.6 - 17.1	EARTH EXPLORATION SATELLITE (Active Sensors)
	SPACE RESEARCH (Active Sensors)
17.7 - 17.9	METEOROLOGICAL SATELLITE (Downlink)
17.7 - 21.2	FIXED SATELLITE (Downlink)
20.2 - 21.2	MOBILE SATELLITE (Downlink)
	STANDARD FREQUENCY SATELLITE (Downlink)
21.2 - 21.4	EARTH EXPLORATION SATELLITE (Passive)
22.21 - 22.5	EARTH EXPLORATION SATELLITE (Passive)
	SPACE RESEARCH (Passive)

TABLE 3 (Continued)

FREQUENCY (GHz)	SERVICE
	RADIO ASTRONOMY
22.6 - 23.6	INTER-SATELLITE
23.6 - 24	EARTH EXPLORATION SATELLITE (Passive)
	SPACE RESEARCH (Passive)
	RADIO ASTRONOMY
24.0 - 24.05	AMATEUR SATELLITE
25.25 - 27.5	STANDARD FREQUENCY SATELLITE (Downlink)
	EARTH EXPLORATION SATELLITE (Space-to-Space)
25.25 - 26.25	INTER-SATELLITE
27.5 - 31.0	FIXED SATELLITE (Uplink)
30.0 - 31.0	MOBILE SATELLITE (Uplink)
30 - 31.3	STANDARD FREQUENCY SATELLITE (Downlink)
31 - 31.3	SPACE RESEARCH
31.3 - 31.8	SPACE RESEARCH (Passive)
	EARTH EXPLORATION SATELLITE (Passive)
	RADIO ASTRONOMY
31.8 - 32.3	SPACE RESEARCH
34.2 - 35.2	SPACE RESEARCH (Active)
	EARTH EXPLORATION SATELLITE (Active)
36.0 - 37.0	SPACE RESEARCH (Passive)
	EARTH EXPLORATION SATELLITE (Passive)
40.0 - 41.0	FIXED SATELLITE (Downlink)
	MOBILE SATELLITE (Downlink)

TABLE 3 (Continued)

FREQUENCY (GHz)	SERVICE
41.0 - 43.0	BROADCASTING SATELLITE
43.0 - 45.0	FIXED SATELLITE (Uplink) MOBILE SATELLITE (Uplink)
45.0 - 49.8	AERONAUTICAL MOBILE SATELLITE MARITIME MOBILE SATELLITE AERONAUTICAL RADIONAVIGATION SATELLITE MARITIME RADIONAVIGATION SATELLITE
49.8 - 50.0	AMATEUR SATELLITE
50.0 - 51.4	FIXED SATELLITE (Uplink)
50.2 - 50.4	SPACE RESEARCH (Passive) EARTH - EXPLORATION SATELLITE (Passive)
50.4 - 51.4	MOBILE SATELLITE (Uplink)
51.0 - 51.4	FIXED SATELLITE (Uplink)
51.4 - 59.0	EARTH EXPLORATION SATELLITE (Passive) SPACE RESEARCH (Passive) INTERSATELLITE
54.25 - 58.2	INTERSATELLITE
59.0 - 64.0	EARTH EXPLORATION SATELLITE (Passive) SPACE RESEARCH (Passive)
64.0 - 66.0	SPACE RESEARCH
64.0 - 65.0	AERONAUTICAL MOBILE SATELLITE
65.0 - 66.0	MARITIME MOBILE SATELLITE
66.0 - 71.0	

TABLE 3 (Continued)

FREQUENCY (GHz)	SERVICE
	AERONAUTICAL RADIONAVIGATION SATELLITE
	MARITIME RADIONAVIGATION SATELLITE
71.0 - 74.0	FIXED SATELLITE (Uplink)
	MOBILE SATELLITE (Uplink)
76.0 - 77.0	SPACE RESEARCH (Active)
	EARTH EXPLORATION SATELLITE (Active)
81.0 - 84.0	MOBILE SATELLITE (Downlink)
	FIXED SATELLITE (Downlink)
84.0 - 86.0	BROADCASTING SATELLITE
86.0 - 92.0	EARTH EXPLORATION SATELLITE (Passive)
	RADIO ASTRONOMY
	SPACE RESEARCH (Passive)
92.0 - 95.0	FIXED SATELLITE (Uplink)
95.0 -100.0	AERONAUTICAL MOBILE SATELLITE
	MARITIME MOBILE SATELLITE
	AERONAUTICAL RADIONAVIGATION SATELLITE
	MARITIME RADIONAVIGATION SATELLITE

A review of Table 3 indicates that most of the frequency spectrum above 10 GHz is assigned to the satellite services or the radio astronomy services. This does not mean that the FCC and DOC will utilize them, but it does highlight the potential for use of these frequency bands. In Figure 1 is shown those frequency segments not assigned for potential use by the services listed in Table 2.

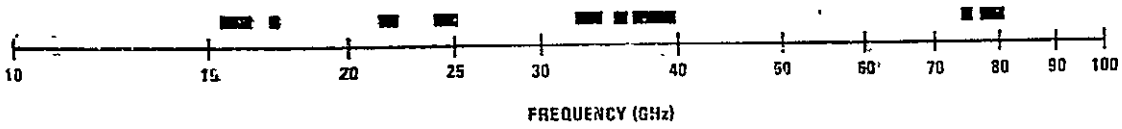

Figure 1. Frequencies NOT Potentially Available for Earth-Space Transmissions.

4.0 OTHER PROPAGATION EFFECTS NOT ADDRESSED IN THIS REPORT

4.1 IONOSPHERIC EFFECTS

The ionosphere generally has a small effect on the propagation of radio waves in the 10 to 100 GHz range. Whatever effects do exist (scintillation, absorption, variation in the angle of arrival, delay, frequency change and depolarization) arise due to the interaction of the radio wave with the free electrons, electron density irregularities and the earth's magnetic field. The density of electrons in the ionosphere varies as a function of geomagnetic latitude, diurnal cycle, yearly cycle, and solar cycle (among others). Fortunately, most U.S. ground station-satellite paths pass through the midlatitude (lowest) electron density region yielding an even lesser effect on propagation. Canadian stations may be affected by the auroral region electron densities which are normally higher. A more complete discussion of these effects is included in CCIR Report 263-3 (Ref. 4).

A mean vertical one-way attenuation for the ionosphere at 15 GHz for the daytime is typically 0.0002 dB (Ref. 5), the amplitude scintillations are generally not observable (Ref. 6) and the transit time delay increase over the free space propagation time delay is of the order of 1 nanosecond (Ref. 7). Clearly for most systems operating above 10 GHz these numbers are sufficiently small that other system error budgets will be much larger than the ionospheric contributions.

4.2 TROPOSPHERIC DELAYS

Highly accurate satellite range, range-rate and position-location systems will need to remove the propagation group delay effects introduced by the troposphere. Extremely high switching rate TDMA systems may require these corrections in the future. The effects arise primarily due to the oxygen and water vapor in the lower troposphere. Typical total additional propagation delay errors have been measured to be of the order of 8 nanoseconds (Ref. 8).

Estimation techniques, based on the measurement off the surface pressure, temperature and relative humidity have been developed (Refs. 8, 9, 10) which can readily reduce this error to less than 1 nanosecond. In addition, algorithms for range (Ref. 11) and range-rate (Ref. 12) have been prepared to reduce tropospheric contributions to satellite tracking errors.

Since this topic is quite specialized and generally results in an additional one-way delay of less than 10 nanoseconds it is not addressed further in this report. An overview of this subject and additional references are available in CCIR Report 564 Revised (Ref. 13).

SECTION II

ORI
Silver Spring, Maryland 20910

PREDICTION OF ATTENUATION ON EARTH-SPACE PATHS

DR. ROGER KAUL

ORI, INC.
SILVER SPRING, MD 20910
CONTRACT NAS5-23438, MOD. 68

SEPTEMBER 1978

TABLE OF CONTENTS

LIST OF FIGURES

LIST OF TABLES

1.0 OVERVIEW

Earth-space path attenuation for systems operating above 10 GHz will usually degrade the performance of the path. Consequently, system engineers must consider both the magnitude, frequency and duration of attenuation events along the path to realize a workable system. However, because of the randomness of events in the troposphere only statistical predictions can be made of path performance. The predictions usually apply on several time scales: long times of the order of minutes or more (resulting in an average attenuation) and short times of the order of seconds (termed amplitude scintillations). The scintillations are always present to some degree and arise due to the inhomogeneity of the troposphere.

The chief contributors to the average attenuation along an earth-space path are:

- Gaseous attenuation
  (primarily due to oxygen and water vapor in the 10 to 100 GHz frequency range)
- Rain.

Some minor levels of attenuation can be obtained from clouds, fog, dust, and sand. The latter contributors have not been studied in detail, but the results to date will be included to demonstrate the existing level of knowledge. Snow and ice appear to cause very low levels of attenuation, but can contribute to wave depolarization.

The gaseous specific attenuation, (i.e., attenuation per unit length) has been studied and measured so that its contribution can be predicted quite accurately given the path length of the link through the medium. The rain attenuation, however, can only be statistically obtained, even though the specific attenuation of rain is now fairly well known. The rain attenuation is usually presented in two formats. The first format consists of the percentage of time the rain attenuation exceeds a specified level (long term cumulative statistics) based on knowledge of the rainfall in a giver region, the specific attenuation, and geometric parameters of the path. The second format consists of the worst month statistics (or better, the worst 30-day statistics) based on the local climatological data, the specific attenuation and the geometry of the earth-space path.

Most of the rain attenuation statistics in this report have been developed from the common base of the rain rate statistics. Given these rain statistics, the models develop the total attenuation statistics utilizing different techniques. Some techniques are easy to utilize, while others require more computational time and are expected to be more accurate. Parts of four models which have been used in the U.S. have been described in some detail in this report. The rationale for utilizing the particular elements of each model are described along with the model. However, other models now being developed or models not as widely applied are referenced, since they may ultimately prove to be more accurate for particular applications.

Several approaches to obtaining the rain attenuation statistics are presented in this chapter. For any specific design, it is recommended that the simplest approach be applied first and then more sophisticated techniques until the required level of accuracy is obtained. The use of these approaches is dependent on the known data. For example, if no rain data is available for a specific site, utilize the CCIR Global model. In contrast, if long-term satellite-to-ground attenuation statistics are available at another frequency, then only frequency scaling will be necessary resulting in a much more accurate prediction of the link performance. These methods are described in detail in Paragraph 3 along with specific examples.

In the remainder of this section, data needed for the more detailed analyses is also presented. This data forms the basis for the predictive models.

2.0 GASEOUS CONTRIBUTIONS*

In the frequency range from 10 to 100 GHz the water vapor absorption at 22.235 GHz and the oxygen lines extending from 53.5 to 65.2 GHz are the only significant contributors. The absorption lines are broadened by collisions at high pressures (low elevations) thus the specific attenuation is altitude dependent. The vertical one-way attenuation for a moderately humid atmosphere (7.5 gm/m^3) at various station altitudes above sea level is presented in Figure 2-1. For other elevation angles θ ($\theta \geq 5^o$) multiply the indicated attenuation by cosecant θ. The range of values C indicated in Figure 2-1 refer to the fine absorption lines which may be observed between high flying aircraft and satellites (Ref. 2-1). For station altitudes not shown, a linear extrapolation between curves is recommended assuming an exponentially distributed atmosphere for both water vapor and oxygen.

The water vapor content is the most variable component of the atmosphere. Therefore, for more arid regions a correction should be made for the expected values of water vapor. To first order, the vertical one-way attenuation at sea-level is given in Figure 2-2 for 7.5 gm/m^3 (solid line)

---

* The primary references for the material presented in this section are Report 234-3, CCIR, Geneva, 1974 and Doc. 5/270-E Working Group 5-2, 19 Sept. 1977.

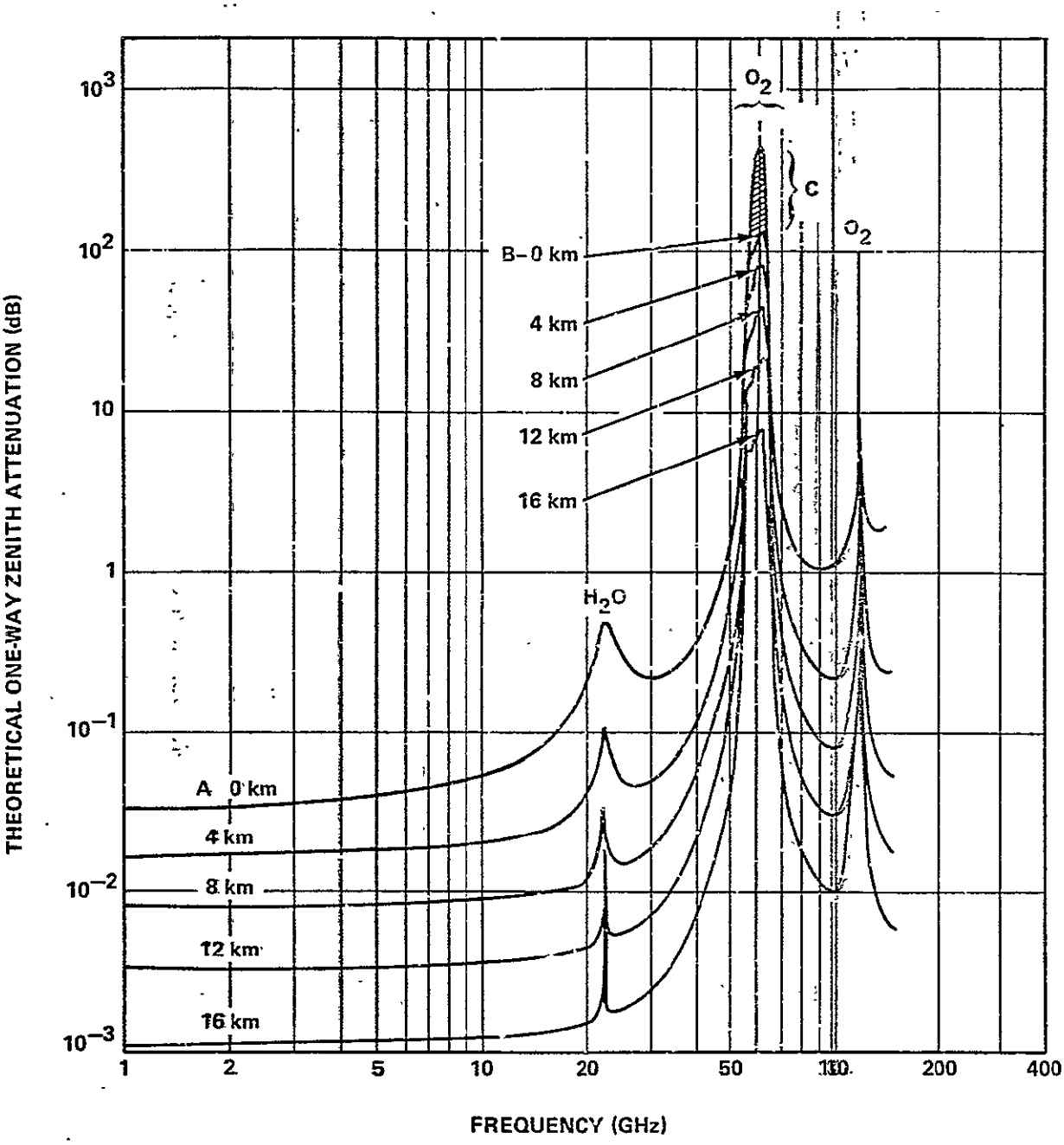

FIGURE 2-1. THEORETICAL VERTICAL ONE-WAY ATTENUATION FROM SPECIFIED HEIGHT TO TOP OF THE ATMOSPHERE FOR A MODERATE HUMID ATMOSPHERE (7.5 G/M^3 AT THE SURFACE)

A: STARTING HEIGHTS (KM)
B: MINIMUM VALUES FOR PATHS STARTING AS INDICATED HEIGHTS (KM)
C: RANGE OF VALUES FOR THE PATH FROM THE SURFACE TO 50 KM

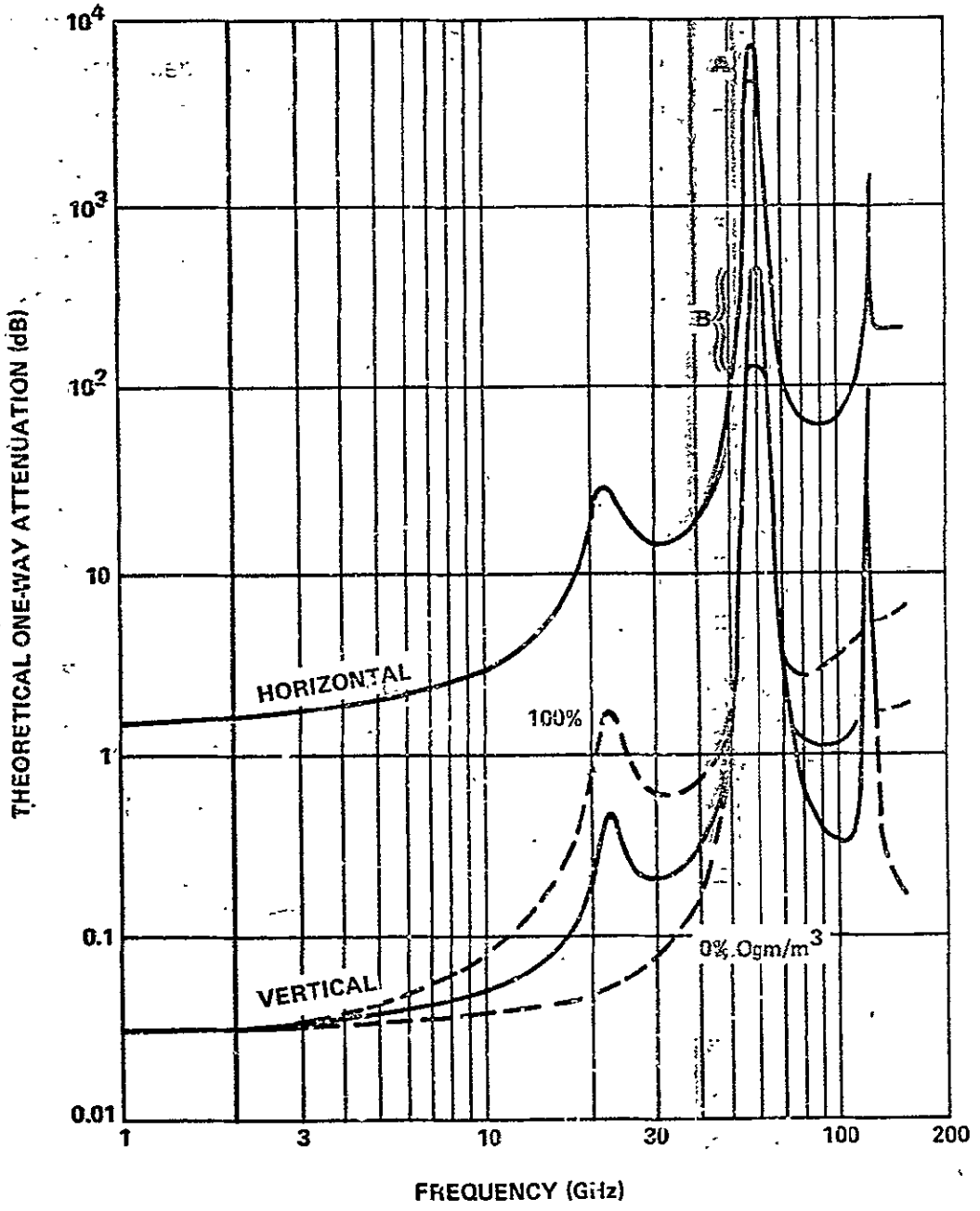

FIGURE 2-2. THEORETICAL ONE-WAY ATTENUATION FOR VERTICAL PATHS THROUGH THE ATMOSPHERE (CALCULATED USING THE UNITED STATES' STANDARD ATMOSPHERE FOR JULY AT 45° N LATITUDE). SOLID CURVES ARE FOR A MODERATE HUMID ATMOSPHERE (7.5 G/M^3 AT THE SURFACE); DASHED CURVES FOR VERTICAL ATTENUATION REPRESENT THE LIMITS FOR 0 AND 100% RELATIVE HUMMIDITY

A: RANGE OF VALUES
B: RANGE OF VALUES

and 0 gm/m^3 (0% dashed line) for the US Standard Atmosphere in July at 45°N latitude. Linear interpolation may be used between the curve for 7.5 gm/m^3 and the 0 gm/m^3 and extrapolated to at least 15 gm/m^3. The elevation angle ($5^\circ \leq \theta \leq 90^\circ$) dependence is proportional to cosecant θ. The horizontal curve (7.5 gm/m^3) in Figure 2-2 can be utilized as a limit for angles below 10° elevation angle.

For a station at arbitrary altitude and surface water vapor density, a combination of the results in Figures 2-1 and 2-2 is required. A suggested procedure follows:

1. Determine the one-way vertical attenuation due to altitude from Figure 2-1 at the frequency of interest
2. Determine the decrease (increase) in dB below (above) the 7.5 gm/m^3 curve in Figure 2-1 based on a linear extrapolation between the solid curve and the 0%, 0 gm/m^3 curve.
3. Add 1) and 2) in dB and multiply by the cosecant of the elevation angle θ ($5^\circ \leq \theta \leq 90^\circ$).

Note: The water vapor content at the surface is usually measured as relative humidity or the partial vapor pressure. The conversions between these units are given in an Appendix at the end of this section.

As an example, the Rosman ground station altitude is $\approx$ 880 meters so the vertical one-way attenuation is 0.17 dB at 20 GHz. Using the example numbers in the Appendix, namely 80°F, R.H. = 60% and elevation angle = 47°, the water vapor density is 15 gm/m^3. Extrapolating this value on Figure 2-2 yields an additional 0.7 dB attenuation above the 7.5 gm/m^3 value. Thus the total attenuation is 0.87 dB vertically. Note that this nearly corresponds to the 100% RH curve on Figure 2-2, but this is coincidental and indicates that the moisture level selected for the example is higher than the averages displayed in Figure 2-2. The total one-way attenuation to ATS-6 from the Rosman ground station due to gases is computed for a 47-degree elevation angle to be 0.87 csc (47) dB = 1.2 dB at 20 GHz. At 30 GHz, the result is lower (0.96 dB) for the same conditions since 30GHz is near the local minimum in the gaseous specific attenuation values.

3.0 RAIN ATTENUATION

3.1 OVERVIEW

3.1.1 Scattering

Rain drops both attenuate and scatter microwave energy along an earth-space path. From the basic Rayleigh scattering criteria (the dimensions of the scatterer are much smaller than the wavelength) and the fact that the median rain drop diameter is approximately 1.5 mm, one would expect that Rayleigh scattering theory should be applied in the frequency (wavelength) range from 10 GHz (3cm) to 100 GHz (3mm). However, Rayleigh scattering also requires that the imaginary component of the refractive index be small, which is not the case for water drops (Ref. 3-1). Because of this effect and the wide distribution of rain drop diameters, the Rayleigh scattering theory appears to apply only up to 3 GHz (Ref. 3-2). Above 3 GHz Mie scattering applies and is the primary technique utilized for specific rain attenuation (attenuation per unit length, dB/km) calculations. Mie scattering accounts for the deficiencies of Rayleigh scattering and has proved to be the most accurate.

3.1.2 Drop-Size Distributions

Several investigators have studied the distribution of rain drop sizes as a function of rain rate and type of storm activity. The three most commonly used distributions are:

- Laws and Parsons (LP)
- Marshall-Palmer (MP)
- Joss-thunderstorm (J-T) and drizzle (J-D)

In general the Laws and Parsons distribution (Ref. 3-3) is favored for design purposes because it has been widely tested by comparison to measurements for both widespread (lower rainrates) and convective rain (higher rainrates) at the present time. Also in the higher rainrate R regime ($R \geq 25$ mm/hr) and at frequencies above 10 GHz, the LP values give higher specific rain attenuations than the J-T values (Ref. 3-4). In addition it has been observed that the raindrop temperature is most accurately modeled by the $0^{\circ}C$ data rather than $20^{\circ}C$, since for most high elevation angle earth-space links the raindrops are cooler at high altitudes and warm as they fall to earth.

An example of the measured number distribution of raindrops with drop diameter as a function of rain rate R (mm/hr) is given in Figure 3-1. Here the measurements of Laws and Parsons (broken lines, Ref. 3-3) and Marshall and Palmer (dotted lines, Ref. 3-5) are fitted by an exponential relation of the form

$$N_D = N_0 e^{-\Lambda D_{cm}^{-4}}$$

where

$$N_0 = 0.08 \text{ cm}^{-4}$$

and

$$\Lambda = 41 \, R^{-0.21}_{cm^{-1}}$$

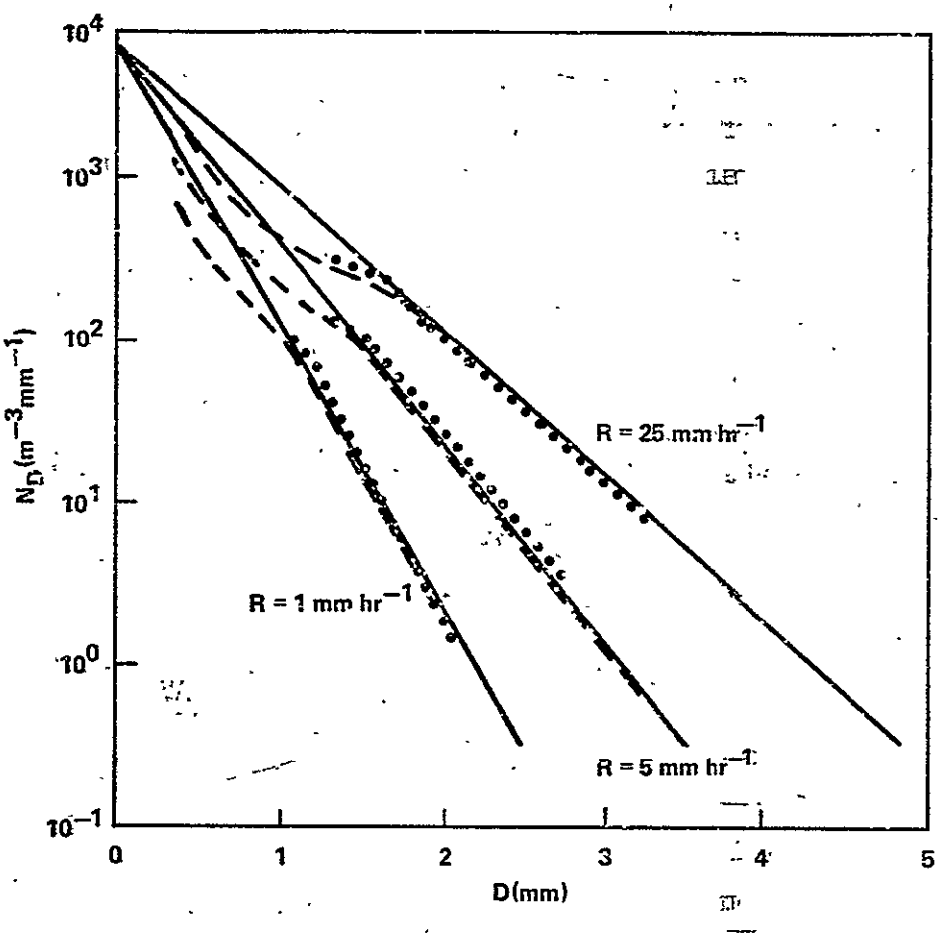

FIGURE 3-1. RAIN DROP SIZE DISTRIBUTION FUNCTION (SOLID STRAIGHT LINES) COMPARED WITH RESULTS OF LAWS AND PARSONS (BROKEN LINES) AND OTTAWA OBSERVATIONS (DOTTED LINES)
REFERENCE: FIGURE 2 OF REF. 3-5

Note that the units in the equations and Figure 3-1 are different. Multiply the N_D by 10^5 to convert to the units of Figure 3-1. The number of rain drops with diameters between D and D + δD in a volume V (cm^3) at rainrate R is

$$N_R = N_D \, \delta D \, V$$

As shown in Figure 3-1, the measured data deviates from the exponential relation for diameters below 1.5 mm. However, the larger drops tend to dominate the specific attenuation at the higher rainrates of most concern for the system engineer, and so this deviation tends not to be reflected in the integral over drop diameters utilized in specific attenuation calculations.

Joss, et al., (Ref. 3-6) have found significant variations of N_D and Λ for different types of rainfall based on one year's measurements at Locarno, Switzerland. These results are presented in Table 3-1; however, the climatic regions where the Joss statistics apply have not been determined. Therefore, it appears best to utilize the Laws and Parsons results, realizing that in certain areas of the U.S. and Canada they have not been verified.

TABLE 3-1

VALUES OF N_0, Λ VERSUS RAIN EVENT AS DETERMINED BY JOSS, ET AL. (REF. 3-6)

Rainfall Type	N_0 cm^{-4}	Λ cm^{-1}
drizzle	0.3	$57R^{-0.21}$
widespread	0.07	$41R^{-0.21}$
thunderstorm	0.014	$30R^{-0.21}$

3.1.3 Specific Attenuation

It has been determined (Ref. 3-7) that the specific attenuation A (dB/km) is related to the rain rate R (mm/hr) by a relation

$$A = a(f)R^{b(f)}$$

where the coefficients a and b are functions of frequency. At this time the most thorough calculations of A have been made by Olsen, et al. (Ref. 3-4). These calculations extend from 1 to 1000GHz and have been presented in both tabular and empirical format for several raindrop distributions and temperatures. For the U.S. and Canada the $0^{o}C$ numbers are most applicable (Ref. 3-2). Table I of Ref. 2-5 is given below (Table 3-2) for selected frequencies of interest in this report. The LP_L and LP_H refer to Laws and Parsons drop size distributions associated with rainrates R from 1.27 to 50.8 mm/hr and 25.4 to 152.4 mm/hr, respectively. Olsen, et al. have also provided analytic approximations for a(f) and b(f) which are quite adequate for use by system engineers. These are

$$a(f) = 4.21 \times 10^{-5}(f)^{2.42} \qquad 2.9 \leq f < 54 \text{ GHz}$$

$$= 4.09 \times 10^{-2}(f)^{0.699} \qquad 54 \leq f < 180 \text{ GHz}$$

and

$$b(f) = 1.41\,(f)^{-0.0779} \qquad 8.5 \leq f < 25 \text{ GHz}$$

$$= 2.63\,(f)^{-0.272} \qquad 25 \leq f < 164 \text{ GHz}$$

where f is in GHz.

Thus for 20 GHz

$$A = a(f)R^{b(f)} \text{ dB/km}$$

$$= 4.21 \times 10^{-5}(20)^{2.42}R^{\,1.41(20)^{-0.0779}} \text{ dB/km}$$

$$= 0.059R^{1.117} = 2.19 \text{ dB/km @ } R = 25.4 \text{ mm/hr.}$$

TABLE 3-2

REGRESSION CALCULATIONS FOR a and b in $A = aR^b$ (dB/km) AS FUNCTIONS OF FREQUENCY AND DROPSIZE DISTRIBUTION, RAIN TEMPERATURE = 0°C

FREQ. (GHz)	a					b				
	LP_L	LP_H	MP	J-T	J-D	LP_L	LP_H	MP	J-T	J-D
10	1.17×10^{-2}	1.14×10^{-2}	1.36×10^{-2}	1.69×10^{-2}	1.14×10^{-2}	1.178	1.189	1.150	1.076	0.968
11	1.50×10^{-2}	1.52×10^{-2}	1.73×10^{-2}	2.12×10^{-2}	1.41×10^{-2}	1.171	1.167	1.143	1.065	0.977
12	1.86×10^{-2}	1.96×10^{-2}	2.15×10^{-2}	2.62×10^{-2}	1.72×10^{-2}	1.162	1.150	1.136	1.052	0.985
15	3.21×10^{-2}	3.47×10^{-2}	3.68×10^{-2}	4.66×10^{-2}	2.82×10^{-2}	1.142	1.119	1.118	1.010	1.003
20	6.26×10^{-2}	7.09×10^{-2}	7.19×10^{-2}	9.83×10^{-2}	5.30×10^{-2}	1.119	1.083	1.097	0.946	1.020
25	0.105	0.132	0.121	0.173	8.61×10^{-2}	1.094	1.029	1.074	0.884	1.033
30	0.162	0.226	0.186	0.274	0.128	1.061	0.964	1.043	0.823	1.044
35	0.232	0.345	0.268	0.372	0.180	1.022	0.907	1.007	0.783	1.053
40	0.313	0.467	0.362	0.451	0.241	0.981	0.864	0.972	0.760	1.058
50	0.489	0.669	0.579	0.629	0.387	0.907	0.815	0.905	0.709	1.053
60	0.658	0.796	0.801	0.804	0.558	0.850	0.794	0.851	0.682	1.035
70	0.801	0.869	1.00	0.833	0.740	0.809	0.784	0.812	0.661	1.009
80	0.924	0.913	1.19	0.809	0.922	0.778	0.780	0.781	0.674	0.980
90	1.02	0.945	1.35	0.857	1.10	0.756	0.776	0.753	0.663	0.953
100	1.08	0.965	1.48	0.961	1.26	0.742	0.774	0.730	0.637	0.928
82	.943	.919				.774	.779			

The value in Table 3-2 for this frequency is $0.0626\ R^{1.119} = 2.34$ dB/km @ R = 25.4 mm/hr, an error of 6 %.

Based on the Olson, et al., results (Ref. 3-4), the following specific attenuation relations are recommended in the 10 to 100 GHz frequency range (see Table 3-3). These specific attentuations will be utilized throughout this report.

TABLE 3-3

RECOMMENDED SPECIFIC ATTENUATION APPROXIMATIONS

Frequency Range	Specific Attenuation, A, (dB/km) (R in mm/hr, f in GHz)
10 - 25 GHz	$A = 4.21 \times 10^{-5}(f)^{2.42} R^{[1.41(f)^{-0.0779}]}$
25 - 54 GHz	$A = 4.21 \times 10^{-5}(f)^{2.42} R^{[2.63(f)^{-0.272}]}$
54 - 100 GHz	$A = 4.09 \times 10^{-5}(f)^{0.699} R^{[2.62(f)^{-0.272}]}$

The specific attenuations for several of the common earth-space bands are shown in Figure 3-2 for raindates from 0.1 to 10 inches/hr (2.54 to 254 mm/hr) using the equations in Table 3-3. The 85 and 94 GHz curves overlap the 50 GHz data because of inaccuracies in the approximations in Table 3-3. More accurate results are obtained from interpolation of Table 3-2.

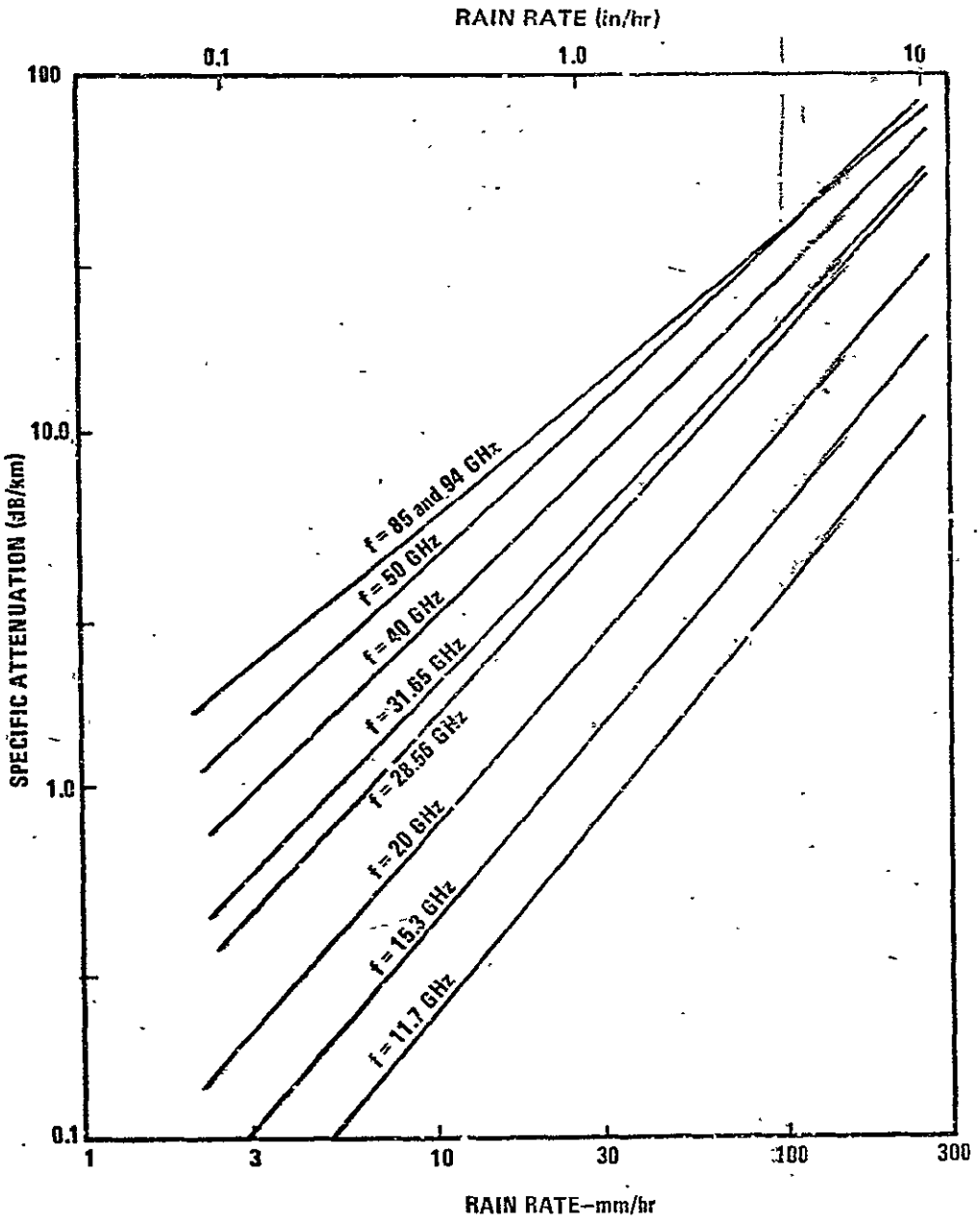

FIGURE 3-2. SPECIFIC ATTENUATION VERSUS RAIN RATE FOR COMMON EARTH-SPACE FREQUENCIES

3.2 RAIN RATE DATA

3.2.1 U.S. Sources

In the U.S. the National Weather Service's National Climatological Center* prepares and maintains extensive precipitation records obtained from Weather Service Offices and over 12,000 observers and agencies. This rain data is available in several documents available from the National Climatological Center. Several of these publications of interest to the earth-space path engineer are:

- Hourly Precipitation Data (HPD)
  - 15 minute rain rate resolution
  - published monthly by state
  - District of Columbia included in the Virginia HPD
  - available about 6 months following date of recording
  - $0.40 per copy
- Climatological Data (CD)
  - 1 hour rain rate resolution
  - published monthly by state
  - District of Columbia included in the Maryland and Delaware CD
  - Washington National Airport WSO is included in the Virginia CD
  - available about 3 months following date of recording
  - $0.40 per copy
- Climatological Data-National Summary
  - greatest 24 hour rain rate data
  - published monthly
  - available about 4 months following date of recording
  - $0.70 per copy
- Climatological Data-National Summary, Annual Summary
  - one 5 minute rain rate resolution per month
  - available about 18 months following last date of recording
  - $1.80 per copy

---

* National Climatic Center, Federal Building, Asheville, North Carolina 28801

- Local Climatological Data (LCD)
  - hourly rain rate resolution
  - published monthly by location
  - available about 4 months following date of recording
  - $0.20 per copy
  - annual issue also published for each location, $0.15 per copy
- Storm Data
  - published monthly for the U.S.
  - describes type of storm and extent of damage.

The Local Climatological Data is available for the 291 stations shown in Table 3-4; however, the Hourly Precipitation Data is available for many more stations.

Examples of the precipitation-related data available in each of these publications are given in Figures 3-3 to 3-7. Comparing the results for either the Baltimore Weather Station Office (WSO) at the Airport (AP) or the Beltsville results, one observes that precipitation data up to 15-minute resolution is available in the HPD's, while the monthly CD lists only the total precipitation per hour (see Figure 3-4). The monthly CD, National Summary, lists the total precipitation per month in liquid form and the total snow or ice pellet depth at most airports. Also included (see Figure 3-5) is the number of thunderstorms recorded during the month. In the Annual Summary of the National CD (see Figure 3-6) the total precipitation, snowfall (all frozen precipitation except hailstones) and the amount and date(s) of the highest precipitation rate during the year for periods of 5 to 180 minutes are given. Unfortunately it only includes one 5 minute event per month, i.e., if there were several significant high rain rate periods per month, only the highest will be indicated in the data. Additional techniques to retrieve more data will be described below.

The Local Climatological Data (LCD) provides the rainfall by hour at each of the 291 stations shown in Table 3-4. An example for Asheville, NC, is shown in Figure 3-7. In this publication the type of weather is

TABLE 3-4

LOCAL CLIMATOLOGICAL DATA STATIONS

U.S. DEPARTMENT OF COMMERCE
NATIONAL OCEANIC AND ATMOSPHERIC ADMINISTRATION
ENVIRONMENTAL DATA SERVICE

(Stations for which Local Climatological Data are issued, as of January 1, 1978)

ALABAMA

abc BIRMINGHAM
abc HUNTSVILLE
abc MOBILE
abc MONTGOMERY

ALASKA

abc ANCHORAGE
abc ANNETTE
abc BARROW
abc BARTER ISLAND
abc BETHEL
abc BETTLES
abc BIG DELTA
abc COLD BAY
abc FAIRBANKS
abc GULKANA
abc HOMER
abc JUNEAU
abc KING SALMON
abc KODIAK
abc KOTZEBUE
abc McGRATH
abc NOME
abc ST. PAUL ISLAND
abc TALKEETNA
abc UNALAKLEET
abc VALDEZ
abc YAKUTAT

ARIZONA

abc FLAGSTAFF
abc PHOENIX
abc TUCSON
abc WINSLOW
abc YUMA

ARKANSAS

abc FORT SMITH
abc LITTLE ROCK

CALIFORNIA

abc BAKERSFIELD
abc BISHOP
abc BLUE CANYON
ac EUREKA
abc FRESNO
abc LONG BEACH
abc LOS ANGELES AIRPORT
ac LOS ANGELES CIVIC CENTER
abc MT. SHASTA
abc OAKLAND
abc RED BLUFF
abc SACRAMENTO
abc SANDBERG
abc SAN DIEGO
SAN FRANCISCO
abc AIRPORT
ac CITY
abc SANTA MARIA
abc STOCKTON

COLORADO

abc ALAMOSA
abc COLORADO SPRINGS
abc DENVER
abc GRAND JUNCTION
abc PUEBLO

CONNECTICUT

abc BRIDGEPORT
abc HARTFORD

DELAWARE

abc WILMINGTON

DISTRICT OF COLUMBIA

abc WASHINGTON - NATIONAL AP
abc WASHINGTON - DULLES INT'L AP

FLORIDA

abc APALACHICOLA
abc DAYTONA BEACH
abc FORT MYERS
abc JACKSONVILLE
abc KEY WEST
ac LAKELAND
abc MIAMI
abc ORLANDO
abc PENSACOLA
abc TALLAHASSEE
abc TAMPA
abc WEST PALM BEACH

GEORGIA

abc ATHENS
abc ATLANTA
abc AUGUSTA
abc COLUMBUS
abc MACON
abc ROME
abc SAVANNAH

HAWAII

abc HILO
abc HONOLULU
abc KAHULUI
abc LIHUE

IDAHO

abc BOISE
abc LEWISTON
abc POCATELLO

ILLINOIS

ac CAIRO
CHICAGO
abc MIDWAY AIRPORT
abc O'HARE AIRPORT
abc MOLINE
abc PEORIA
abc ROCKFORD
abc SPRINGFIELD

INDIANA

abc EVANSVILLE
abc FORT WAYNE
abc INDIANAPOLIS
abc SOUTH BEND

IOWA

abc BURLINGTON
abc DES MOINES
abc DUBUQUE
abc SIOUX CITY
abc WATERLOO

KANSAS

abc CONCORDIA
abc DODGE CITY
abc GOODLAND
abc TOPEKA
abc WICHITA

KENTUCKY

abc LEXINGTON
abc LOUISVILLE

LOUISIANA

abc ALEXANDRIA (1)
abc BATON ROUGE
abc LAKE CHARLES
abc NEW ORLEANS
abc SHREVEPORT

MAINE

abc CARIBOU
abc PORTLAND

MARYLAND

abc BALTIMORE

MASSACHUSETTS

abc BOSTON
ac BLUE HILL OBS.
abc WORCESTER

MICHIGAN

abc ALPENA
DETROIT
abc CITY AIRPORT
abc DETROIT METRO AP
abc FLINT
abc GRAND RAPIDS
abc HOUGHTON LAKE
abc LANSING
ac MARQUETTE
abc MUSKEGON
abc SAULT STE. MARIE

MINNESOTA

abc DULUTH
abc INTERNATIONAL FALLS
abc MINNEAPOLIS ST PAUL
abc ROCHESTER
abc ST CLOUD

MISSISSIPPI

abc JACKSON
abc MERIDIAN

MISSOURI

abc COLUMBIA
abc KANSAS CITY
abc ST JOSEPH
abc ST. LOUIS
abc SPRINGFIELD

MONTANA

abc BILLINGS
abc GLASGOW
abc GREAT FALLS
abc HAVRE
abc HELENA
abc KALISPELL
abc MILES CITY
abc MISSOULA

NEBRASKA

abc GRAND ISLAND
abc LINCOLN
abc NORFOLK
abc NORTH PLATTE
abc OMAHA
ac OMAHA (NORTH) (2)
abc SCOTTSBLUFF
ac VALENTINE

NEVADA

abc ELKO
abc ELY
abc LAS VEGAS
abc RENO
abc WINNEMUCCA

NEW HAMPSHIRE
abc CONCORD
ac MT WASHINGTON

NEW JERSEY

ATLANTIC CITY
abc AIRPORT
a STATE MARINA
abc NEWARK
ac TRENTON

NEW MEXICO

abc ALBUQUERQUE
abc CLAYTON
abc ROSWELL

NEW YORK

abc ALBANY
abc BINGHAMTON
abc BUFFALO
NEW YORK
abc CENTRAL PARK
abc J F KENNEDY INT'L AP
abc LaGUARDIA FIELD
abc ROCHESTER
abc SYRACUSE

NORTH CAROLINA

abc ASHEVILLE
abc CAPE HATTERAS
abc CHARLOTTE
abc GREENSBORO
abc RALEIGH
abc WILMINGTON

NORTH DAKOTA
abc BISMARCK
abc FARGO
abc WILLISTON

OHIO

abc AKRON-CANTON
CINCINNATI
ac ABBE OBS.
abc AIRPORT
abc CLEVELAND
abc COLUMBUS
abc DAYTON
abc MANSFIELD
abc TOLEDO
abc YOUNGSTOWN

OKLAHOMA

abc OKLAHOMA CITY
abc TULSA

OREGON

abc ASTORIA
abc BURNS
abc EUGENE
abc MEDFORD
abc PENDLETON
abc PORTLAND
abc SALEM
abc SEXTON SUMMIT

PACIFIC ISLANDS

abc GUAM
abc JOHNSTON
abc KOROR
abc KWAJALEIN
abc MAJURO
abc PAGO PAGO
abc PONAPE
abc TRUK (MOEN)
abc WAKE
abc YAP

PENNSYLVANIA

abc ALLENTOWN
abc AVOCA, WILKES-BARRE SCRANTON AP
abc ERIE
abc HARRISBURG
abc PHILADELPHIA
PITTSBURGH
abc AIRPORT
ac CITY
abc WILLIAMSPORT

RHODE ISLAND

ac BLOCK ISLAND
abc PROVIDENCE

SOUTH CAROLINA

CHARLESTON
abc AIRPORT
ab CITY
abc COLUMBIA
abc GREENVILLE SPARTANBURG

SOUTH DAKOTA

abc ABERDEEN
abc HURON
abc RAPID CITY
abc SIOUX FALLS

TENNESSEE

abc BRISTOL
abc CHATTANOOGA
abc KNOXVILLE
abc MEMPHIS
abc NASHVILLE
ac OAK RIDGE

TEXAS

abc ABILENE
abc AMARILLO
abc AUSTIN
abc BROWNSVILLE
abc CORPUS CHRISTI
abc DALLAS FORT WORTH
abc DEL RIO
abc EL PASO
ac GALVESTON
abc HOUSTON
abc LUBBOCK
abc MIDLAND
abc PORT ARTHUR
abc SAN ANGELO
abc SAN ANTONIO
abc VICTORIA
abc WACO
abc WICHITA FALLS

UTAH

abc MILFORD
abc SALT LAKE CITY

VERMONT

abc BURLINGTON

VIRGINIA

abc LYNCHBURG
abc NORFOLK
abc RICHMOND
abc ROANOKE
ab WALLOPS ISLAND

WASHINGTON

abc OLYMPIA
abc QUILLAYUTE AIRPORT
abc SEATTLE TACOMA AP
ac SEATTLE URBAN SITE
abc SPOKANE
abc STAMPEDE PASS
ac WALLA WALLA
abc YAKIMA

WEST INDIES

abc SAN JUAN, P R

WEST VIRGINIA

abc BECKLEY
abc CHARLESTON
abc ELKINS
abc HUNTINGTON
ac PARKERSBURG

WISCONSIN

abc GREEN BAY
abc LA CROSSE
abc MADISON
abc MILWAUKEE

WYOMING

abc CASPER
abc CHEYENNE
abc LANDER
abc SHERIDAN

a. Monthly summary issued.   b. Monthly summary includes available 3-hourly observations   c. Annual Summary issued.

Subscription Price: Local Climatological Data $2.55 per year including annual issue if published, $1.85 additional for foreign mailing. Single copy $.20 for monthly issue, $.20 for annual issue. These costs are for only the station(s) requested. A complete set of all of the stations [illegible] is available [illegible] $20.00 [illegible] $25.00. Make checks payable to DOC, NOAA, N.C. [illegible] send payments to: National Climatic Center, Federal Building, Asheville, NC 28801

(1) September 1977 was the last monthly issue; last published Annual Summary was 1976.

(2) June 1977 was the first monthly issue; available data published for entire year.

HOURLY PRECIPITATION

HOURLY AMOUNTS

MARYLAND AND DELAWARE
DECEMBER 1977

STATION	DATE	A. M. HOUR ENDING 1	2	3	4	5	6	7	8	9	10	11	12	P. M. HOUR ENDING 1	2	3	4	5	6	7	8	9	10	11	12	TOTAL
		MONTHLY MAXIMUM AMOUNTS																								
		HOURS	1			2			3			6			12			24			ACCUMULATION				
		MINUTES	15			30			45			60			120			180							
		(APPLY HEADING AS APPROPRIATE)																								
MARYLAND																										
BALTIMORE WSO AP	1	.15	.01	.03																						.19
	5							.01	.01	.01		.02	.02		.08	.04	.26									.25
	6								.01																	.01
	9				.01	.07																				.08
	13						.03																			.03
	14									.01	.09	.08	.08	.05	.02	.02	.08	.04	.08	.03	.05	.05	.04			.67
	18	.09	.20	.17	.27	.04	.20	.30	.35	.31	.28	.25	.12	.09		.05						.13	.21	.18	.13	3.35
	19	.12	.05	.05	.05	.01	.04	.03	.02							.05										.37
	22													.05	.04	.03	.03			.02	.01	.03	.01			.22
	21	.01	.01		.01	.09	.09	.04	.05	.01																.31
	25		.04	.03	.01	.02	.04	.01										.02	.04				.01			.15
	30																									.11
	31						.01																			.01
		AMOUNT				.35			.66			.95			1.69			2.39			3.39					
		DATE/TIME OF ENDING				18/8:00A			18/9:00A			18/9:00A			18/11:00A			18/12:00P			19/1:00A					
BALTIMORE WSO CI	1	.03	.04	.03																						.15
	5							.01	.01	.01		.01	.03	.01		.04	.09	.07								.28
	6	.01	.01							.01																.03
	9			.01		.05																				.06
	13	.03		.01																						.04
	14								.01	.01	.09	.08	.03	.07	.02	.04	.03	.04	.06	.04	.05		.03			.66
	18	.08	.25	.11	.28	.13	.20	.29	.56	.62	.33	.33	.18	.14	.02		.01		.01				.11	.18	.15	3.99
	19	.09	.04	.05	.05	.05	.03	.02	.01	.01	.03	.01														.41
	20													.01	.08	.06	.02	.02	.01	.02	.02	.03	.02			.29
	21	.02	.01	.01	.01	.11	.12	.04	.05	.03																.40
	25		.03	.01	.01	.03	.02	.02										.02	.03	.06						.12
	30																									.11
		AMOUNT				.62			1.13			1.51			2.37			3.02			3.99					
		DATE/TIME OF ENDING				18/9:00A			18/9:00A			18/11:00A			18/11:00A			18/1:00			19/1:00A					
BELTSVILLE	1	.1														.1										.2
	5															.1										.2
	9					.1																				.1
	14										.2		.1				.1		.1		.1					.6
	17																								.1	.1
	18	.2	.1	.4	.1	.2	.3	.6	.3	.4	.3	.1	.1		.1						.1	.2	.1	.3	.2	4.1
	19			.1										.1												.3
	20													.1											.1	.3
	21					.1	.1		.1																	.3
	25		.1															.1			.1					.1
	30																									.2
		AMOUNT				.6			.9			1.3			2.1			3.1			4.1					
		DATE/TIME OF ENDING				18/7:00A			18/8:00A+			18/9:00A			18/10:00A			18/12:00A+			18/12:00P					
		AMOUNT				.4			.5			.6			.7			1.0			1.4					
		DATE/TIME OF ENDING				18/6:45A			18/7:00A+			19/7:15A+			18/7:30A+			18/8:30A+			18/9:30A+					
BELTSVILLE PLANT STA 5	1	.04	.01	.02																						.07
	5							.01	.01	.01	.01	.01	.01	.02	.01	.08	.03							.01		.21
	6							.01	.33																	.04
	9					.05	.02																			.07
	14										.12	.03	.04	.04	.02	.01	.01	.03	.07	.02	.07	.01	.01			.48
	17																								.21	.21
	18	.21	.10	.25	.08	.22	.29	.31	.40	.30	.24	.08	.08	.03	.05	.01				.01	.30	.10	.14	.11	.05	3.36
	19	.02	.02	.04	.04	.04	.04	.03	.02					.01			.01	.01	.01							.27
	20						.01		.01		.01			.05	.04		.02		.02	.01	.01	.02	.02	.01	.01	.24
	21			.01	.04	.10	.10	.02	.02	.02	.04															.35
	25	.01	.03	.01		.03	.02										.01	.01	.03	.01	.01				.03	.10
	30																									.10
		AMOUNT				.40			.71			1.01			1.76			2.66			3.52					
		DATE/TIME OF ENDING				18/8:00A			18/8:00A			18/9:00A			18/10:00A			18/11:00A			18/11:00P					

Monthly Max. Amounts Temporal Resolution:

1 hour →

15 minute →

FIGURE 3-3. AN EXAMPLE OF THE HOURLY PRECIPITATION DATA (HDP) ISSUED MONTHLY BY STATE

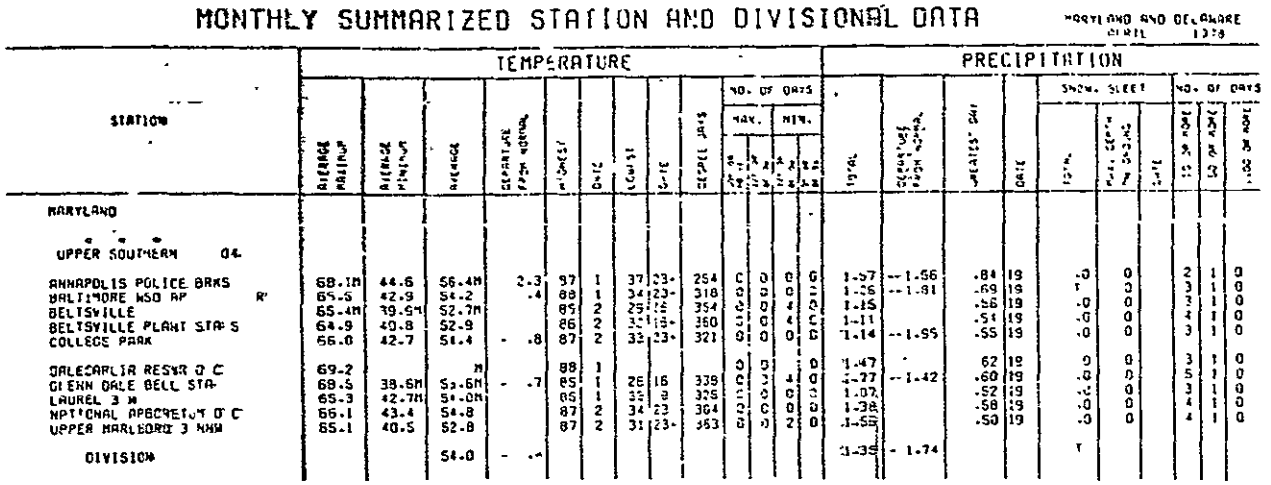

MONTHLY SUMMARIZED STATION AND DIVISIONAL DATA

MARYLAND AND DELAWARE
APRIL 1979

STATION	TEMPERATURE												PRECIPITATION								
	AVERAGE MAXIMUM	AVERAGE MINIMUM	AVERAGE	DEPARTURE FROM NORMAL	HIGHEST	DATE	LOWEST	DATE	DEGREE DAYS	NO. OF DAYS MAX. 90 OR ABOVE	NO. OF DAYS MAX. 32 OR BELOW	NO. OF DAYS MIN. 32 OR BELOW	TOTAL	DEPARTURE FROM NORMAL	GREATEST DAY	DATE	SNOW, SLEET TOTAL	SNOW, SLEET DEPTH ON GROUND	SNOW, SLEET DATE	NO. OF DAYS 1.0 OR MORE	NO. OF DAYS .50 OR MORE	NO. OF DAYS .10 OR MORE
MARYLAND																					
UPPER SOUTHERN 04																					
ANNAPOLIS POLICE BRKS	68.1M	44.6	56.4M	2.3	97	1	37	23+	254	0	0	0	1.97	--1.56	.84	19	0	0		2	1	0
BALTIMORE WSO AP R'	65.6	42.9	54.2	.4	88	1	34	23+	318	0	0	0	1.26	--1.81	.69	19	T	0		3	1	0
BELTSVILLE	65.4M	39.6M	52.7M		85	2	29	16	354	0	0	4	1.45		.56	19	0	0		3	1	0
BELTSVILLE PLANT STA S	64.9	40.8	52.9		86	2	32	16+	350	0	0	4	1.11		.54	19	0	0		4	1	0
COLLEGE PARK	66.0	42.7	54.4	- .8	87	2	33	23+	321	0	0	0	1.14	--1.95	.55	19	0	0		3	1	0
DALECARLIA RESVR D C	69.2		M		88	1				0	0	0	1.47		.62	19	0	0		3	1	0
GLENN DALE BELL STA	68.6	38.6M	53.6M	- .7	85	1	26	16	339	0	0	4	1.27	--1.42	.60	19	0	0		5	1	0
LAUREL 3 W	65.3	42.7M	54.0M		85	1	35	8	325	0	0	0	1.07		.52	19	0	0		3	1	0
NATIONAL ARBORETUM D C	66.1	43.4	54.8		87	2	34	23	304	0	0	0	1.38		.58	19	0			4	1	0
UPPER MARLBORO 3 NNW	65.1	40.5	52.8		87	2	31	23+	363	0	0	2	1.55		.50	19	0	0		4	1	0
DIVISION			54.0	- .4									1.35	- 1.74			T					

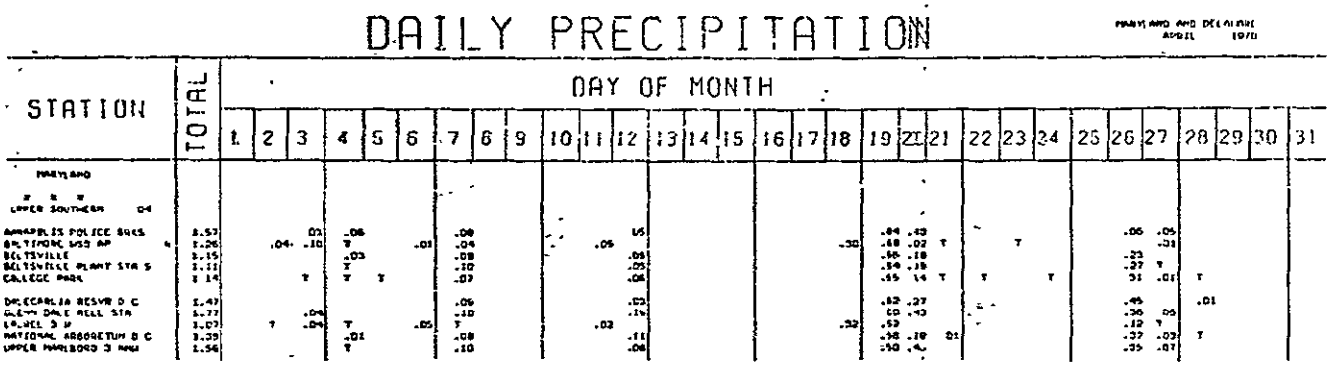

DAILY PRECIPITATION

MARYLAND AND DELAWARE
APRIL 1979

STATION	TOTAL	DAY OF MONTH																														
		1	2	3	4	5	6	7	8	9	10	11	12	13	14	15	16	17	18	19	20	21	22	23	24	25	26	27	28	29	30	31
MARYLAND																																
UPPER SOUTHERN 04																																
ANNAPOLIS POLICE BRKS	3.57			.03	.08			.09					.55							.44	.43						.06	.05					
BALTIMORE WSO AP R	1.26		.04	.10	T		.01	.04				.05							.30	.48	.02	T		T			.01					
BELTSVILLE	1.45				.03			.09					.08							.66	.18						.23					
BELTSVILLE PLANT STA S	1.11				T			.10					.03							.54	.18						.27	T				
COLLEGE PARK	1.14			T	T	T		.07					.04							.65	.14	T		T			.21	.01	T			
DALECARLIA RESVR D C	1.47							.06					.03							.62	.27						.45		.01			
GLENN DALE BELL STA	1.27							.10					.14							.60	.43						.36	.05				
LAUREL 3 W	1.07		T	.02	T		.05	T				.02							.32	.62						.12	T				
NATIONAL ARBORETUM D C	1.38				.01			.08					.11							.58	.28	01					.27	.03	T			
UPPER MARLBORO 3 NNW	1.55				T			.10					.08							.50	.42						.35	.01				

FIGURE 3-4. AN EXAMPLE OF THE CLIMATOLOGICAL DATA ISSUED MONTHLY BY STATE

CLIMATOLOGICAL DATA
METRIC UNITS

FEBRUARY 1978

State and Station	Elevation (ground) m	Pressure: Station mb	Pressure: Sea level mb	Temperature: Average maximum °C	Average minimum °C	Average °C	Departure from normal °C	Highest °C	Date	Lowest °C	Date	No. of days: Max. 32.2 °C or above	No. of days: Min. 0 °C or lower	Average dew point °C	Average relative humidity %
INDIANA															
EVANSVILLE	118	1006.5	1023.3	-1.2	-11.1	-6.1	-8.3	5.6	24	-19.4	7	0	28	-10.0	69
FORT WAYNE	241	991.2	1022.9	-4.9	-17.5	-11.2	-8.8	1.7	25+	-24.4	10	0	28	-15.0	73
INDIANAPOLIS	241	992.2	1022.9	-2.9	-12.9	-7.9	-7.2	6.4	24	-21.1	7	0	28	-11.1	77
SOUTH BEND	234	977.6	1022.2	-3.8	-15.3	-9.6	-6.4	2.4	24	-25.6	7	0	25	-12.0	75
IOWA															
BURLINGTON	211			-3.9	-13.9	-8.9	-6.3	5.6	24	-23.3	6	0	28		
DES MOINES	284	987.8	1024.6	-5.9	-14.9	-10.4	-6.1	3.9	24	-24.4	6	0	28	-13.9	72
DUBUQUE	322	982.7		-6.7	-16.1	-11.4	-5.8	2.8	24	-23.3	17	0	28		
SIOUX CITY	334	981.4	1025.7	-7.3	-17.0	-12.2	-7.4	1.3	24+	-28.9	2	0	28	-14.4	78
WATERLOO	269	971.2	1025.2	-8.2	-19.2	-13.7	-7.4	7.2	24	-27.8	5+	0	28	-16.7	74
KANSAS															
CONCORDIA	448	968.2	1023.9	-2.9	-12.3	-7.6	-7.3	7.2	24	-23.3	18+	0	28	-11.1	74
DODGE CITY	787	927.2	1021.9	-1.3	-10.6	-5.9	-7.7	12.8	6	-20.6	17	0	28	-8.3	82
GOODLAND	1114	889.3	1020.9	-1.6	-12.7	-6.8	-6.6	10.6	4+	-21.1	17	0	28	-9.4	84
TOPEKA	267	990.9	1024.3	-1.6	-11.3	-6.4	-7.2	9.4	24	-21.9	15	0	28	-9.4	76
WICHITA	408	974.2	1023.3	-0.8	-8.3	-4.6	-6.9	10.0	24	-18.3	18+	0	28	-8.3	75
KENTUCKY															
COVINGTON	265	988.8	1021.9	-2.8	-12.6	-7.7	-6.4	1.7	25	-23.3	7	0	28	-13.3	67
LEXINGTON	294	984.4	1021.6	-1.3	-10.4	-5.9	-7.8	3.3	25	-22.2	7	0	28	-10.0	74
LOUISVILLE	145	1003.7	1022.2	-0.3	-8.8	-4.5	-6.7	4.4	24	-17.8	7	0	28	-9.9	71
LOUISIANA															
BATON ROUGE	20	1018.0	1020.7	12.9	1.8	7.4	-4.8	23.9	28	-4.4	22	0	13	0.6	66
LAKE CHARLES	3	1019.5	1023.3	12.6	2.6	7.5	-5.3	24.4	25	-5.0	22	0	4	1.7	72
NEW ORLEANS	1	1019.0	1020.0	11.9	2.6	7.3	-5.9	22.8	28	-3.3	22+	0	7	1.1	67
SHREVEPORT	79	1011.5	1021.0	9.4	-2.7	3.4	-6.9	21.7	28+	-11.1	22	0	22	-8.7	77
MAINE															
CARIBOU	190	987.8		-5.2	-15.8	-10.8	+0.2	1.1	27+	-24.4	6	0	28		
PORTLAND	13	1011.9	1019.3	-0.8	-13.4	-7.1	-2.1	3.9	25	-25.6	4	0	28	-12.4	66
MARYLAND															
BALTIMORE	45	1012.9	1018.5	1.6	-6.8	-2.6	-5.2	10.6	25	-11.7	10	0	27	-10.3	58
MASSACHUSETTS															
BLUE HILL OBS R	192			-0.9	-9.0	-5.4	-2.9	4.4	17	-19.4	4	0	28		
BOSTON	5	1013.9	1014.8	1.1	-6.5	-2.7	-1.8	6.7	17+	-16.1	4	0	28		
WORCESTER	301	975.6		-2.4	-10.9	-6.7	-2.8	3.3	15	-19.4	4	0	28	-15.0	55

State and Station	Precipitation: Total mm	Departure from normal mm	Greatest in 24 hours mm	No. of days: .25 mm or more	No. of days: With thunderstorms	Snow, ice pellets: Total mm	Maximum depth on ground mm	Wind: Resultant speed m/s	Resultant direction	Fastest mile (1.6 kilometers): Speed m/s	Direction	Date	No. of days (sunrise to sunset): Clear, 0-3	Partly cloudy, 4-7	Cloudy, 8-10	Sky cover, tenths (sunrise to sunset)	Possible sunshine %
INDIANA																	
EVANSVILLE	10	-64	13	9	0	135	152	1.4	35	11.2	34	24	6	8	16	6.9	59
FORT WAYNE	6	-44	4	5	0	155	432	1.5	27	11.6	W	24	7	5	16	6.8	75
INDIANAPOLIS	6	-51	5	10	0	99	381	1.1	32	10.7	E	13	6	9	13	6.5	54
SOUTH BEND	22	-27	8	8	0	427	649	1.4	26	11.2	30	25	6	3	19	7.3	
IOWA																	
BURLINGTON	19	-17	10	6	0	292	254	1.4	35	10.3	32	25+	7	5	15	6.7	
DES MOINES	33	6	17	8	0	472	356	1.3	35	12.5	35	24+	6	2	20	7.4	37
DUBUQUE	17	-15	7	9		246	279										
SIOUX CITY	29	1	12	10	0	274	229	1.6	1	19.7	36	22	6	0	16	7.5	53
WATERLOO	11	-17	5	7	0	163	279	1.6	33	10.1	31	24	5	7	16	7.1	
KANSAS																	
CONCORDIA	14	-6	14	7	0	297	279	1.3	2	15.2	36	20	5	4	19	7.4	54
DODGE CITY	34	15	11	9	0	419	279	0.6	35	17.0	36	20	6	8	14	6.4	57
GOODLAND	27	17	12	8	0	300	229	0.9	23	14.3	35	20	10	4	14	6.4	
TOPEKA	21	-6	13	8	0	315	254	1.7	2	13.0	N	13	6	2	20	7.5	38
WICHITA	41	19	12	11	0	198	102	1.6	3	15.6	N	13	5	7	16	7.3	42
KENTUCKY																	
COVINGTON	4	-71	1	7	0	117	279	1.2	34	8.0	31	25+	5	9	11	6.0	
LEXINGTON	17	-70	10	7	0	160	152	0.7	36	8.9	26	23+	5	9	14	7.3	
LOUISVILLE	19	-69	10	8	0	135	254	1.6	35	9.8	N	21	7	9	12	6.3	69
LOUISIANA																	
BATON ROUGE	57	-64	26	7	3	0	0	1.5	35	11.6	14	22	10	6	12	5.7	
LAKE CHARLES	54	-69	14	10	2	T	0	1.7	3	13.0	15	12	5	8	12	5.7	
NEW ORLEANS	64	-59	16	9	2	T	0	1.5	1	9.4	16	12	10	3	15	6.2	49
SHREVEPORT	48	-44	17	7	1	51	25	1.5	2	12.9	20	12	12	3	13	5.4	54
MAINE																	
CARIBOU	7	-47	4	5		112	559						8	9	11	[illegible]	
PORTLAND	22	-67	20	4	0	248	406	2.2	33	13.0	NE	7+	13	5	10	[illegible]	78
MARYLAND																	
BALTIMORE	14	-57	9	6	0	312	229	2.6	32	13.4	[illegible]	7	12	[illegible]	9	4.0	57
MASSACHUSETTS																	
BLUE HILL OBS R	75	-25	68	3		772	838			30.0	NE	6					68
BOSTON	73	-17	67	4	0	691	737	3.9	32	27.3	NE	6	13	5	10	4.7	69
WORCESTER	53	-24	43	4	0	528	762	3.4	31	14.3	W	6	11	7	10	5.1	

FIGURE 3-5. AN EXAMPLE OF NATIONAL SUMMARY OF CLIMATOLOGICAL DATA ISSUED MONTHLY

ANNUAL CLIMATOLOGICAL DATA
METRIC UNITS

State and Station	Temperature: Averages: Daily maximum	Daily minimum	Annual	Extremes: Highest	Date	Lowest	Date	Heating degree days	Cooling degree days	Precipitation: Total	Greatest in 24 hours	Date(s)	Snow: Total	Greatest in 24 hours	Date(s)	Relative humidity: 1:00am EST	7:00am EST	1:00pm EST	7:00pm EST	Wind: Average speed	Resultant speed	Resultant direction	Fastest mile (1.6 kilometers): Speed	Direction	Date	Average sky cover sunrise to sunset	Number of days: Sunrise to sunset: Clear 0-0.3	Partly cloudy 0.4-0.7	Cloudy 0.8-1.0	Precipitation .25mm or more	Snow 25.4mm or more	Thunderstorms	Heavy fog	Max temp. 32.2 C and above	Max temp. 0 C and below	Min temp. 0 C and below	Min temp. -17.8 C and below
	C	C	C	C		C		Base 18.3 C	Base 18.3 C	mm	mm		mm	mm		%	%	%	%	m/s	m/s		m/s			Tenths											
MARYLAND BALTIMORE	18.4	7.1	12.8	36.4	JUL 28	-15.0	JAN 19	2651	698	1103	125	SEP 15-16	340	198	MAR 9	74	77	53	59	3.9	1.4	28	27.4	[illegible]	MAR 13	5.6	128	87	151	102	2	33	19	27	17	108	[illegible]

NORMALS, MEANS AND EXTREMES

YEAR 197[illegible]

State and Station	Elevation Ground (Meters)	Temperature (°C): Normal (1941-1970): January Daily Maximum	January Daily Minimum	July Daily Maximum	July Daily Minimum	Annual	Extremes: Length (Yrs)	Record Highest	Record Lowest	Normal Heating Degree Days (1941-1970): January	Seasonal	Precipitation (Millimeters): Normal (1941-1970): Wettest Month	Driest Month	Annual	Extremes: Wettest Month	Driest Month	Maximum In 24 Hours	Snow: Mean Total: January	Seasonal	Extreme: Maximum In 24 Hours	Relative Humidity (Percent): January 7:00 a.m. EST	January 1:00 p.m. EST	January 7:00 p.m. EST	July 7:00 a.m. EST	July 1:00 p.m. EST	July 7:00 p.m. EST	Wind Speed (m.p.s.): Mean Speed: January	July	Fastest Mile (1.6 Kilometers)	Sunshine (% of Possible): January	July	Annual Mean Number of Days: Sunrise to Sunset: Clear	Partly Cloudy	Cloudy	Precipitation .25mm or More	Snow Sleet Hail 25.4mm or More	Thunderstorms	Heavy Fog	Temperature: Max 32.2°C and Above	Min 0°C and Below	Min -17.8°C and Below
MARYLAND BALTIMORE INTL AP	45	5.5	-?.9	30.4	19.?	12.?	81 / 27	42.6 / 38.?	-40.0 / -21.7	544	2647	107	71	1028	464	7	375 / 197	124	546	394	72	[illegible]	[illegible]	[illegible]	53	74	4.4	3.6	[illegible]	[illegible]	[illegible]	[illegible]	[illegible]	[illegible]	112	7	27	49	31	10?	•

MAXIMUM SHORT DURATION PRECIPITATION

[illegible]

FIGURE 3-6
AN EXAMPLE OF THE ANNUAL SUMMARY OF CLIMATOLOGICAL DATA

LOCAL CLIMATOLOGICAL DATA

U.S. DEPARTMENT OF COMMERCE
NATIONAL OCEANIC AND ATMOSPHERIC ADMINISTRATION
ENVIRONMENTAL DATA SERVICE

ASHEVILLE, NORTH CAROLINA
NATIONAL WEATHER SERVICE OFC
ASHEVILLE AIRPORT
AUGUST 1975

LATITUDE 35° 26' N LONGITUDE 82° 33' W ELEVATION (GROUND) 2140 FT. STANDARD TIME USED: EASTERN WBAN #03812

Date	Temp. °F Maximum	Minimum	Average	Departure from normal	Average dew point	Degree days base 65° Heating	Cooling	Weather types on dates of occurrence (1 Fog, 2 Heavy fog, 3 Thunderstorm, 4 Ice pellets, 5 Hail, 6 Glaze, 7 Duststorm, 8 Smoke, haze, 9 Blowing snow)	Snow, ice pellets or ice on ground at 07AM In.	Precipitation Water equivalent In.	Snow, ice pellets In.	Avg. station pressure In. Elev. 2170 feet m.s.l.	Wind Resultant direction	Resultant speed m.p.h.	Average speed m.p.h.	Fastest mile Speed m.p.h.	Fastest mile Direction	Sunshine Minutes	Percent of possible	Sky cover tenths Sunrise to sunset	Midnight to midnight	Date
1	2	3	4	5	6	7A	7B	8	9	10	11	12	13	14	15	16	17	18	19	20	21	22
1	83	63	73	-1	66	0	8	2 8	0	0	0	27.99	17	4.6	5.3	[illegible]	[illegible]	483	58	6	6	1
2	85	61	73	-1	65	0	8	2 3	0	T	0	27.87	10	2.7	5.6	[illegible]	[illegible]	612	73	4	3	2
3	88	62	75	1	66	0	10	2	0	0	0	27.81	16	4.0	6.2	[illegible]	[illegible]	634	76	5	5	3
4	86	63	75	1	68	0	10	2	0	0	0	27.80	17	6.2	7.3	[illegible]	[illegible]	506	61	6	6	4
5	84	65	75	1	68	0	10	2 3	0	.25	0	27.76	24	.5	5.8	[illegible]	[illegible]	319	38	7	7	5
6	75	64	70	-4	67	0	5	1 8	0	.55	0	27.71	32	2.8	5.2	[illegible]	[illegible]	0	0	10	10	6
7	75	63	69	-5	65	0	4	1 8	0	T	0	27.84	07	1.8	5.8	[illegible]	[illegible]	59	7	9	9	7
8	74	59	67	-7	62	0	2	2 8	0	0	0	28.01	16	3.9	4.3	[illegible]	[illegible]	109	13	9	8	8
9	81	57	69	-5	52	0	4	2 8	0	0	0	28.02	12	1.6	4.2	[illegible]	[illegible]	341	41	9	8	9
10	71	63	67*	-7	66	0	2	2	0	.04	0	27.95	01	4.2	4.8	[illegible]	[illegible]	0	0	10	10	10
11	83	62	73	0	54	0	8	1	0	[illegible]	0	27.68	35	6.7	7.6	[illegible]	[illegible]	717	88	4	4	11
12	86	59	73	0	64	0	8	1 8	0	T	0	27.92	36	4.2	5.0	[illegible]	[illegible]	547	67	3	2	12
13	85	60	73	0	64	0	9	2 8	0	0	0	27.94	03	1.5	4.3	[illegible]	[illegible]	550	80	2	2	13
14	84	59	72	-1	66	0	7	23 8	0	.01	0	27.92	31	2.5	3.2	[illegible]	[illegible]	394	49	6	5	14
15	87	64	76	3	68	0	11	23 8	0	.10	0	27.86	22	.1	4.5	[illegible]	[illegible]	456	56	5	5	15
16	87	65	76	3	67	0	11	23 8	0	.31	0	27.87	04	1.3	5.3	[illegible]	[illegible]	488	60	5	6	16
17	86	63	75	2	68	0	10	23 8	0	.91	0	27.85	35	4.7	6.0	[illegible]	[illegible]	319	40	8	7	17
18	86	65	76	3	66	0	11	1 8	0	T	0	27.84	36	6.9	7.1	[illegible]	[illegible]	497	62	6	7	18
19	82	64	73	0	66	0	8	1 3 8	0	.05	0	27.89	32	1.4	5.6	[illegible]	[illegible]	318	40	7	7	19
20	83	64	74	1	67	0	9	2 8	0	.05	0	27.97	12	.5	4.9	[illegible]	[illegible]	406	51	4	5	20
21	84	64	74	2	57	0	9	2 8	0	0	0	28.04	18	3.7	5.2	[illegible]	[illegible]	475	59	3	3	21
22	87	63	75	3	67	0	10	2 8	0	0	0	28.02	02	2.3	5.9	[illegible]	[illegible]	502	63	5	5	22
23	89	63	76	4	69	0	11	2 8	0	T	0	28.00	34	4.6	5.6	[illegible]	[illegible]	593	75	3	6	23
24	88	65	77*	5	68	0	12	23 8	0	.73	0	27.94	05	1.2	3.5	[illegible]	[illegible]	493	62	4	4	24
25	89*	63	76	4	67	0	11	2	0	0	0	27.90	34	4.0	5.0	[illegible]	[illegible]	714	90	3	3	25
26	83	62	75	3	66	0	10	2 8	0	0	0	27.96	34	5.1	5.5	[illegible]	[illegible]	546	69	4	5	26
27	87	65	76	3	66	0	11	1 3	0	.50	0	28.05	01	2.5	5.4	[illegible]	[illegible]	205	26	9	9	27
28	80	63	72	2	66	0	7	2	0	.13	0	28.04	13	2.3	[illegible]	[illegible]	[illegible]	266	38	9	8	28
29	80	61	71	0	63	0	6	2 8	0	0	0	27.97	16	4.4	4.9	[illegible]	[illegible]	393	50	6	6	29
30	83	57*	70	-1	63	0	5	2	0	0	0	27.84	16	2.2	3.9	[illegible]	[illegible]	460	59	4	3	30
31	82	60	71	0	55	0	6	23	0	T	0	27.78	24	1.7	4.5	[illegible]	[illegible]	[illegible]	63	[illegible]	6	31

Sum 2589	Sum 1931					Total 0	Total 252
Avg. 83.5	Avg. 62.3	Avg. 72.9	Dep. 0.1	Avg. [illegible]		Dep. 0	Dep. [illegible]
						Season to date Total 0	Total 706
Number of days: Maximum temp. ≥ 90° 0	≤ 32° 0	Minimum temp. ≤ 32° 0	≤ 0° 0			Dep. 0	Dep. -53

Number of days: Precipitation ≥ .01 inch 12; Snow, ice pellets ≥ 1.0 inch 0; Thunderstorms 10; Heavy fog X 24; Clear 5; Partly cloudy 17; Cloudy 9.

Precipitation Total 3.53; Dep. -1.87 (?). Snow, ice pellets Total 0. Avg. station pressure 27.91. Resultant wind 32, 5.5 (?). Fastest mile [illegible]. Sunshine total 13015, % 52. Sky cover avg. 5.9, 5.8 (?).

Greatest in 24 hours and dates: Precipitation 2.23 (?) 15–17; Snow, ice pellets 0. Greatest depth on ground of snow, ice pellets or ice and date 0.

HOURLY PRECIPITATION (WATER EQUIVALENT IN INCHES)

Date	A.M. 1	2	3	4	5	6	7	8	9	10	11	12	P.M. 1	2	3	4	5	6	7	8	9	10	11	12	Date
2															T										2
5													T		.02	.02	T	T		T	.10	.11			5
6					.01	.11	.05	T	T			T	T	.23	.04	.08	T		T	T					6
7												T	T												7
10								T	T	.01	.01	.01	T	T	.01	T	T								10
12																T									12
14														T						T	.01				14
15																	.01	.06	.03	T					15
16																		.31							16
17															.15	.75	.01			T	T				17
18																				T					18
19									T	T				T	T	.05									19
20															.05										20
23																T									23
24																.43	.30								24
27														T	.02	.03	T	.02	T			.14	.29	T	27
28	.02	T														.04	.06	.01							28
31																T									31

ASHEVILLE, NORTH CAROLINA

* Extreme temperatures for the month, may be the last of more than one occurrence.
- Below zero temperature or negative departure from normal.
* ≥ 70° at Alaskan stations.
* Also on an earlier date, or dates.
X Heavy fog restricts visibility to 1/4 mile or less.
T In the hourly precipitation table and in columns 9, 10, and 11 indicates an amount too small to measure.
The season for degree days begins with July for heating and January for cooling.
Data in columns 6, 12, 13, 14, and 15 are based on 8 observations per day at 3-hour intervals.
Wind directions are those from which the wind blows. Resultant wind is the vector sum of wind directions and speeds divided by the number of observations. Figures for directions are tens of degrees from true north; i.e., 09 = east, 18 = south, 27 = west, 36 = north, and 00 = calm. Wind directions are in tens of degrees in col. 17. Entries in col. 16 are fastest observed 1-minute speeds. If the # appears in col. 17, speeds are gusts.
Any errors detected will be corrected and changes in summary data will be annotated in the annual summary.

SUBSCRIPTION PRICE LOCAL CLIMATOLOGICAL DATA $2.55 PER YEAR INCLUDING ANNUAL ISSUE IF PUBLISHED. FOREIGN MAILING $2.10 EXTRA. SINGLE COPY: 20¢ FOR MONTHLY ISSUE; 15¢ FOR ANNUAL SUMMARY. MAKE CHECKS PAYABLE TO DEPARTMENT OF COMMERCE, NOAA. SEND PAYMENTS AND ORDERS TO NATIONAL CLIMATIC CENTER, FEDERAL BUILDING, ASHEVILLE, NORTH CAROLINA 28801.

I CERTIFY THAT THIS IS AN OFFICIAL PUBLICATION OF THE NATIONAL OCEANIC AND ATMOSPHERIC ADMINISTRATION, AND IS COMPILED FROM RECORDS ON FILE AT THE NATIONAL CLIMATIC CENTER, ASHEVILLE, NORTH CAROLINA, 28801

William H. Haggard

DIRECTOR, NATIONAL CLIMATIC CENTER

SUMMARY BY HOURS

Hour (local time)	Averages: Sky cover (tenths)	Station pressure In.	Temperature Air °F	Wet bulb °F	Dew pt. °F	Relative humidity %	Wind speed m.p.h.	Resultant wind Direction	Speed m.p.h.
01	5	27.92	65	65	65	94	3.0	06	.6
04	7	27.90	64	64	64	100	3.4	35	[illegible]
07	8	27.97	64	64	64	100	4.1	34	2.5
10	4	27.94	75	71	68	79	6.4	[illegible]	3.3
13	5	27.92	[illegible]	71	67	67	7.6	0[illegible]	1.4
16	7	27.38	[illegible]	70	67	62	7.8	17	2.4
19	6	27.88	73	59	67	67	5.0	13	.8
22	4	27.92	53	57	66	94	3.7	11	.5

USCOMM - NOAA - ASHEVILLE 425
09/18/75

FIGURE 3-7. AN EXAMPLE OF THE LOCAL CLIMATOLOGICAL DATA FOR ASHEVILLE, NC

provided so that one can ascertain if the rainfall is from a thunderstorm or a general wide-coverage weather system. The water equivalent of the snow is shown in the hourly precipitation data. An example of the LCD rainfall data for Asheville, NC, for the month of August 1975, is shown in Figure 3-7. Note that the same information is available on the Hourly Precipitation Data records but that the type of rainfall event is not noted in the latter.

Finally the National Climatic Center prepares a Storm Summary on a monthly basis. This information is of little value to system engineers since it emphasizes the damage done by the storm rather than the physics of the storm. For example, the most severe rain event in Asheville, NC, in 1975 occurred on August 24; however, this is not indicated in the Storm Summary because it apparently caused no significant damage.

If more information is desired regarding higher rain rates associated with thunderstorms it can be obtained for most first-order Weather Service Office (defined as those offices manned by Weather Service personnel) sites. These sites generally have both tipping bucket and universal weighing gauge precipitation monitors. The tipping bucket gauges generally accumulate the number of 0.01 inch precipitation events in a day which is utilized to collaborate with the accumulation in the other gauges. However, some tipping bucket gauges employ a readout strip chart (triple register chart of operations recorder register) similar to that shown in Figure 3-8. By estimating the time between tips the rain rate may be estimated. The location of those stations having triple register charts was not available from the National Climatic Center.

The universal weighing gauge is also capable of providing rain rate information and is the main instrument utilized to provide the 5-minute to 1 hour precipitation data. This measurement is accomplished by reading directly from the 24-hour strip chart on the gauge. An example of one of these strip charts is shown in Figure 3-9. These charts are available dating back about 10 years from the National Climatic Center for 25 cents per chart. By measuring the slope of the line, the rain rate to at least 5 minute resolution may be obtained and even 1-minute rain rates may be inferred from some charts. It appears that these charts are the best source of information for short duration rate data.

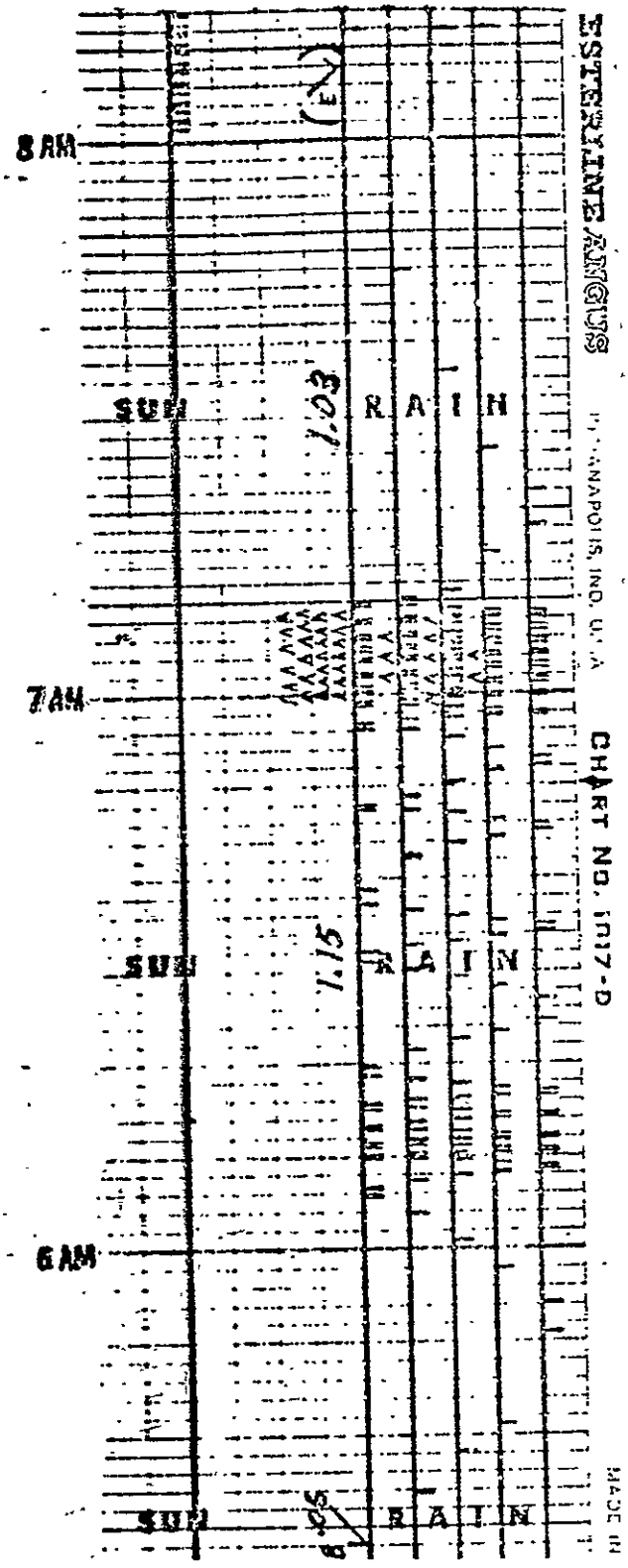

FIGURE 3-8. EXAMPLE OF OPERATIONS RECORDER RECORD
(de N.W.S. FIELD MEASUREMENTS HANDBOOK, NO. 1; PG E7-9)

WS FORM 1028C U.S. DEPARTMENT OF COMMERCE—NOAA NATIONAL WEATHER SERVICE

12 INCH DUAL OR 6 INCH SINGLE TRAVERSE – 24 HOUR

RECORD OF PRECIPITATION

TIME: Standard (✓) Daylight ( )

	TIME	MONTH	DAY	YEAR
OBSERVER _____ CHART ON	7:30 AM PM	AUG	21	75
STATION WSO ASHEVILLE, N.C. CHART OFF	8:00 AM PM	AUG.	25	75

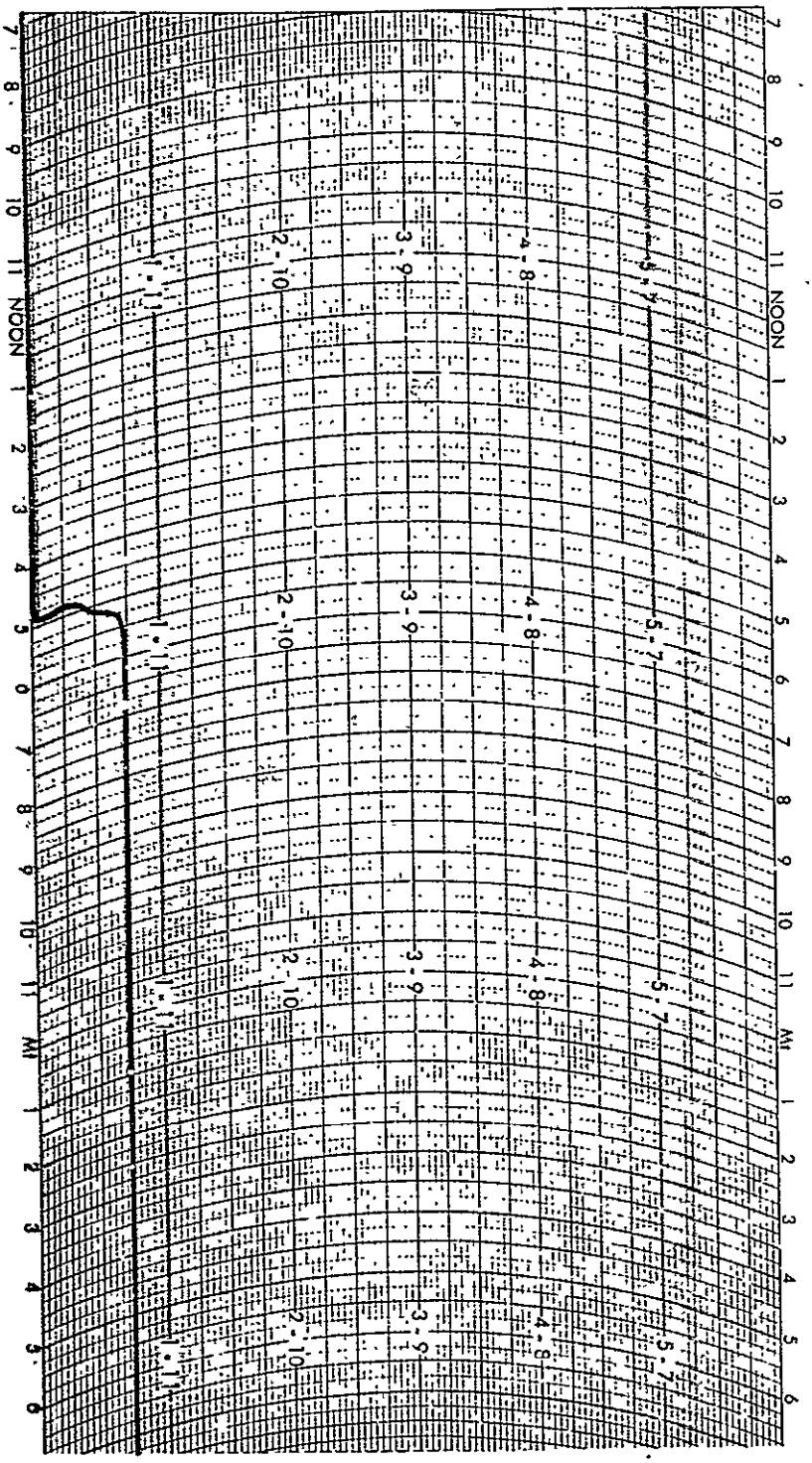

FIGURE 3-9. AN EXAMPLE OF A UNIVERSAL WEIGHING GAUGE STRIP CHART

The last automated rain gauge utilized by the U.S. Weather Service is the Fischer-Porter gauge. This unit is a weighing gauge which punches a paper strip chart in a BCD format every 15 minutes. The gauge may be set to record every 5 minutes, but that resolution is generally not utilized by the Weather Service. The gauge records to only the nearest 0.1 inch.

An example of how intense rain rates may be measured is now given. Note that from Figure 3-6 the most intense rain rates (0.38 inches in 5 minutes) in the Asheville, NC, WSO occurred on August 24, ending at 1658 Eastern Standard Time. This occurred during a thunderstorm (see Figure 3-7) but it was not the most rain in a 24-hour period, which occurred on August 17. The amount of precipitation between 1500 and 1700 EST on August 17 is noted in the LCD in Figure 3-7. However, the most data appears directly in the gauge readout shown in Figure 3-9. Clearly the rainrate just before 4 PM was more than 4.56 inch/hr (116 mm/hr) for the first several minutes. Interpolation yields a rate approaching 150 mm/hr. for 2 minutes. Another example of a cloud burst is shown in Figure 3-10. Herein rain rates approach 300 mm/hr (12 inches/hr) at 8 PM and contributed to the airline crash at this airport at this time. Clearly the attenuation at a ground station would be significant for this type of 2 minute event (0.00038% of a year).

3.2.2 Canadian Sources

The Atmospheric Environment Office* prepares several documents containing rain and snow precipitation data. These documents† are:

- Monthly Record-Western Canada, Part 1,
  - Provinces of:
    - British Columbia
    - Alberta
    - Saskatchewan
    - Manitoba
  - $21.60 foreign per year
  - $ 2.00 foreign per issue

---

* Head Office, 4905 Dufferin Street, Downsview, Ontario M3H 5T4, Canada

† Available from: Supply and Services Canada, Publishing Centre, Hull, Quebec, KDA 0S9, Canada. Make checks payable to Receiver General for Canada. Canadians should request domestic price schedule.

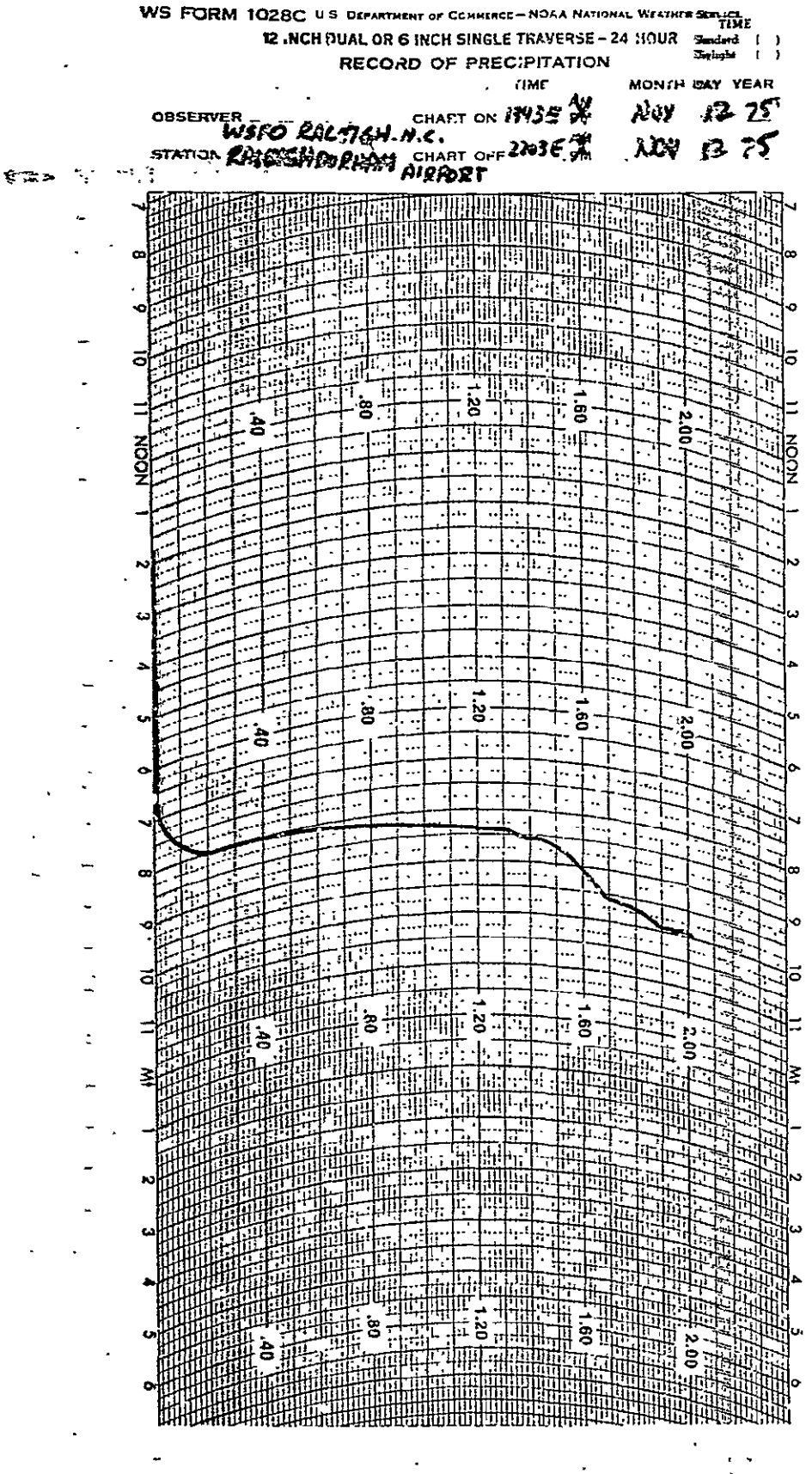

FIGURE 3-10. AN EXAMPLE OF AN INTENSE RAIN EVENT

- Monthly Record-Northern Canada, Part 2
  - Territories of:
    Yukon
    Northwest
  - $12.00 foreign per year
  - $ 1.00 foreign per issue
- Monthly Record-Eastern Canada, Part 3
  - Provinces of:
    Ontario
    Quebec
    Nova Scotia
    New Brunswick
  - $21.60 foreign per year
  - $ 2.00 foreign per issue
- Canadian Weather Review
  - published monthly
  - covers about 250 surface stations throughout Canada
  - $5.40 foreign per year
  - $0.50 foreign per issue
  - available about one month following the date of recording
- Snow Cover Data for Canada
  - published once per winter
  - covers all provinces/territories
  - $1.00 foreign per issue
  - available June/July of each year

The data in the Monthly Reviews (available about four months following recording) is of most importance to the earth-space path engineer. As shown in Figure 3-11, the rainfall, snowfall and total precipitation are given for each day of the month. The Monthly Summary table indicates the number of thunderstorms, etc., and the recording rain gauge data for selected cities is given. These are the maximum amounts for the duration periods indicated on the date of

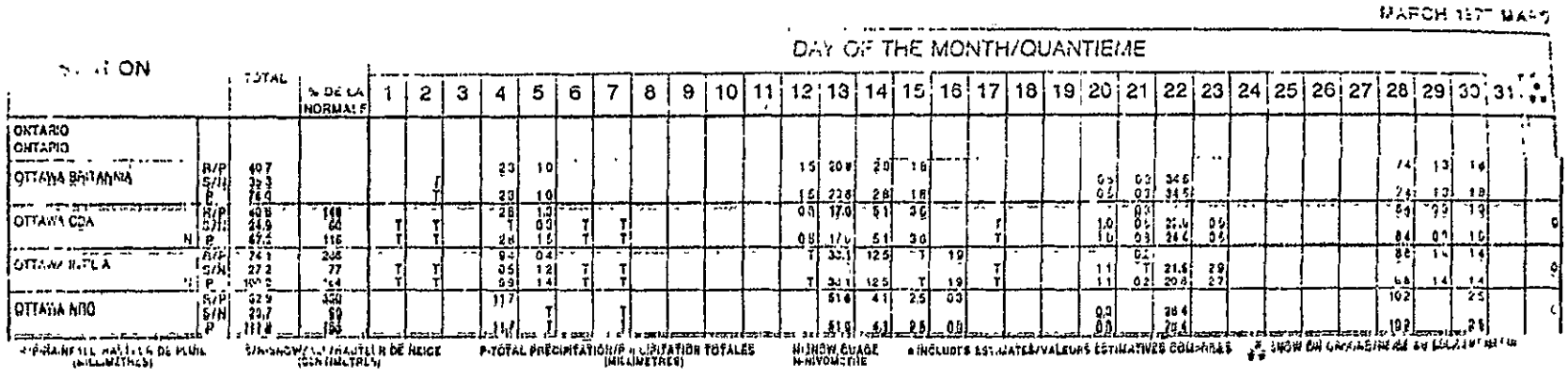

MARCH 1977 MARS

DAY OF THE MONTH/QUANTIEME

STATION		TOTAL	% DE LA NORMALE	1	2	3	4	5	6	7	8	9	10	11	12	13	14	15	16	17	18	19	20	21	22	23	24	25	26	27	28	29	30	31
ONTARIO																																	
ONTARIO																																	
OTTAWA BRITANNIA	R/P	40.7			T		23	10							15	20.9	2.0	1.8					0.3	0.3	34.6					7.4	1.3	1.6	
	S/N	32.3			T																		0.3	0.3	34.6								
	P	72.0			T		23	10							15	22.8	2.8	1.8												7.4	1.3	1.6	
OTTAWA CDA	R/P	40.6	118				2.8	1.3							0.8	17.0	5.1	3.6					1.0	0.3	22.4	0.6				5.9	1.3	1.3	
	S/N	24.9	82	T	T		T	0.3	T	T										T				0.3	24.2	0.6							0
N	P	65.5	116	T	T		2.8	1.6	T	T					0.8	17.0	5.1	3.6		T			1.0	0.3	24.2	0.6				8.4	2.1	1.3	0
OTTAWA INT'L A	R/P	24.1	206				9.3	0.4							T	3.3.1	12.5	1	1.9					0.1						8.8	1.4	1.4	
	S/N	27.2	77	T	T		8.5	1.2	T	T										T			1.1	T	21.6	2.9							0
	P	51.3	144	T	T		8.9	1.4	T	T					T	3.3.1	12.5	T	1.9	T			1.1	0.2	20.8	2.7				6.8	1.4	1.4	
OTTAWA NRC	R/P	32.9	330				11.7									5.1.6	4.1	2.5	0.3											10.2		2.5	
	S/N	23.7	80					T		T													0.3		28.4								0
	P	111.8	193				11.7	T		T						5.1.6	4.1	2.5	0.3				0.3		28.4					10.2		2.5	

P-RAINFALL (MILLIMETRES) DE PLUIE (MILLIMETRES) S/N-SNOWFALL (CENTIMETRES) HAUTEUR DE NEIGE (CENTIMETRES) P-TOTAL PRECIPITATION/PRECIPITATION TOTALES (MILLIMETRES) N-NIVOMETRIE a INCLUDES ESTIMATES/VALEURS ESTIMATIVES COMPRISES * SNOW ON GROUND/NEIGE AU SOL

MARCH 1977 MARS

RECORDING RAIN GAUGE DATA/ DONNEES DES PLUVIOGRAPHES

TABLE/TABLEAU 7

STATION	MAXIMUM AMOUNTS (.01 inch) HAUTEUR MAXIMUM (en .01 de pouce) FOR DURATION INDICATED WITH DATES OF OCCURENCE POUR LES DUREES MENTIONEES ET DATES												HOURLY RAINFALL CHUTE DE PLUIE HORAIRE No. of occurrences in classes shown Frequence par classe					
	5 min.		10 min.		15 min.		30 min.		60 min.		120 min.		6 hr.		12 hr.			
	AMOUNT VALEUR	DATE	AMOUNT VALEUR	DATE	AMOUNT VALEUR	DATE	AMOUNT VALEUR	DATE	AMOUNT VALEUR	DATE	AMOUNT VALEUR	DATE	AMOUNT VALEUR	DATE	AMOUNT VALEUR	DATE	.01–.09	.10–.19	.20–.49	.50–.99	1.00–1.99	2.00 or more ou plus
ONTARIO																						
ONTARIO																						
OTTAWA INT'L A	04	30	05	04	08	13	13	13	19	04	32	13	78	13	111	13	46	11				
SAULT STE MARIE A	04	12	05	12	08	12	15	12	27	12	35	12	71	12	77	12	43	6				
SIMCOE	05	04	11	12	15	12	25	12	32	12	49	12	103	12	129	12	40	6				
SIOUX LOOKOUT A	02	27	03	27	04	27	08	27	13	27	13	27	14	27	14	27	3					
SUDBURY A	M		M		M		M		M		M		M		M		M	M				

MARCH 1977 MARS

MONTHLY SUMMARY

STATION	NUMBER OF DAYS WITH / NOMBRE DE JOURS AVEC											
	TEMPERATURES · 0.0 C	THUNDERSTORMS ORAGES	SNOW OR DRIZZLE PLUIE OU BRUINE	FREEZING PRECIPITATION PRECIPITATIONS SE CONGELANT	HAIL GRELE	SNOW NEIGE	MEASURABLE PRECIPITATION PRECIPITATION MESURABLE	FOG BROUILLARD	SMOKE OR HAZE FUMEE OU BRUME SECHE	DUST OR BLOWING SAND POUSSIERE OU CHASSE - SABLE ELEVE	BLOWING SNOW CHASSE NEIGE ELEVEE
ONTARIO											
[illegible]											

FIGURE 3-11. EXAMPLES OF THE CANADIAN MONTHLY RECORD PRECIPITATION DATA

occurrence. In addition, the number of hourly periods with rainfall accumulations between 0.01-0.09, 0.1-0.19, etc., inches is noted. These data are obtained from tipping bucket rain gauges measuring in increments of 0.01 inches.

The tipping bucket rain gauge data is available for many more Canadian locations. The charts from these gauges are available upon request from the Climatological Recording Services Branch of the Head Office in Downsview, Ontario, at a nominal charge.

3.2.3 Worldwide Sources

Many countries prepare meteorological data similar to the US and Canada. Many of these are on file at the National Weather Service Library, Room 816, Gramax Bldg., 13th Street, Silver Spring, MD. One document, the Monthly Climatic Data for the World does list the number of days per month a station receives more than 1 mm of rain and the total rainfall per month. The data is coarse and can only provide a general indication of the precipitation climate. An example is shown in Figure 3-12. This document is available for $0.70 per monthly copy about 9 months following the recording date from the National Climatic Center.

SURFACE DATA

OCTOBER 1977

STATION	LATITUDE	LONGITUDE	ELEVATION	NUMBER OF DAYS OF OBSNS.	PRESSURE		TEMPERATURE		VAPOR PRESSURE		PRECIPITATION				SUNSHINE
					MEAN STATION	MEAN SEA LEVEL	MEAN	DEPARTURE	MEAN	DEPARTURE	NO. OF DAYS ≥ 1 MM.	TOTAL	DEPARTURE	QUINTILE	PERCENTAGE OF LONG-TERM AVERAGE
	° ′	° ′	METERS		MB	MB	°C	°C	MB	MB		MM	MM		%
CANADA-EASTERN															
ALERT	82 30 N	62 20 W	63	31	1003.7	1012.2	-18.9	+00.9	1.1	-0.1	4	9	- 7		
EUREKA	80 00 N	85 56 W	10	31	1008.5	1009.9	-21.0	+00.5	1.2	+0.1	1	4	- 3		
RESOLUTE	74 43 N	94 59 W	67	31	998.0	1006.9	-14.3	+00.3	2.1	+0.2	6	22	+ 6		106
CLYDE	70 27 N	68 33 W	6	31	1002.1	1005.4	- 7.6	- 1.2	3.2	-0.3	11	55	+ 21		
HALL BEACH	68 47 N	81 15 W	8	31	1004.9	1005.8	- 9.4	+ 1.6	3.0	+0.2	9	27	+ 4		
BAKER LAKE	64 18 N	96 00 W	13	31	1007.0	1006.6	- 5.1	+ 2.4	4.0	+0.5	10	57	+ 32		
CORAL HARBOUR	64 12 N	83 22 W	64	31	999.0	1007.3	- 5.8	+ 2.2	3.9	+0.4	16	46	+ 17		
FROBISHER BAY	63 45 N	68 33 W	34	31	1002.3	1006.7	- 3.8	+ 0.9	4.0	+0.2	13	52	+ 19		97
CHURCHILL	58 45 N	94 04 W	29	31	1005.5	1009.1	2.5	+ 3.6	5.7	+0.6	6	23	- 15		142
INUCDJOUAC	58 27 N	78 07 W	5	31	1007.1	1008.7	1.7	+ 2.1	6.3	+0.7	14	71	+ 22	S	131
FORT CHIMO	58 06 N	68 25 W	37	31	1004.4	1009.1	0.1	+ 0.4	5.4	+0.2	12	48	+ 9		
TROUT LAKE	53 50 N	89 52 W	220	31	987.0	1014.2	4.9	+ 3.1	6.2	-0.1	5	47	- 6		
NITCHEQUON	53 12 N	70 54 W	536	31	948.9	1014.0	0.9	+ 0.3	5.7	0.0	13	64	- 15		
MOOSONEE	51 16 N	80 39 W	10	31	1013.4	1014.7	5.3	+ 1.4	6.8	-0.4	6	58	- 15		173
ARMSTRONG	50 17 N	88 54 W	323	31			4.1	+ 1.0			5	34	- 25		/147
KAPUSKASING	49 25 N	82 28 W	227	31	998.4	1016.5	4.3	- 0.3	6.5	-0.8	9	69	- 3		
GERALDTON	49 42 N	86 57 W	331					U							
SEPT-ILES	50 13 N	66 16 W	55	31	1006.6	1013.4	4.8	+ 0.9	6.5	-0.2	14	157	+ 74		107
GOOSE	53 19 N	60 25 W	49	31	1005.2	1011.3	3.2	0.0	5.9	-0.1	10	78	+ 15		102
NORTH BAY	46 22 N	79 25 W	371	31	972.4	1017.4	5.4	- 1.2	7.2	-1.0	9	62	- 22		128
MANIWAKI	46 23 N	75 58 W	170	31	995.8	1016.7	5.8	- 1.1	7.2	-0.9	9	63	- 5		106
TORONTO/MALTON INT AP	43 41 N	79 38 W	173	31	996.2	1017.3	8.0	- 1.5	8.5	-1.1	6	69	+ 10		
MONTREAL/DORVAL INT AP	45 28 N	73 45 W	36	31	1011.6	1016.0	7.6	- 1.4	8.5	-0.4	11	113	+ 35		
BAGOTVILLE	48 20 N	71 00 W	159	31	995.6	1015.2	5.6	- 0.1	6.7	-0.6	10	61			
CHATHAM	47 01 N	65 27 W	34	31	1009.6	1013.7	7.2	- 0.2	8.1	-0.2	16	257	+174	S	87
STEPHENVILLE	48 32 N	58 33 W	26	31	1009.6	1012.8	7.8	+ 0.6	8.4	0.0	17	183	+ 84		
GANDER INT AP	48 57 N	54 34 W	151	31	993.8	1012.4	6.3	0.0	8.1	+0.1	14	127	+ 28		90
SHEARWATER	44 38 N	63 30 W	51	31	1008.7	1015.0	9.8	+ 0.2	10.2	0.0	13	142	+ 33		108
SYDNEY	46 10 N	60 03 W	62	31	1008.9	1014.4	8.7	- 0.4	8.7	-1.1	13	130	+ 15	4	70
SHELBURNE	43 43 N	65 15 W	30					U							
SABLE ISLAND	43 56 N	60 01 W	4	31	1015.4	1015.9	11.7	+ 0.1	11.7	0.0	14	122	+ 12	4	70
ST. JOHN'S (TORBAY)	47 37 N	52 45 W	141					U							
ST PIERRE AND MIQUELON															
ST PIERRE	46 46 N	56 10 W	5	31	1013.9	1014.5	9.1	+ 0.2	9.8	+0.4	13	87	- 50	1	112
UNITED STATES-NORTHEAST															
INTERNATIONAL FALLS	48 34 N	93 23 W	361	31	975.0	1016.7	5.3	-0.1				20	- 23		
DULUTH	46 50 N	92 11 W	432	31	975.4	1017.3	6.8	-0.6				81	+ 23		104
ST. CLOUD	45 35 N	94 11 W	318	31	979.0	1017.6	7.8	-0.9							
SAULT STE. MARIE	46 28 N	84 22 W	221	31	993.8	1016.8	7.1	-0.8	8.1	0.0	8	47	- 25	2	61
BURLINGTON	44 28 N	73 09 W	104	31	1001.2	1016.5	8.1	-1.2	8.2		10	128	+ 58	5	88
CARIBOU	46 52 N	68 01 W	146	31	991.5		6.4	-0.2				135	+ 51		
DES MOINES	41 32 N	93 39 W	294	31	986.8	1018.0	11.3	-1.1	9.4	-0.2	10	120	+ 75	3	82
COLUMBIA	38 49 N	92 13 W	274	31	990.1	1018.5	13.1	-1.3				112	- 26		85
CHICAGO	41 47 N	87 45 W	190	31	995.6	1018.3	11.0	-2.0	8.9	-0.8	9	42	- 21	2	76
ST. LOUIS	38 45 N	90 23 W	172	31	998.3	1018.9	13.1	-2.0	11.5	+0.7	7	96	+ 25	4	94
DAYTON	39 54 N	84 13 W	306	31	985.8	1018.6	11.0	-2.1	8.6		9	98	+ 49	5	76
COLUMBUS	40 00 N	82 53 W	254	31	985.5	1018.5	13.1	-1.3	8.3	-1.9	9	65	+ 17	4	85
BUFFALO	42 56 N	78 44 W	215	31	985.3	1017.5	9.8	-1.1	9.1	0.0	9	66	- 10	3	91
NEW YORK LA GUARDIA	40 46 N	73 54 W	9	31	1005.4	1016.9	12.7	-1.8	11.1	-0.3	2	148	+ 73	S	
BOSTON	42 22 N	71 02 W	3	31	1011.4	1016.0	12.9	+0.1	11.2	+0.5	2	118	+ 41	S	85
BLUE HILL OBS	42 13 N	71 07 W	195	31	992.1	1015.2	10.7	-1.1	10.6	+0.6	12	183	+ 71	S	89
CHATHAM	41 40 N	69 58 W	16					U							
WASHINGTON DULLES	38 57 N	77 27 W	98					U							
WASHINGTON NATIONAL	38 51 N	77 02 W	20	31	1013.5	1017.8	15.0	-0.4	11.0	-0.7	7	136	+ 68	S	84

FIGURE 3-12. AN EXAMPLE OF THE MONTHLY CLIMATIC DATA FOR THE WORLD

3.3 EFFECTIVE PATH LENGTH

3.3.1 Overview

Given the specific attenuation A at a given frequency and rain rate, the total attenuation along the earth-space path may be calculated given the length of the path through the attenuating medium. The effective path length provides the coupling between the specific attenuation and the total attenuation. However, because the attenuation varies with distance along the path an integral must be calculated. The values of the point rain rate R along the path at any time t are not known so the concept of the effective path length L_e has been introduced. At any given instant t it is defined as

$$L_e(f,s) \; A\,[f,R(s=0)] \;=\; A_T\,[f,s]$$

$$= \int_{s=0}^{s_1} A[f,R(s)]ds$$

where $L_e(f,s)$ is the effective path length at frequency f, time t, and along the earth-space path s. s is zero at the ground station and R(s=0) is the point rain rate at the ground station. A_T is the total path attenuation along the path s at time t, and s_1 is a point along the path above which A is negligibly small. Implicitly s_1 is a function of the elevation angle θ and the 0°C isotherm height where the precipitation exists as ice, and R is a function of s and t because the rain rate varies along the path s as dense rain cells pass through the link.

The value of the integral has been measured by direct observation of satellite beacons (Ref. 3-8) and radar diagnostics of rain systems (Ref. 3-9).

3.3.2 Elevation Angle Dependence

The path length s of the attenuating medium may be closely approximated by the cosecant θ relation. This assumes a planegeometry which is nearly the case for typical heights to the 0°C isotherm (less than 5 km, see Figure 3-16) and elevation angles above 10 degrees.

3.4. RAINFALL MODELS FOR THE U.S. AND CANADA

The information in Sections 3.1 through 3.3 will allow one to compute the attenuation along an earth-space path given the point rain rate R. In this section four models are presented to provide the cumulative statistics for R. The models described here are:

a) the Global Rain Model (Ref. 3-12)

b) the Rice-Holmberg Model (Ref. 3-13)

c) the Dutton-Dougherty Model (Ref. 3-14, 3-15)

d) the Lin Model (Ref. 3-16).

The results presented herein are only those portions of the model which apply to calculation of R and its distribution along the path. In Section 3.5 the total attenuation is calculated.

Other rain and rain attenuation prediction and scaling models have been published and are in the process of being developed. These include:

e) the Synthetic Storm Model developed at the Virginia Polytechnic Institute and State University, R. R. Persinger, W. L. Stutzman, R. E. Castle and C. W. Bostian, preprint; and R. R. Persinger and W. L. Stutzman, VPI & SU Interim Report 1978-1, June, 1978.

f) the Frequency Scaling Model developed at COMSAT Laboratories, F. Tseng and G. Hyde, EASCON 78, Arlington, VA, Sept. 25-27, 1978, pg. 396.

g) the Storm Cell Model developed at Ohio State University, L. R. Zintsmaster, ElectroScience Lab. Status Report 2374-9, May 1972.

h) the Location-Dependent Attenuation Model developed at the Applied Physics Laboratory, J. Goldhirsh, Proc. URSI, Comm. F, La Baule, France, 28 April - 6 May 1978, pg. 305; and Radio Science, vol. 12, Sept - Oct 1977, pg. 741.

These four models should be consulted, as appropriate, where they appear to extend the results of the more frequently utilized models.

3.4.1. The Global Rain Model (Ref. 3-12)

This model is currently being proposed to supplement and update the current CCIR model described in Report 563. The climatic regions are defined and then the distribution curve for the surface point rain rate data in each region is developed. The five rain rate regions for the U.S. and Canada are shown in Figure 3-14. The rain rate distributions for each of the regions are show in Figure 3-15. The adjacent geographic distributions are used as the upper and lower bounds for the point-to-point and year-to-year variation of the observed annual distribution function. A table of values corresponding to Figure 3-15 is shown in Table 3-5.

The relation

$$r = \gamma(D)\, R^{-\delta(D)}$$

is utilized to account for the path averaged rain rate compared to the ground station rain rate, where $D = H/\tan\theta$ is the horizontal projection (basal) length of the path to the height H of the $0^{o}C$ isotherm (see Figure 3-16) and $\gamma(D)$ and $\delta(D)$ shown in Figure 3-17 are the parameters for the path averaging model. The path averaged rain rate is then

$$R_{ave} = r\, R$$

for a given probability of occurrence. The effective path length is $L_e = H \csc\theta$. For ground stations above one kilometer, it appears desirable to subtract the ground station altitude from the value of H given in Figure 3-16 and use this value for the effective path length.

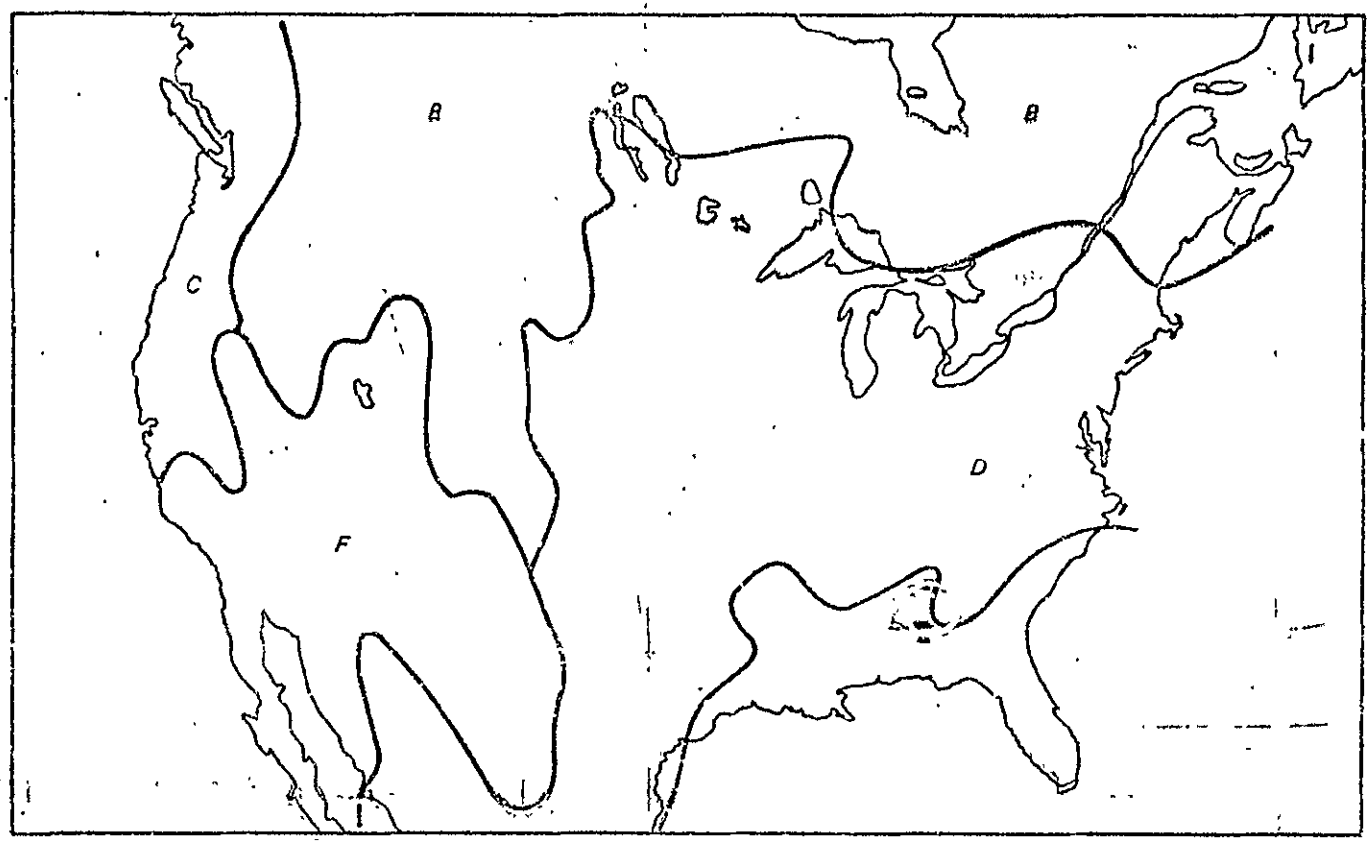

FIGURE 3-14. RAIN RATE CLIMATE REGIONS FOR THE U.S. AND CANADA (FROM REF. 3-12)

804148

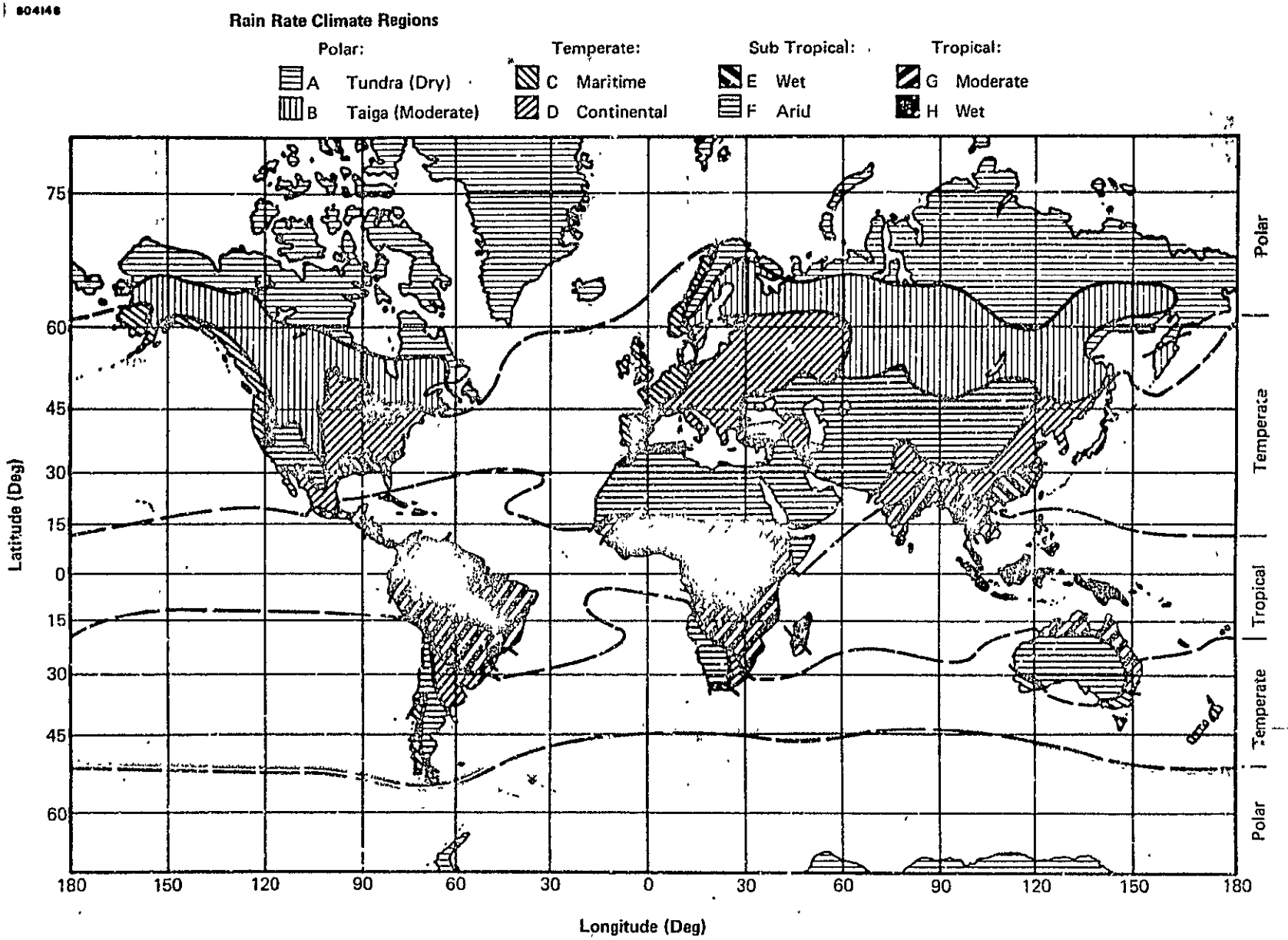

FIGURE 3.14A. GLOBAL RAIN RATE CLIMATE REGIONS
(FROM REF. 3-12)

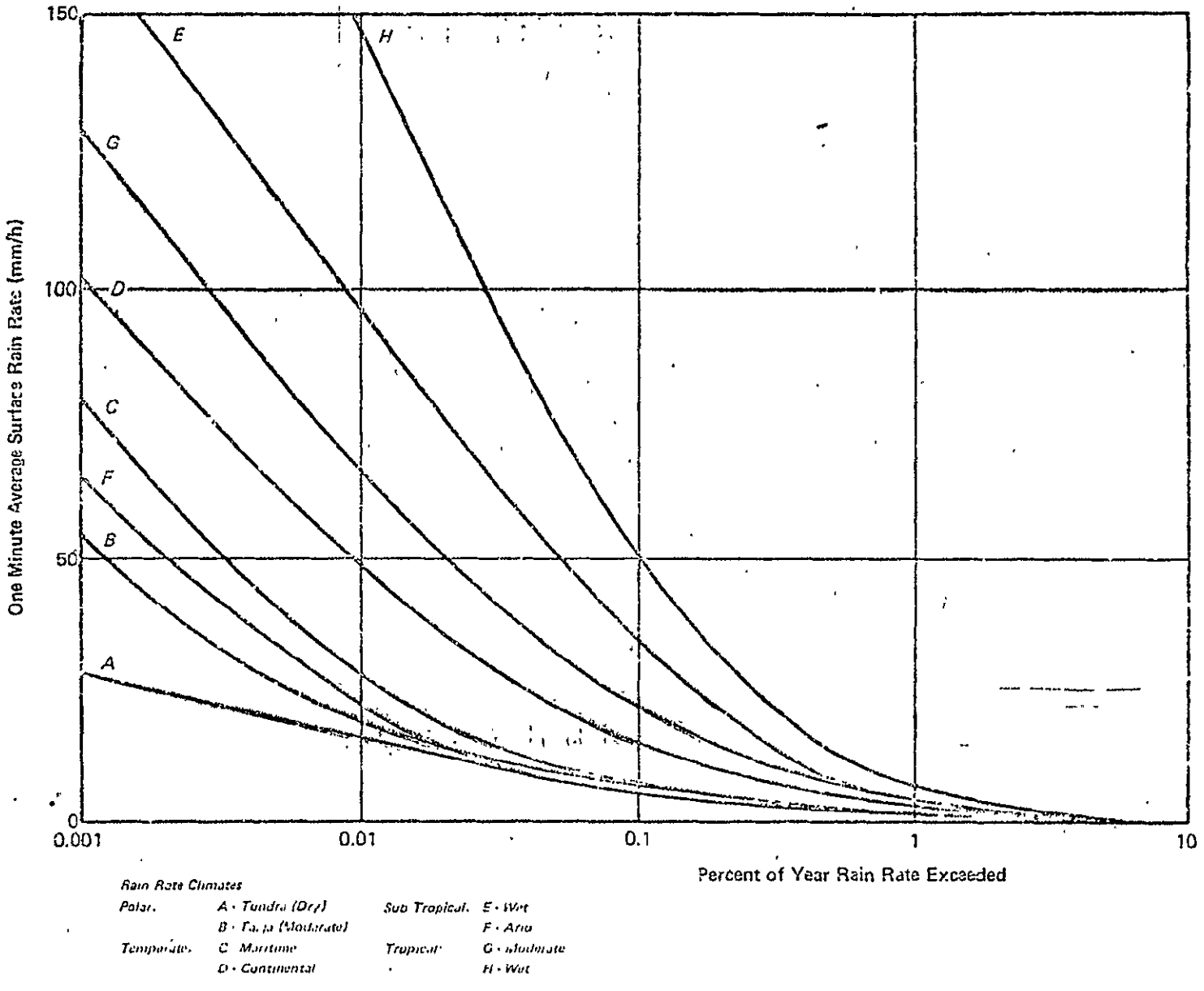

FIGURE 3-15. RAIN RATE DISTRIBUTIONS FOR THE U.S. AND CANADA (FROM REF. 3-12)

TABLE 3-5

RAIN RATE DISTRIBUTION VALUES (mm/hr)

PERCENT OF YEAR	RAIN RATE CLIMATE REGIONS							
	A	B	C	D	E	F	G	H
0.001	28	54	80	102	164	66	129	251
0.002	24	40	62	86	144	51	109	220
0.005	19	26	41	64	117	34	85	178
0.01	15	19	28	49	98	23	67	147
0.02	12	14	18	35	77	14	51	115
0.05	8.0	9.5	11	22	52	8.0	33	77
0.1	6.5	6.8	7.2	15	35	5.5	22	51
0.2	4.0	4.8	6.8	9.5	21	3.8	14	31
0.5	2.5	3.0	2.8	5.2	8.5	2.4	7.0	13
1.0	1.7	1.8	1.9	3.0	4.0	1.7	4.0	6.4
2.0	1.1	1.4	1.0	1.8	2.0	1.1	1.6	2.8

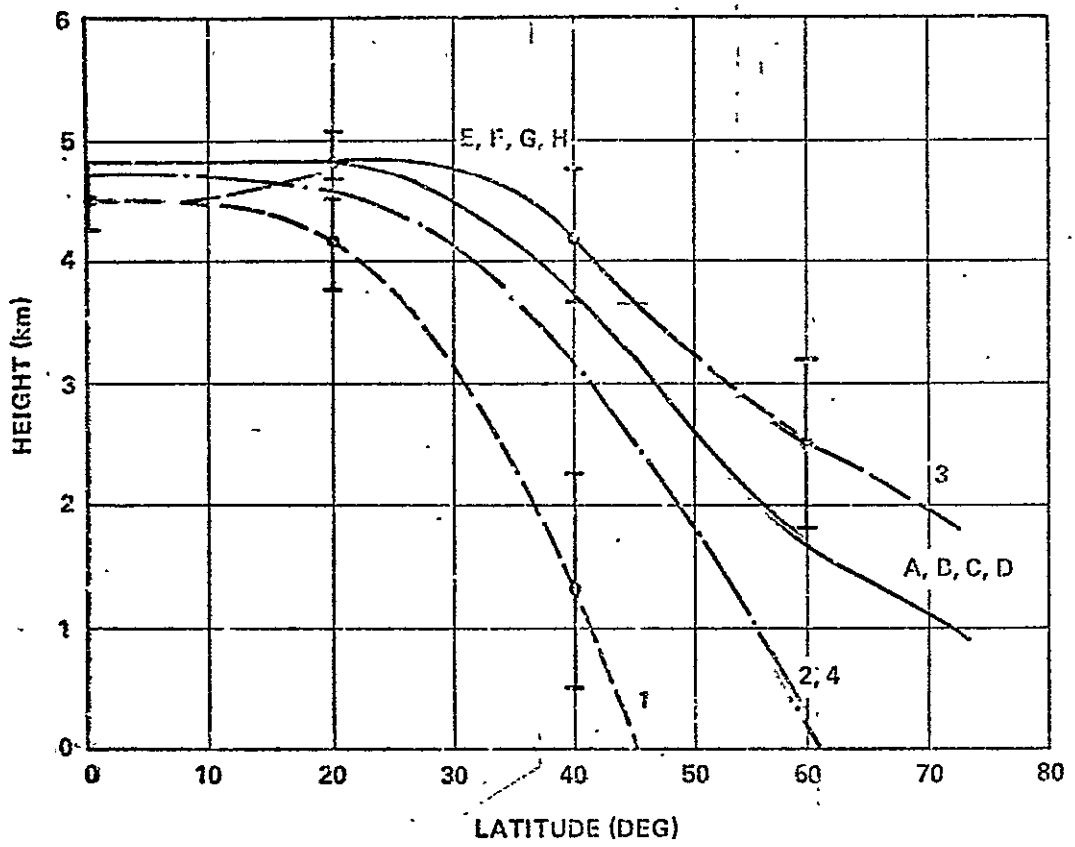

MODEL FOR RAIN RATE CLIMATES A THROUGH H

ANNUAL

SEASONAL 1 — WINTER (NORTHERN HEMISPHERE)
2 — SPRING
3 — SUMMER
4 — FALL

FIGURE 3-16. LATITUDE DEPENDENCE OF ZONALLY AVERAGED 0°C ISOTHERM HEIGHT

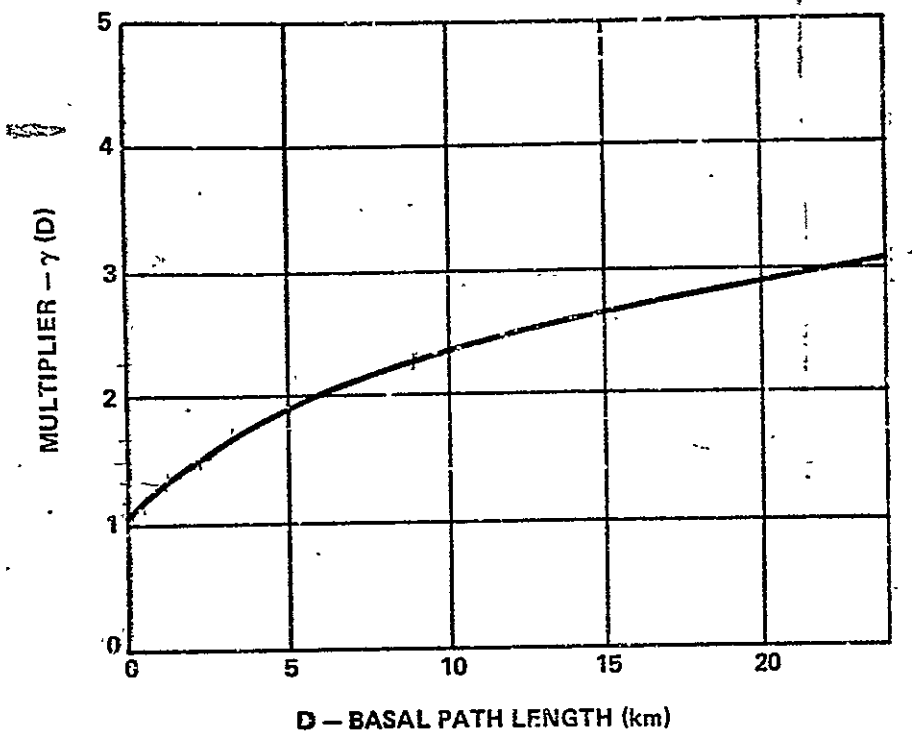

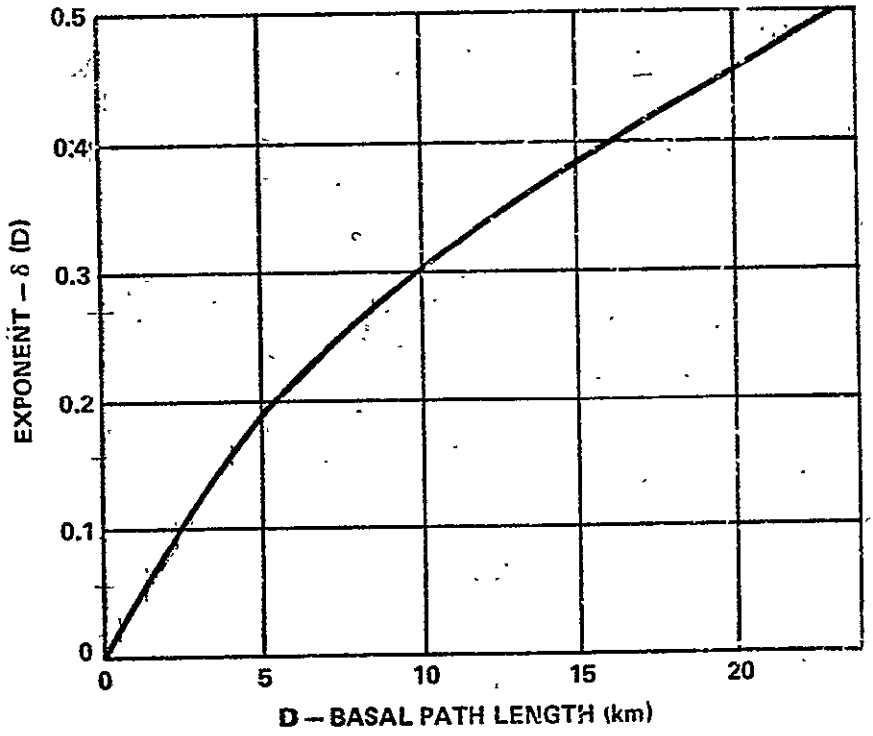

FIGURE 3-17. MULTIPLIER AND EXPONENT IN THE PATH AVERAGING MODEL

3.4.2 The Rice-Holmberg Model (Ref. 3-13)

The Rice-Holmberg model is the basis for the CCIR rainfall model used in Report 563. In the R-H model the rain events are divided into two groups. The first group applies to convective storms (thunderstorms). The second group includes all other rain events. The model yields the amount of time $T_t(R)$ that a t - minute average rainfall rate exceeds a given value R.

For one-minute time intervals (the motivation for selecting a one-minute average is based on weather data and statistics (see Figure 3-20)).

$$T_1(R) = M\{0.03\beta\exp(-0.03R) + 0.2(1-\beta)[\exp(-0.258R) + 1.86\exp(-1.63R)]\} \text{ hours}$$

where M is the total annual rainfall in millimeters, and β is the ratio of the rainfall during thunderstorms to the total rainfall for the year. To utilize this formula, M the average annual rainfall, must be determined (not including snowfall) from the weather records for a given location. The Annual Summary of Climatological Data (Figure 3-6) indicates, for example, that the normal precipitation for Baltimore averaged from 1941 to 1970 is 1028 mm minus the snowfall. The snowfall data is obtained from reviewing many years of the data and assuming that 10 mm of snow equals 1 mm of liquid water.

The ratio of the thunderstorm rainfall to the total rainfall, β, is obtainable from the local Climatological Data for the location. For example, referring to Figure 3-7, in August 1975 in Asheville, NC, 2.97 inches of rain was associated with the 10 thunderstorms during the month. The total precipitation for August was 3.63 inches, so $\beta = 2.97/3.63 = 0.82$. When averaged over the entire year this number would be much lower.

Maps showing M and β are shown in Figures 3-18 and 3-19. These numbers may also be used in the one-minute average rainfall formula given above to obtain the number of hours per year during which the rainfall rate exceeds R. The percentage per year is obtained by dividing by 87.66 (there are 8766 hours per year).

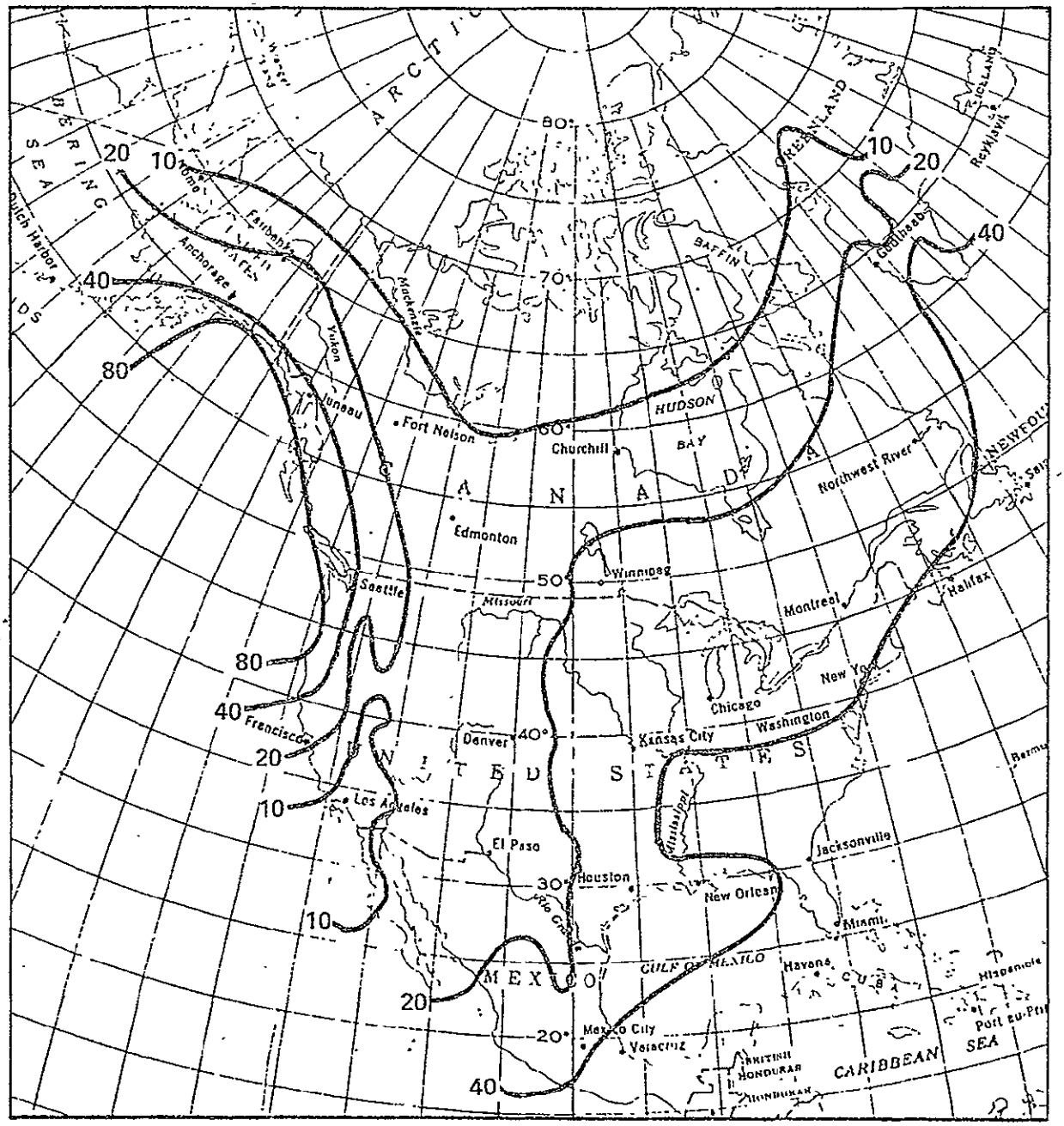

FIGURE 3-18. MEAN ANNUAL PRECIPITATION IN INCHES IN U.S. AND CANADA (1 inch = 25.4 mm)

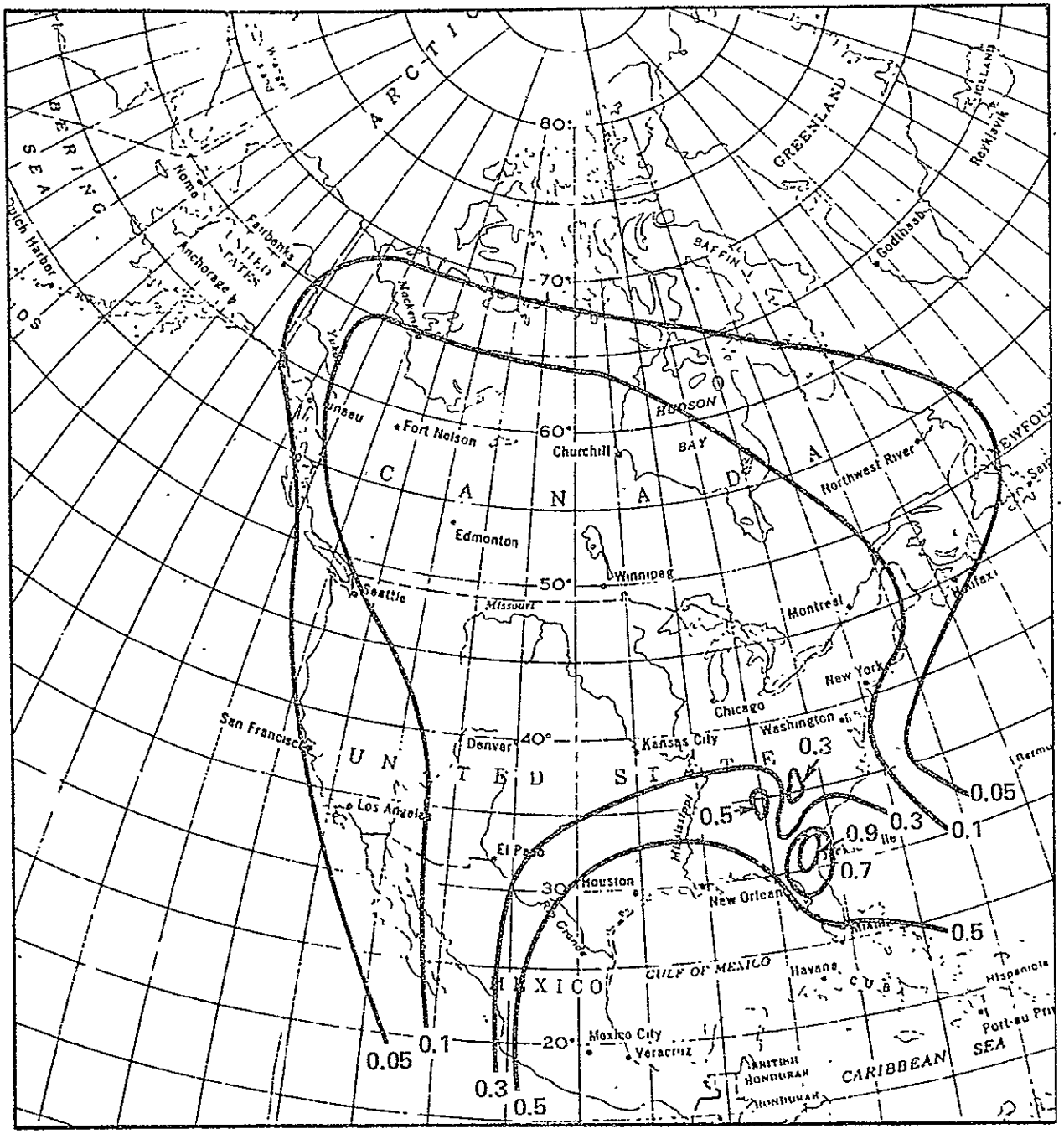

FIGURE 3-19. THE PARAMETER β IN THE RICE-HOLMBERG MODEL OVER THE U.S. AND CANADA

Adapted from Miller, Albert, Meteorology, p110, C E Merrill Books, Columbus, Ohio 1966
Compare with U S Dept of Commerce Climates of the World, p4, GPO Jan 1969

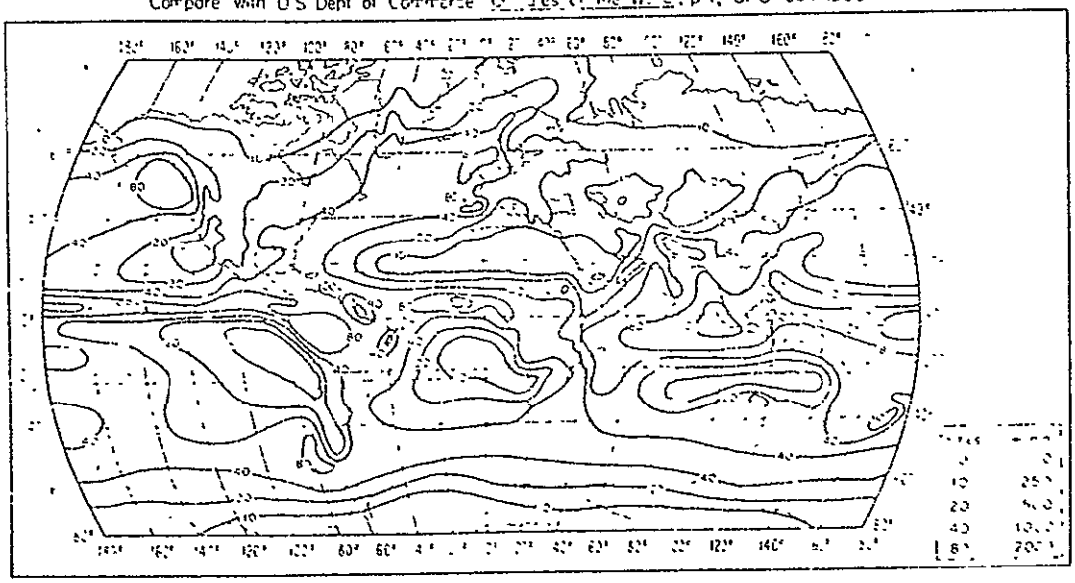

FIGURE 3-18A. MEAN ANNUAL PRECIPITATION IN INCHES (1 inch = 25.4 mm).

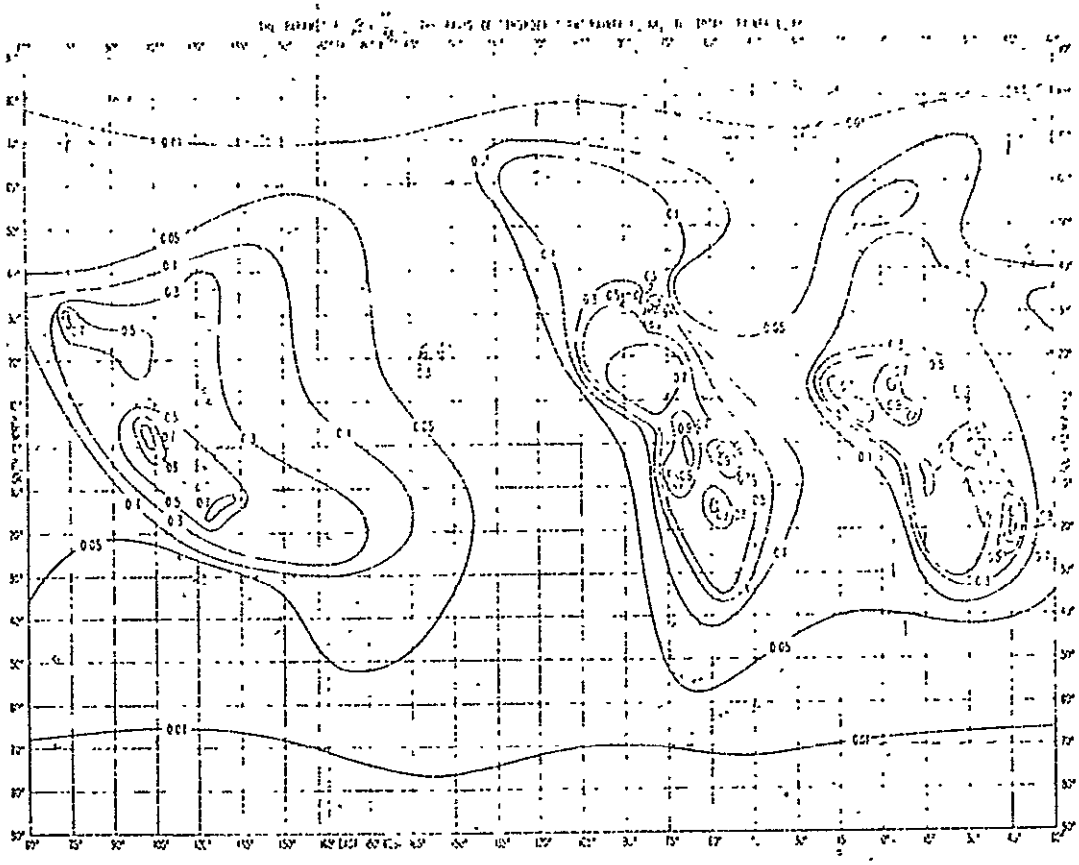

FIGURE 3-19A. THE PARAMETER β IN THE RICE-HOLMBERG MODEL

3.4.3. The Dutton-Dougherty Model (Refs. 3-14, 3-15)

This model is also referred to as the modified Rice-Holmberg model. The model yields an improved estimate of $T_t(R)$, i.e., the number of hours that the t - minute averaged rain rate will exceed R at the surface. Usually t = 1 minute is considered to be representative of the instantaneous rain rate.

In the Dutton-Dougherty model the percent of an average year $P_t(R)$ that t - minute rainfall rates R are expected are grouped into three rainfall rate regimes, namely

$$P_t(R) = 0.0114\ T_{1t}\ \exp(-R/\overline{R}_{1t}) \qquad R > 30 \text{ mm/hr}$$

$$P_t(R) = 0.0114\ T_{st}\ \exp(-\sqrt[4]{R/\overline{R}_{st}}) \qquad 5 \leq R \leq 30 \text{ mm/hr}$$

$$P_t(R) = 0.0114\ (T_{1t} + T_{2t})\ \exp\ (-R/R'_t) \qquad R < 5 \text{ mm/hr}$$

Here the $\overline{R}_{1t}$, R'_t, and T_{2t} are linear combinations of M, β and D = 24 + 3M hours (Ref. 3-13) by the relation

$$\overline{R}_{1t} = a_{1t}M + a_{2t}\beta + a_{3t}D + a_{4t} \pm S_1$$

$$T_{2t} = b_{1t}M + b_{2t} \pm S_2$$

$$R'_t = b_{3t}M + b_{4t}\ \beta + b_{5t}D + b_{6t} \pm S_3$$

where S_1, S_2 and S_3 are the standard errors which can be shown to be small compared to $\overline{R}_{1t}$, T_{2t} and R'_t (Ref. 3-17). The Natl. Telecom. Inform. Ag. will make available a well annotated computer program (DEGP76) to do these calculations (Ref. 3-18). This program does not include all of the smoothing algorithms currently being added to an updated program. The parameters $T_{1t} = M/\overline{R}_{1t}$, T_{st} and T_{1t} are found from the boundary condition equations between the regimes at 5 and 30 mm/hr.

Dutton (Ref. 3-15) has extended the model to include the variance of R for a given $T_t(R)$. This allows calculation of confidence limits on the average cumulative statistics. These calculations are not included in the DEGP76 program and require additional regression analyses of data from several locations within the same climatic zone. In addition, Dutton (Ref. 3-15) has demonstrated how to

obtain a zonally averaged rain rate distribution for a climatic zone (similar to the curves in Figure 3-15) and it is suggested that these analyses be utilized to define the zone boundaries.

3.4.4 The Lin Model (Ref. 3-16)

Lin has observed that the rain rate probability is approximately lognormal. Namely,

$$P(R) \approx P_0(0) \left\{ \tfrac{1}{2} \operatorname{erfc} \left[\frac{\ln R_i - \ln R_m}{2 S_R} \right] \right\}$$

where $P(R)$ is the probability that the surface point rain rate exceeds rain rate R, $P_0(0)$ is the probability that it is raining, R_i is the instantaneous rain rate, R_m is the mean value of R_i and S_R is the standard deviation of ln R.

The value of $P_0(0)$ is usually calculated for a rain rate of 0.25 mm/hr or more. This selection is made because 0.25 mm/hr has little effect on links below 60 GHz and most rain gauges can not measure more accurately than 0.25 mm/hr. In addition, since the Weather Service measures rain accumulations during a period of one hour, the effect of integration time has been experimentally estimated to be

$$P(R \geq 0.25 \text{ mm/hr} \mid T \leq 1 \text{ min}) \approx \tfrac{1}{2} P(R \geq 0.25 \text{ mm/hr} \mid T = 1 \text{ hr}).$$

This relation allows one to estimate $P_0(0)$ from the HPD's shown in Figure 3-4, the LCD's shown in Figure 3-8 or the Canadian Recording Rain Gauge Data as shown in Figure 3-13. This formula is dominated by the low rain rates and should not be applied to higher rates where convective storms lasting several minutes yield lognormal statistics.

The initial value selected for R_m should be obtained from the total rainfall for the year (precipitation minus snowfall) divided by the number of hours the rainfall exceeds 0.25 mm/hr (0.01 inch/hr). This data is found in the HPD's, the LCD's or the Canadian Monthly Review. The final values for R_m and S_R are obtained by a least-squares approximation that minimizes the differences between the data points and the lognormal approximation. Typical values for Merrimack Valley, MA (Climate Region D, see Figure 3-14) are (Ref. 3-16) $R_m \approx 1.23$ mm/hr, $S_R \approx 1.34$, $P_0(0) \approx 0.033 = 3.3\%$.

The instantaneous rain rate R_i is assumed to be averaged over a 2-second interval which corresponds to the volume in the main Fresnel zone divided by the raindrop terminal velocity. Measurements of the rain rate distribution dependence on the gauge integration time have been made in the range 1.5 sec $\leq t \leq$ 2 min. for at least one location. The data is shown in Figure 3-20 from Ref. 3-19.

The probability $P_0(0)$ is the probability of rainfall at a point. However, intuitively one would expect that for a path of elevation angle θ that rain may be occurring along the path but not at the gauge. This has been compensated for in the Global model by the factor r. In the Lin model, the P_0 is modified to be $P_0(D)$, where D is the horizontal projection of the path. Experimental data in Florida has yielded an empirical relation (Ref. 3-20)

$$P_0(D) \approx 1 - \frac{1 - P_0(0)}{\left[1 + \frac{D^2}{21.5}\right]^{0.014}}$$

where D is in kilometers. Thus for earth-space paths, the $P_0(D)$ value should be used instead of $P_0(0)$.

Later models developed by Lin have recently been published and are also recommended for use here. Measurements at US locations have shown that the total attenuation = $(AL)/(1+L/\bar{L}(R))$, where A is the specific attenuation, L is path length through the storm, R is the 5-minute point rain rate in mm/hr and $\bar{L}(R)=(2636/(R-6.2))$km (see Refs. 3-21 and 3-22). Typically Lin finds that storm height are 4 km, so L-(H-G)csc θ, where G is the ground station altitude.

3.4.5 Worst-Month Statistics

Designers of communications systems who must meet "any month" performance criteria will need a model for the worst-month or worst 30-day statistics. These statistics are the average percentage of time within the worst month which comes once per year when a threshold is exceeded.

Recently Crane and DeBrunner (Ref. 3-23) have applied an exponential model to fit the tail of the distribution curve. Using the notation in Ref. 3-23, the probability of exceeding the worst-month threshold value is $P(x_{hj})$, where h denotes the worst month and j denotes the threshold rain rate value related to the path attenuation margin budget and other system parameters.

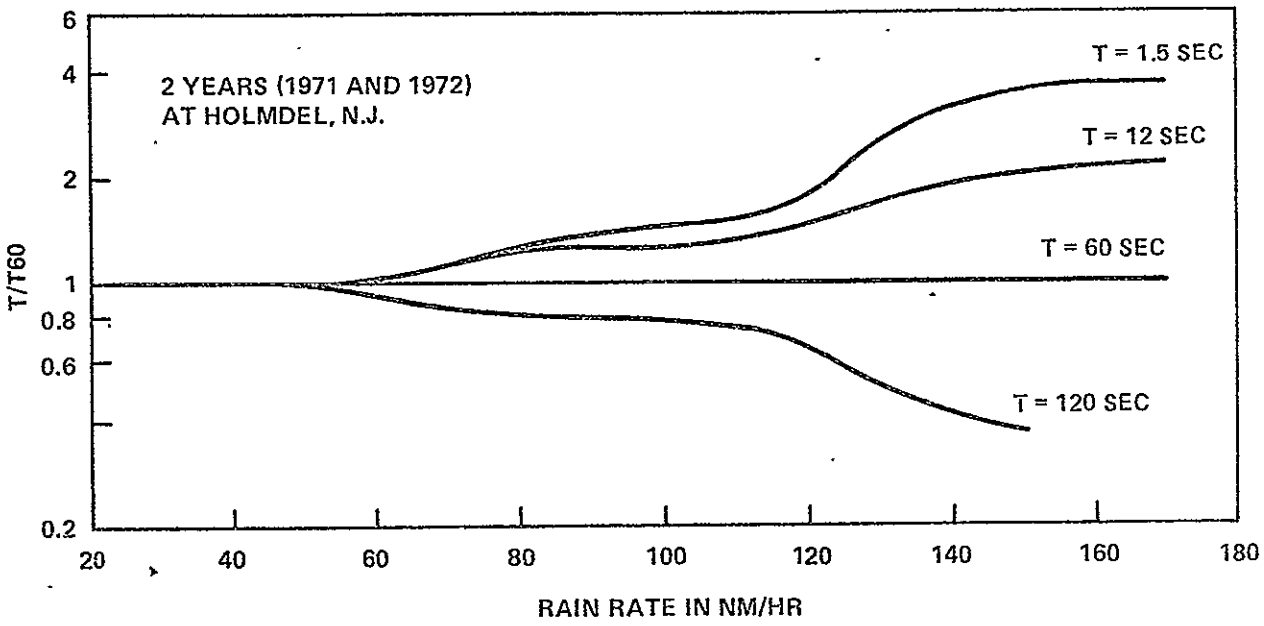

FIGURE 3-20. THE INSTANTANEOUS RAIN RATE DISTRIBUTION VERSUS GAUGE INTEGRATION TIME

The distribution for N years is

$$P(x_{hj}) = \frac{1}{12\ N} = C_{oj}\ \exp(-x_{hj}/C_{1j})$$

where x_{hj} is the probability of exceeding j during the worst month. Inverting the equation yields

$$x_{hj} = C_{1j}\ \ln(12\ N\ C_{oj}) = C_{1}\ \ln(C_{oj}/P(x_{hj})).$$

An example of this distribution is shown in Figure 3-21. The values C_{oj} and C_{1j} may be obtained from the figure, e.g., $C_{oj} = 0.2$ and $C_{1j} = 7.9 \times 10^{-5}$.

For the case where N = 1 year, a bound on C_{oj} may be obtained from

$$\frac{12}{M} \leq \frac{\ln(12\ C_{oj})}{C_{oj}} \leq 4.41$$

where M (M > 3) is the number of months during the year that rain typically occurs. If M < 3, the use of the exponential distribution model should be questioned.

The data in Figure 3-21 is best obtained from the CD (Figure 3-4) where the number of days with heavy precipitation is recorded or from Table 7 of the Canadian Monthly Record (Figure 3-11). Ultimately, the rain gauge charts for the dates and locations identified above will be required to obtain the high rain rate data.

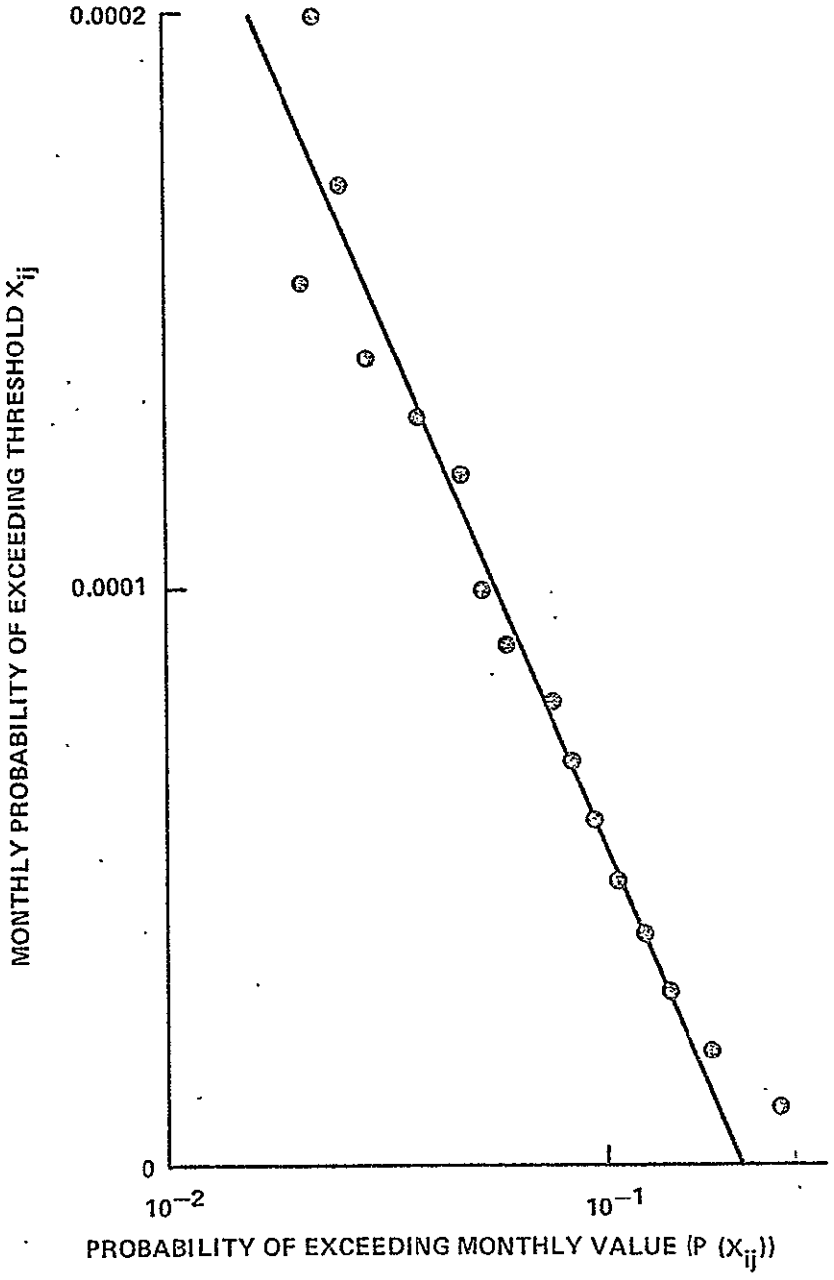

FIGURE 3-21. WORST-MONTH DISTRIBUTION FUNCTION FOR A 347 MONTH PERIOD AND A 90 MM/HR THRESHOLD

3.5 TOTAL RAIN ATTENUATION PREDICTIONS

3.5.1 General Approaches

An estimate of the rain attenuation cumulative statistics may be determined in several ways. The optimum way depends both on the amount of rain and/or attenuation data available and on the level of sophistication desired. In general the cumulative statistics can be calculated over a period of a year with 99% error bounds, so that only 1 year in 100 will be the exception. The system engineer, based on the path margin available for attenuation, can then judge how the attenuation will affect the performance and availability of the system. Depending on the data base available, the designer may compute the cumulative statistics in several ways; however, it is recommended that the simplest calculations be carried out first to give a general feeling for the statistics and also to act as a check on the results of more sophisticated calculations.

The several flow charts in Figures 3-22 to 3-24 will assist with deciding which calculations are to be pursued. The steps are numbered to allow easy reference with the discussions to follow.

Generally the yearly cumulative statistics are desired. The worst 30-day or worst-month statistics were discussed in an earlier section. Again it is emphasized that only the rain statistics are desired, since snow has a much lower specific attenuation. The examples used here are for synchronous or near-synchronous satellites with relatively stable orbital positions.

3.5.2 Analytic Estimates of Attenuation Statistics (Figure 3-22)

Referring to Figure 3-22, the required given parameters are the ground station latitude, longitude and elevation; the satellite orbital position which allows calculation of the elevation angle; and the operating frequency. Step 1 is to determine the rain zone climate region from Figure 3-14 and utilize the appropriate one-minute average surface rain rate curve shown in Figure 3-15. Given the latitude, elevation and season of the year, the averaged rain rate along the link is computed using Figures 3-16 and 3-17. In Step 2 the effective path length is computed from $L_e = H \csc\theta$ and the total attenuation is then computed from Table 3-3 and L_e.

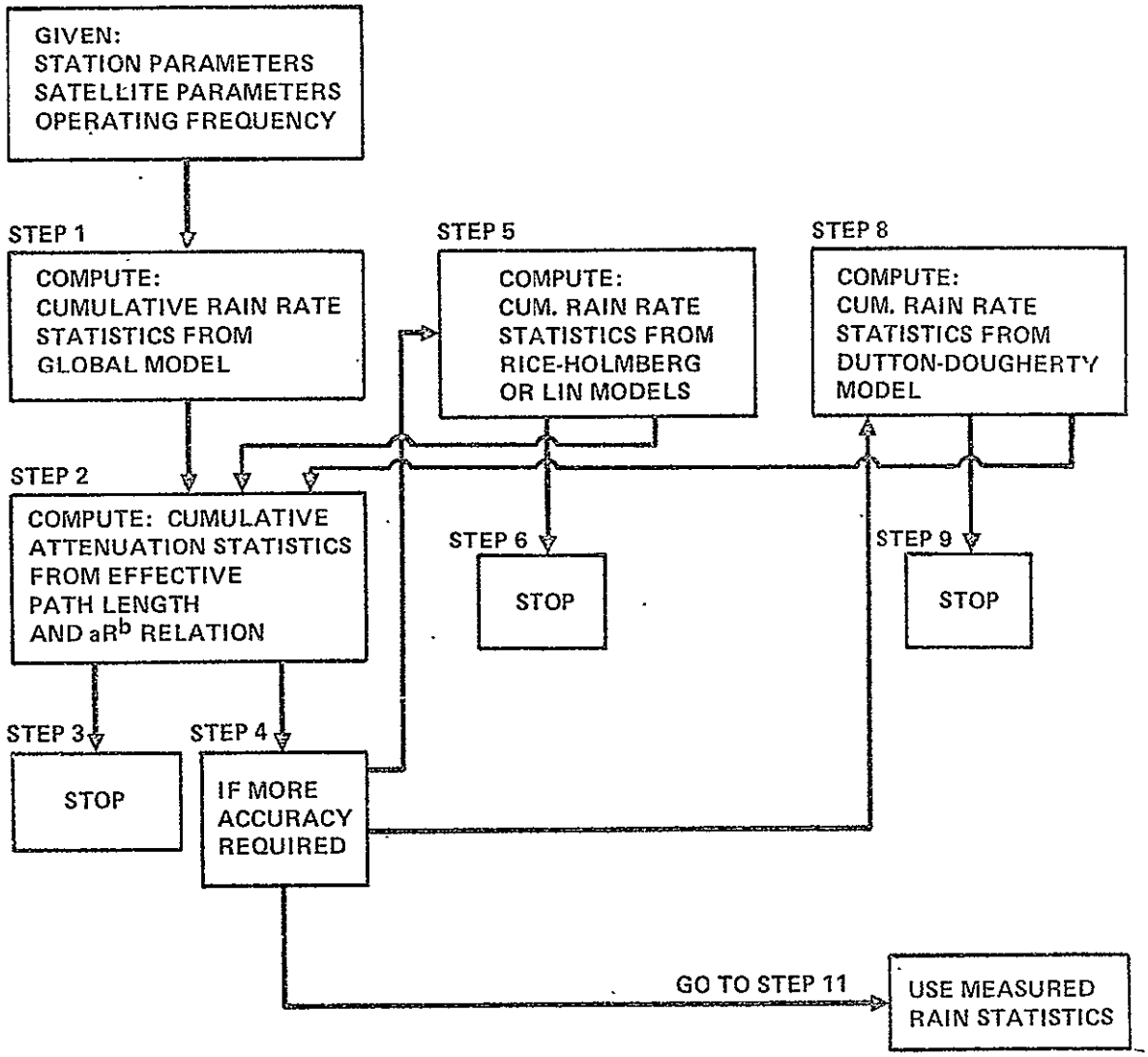

FIGURE 3-22. ANALYTIC ESTIMATE OF CUMULATIVE RAIN RATE AND ATTENUATION STATISTICS

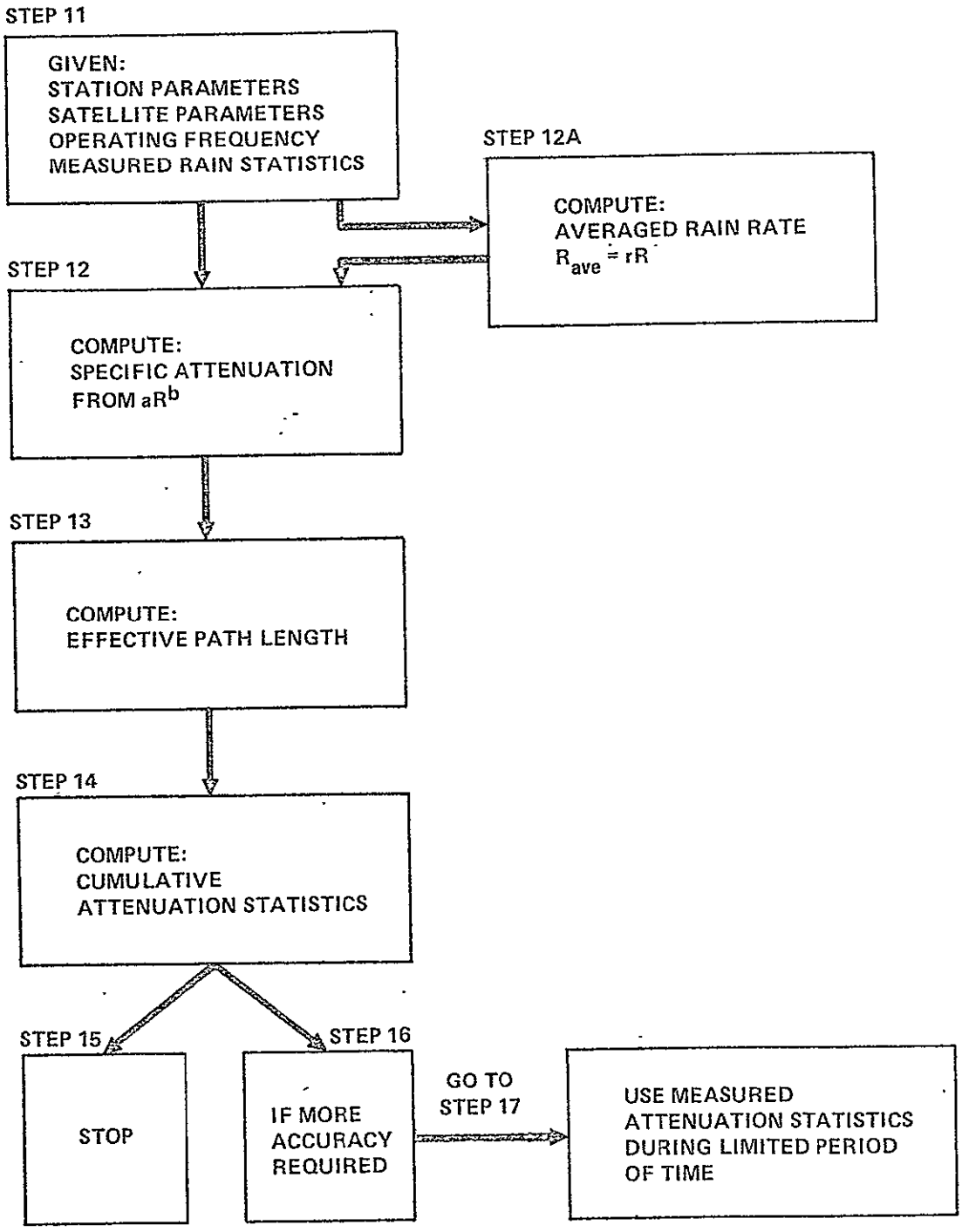

FIGURE 3-23. ATTENUATION STATISTICS GIVEN RAIN RATE STATISTICS

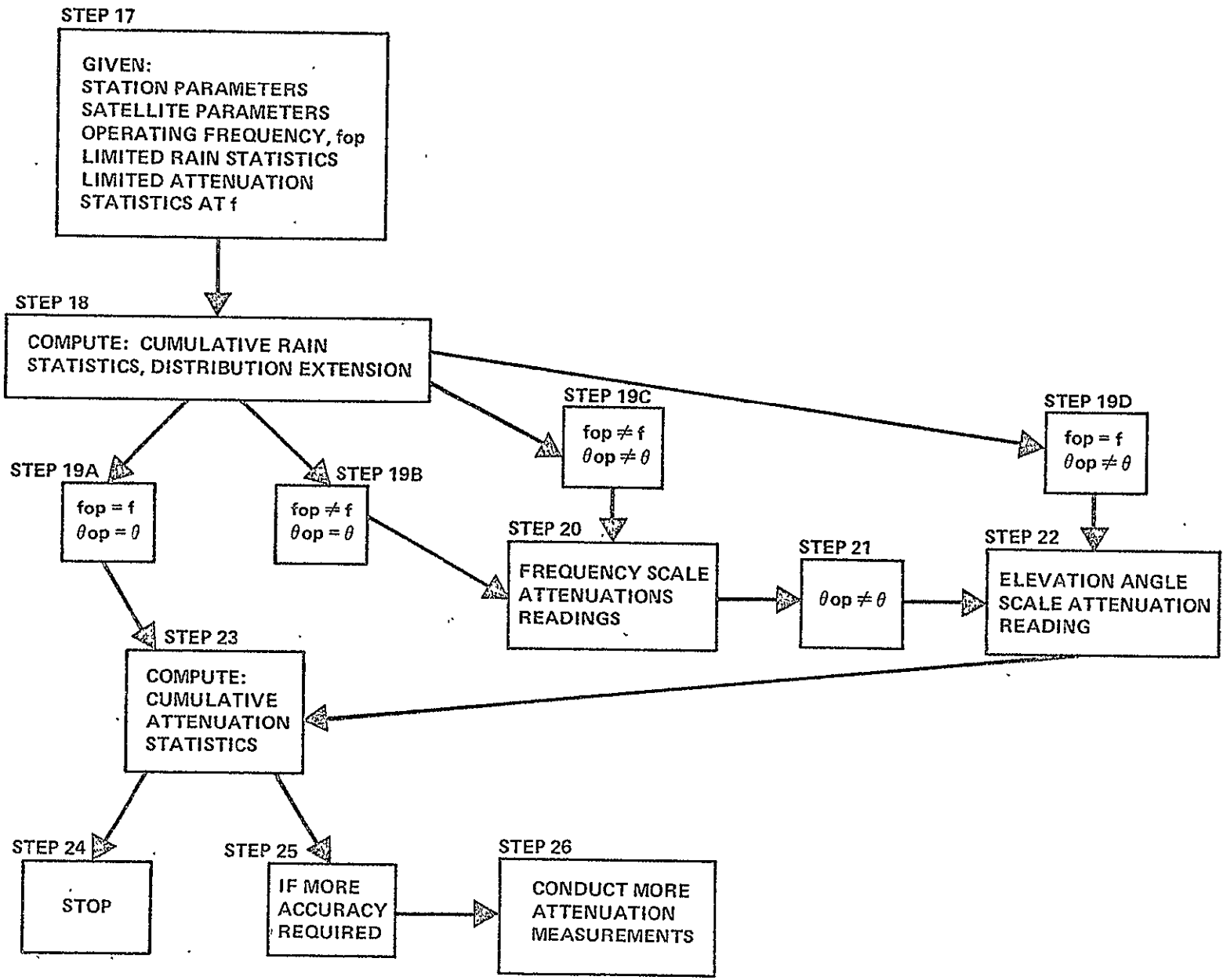

FIGURE 3-24. CUMULATIVE ATTENUATION STATISTICS GIVEN LIMITED RAIN RATE AND ATTENUATION STATISTICS

3.5.2.1 Example: Analytic Estimate Procedure (Figure 3-22)

3.5.2.1.1 Global Model. For the case of the 20 GHz ATS-6 link from Rosman, NC, latitude = 35 degrees N, longitude = 82 degrees W, elevation = 880 meters, the elevation angle = 47 degrees, so it is located in rain region D. The 0°C isotherm height H = 3.7 km so the horizontal path length $D = H/\tan\theta = 3.7/\tan(47^{\circ})$ = 3.45 km ≈ 3 km.* The rain rate average parameter $r = \gamma(D)\, R^{-\delta(D)} = 1.6\, R^{-0.13}$, so the averaged rain rate = $r\,R = 1.6\, R^{0.87}$. This factor is used to modify the ordinate of Figure 3-15, i.e., for a surface rain rate of 50 mm/hr, the averaged rain rate is 48 mm/hr. The effective path length is $L_e = H \csc\theta$ = 5.1 km. The specific attenuation (from Table 3-3) is

$$A = 0.06\, R_{ave}^{1.12} \text{ dB/km}$$

where the path averaged rain rate R_{ave} is utilized. The total attenuation due to rain will exceed

$$AL_e = 0.06\,(48)^{1.12}(5.1) \text{ dB} = 23.4 \text{ dB}$$

for 0.01% of a year (53 minutes) using the Global Model. The lower bound for 0.01% of the year is computed from curve E of Figure 3-15 and the upper bound from curve B of Figure 3-15.

3.5.2.1.2 Rice-Holmberg and Lin Models. If a more accurate estimation is desired, the Rice-Holmberg model may be applied (see Step 5). The M and β paramters may be computed by averaging several years records from a nearby Weather Station Office or from the maps in Figures 3-18 and 3-19. Using the data in these Figures for the Asheville, NC area, M ≈ 1150 mm and β = 0.3. For the surface rain rate of 50 mm/hr

$$T_1(50) = 1150 \left\{(0.03)(0.3)\exp\left[(0.03)(50)\right] + (0.2)(0.7)\exp\left[(-0.258)(50)\right] + 1.86\exp\left[(-1.63)(50)\right]\right\}$$

= 2.3 hours = 0.026% of the year.

Clearly, this is higher than the 0.01% predicted by the Global Model.

The Lin model would use the 5-minute rain rate data from the Weather Station office. This has not been done in this report, however, data for Palmetto, GA (Ref. 3-22) yields $T_5(50) \cong 1.1$ hours = 0.012% of the year.

---

*Some compensation for the ground station height has been considered by rounding 3.45 km down to 3 km.

3.5.2.1.3 Dutton-Dougherty Model. Because of this disparity it appears worthwhile to check these estimates with other models (e.g., the Dutton-Dougherty model, Step 8). The results for all three models along with the measured ATS-6 data are shown in Figure 3-25. The Dutton-Dougherty model best approximates the measured 20 GHz data from ATS-6. Unfortunately, the Dutton-Dougherty model also includes the clear attenuation of approximately 2.5 dB. This value appears high (see calculations in Section 2 yielding 1.2 dB) and so the Dutton-Dougherty model results should be shifted by about 1 dB.

3.5.2.2 Discussion of Example. In this case the more difficult model to apply yields the most accurate results. The Rice-Holmberg model fits quite well for low values of attenuation but begins to deviate at values of probability in excess of 0.02% or less. For percentages near 0.1% the model tends to underestimate the data. The Global model also tends to underestimate the statistics of the attenuation. Similar estimates made for White Sands, NM (Region F) also indicate that the attenuation is underestimated with the Global model.

3.5.3 Attenuation Estimates Given Rain Rate Statistics. (Figure 3-23)

If the rainfall is measured by a weather service for a period of 10 years or more near a ground station site, the rain rate statistics may be generated from the LCD's or HPD's supplemented by the universal weighing gauge charts (see Figures 3-9 and 3-10) or a tipping bucket chart as shown in Figure 3-8 during the heavy rain events. It is desirable to obtain the data in one-minute rain rate averaged increments. This is close to the instantaneous rain rate needed for the statistics (Ref. 3-19).

The rain rate statistics are now averaged along the link path using the relation $R_{ave} = r\ R$ (Step 12A), or the point rain rate may be utilized directly in the specific attenuation formula (Step 12). If the averaged rain rate is utilized, then the effective path length is $L_e = H \csc\theta$.

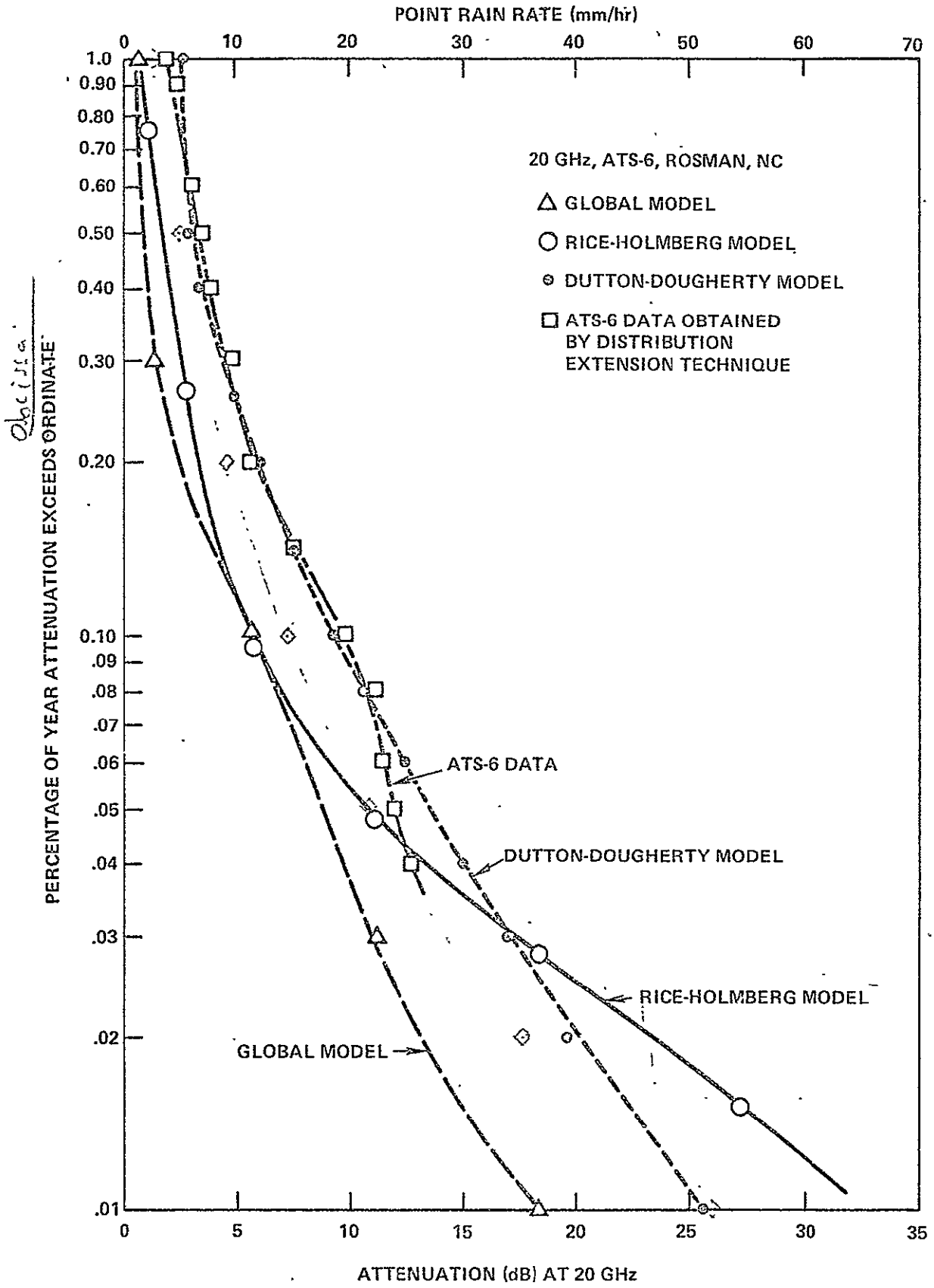

FIGURE 3-25. CUMULATIVE ATTENUATION PREDICTIONS (3 MODELS) AND DATA FOR 20 GHz SIGNALS AT ROSMAN, N.C.

If the point rain rate is utilized in the specific attenuation calculation, the effective path length is found in Figure 3-13 or the formula $L_e(R) = 12.82\ R^{-0.3}$ should be utilized. Since the effective path lengths in Figure 3-13 have been measured, it appears more accurate to use the experimental relations. The results of these calculations will be the total attenuation at the operating frequency. These attenuations are then plotted on the parallel to the rain rate axis similar to Figure 3-25.

3.5.3.1 Example of Attenuation Statistics Given Rain-Rate Statistics. (Figure 3-23). At Rosman, NC, the rain rate from the near bucket was measured over a period of six months (July to December, 1974). The resulting distribution is shown in Figure 3-26. The attenuation values for a given probability of occurrence are then computed using the specific attenuation and the effective path length relation $L_e = 12.82\ R^{-0.3}$. The L_e term causes the attenuation estimate to deviate from the rain rate distribution for high values of rain rate.

3.5.4 Attenuation Estimates Given Limited Rain Rate and Attenuation Statistics (Figure 3-24)

3.5.4.1 Distribution Extension. Referring to Figure 3-24, the amount of given data is more extensive than the other methods mentioned, except that both the rain rate and attenuation statistics were measured over a limited period of time (typically less than a year). It is desirable to extend these statistics to a one-year period through a procedure called distribution extension.

Consider the rain rate distribution first. Two situation are likely to occur. First, if the measurements were made for a total time T only occasionally during a time period T_1 to T_2, and one desires to extrapolate the measured distribution to the total time $T_2 - T_1$. The second situation occurs when the measurements made between T_1 and T_2 are to be extrapolated to a larger time period T_0 to T_3 which includes T_1 and T_2.

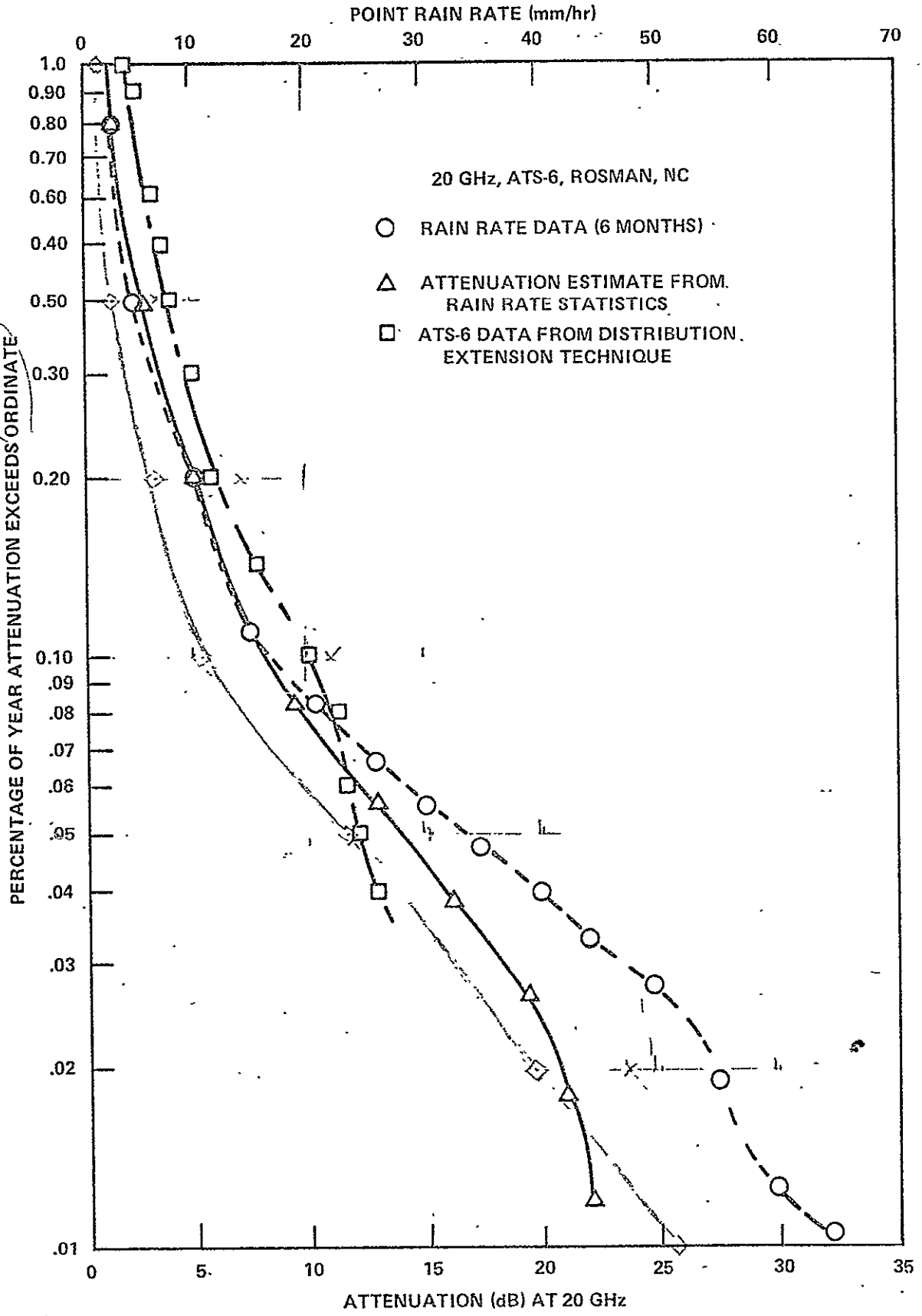

FIGURE 3-26. RAIN RATE AND ATTENUATION STATISTICS BASED ON PROCEDURES IN FIGURE 3-23

For the first case of distribution extension, Bayes' rule indicates how the extension is to be performed. Namely

$$P(R_i \geq R_0 | T \leq T_2 - T_1)\ P(T \leq T_2 - T_1) =$$
$$P(T \leq T_2 - T_1 \mid R_i \geq R_0)\ P(R_i \geq R_0),$$

which states that the (probability that the instantaneous rain rate R_i is greater than or equal to some specified rain rate R_0 during the measurement time T less than or equal to the period from T_1 to T_2) times (the probability that T is less than or equal to $T_2 - T_1$) equals (the probability that a measurement was made given that $R_i \geq R_0$) times (the probability that $R_i \geq R_0$). For the obvious limit that $T = T_2 - T_1$, this results in the identity

$$P(R_i \geq R_0 \mid T = T_2 - T_1)\ (1) = (1)\ P(R_i \geq R_0).$$

The term $P(T \leq T_2 - T_1 \mid R_i \geq R_0)$ accounts for the fact that if one made a nonrepresentative set of measurements during T when $R_i \geq R_0$ this term would correct the measured distribution to the true distribution. The desired quantity is

$$P(R_i \geq R_0) = \frac{P(R_i \geq R_0 \mid T \leq T_2 - T_1)\ P(T \leq T_2 - T_1)}{P(T \leq T_2 - T_1 \mid R_i \geq R_0)}.$$

For the second situation, namely measurements were made during a time T between T_1 and T_2 and one wishes to extend the distribution to a longer sampling period T_0 to T_3, where $T_0 \leq T_1 < T_2 \leq T_3$, the same formula applies except T_1 becomes T_0 and T_2 becomes T_3. Here, for example, the term $P(T \leq T_3 - T_0 \mid R_i \geq R_0)$ will account for the seasonal frequency dependence of thunderstorms, etc. The value of this term is difficult to determine, however the frequency of thunderstorms and number of hours with rain in excess of a specified level will give approximations to the $P(T \leq T_3 - T_0 \mid R_i \geq R_0)$.

Referring to Figure 3-24, the cumulative rain distribution has been determined (Step 18) by distribution extension. If the attenuation statistics were taken at the operating frequency, the cumulative attenuation statistics may be plotted. The construction of this curve, $P(AL_i \geq AL_0 \mid T \leq T_3 - T_0)$, is shown in Figure 3-27. In this figure, the $P(R_i \geq R_0 \mid T \leq T_2 - T_1)$, $P(R_i \geq R_0 \mid T \leq T_3 - T_0)$ and $P(AL_i \geq AL_0 \mid T \leq T_2 - T_1)$ are available from the

* Note: In this section L_e, the effective path lengths, has been abbreviated L.

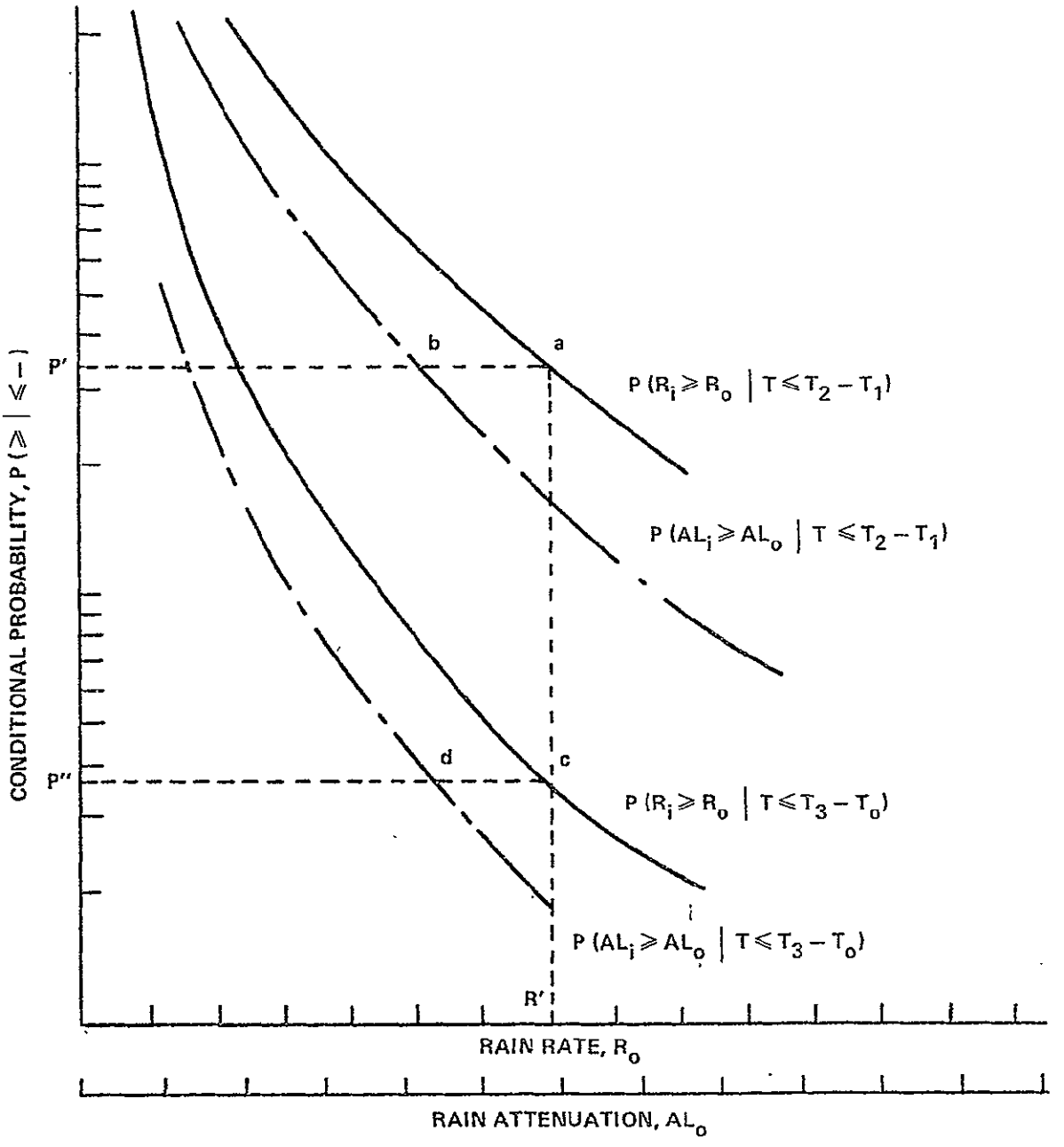

FIGURE 3-27. CONSTRUCTION OF CUMULATIVE ATTENUATION STATISTICS USING THE DISTRIBUTION EXTENSION TECHNIQUE

measurements and the distribution extension. The desired curve $P(AL_i \geq AL_0 \mid T \leq T_3 - T_0)$ is constructed by noting that the distance c - d is equal to a - b. For example, if the rain rate during the attenuation measurement period T exceeded R' mm/hr with probability P' (point a), and the measured attenuation for the same probability was about A' dB (point b), and the rain rate exceeded R' for probability P" of the total period $T_3 - T_0$ (point c), then the attenuation for the entire period T_0 to T_3 would be expected to exceed A' dB for that same probability P" (point d). Using this technique, the entire curve $P(AL_1 \geq AL_0 \mid T \leq T_3 - T_0)$ is generated. The probabilities P during the period T_0 to T_3 may also be expressed as a percentage of the time $T_3 - T_0$ or, e.g., as the number of minutes during the period $T_3 - T_0$.

3.5.4.2 Frequency Scaling. If Steps 19B, C or D are the case, Steps 20, 21 and/or 22 may be required. Step 20 is carried out by one of the following frequency scaling techniques. These are

20-1) empirical scaling

20-2) specific attenuation scaling

20-3) Gaussian rain distribution scaling.

Technique 20-1 utilizes experimental data to relate the total rain-induced attenuation at one frequency to another frequency. The attenuation also depends on polarization because of the ellipsivity of the raindrops, but this effect is small compared to the accuracy of the above estimates and results primarily in depolarization. A general rule for scaling data based on 11 and 19 GHz radar data is (Ref. 3-24)

$$\frac{AL(f_2)}{AL(f_1)} = \left(\frac{f_2}{f_1}\right)^{1.72}$$

where AL is the total attenuation along the path and f_i are the operating frequencies for the measurements.

Technique 20-2 utilizes the specific attenuation data (Ref. 3-4) in Section 3.1.3 to scale $A(f_2)/A(f_1)$. L is assumed to be independent of frequency. The result is

$$\frac{A(f_2)}{A(f_1)} = \frac{a(f_2)}{a(f_1)} R^{(b(f_2)-b(f_1))} = \frac{a(f_2)}{a(f_1)}$$

since $b(f_2) - b(f_1) \approx 0$. Note that this result is dependent on rain rate R.

Finally, technique 20-3 assumes that each cell is spatially distributed along the earth-space path according to the relation (Ref. 3-28)

$$R(s) = R_o \exp(-s^2/\ell_o^2)$$

where s is along the path, ℓ_o is the characteristic cell dimension and R_o is the peak rain rate in the cell. Neglecting the term $\ell_o^{(b(f_1)-b(f_2))/b(f_1)}$, the result is

$$\frac{AL(f_2)}{AL(f_1)} = \frac{a(f_2)}{a(f_1)} \sqrt{\frac{b(f_1)}{b(f_2)}} \left\{ \left(\frac{AL(f_1)}{a(f_1)} \sqrt{\frac{b(f_1)}{\pi}} \right)^{\frac{b(f_2)-b(f_1)}{b(f_1)}} \right\}$$

which is implicity dependent on R through the term $AL(f_1)$.

Dropping the term $\ell_o^{(b(f_1)-b(f_2))/b(f_1)}$, can result in errors when frequency scaling over wide frequency ranges. For a typical value of ℓ_o = 5 km, the error in scaling from 11.7 to 31.65 GHz is 20% due to this term alone. Therefore, for frequency scaling of more than two to one, it is recommended that the full relation

$$AL(f_2) = \frac{a(f_2)}{a(f_1)^{b(f_2)/b(f_1)}} \sqrt{\frac{b(f_1)^{b(f_2)/b(f_1)}}{b(f_2)}} \pi^{(\frac{1}{2} - b(f_2)/2b(f_1))} \cdot$$

$$\ell_o^{(1 - b(f_2)/b(f_1))} AL(f_1)^{b(f_2)/b(f_1)}$$

be utilized.

Tables of these frequency scaling factors are presented here for the common frequencies of 11.7, 15.3, 20, 28.56 and 31.65 GHz (see Tables 3-6 and 3-7). The values of $a(f_1)$, etc., are taken from the analytic relations in Section 3.1.3.

3.5.4.3 Elevation Angle Scaling. Step 21, the elevation angle scaling between the operational elevation angle θ_{op} and the measured data angle θ, may be corrected for by using the relation

$$\frac{AL(\theta_{op})}{AL(\theta)} = \frac{\csc\theta_{op}}{\csc\theta} = \frac{\sin\theta}{\sin\theta_{op}}$$

The corrections for the frequency and elevation angle scaling are first applied to the $P(AL_i \geq AL_0 \mid T \leq T_2 - T_1)$ curve by varying the value of AL_0, e.g., AL_0 becomes AL_0' due to frequency scaling and elevation angle corrections. The curve $P(AL_i \geq AL_0' \mid T \leq T_3 - T_0)$ is then computed using the procedure shown in Figure 3-24.

If more accurate cumulative attenuation statistics are required, it will be necessary to increase the attenuation measurement time T to obtain a truly representative sample of measurements.

3.5.4.4 Example of Attenuation Estimate Given Limited Rain Rate and Attenuation Statistics. The distribution extension technique has been applied to a six-month period from July to December 1974 at Rosman, NC. Here attenuation measurements were made for T = 608 minutes during the T = 725 minutes of measurable rainfall. Rainfall measurements were then made from July (T_0) to December (T_3). Using the technique in Figure 3-27, the attenuation distribution for the $T_3 - T_0$ period was estimated (see Figure 3-28).

In this case steps 19 and 20 were not required, since the measurements were made at 20 GHz and at the ATS-6 elevation angle. If an estimate were desired for another satellite at another frequency steps 19 and 20 would be carried through using the attenuation statistics obtained from the distribution extension technique.

TABLE 3-6

FREQUENCY SCALING RATIOS FROM SPECIFIC ATTENUATION
(Technique 20-2)

Frequency f_1, GHz	Frequency f_2, GHz: 11.7	15.3	20	28.56	31.65
11.7	1	$1.91R^{-0.024}$	$3.66R^{-0.048}$	$8.67R^{-0.007}$	$11.0R^{-0.136}$
15.3	$0.52R^{0.024}$	1	$1.91R^{-0.024}$	$4.53R^{-0.083}$	$5.76R^{-0.11}$
20	$0.27R^{0.48}$	$.52R^{0.024}$	1	$2.37R^{-0.06}$	$3.01R^{-0.068}$
28.56	$0.12R^{.11}$	$0.22R^{0.083}$	$0.42R^{0.06}$	1	$1.27R^{-0.028}$
31.65	$0.09R^{.136}$	$0.17R^{.112}$	$.33R^{0.088}$	$.79R^{0.028}$	1

Note: R in mm/hr

f = 11.7 GHz	a = 0.0162 dB·hr/km·mm	b = 1.1641
f = 15.3	a = 0.0310	b = 1.1401
f = 20.0	a = 0.0593	b = 1.1165
f = 28.56	a = 0.1404	b = 1.0568
f = 31.65	a = 0.1787	b = 1.0285

a and b are derived from the analytic formulas in Table 3-3. More accurate values may be obtained by interpolating Table 3-2.

TABLE 3-7

FREQUENCY SCALING RATIOS FROM GAUSSIAN RAIN DISTRIBUTION SCALING

(Technique 20-3)

Frequency f_1, GHz \ Frequency f_2, GHz	11.7	15.3	20.0	28.56	31.65
11.7	1.0	1.85β	3.41β	7.40β	9.04β
15.3	0.53β	1.0	1.87β	4.19β	5.20β
20.0	0.28β	0.53β	1.0	2.32β	2.92β
28.56	0.11β	0.21β	0.41β	1.0	1.29β
31.65	0.083β	0.16β	0.31β	0.77β	1.0

Note: $\beta = AL(f_1)^{(b(f_2)/b(f_1))}$ and ℓ_o = 4 km

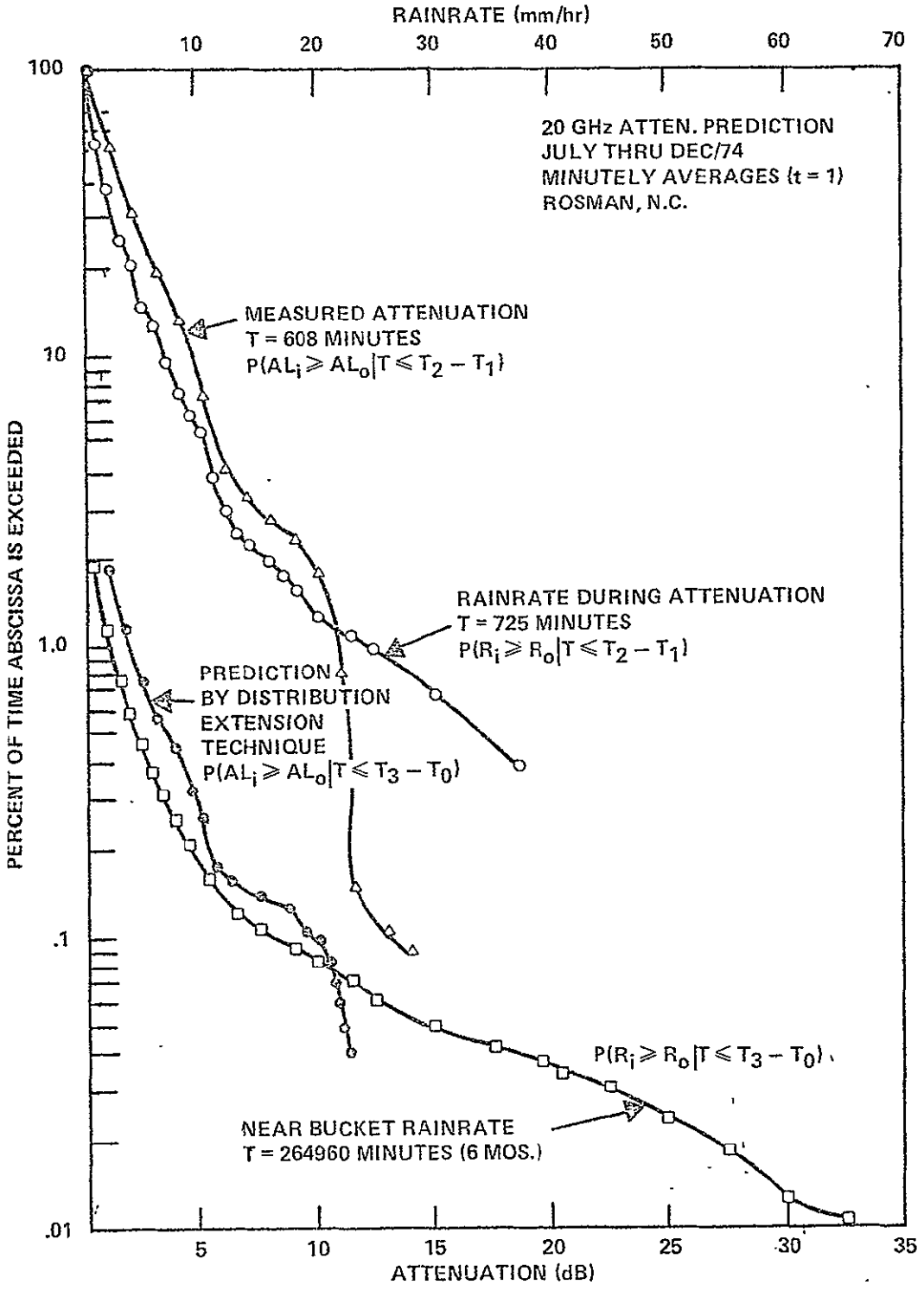

FIGURE 3-23. ATTENUATION STATISTICS BASED ON DISTRIBUTION EXTENSION TECHNIQUE (FIGURE 3-24)

4.0 CLOUD, FOG, SAND AND DUST ATTENUATION

4.1 SPECIFIC ATTENUATION OF WATER DROPLETS

The attenuation of clouds and fog arises from the small droplets (generally less than 0.01 cm diameter) and can be computed in the Rayleigh approximation. Therefore specific attenuation is related to the water vapor density of the cloud or fog (Ref. 4-1) as described in the Appendix. The resulting specific attenuation for clouds or fog is

$$A_c = K_c \rho_w \quad \text{dB/km}$$

where K_c is the specific attenuation per unit water vapor density ρ_w. K_c is in the units $dB \cdot m^3/g \cdot km$ or $dB \cdot m^3/kg \cdot km$ depending on the units of ρ_w.

Values of K_c versus frequency are given in Figure 4-1 (Ref. 4-2). In engineering calculations for fog, which is generally most intense at the surface on a cool evening, the 10^oC curve is recommended for summer and the 0^oC is more appropriate for other seasons. For clouds, as with rain, the 0^oC curve is recommended. Note that these are theoretically-derived curves and so their value is unverified.

4.2 CLOUDS*

For heavy cumulus or cumulonimbus clouds, ρ_w is typically between $1 gm/m^3$ and $2.5 gm/m^3$ (Ref. 4-3), although values as high as 4 to 5 gm/m^3 are occasionally

*Much of this work is taken from ORI Tech. Report 1187, D. Rogers and R. Kaul, June 1977.

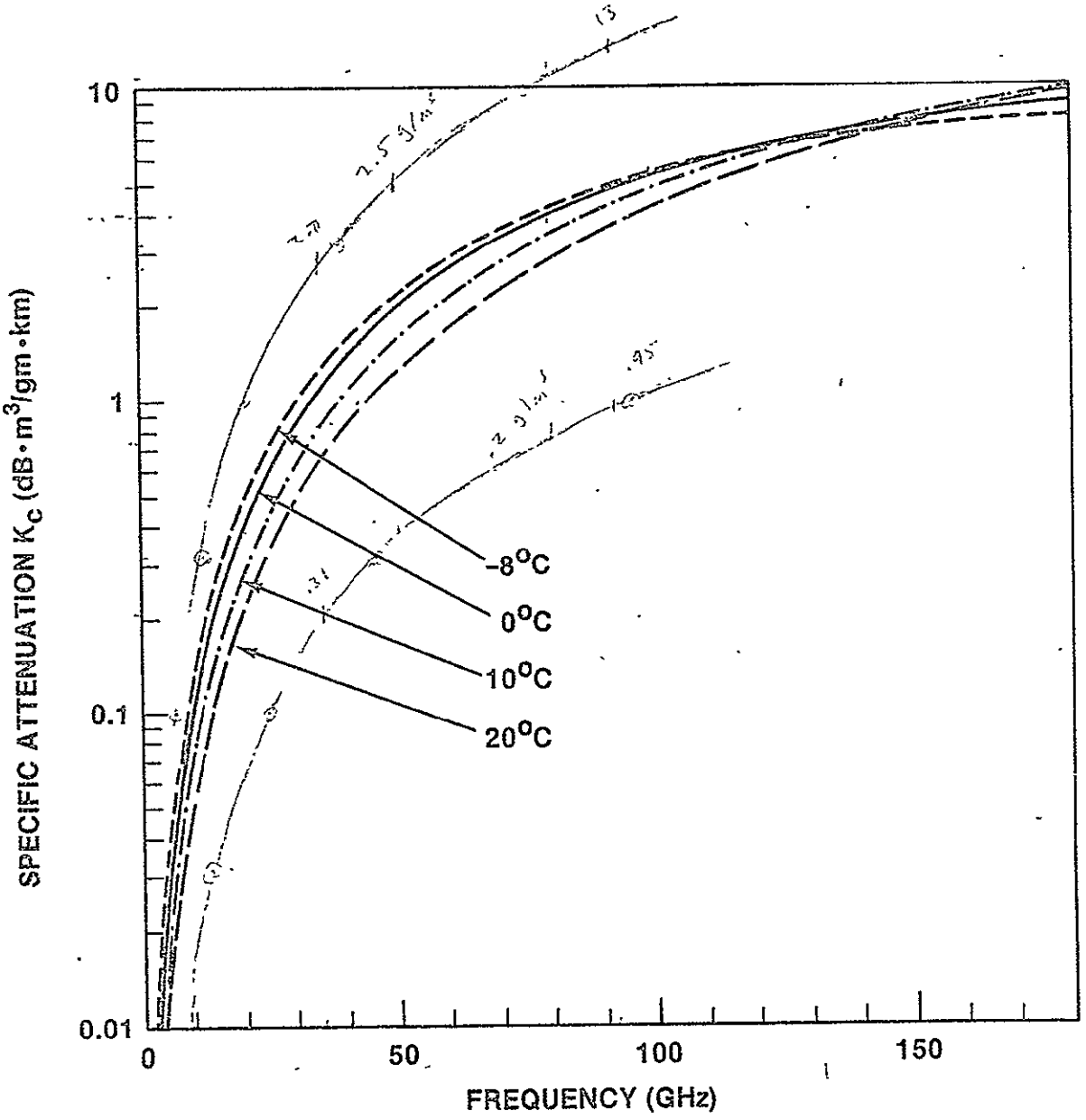

IGURE 4-1. THEORETICAL ATTENUATION BY WATER CLOUD AT VARIOUS TEMPERATURES AS A FUNCTION OF FREQUENCY

observed (Ref. 4-4). Fair weather cumulus clouds have liquid water contents about an order of magnitude smaller (Ref. 4-5). For nonprecipitating events an upper limit of 2.5 gm/m^3 seems appropriate for system design in the U.S. and Canada. More detailed calculations may be made using the data in Table 4-1 (adapted from Ref. 4-6) and local cloud data.

Estimates of the path length L_c through the clouds are more difficult to make. The maximum dimensions (horizontal and vertical) for heavy cumulus and cumulonimbus clouds are about 10 km (Ref. 4-7). If one assumes a right circular cylinder configuration and knowing the elevation angle, an approximate length L_c may be determined. However for elevation angles below 30 degrees the effects of multiple clouds should be considered. As a general rule, a maximum $L_c \approx 10$ km is not unreasonable, resulting in total cloud attenuation (upper bound) at 11.7 GHz of

$$K_c \rho_w L_c|_{max} = (0.13 \text{ dBm}^3/\text{km} \cdot \text{gm})(2.5 \text{ gm/m}^3)(10 \text{ km})$$
$$= 3.25 \text{ dB}$$

This result is quite high and should be considered an upper bound. The corresponding upper bounds at 20 and 30 GHz are 10 dB and 20 dB, respectively.

Measurements made at Slough, United Kingdon, do not confirm these results (Ref. 4-1). The vertical attenuations at 95 and 150 GHz made between October 1975 and May 1976 are shown in Table 4-2.

TABLE 4-2

ADDITIONAL ATTENUATION IN CLOUDS

Type	Attenuation (dB) f=95 GHz	Attenuation (dB) f=150 GHz
Strato-cumulus	0.5 -1	0.5 - 1
Small, fine weather cumulus	0.5	0.5
Large cumulus	1.5	2.0
Cumulo-nimbus	2-7	3-8
Nimbus-strato (rain cloud)	2-4	5-7

Note: Water vapor density at ground level was 4 to 11 gm/m^3 resulting in a clear-air attenuation of 0.7 to 1 dB and 1 to 3 dB at 95 and 150 GHz, respectively.

TABLE 4-1

PROPERTIES OF CLOUDS

Cloud Type	Water Density (g/m^3)	Base Height (m)	Top Height (m)
Cirrostratus, Arctic	0.1	4000	6000
Cirrostratus, Midlatitude	0.1	5000	7000
Cirrostratus, Tropical	0.1	6000	8000
Altocumuls and Altostratus	0.15	2400	2900
Low-lying Stratus	0.25	150	1000
Stratocumulus	0.25	1320	660
Fair Weather Cumulus	0.5	500	1000
	1.0	1000	1500
	0.5	1500	2000
Cumulus with Rain, 2.4 mm/hr	0.1	0	500
	1.0	500	1000
	2.0	2000	3000
Cumulus with Rain, 12 mm/hr	0.5	0	400
	2.0	400	1000
	4.0	1000	4000
Cumulus Congestus	0.3	1000	1200
	0.5	1200	1600
	0.8	1600	2000
	1.0	2000	2500
	0.5	2500	3000
Cumulonimbus with Rain, 150 mm/hr	6.3	0	300
	7.0	300	1000
	8.0	1000	4000
	4.0	4000	6000
	3.0	6000	8000
	0.2	8000	10000

These results, assuming the data in Figure 4-1 is correct and L_c = 10 km, yield values for ρ_w = (8 dB)/(5 dB· m^3/kg·gm)(10 km)

= 0.16 gm/m^3.

If one assumes ρ_w = 2.5 gm/m^3, then

L_c = (8 dB)/(5 dB·m^3/kg·gm)(2.5 gm/m^3)

= 0.64 km.

Neither result seems reasonable and so some engineering judgement must be used here for the total cloud attenuation.

Measurements made near Austin, Texas (Ref. 4-2) at frequencies of 35 and 95 GHz indicated mean attenuations of 0.18 and 0.61 dB, respectively for strato-cumulus clouds. Correspondingly for cumulus clouds (probably ranging between the small and large cumulus values in Table 4-2), attenuations between 0.12 and 0.34 dB were observed, respectively. The maximum cloud attenuations at 35 and 95 GHz were 2.3 and 10 dB, respectively, arising from rain-bearing clouds.

Measurements of cloud attenuation can be most easily made with radiometers and verified with satellite beacon measurements. These attenuation values fall in the range where radiometers are most accurate.

4.3 FOG

Fog results from the consideration of atmospheric water vapor into water droplets that remain suspended in air. When the resulting cloud of water droplets or ice crystals envelops an observer and restricts his ability to detect a black target against the sky horizon background by the 2 to 5% threshold contrast of the human eye at a distance of one kilometer or less, the international definition of fog has been satisfied (Ref. 4-8 and 4-9). The relation (Ref. 4-10)

$$\rho_w = 0.0156\ V^{-1.43}$$

appears to adequately relate ρ_w to the visibility V in km for $\rho_w \leq 0.4$ gm/m^3. This applies only to advective (coastal) fogs which form over open water as a result of the advection (movement) of warm, moist air over colder water. For radiation (inland) fog which forms in air that has been over land during daylight

hours preceding the night of formation, the relation (Ref. 4-11)

$$\rho_w = (42\ V)^{-1.54}$$

has been derived. The conditions favorable for radiative fog are: (1) air that has been under a cloud cover (with or without precipitation) during the day previous to its formation and (2) pools of air cooled to an excessive degree which collect in valleys, low, marshy land and along rivers on calm, clear nights. The maximum ρ_w is generally less than 1.0 gm/m^3.

The attenuation due to fog is modelled by the same relation as clouds, but using the 0 or 10°C value for the specific attenuation per gm/m^3. Unfortunately, the spatial distribution of ρ_w or L_c has not been measured via satellite beacons. Typical ρ_w values for fog and haze are given in Table 4-3.

TABLE 4-3
PROPERTIES OF FOG AND HAZE

Type	Water Density gm/m^3	Base Height (m)	Top Height (m)	Visibility (m)
Fog Layer*	0.15	0	50	-
Radiation (inland) Fog†	0.11	-	-	100
Advection (coastal) Fog†	0.17	-	-	200
Haze, Heavy*	0.001	0	1500	-

*Adapted from Ref. 4-6.
†Adapted from Ref. 4-8.

4.4 SAND AND DUST ATTENUATION

Sand and dust scatter electromagnetic energy and their effect may be evaluated via Mie scattering. To date simulated measurements have been carried out in the laboratory (Ref. 4-12). At 10 GHz and concentrations of sand and dust less than 10^{-15}gm/cm^3 the measured specific attenuation was less than 0.1 dB/km for sand and 0.4 dB/km for clay. Severe storms have concentrations exceeding these values.

Blowing sand and dust storms occur in some regions of the U.S. These are recorded by the Weather Service as part of the Local Climatological Data (LCD) at the 291 stations. Ground stations needing this information should review the data recorded by a nearby LCD recording station.

The vertical extent of these sand storms is unknown, but it seems unlikely that high concentrations would exceed 1 km. The path length is expected to vary between ½ and 3 km, generally resulting in a total additional attenuation due to sand of the order of 1 dB or less. No measured satellite beacon link data is available to confirm these results.

APPENDIX

CONVERSION OF WATER VAPOR PARAMETERS

The U.S. and Canadian weather services provide measurements of the surface relative humidity. To calculate the attenuation due to water vapor, it is necessary to convert this quantity to the mass of water in a unit volume of air (gm/m^3) at the surface. In calculations of the refractivity the partial pressure (mbar) of water vapor is frequently required. In this appendix the conversion formulas are presented.

CONVERSION OF RELATIVE HUMIDITY TO PARTIAL PRESSURE OF WATER VAPOR

To a very good approximation the earth's atmosphere obeys an ideal gas law equation of state, except during periods when the water vapor will be supersaturated or supercooled. Fortunately, except for cloud physics, this is not a contributing factor for earth-space propagation.

The equation of state for dry air is $pv = R_d T$ where $R_d = 287$ joule/kg $\cdot$ ^{o}K, p is the pressure in newtons/m^2 (1 newton/m^2 = 1.45 x 10^{-4} lb/in^2), v is the specific volume in m^3/kg ($v = 1/\rho$, ρ = density) and T is the temperature in ^{o}K.

The equation of state for water vapor at atmospheric pressures and temperatures has been experimentally determined to be

$$ev = 461\ T$$

where e is the partial pressure of the water vapor.

Since both dry air and water vapor act like perfect gasses, the Gibbs-Dalton law may be utilized for humid air so that

$$pv = \left(\frac{M_d R_d + M_w R_w}{M_d + M_w} \right) T = (p_d + e)\, v$$

where p, v and T are the total pressure, specific volume and temperature of the humid air. M_d and M_w are the masses of dry air and water vapor in grams, and $R_d = 287$ and $R_w = 461$ joule/kg · ^oK, respectively.

The relative humidity is defined as

$$R.H. = \frac{e}{e_s}$$

where e_s is the saturation vapor pressure corresponding to the temperature of the mixture. The saturated partial pressure may be found in the ASME Steam Tables or the Handbook of Chemistry and Physics. A plot of e_s in newtons/m^2 versus temperature is given in Figure A-1.

CONVERSION OF RELATIVE HUMIDITY TO WATER VAPOR DENSITY

The water vapor density ρ_w (kg/m^3) at a given temperature T and vapor pressure e may be found from the ideal gas law; i.e.,

$$\rho_w = 1/v_w = e/(R_w T) = (R.H.)e_s/(R_w T)$$

where e is the vapor pressure in newtons/m^2, $R_w = 461$ joule/kg · ^oK, and T is the absolute temperature.

Alternatively, the saturated water vapor specific volume v_w is given in the ASME Steam Tables and the Handbook of Chemistry and Physics. The conversion for the specific volume is

$$v_w(m^3/kg) = 0.062\ v_w(ft^3/lbm)$$

where lbm is the mass equivalent to a pound in a standard acceleration field. Then $\rho_w = (v_w)^{-1}$.

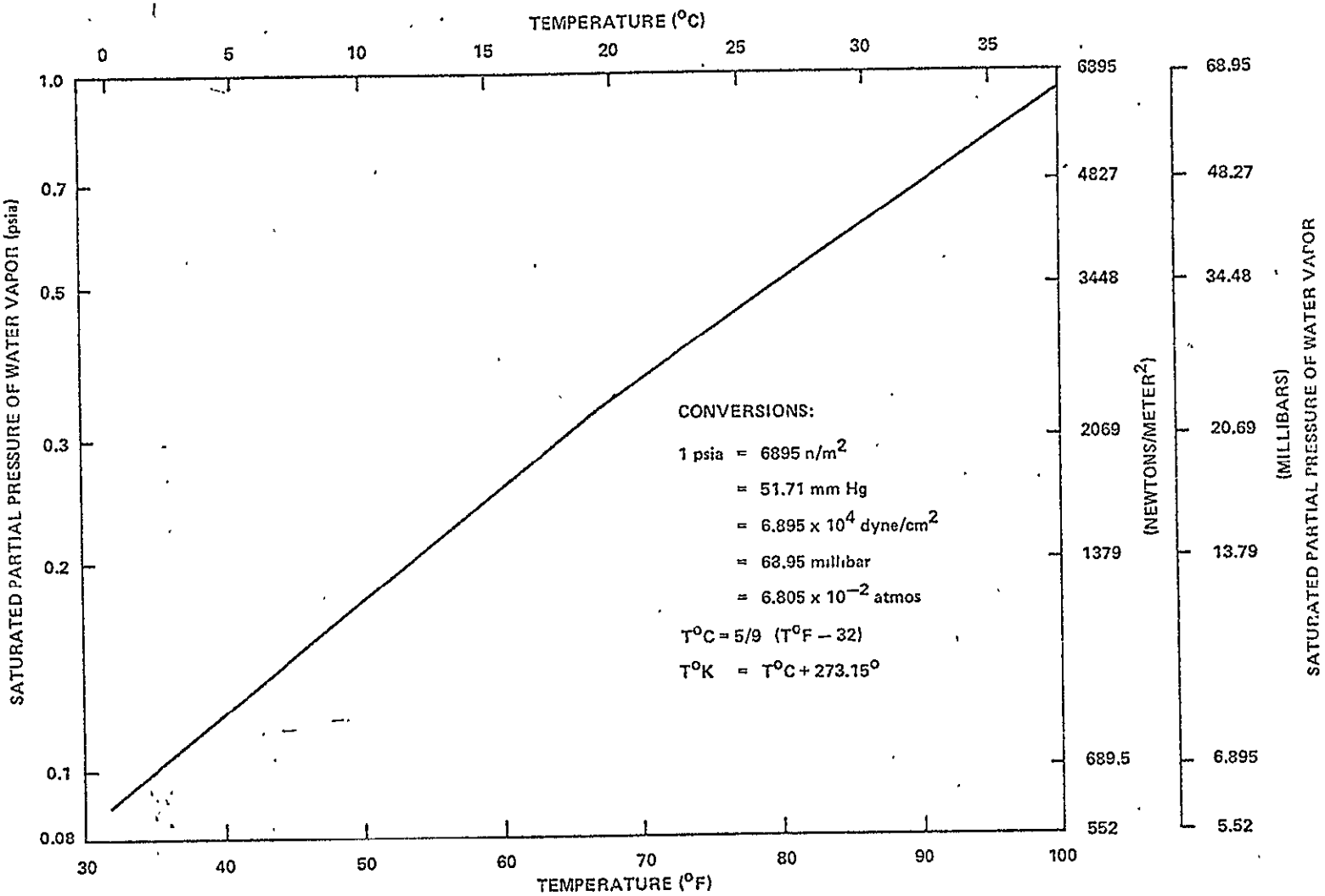

FIGURE A-1. THE SATURATED PARTIAL PRESSURE OF WATER VAPOR VERSUS TEMPERATURE.

APPROXIMATE CONVERSION OF RELATIVE HUMIDITY TO COLUMNAR WATER CONTENT

For radiometric measurements, it is useful to know the total amount of water vapor in a column along the line of sight. To a first approximation, one can assume that the water vapor density ρ_w is distributed exponentially from the surface to the 0^oC altitude. The zonally averaged height of this isotherm is given in Figure A-2 for the rain climates shown in Chapter II. The amount of water in a column along the line of sight is

$$R = \csc\Theta \, \rho_{w_s} \int_{A_1}^{A_z} e^{-\gamma(x-A_1)} \, dx$$

where A_1 is the ground station altitude, A_2 is the 0^oC altitude, $\rho_{w_s} = (R.H.)\, e_{ss}$ is the surface water vapor density and γ is the scale height. The γ is determined by the boundary conditions

$$\gamma = - \frac{\ln\rho_{w_s} - \ln\rho_{w_{0^oC}}}{A_1 - A_2}$$

where ρ_{w_s} and $\rho_{w_{0^oC}}$ are computed from Figure A-1 for the appropriate surface temperature. The total column of water is then

$$R(kg/m^2) = \frac{(\csc\Theta)(\rho_{ws} - \rho_{w0^oC})(A_2 - A_1)}{\ln \rho_{w_s} - \ln \rho_{w_{0^oC}}}.$$

AN EXAMPLE

The following example applies to the Rosman, N.C. ground station (elevation = 880m, latitude = 35^oN) to ATS-6 (elevation angle = 47^o) for the month of September (T surface = 80^oF = 26.7 ^oC, R.H. = 60%).

At this temperature the saturated water vapor content e_s is 0.51 psia or 3516 newtons/m^2 (from Figure A-1), so the surface vapor pressure is 2110 newtons/m^2.

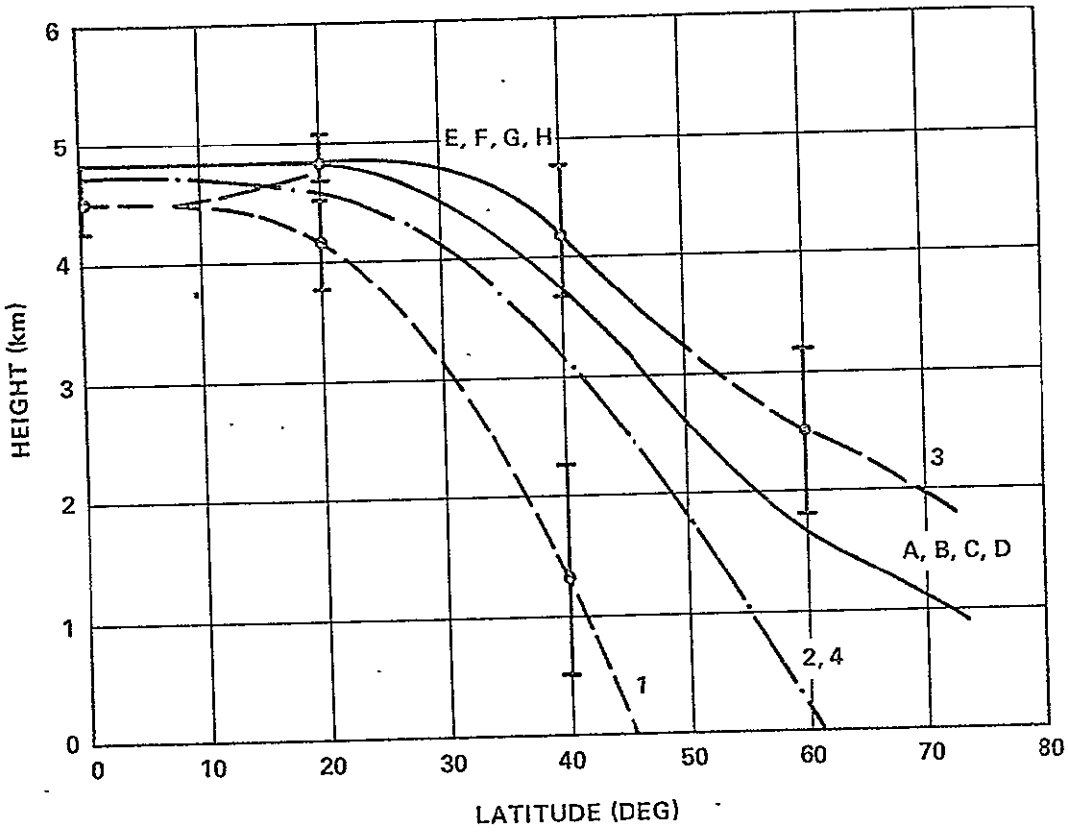

——— MODEL FOR RAIN RATE CLIMATES A THROUGH H

—·— ANNUAL

— — — SEASONAL 1 – WINTER (NORTHERN HEMISPHERE)
2 – SPRING
3 – SUMMER
4 – FALL

FIGURE A-2. LATITUDE DEPENDENCE OF ZONALLY AVERAGED 0°C ISOTHERM HEIGHT

The water vapor densities are computed from the ideal gas law at the ground station altitude A_1.

$$\rho_{w_s} = \frac{(R.H.)\ e_s}{R_w\ T} = \frac{(0.6)\ (3516)}{(461)\ (300)} = 1.53 \times 10^{-2}\ kg/m^3$$

$$\rho_{w_{0^oC}} = \frac{(0.6)\ (607)}{(461)\ (273.2)} = 2.9 \times 10^{-3}\ kg/m^3$$

The altitude of the 0°C isotherm is approximated from Figure A-2:

$$A_2 = 3700\ m$$

Using the formula to calculate the columnar water content yields:

$$R = \csc(47^o)\frac{(3700-880)\ (15.3 - 2.9) \times 10^{-3}}{\ln 15.3 - \ln 2.9} = 28.75\ kg/m^2$$

REFERENCES

2-1. H. J. Liebe, "Molecular Transfer Characteristics of Air Between 40 and 140 GHz," IEEE Trans. Micro. Th. Tech., Vol. MTT-23, No. 4, April, 1975, pp. 380-386.

3-1. M. Kerker, The Scattering of Light and Other Electromagnetic Radiation, Academic Press, New York, 1969.

3-2. D. V. Rogers, Comsat Laboratories, Clarksburg, MD, private communication, 1978.

3-3. J. O. Laws and D. A. Parsons, "The Relation of Raindrop-Size to Intensity," Trans. Am. Geophys. Union, Vol. 24, Oct./Nov., 1943, pp. 452-460.

3-4. R. L. Olsen, D. V. Rogers and D. B. Hodge, "The aR^b Relation in the Calculation of Rain Attenuation," IEEE Trans. Ant. and Prop., Vol. AP-26, March, 1978, pp. 318-329.

3-5. J. S. Marshall and W. McK. Palmer, "The Distribution of Raindrops With Size," Jrnl. Meteorology, Vol. 5, August, 1948, pp. 165-166.

3-6. J. Joss, J. C. Thans and A. Waldvogel, "The Variation of Raindrop Size Distributions at Locarno," Proc. Int. Conf. Cloud Phys., Toronto, Canada, August 26-30, 1968, pp. 369-373.

3-7. R. K. Crane, "Prediction of the Effects of Rain on Satellite Communication Systems," Proc. IEEE, Vol. 65, March, 1977, pp. 456-474.

3-8. R. Kaul, D. Rogers, and J. Bremer, "A Compendium of Millimeter Wave Propagation Studies Performed by NASA," ORI Report prepared under NAS5-24252, November, 1977.

3-9. J. Goldhirsh, "Attenuation of Propagation Through Rain for an Earth-Satellite Path Correlated with Predicted Values Using Radar," IEEE Trans. Ant. Prop., Vol. AP-24, pp. 800-806, November, 1976.

3-10. L. J. Ippolito, "Millimeter Wave Space Communications," Course Outline and Notes, The George Washington University, February 22-24, 1978.

3-11. D. C. Hogg and T. S. Chu, "The Role of Rain in Satellite Communications," Proc. IEEE, Vol. 63, No. 9, September 1975.

3-12. "Rain Attenuation Prediction," CCIR Doc. F5/003, 25 April 1978, prepared for the Special Preparatory Meeting, Geneva, 1978.

3-13. P. L. Rice and N. R. Holmberg, "Cumulative Time Statistics of Surface-Point Rainfall Rates," IEEE Trans. Comm., Vol. COM-21, pp. 1131-1136, October, 1974.

3-14. E. J. Dutton and H. T. Dougherty, "Modeling the Effects of Clouds and Rain Upon Satellite-to-Ground System Performance," Off. of Telecom. Report 73-5, March, 1973, NTIS No. COM-75-10950.

3-15. E. J. Dutton, "Earth-Space Attenuation Prediction Procedures at 4 to 16 GHz," Office of Telecomm. Report 77-123, May, 1977.

3-16. S. H. Lin, "A Method of Calculating Rain Attenuation Distribution on Microwave Paths," Bell Syst. Tech. Jrnl., Vol. 54, pp. 1051-1086, July-August, 1975.

3-17. E. J. Dutton, H. T. Dougherty and R. F. Martin, Jr., "Prediction of European Rainfall and Link Performance Coefficients at 8 to 30 GHz, U. S. Army Communications Command Tech. Report No. ACC-ACO-16-74, 1974, (NTIS AD-A000804).

3-18. H. B. Janes, J. T. Collins and F. K. Staeele, "Preliminary Catalog of Programs and Data for 10-100 GHz Radio System Predictions," Off. Telecom. Rpt. 78-141, March, 1978.

3-19. W. F. Bodtmann and C. L. Ruthroff, "Rain Attenuation on Short Radio Paths: Theory, Experiment, and Design," Bell Syst. Tech. Jrnl., Vol. 53, pp. 1329-1349 (September, 1974).

3-20. D.M.A. Jones and A. L. Sims, "Climatology of Instantaneous Precipitation Rates," Illinois State Water Survey at the Univ. of Illinois, Urbana, Ill. Project No. 8624, Final Report, December 1971.

3-21. S. H. Lin, "Nationwide Long-Term Rain Rate Statistics and Empirical Calculation of 11-GHz Microwave Rain Attenuation," Bell Syst. Tech. Jrnl., Vol. 56, p. 1581, November 1977.

3-22. S. H. Lin, "Empirical Calculation of Microwave Rain Attenuation Distributions on Earth-Satellite Paths," EASCON '78 Record, Arlington, VA, Sept. 25-27, 1978, pp. 372-378.

3-23. R. K. Crane and W. E. DeBrunner, "Worst-Month Statistics," Elect. Letters, Vol. 14, pp 38-40, 19 January 1978.

3-24. G. Drufuca, "Rain Attenuation Studies for Frequencies Above 10 GHz from Rain Gauge Observation," I.U.C.R.M. Colloquium on the Fine Scale Structure of Precipitation and EM Propagation, Nice, France, October 1975.

3-25. D. B. Hodge, "Frequency Scaling of Rain Attenuation," IEEE Trans. Ant. Prop., Vol AP-25, pp 446-7, May, 1977.

4-1. CCIR, Doc 5/287-E, "Attenuation and Scattering by Rain and Other Atmospheric Particles, "Working Group 5, 22 Sept. 1977.

4-2. Lao-Iun Lo, B. M. Fannin, and A. W. Straiton, "Attenuation of 8.6 and 3.2 mm Radio Waves by Clouds," IEEE Trans. Ant. Prop., Vol AP-23, pp 782-786, 1975

4-3. B. R. Bean and D. J. Dutton, Radio Meteorology, Ch. 7, Dover Publishing Co., New York, N.Y. 1968.

4-4. H. K. Weickmann and H. J. aufm Kampe, "Physical Properties of Cumulus Clouds," Jrnl. Meteor., Vol 10, pp 204-221, June 1953

4-5. R. K. Crane, "Propagation Phenomena Affecting Satellite Communications Systems Operating in the Centimeter and Millimeter Wavelength Bands," Proc. IEEE, Vol. 59, pp 173-188, February, 1971.

4-6. N. E. Gaut, E. C. Reifenstein III and D. T. Chang, "Microwave Properties of the Atmosphere, Clouds and the Oceans", Environment Research and Technology, Inc. Report for Project P-280, NASA/GSFC Contract NAS5-21624, March 1972, pg 4-4.

4-7. B. J. Mason, The Physics of Clouds, The Claredon Press, Oxford, 1971.

4-8. K. L. Koester and L. H. Kosowsky, "Attenuation of Millimeter Waves in Fog," 14th Radar Meteorology Conf., Tucson, Arizona, 17-20 November 1970.

4-9. J. J. George, "Fog in Compendium of Meteorology", Amer. Meteor. Soc., Boston, pp 1179-1189.

4-10. J. W. Ryde and D. Ryde, "Attenuation of Centimeter and Millimeter Waves by Rain, Fog and Clouds," Tech. Rept 8670, British General Electric Co, 1945

4-11. R. G. Eldridge, "Haze and Fog Aerosol Distributions," J. Atmos. Sci, Vol. 23, pp 605-613, 1966.

4-12. I. Y. Ahmed and L. J. Auchterlouie, "Microwave Measurements of Dust Using an Open Resonator," Electronics Letters, Vol. 12, No. 17, pp 445, 1976.

SECTION III

ORI
Silver Spring, Maryland 20910

PREDICTION OF PATH DIVERSITY FOR EARTH-SPACE PATHS

PROF. D.B. HODGE
ELECTROSCIENCE LABORATORY
OHIO STATE UNIVERSITY

A CONSULTANT FOR

ORI, INC.
SILVER SPRING, MD 20910
CONTRACT NAS5-23438, MOD. 68

OCTOBER 1978

TABLE OF CONTENTS

LIST OF FIGURES

LIST OF TABLES

1.0 PATH DIVERSITY

1.1 THE PATH DIVERSITY CONCEPT

Rain attenuation often degrades earth-space paths operating above 10 GHz so seriously that the requirements of economical design and reliable performance cannot be achieved simultaneously. To overcome this problem, Hogg (1968) proposed the use of path diversity on earth-space paths to achieve the desired level of system reliability at a reasonable cost compromise. This proposal was based on the hypothesis that rain cells and, in particular, the intense rain cells that cause the most severe fading are rather limited in spatial extent. Furthermore, these rain cells do not occur immediately adjacent to one another. Thus, one might expect that the probability of simultaneous fading on two paths to spatially separated earth terminals would be less than that associated with either individual path. This hypothesis was tested first by Wilson (1970) using radiometric noise emission measurements to determine the rain attenuation on separated paths and by Hodge (1974a) using actual earth-space paths. These and other ensuing experiments have clearly demonstrated that path diversity is an effective technique for improving system reliability in the presence of rain attenuation.

The reliability improvement resulting from the use of path diversity must ultimately be balanced against the increased system costs arising from the need for a second earth terminal site, antenna, equipment, and connecting link between the two earth terminals. Of course, redundant equip-

ment normally utilized at a single terminal might simply be separated physically to achieve this improvement at a reduced cost. Also, a judicious design might incorporate the connecting link as part of the trunk link to the earth terminals in order to further reduce the overall cost. Finally, the overall system reliability degradation due to the requirement of additional system equipment must be weighed also. This cost and equipment reliability will not be considered further in this discussion. The remainder of this discussion will be directed toward the design and performance of path diversity systems independent of cost and equipment reliability aspects.

A typical path diversity earth terminal configuration is shown in Figure 1.1-1 along with the definitions which will be used in the following discussion. The parameters are defined as follows:

Az = azimuth of earth-space path (degrees)

EL = elevation of earth-space path (degrees)

d = separation between earth terminals (km)

β = orientation of earth terminal baseline (degrees $0 \leq \beta < 180$)

$\emptyset$ = major axis of predominant rain cell orientation degrees, $0 \leq \emptyset < 180$)

Two alternative approaches (Brandinger-1978) have also been suggested as techniques for improving reliability in the presence of rain attenuation; these are angle and frequency diversity. The first, angle diversity, uses one ground site with more than one earth-space path to satellites located in separated orbital positions; thus, the paths are oriented along different azimuths. If a rain cell is located on one path at some distance from the terminal, the result will be quite similar to that for path diversity; however, if a rain cell is located near the terminal, little improvement results. This approach is not as effective as path diversity but may find utility in cases where multiple satellites are available.

The second approach, frequency diversity, is based on the frequency dependence of rainfall attenuation. In this case channel assignments both above and below 10 GHz are incorporated in the same system. Thus, in the event of rainfall, high priority traffic is diverted to the lower frequency which is less susceptible to rain attenuation. Thus, the channel capacity is adaptively reduced to

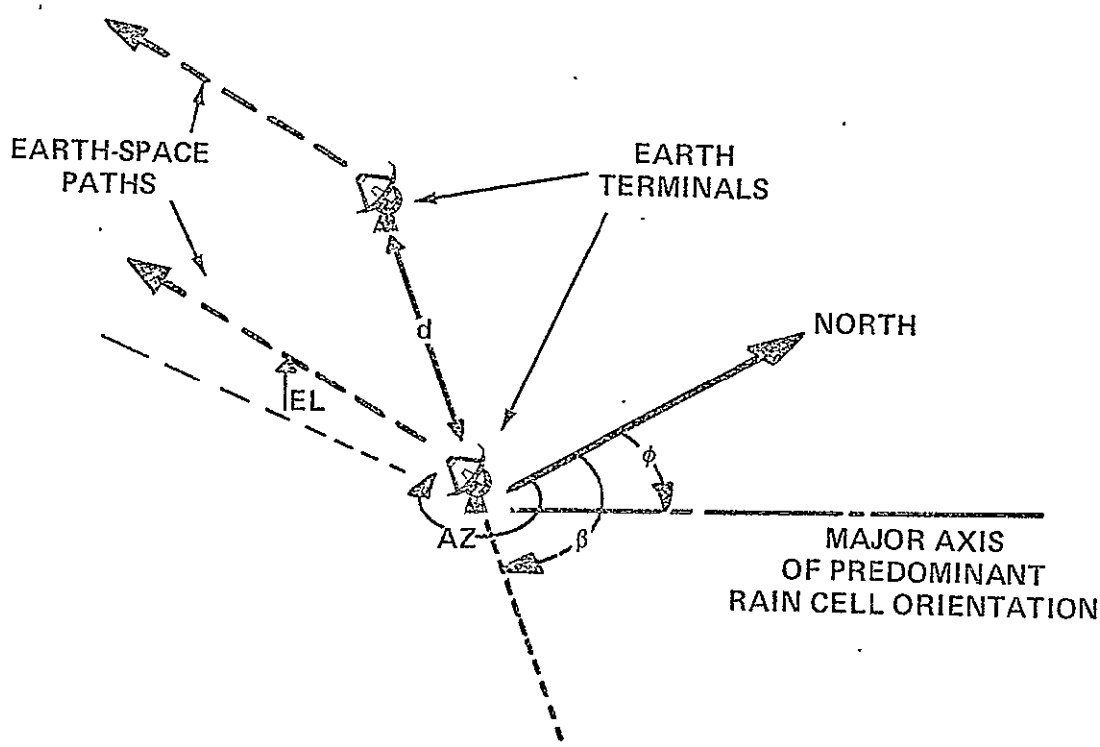

Figure 1.1-1 Path Diversity Configuration and Parameters

maintain reliability for a portion of the traffic. This is equivalent to assigning all high priority traffic to a lower frequency and tolerating a lower reliability channel above 10 GHz. This approach will probably not be useful in general applications.

1.2 DIVERSITY GAIN AND DIVERSITY ADVANTAGE

In order to characterize the performance of a path diversity system, it is convenient to establish a descriptive parameter for this purpose. Two such parameters have been proposed and utilized in the literature; they are diversity gain, G, and diversity improvement, I.

Let us consider the distribution of rain attenuation, i.e., excess path attenuation, fade depth, or attenuation above the clear sky level, exceeded on a single path, $A(T)^{\dagger}$, for a given percentage of time, T, and the rain attenuation, $A_{div}(T)$, exceeded jointly on two separated paths for the same percentage of time as shown in Figure 1.2-1. It appears to be more customary in the literature to plot A along the abscissa and T along the ordinate, even though A is generally taken to be a function dependent upon T. Obviously, if the attenuation distribution is measured or modelled properly, the functional relationship between A and T in any given experiment is unique whether one chooses to think of A being dependent upon T, A(T), or T being dependent upon A, T(A). Furthermore, given A(T), T(A) is immediately known. Therefore, both functional relations will be utilized in the following.

It should also be noted that <u>percentage time</u>, T(A), will be assumed to be equivalent to the probability of occurrence, P(A), multiplied by 100, T(A) = 100 P(A). This, of course, is only an approximation for experimental data of limited duration. Therefore, the term percentage time will be utilized in the following discussion instead of probability in order to emphasize this fact.

Diversity gain, G, (Hodge-1974a) may be defined as the difference between the rain attenuation exceeded on a single path and that exceeded jointly on separated paths for a given percentage of time, i.e.,

$$G(A) = A(T) - A_{div}(T) \qquad (1.2\text{-}1)$$

---

† In this section A denotes the total attenuation. AL_e was used in section II.

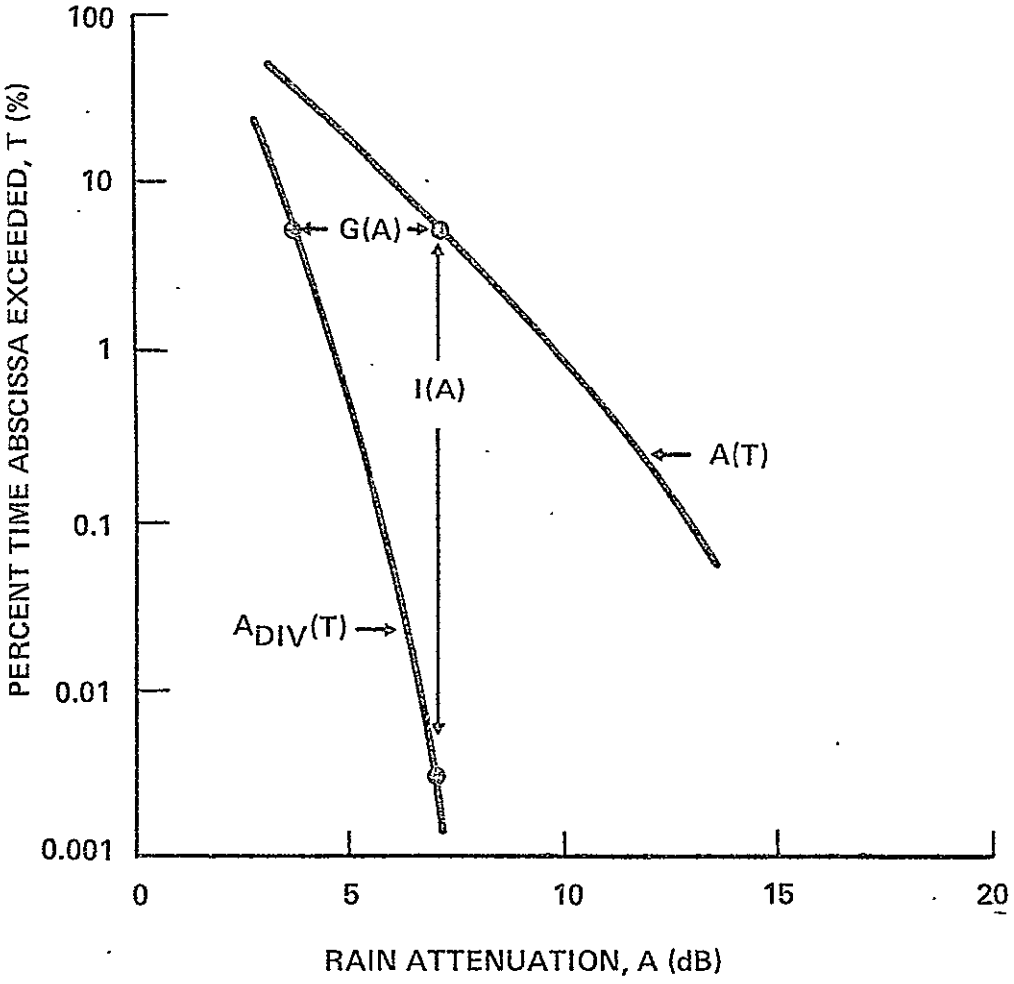

Figure 1.2-1 Hypothetical Rain Attenuation Distribution

Diversity advantage, I, (Wilson and Mammel-1973) may be defined as the ratio of the percentage of time exceeded on a single path to that exceeded jointly on separated paths for a given rain attenuation level, i.e.,

$$I(A) = \frac{T(A)}{T_{div}(A)} \qquad (1.2\text{-}2)$$

Diversity gain may be interpreted as the reduction in the required system margin at a particular percentage of time afforded by the use of path diversity. Alternatively, diversity advantage may be interpreted as the factor by which the fade time is improved at a particular attenuation level due to the use of path diversity.

Clearly, both diversity gain and advantage are functions of attenuation level or, implicitly, percentage of time. Furthermore, referring to Fig. 1.2-1, it is evident that the specification of either diversity gain or improvement along with single terminal fade distribution permits the joint attenuation to be reconstructed. Therefore, in principle, these two parameters are equivalent and contain the same information; however, in actual practice this is not the case. This can be seen by again referring to Fig. 1.2-1 and also observing that the uncertainty of experimental data increases as the percentage time of occurrence decreases. Now, the diversity gain determined at a particular fade depth depends upon two quantities, A(T) and $A_{div}(T)$, subject to uncertainties of the same order. In contrast, the diversity advantage associated with the same fade depth, A, will be a ratio of a quantity, T(A), subject to the same-order of uncertainty as that determining $G_{div}(A)$, to a quantity, $T_{div}(A)$, subject to a much larger uncertainty. Therefore, one may conclude that the diversity advantage factor will be subject to greater uncertainty than the diversity gain parameter associated with the same fade depth. The variability of the diversity advantage factors as compared with the diversity gains reported in the experimental literature and referred to in the following readily confirms this argument.

In the preceding discussion, it has been implicitly assumed that the fade distributions associated with each individual earth terminal were identical. However, in actual practice this is seldom the case. These distributions may differ because the measurement period is not long enough for the spatial rainfall distribution to become uniform; in this case the differences between the distributions are an indication of the uncertainty of the measurement. Alternatively, local climatological variations may give rise to real differences between distributions measured only a few kilometers apart; very little is known definitively about this latter effect. In general, however, since there is little or no basis to give greater weight to one distribution over another, the definitions given in eqs. 1.2-1 and 1.2-2 should be generalized for experimental data analysis to:

$$G(A) = A_{ave}(T) - A_{div}(T) \qquad (1.2\text{-}3)$$

$$I(A) = \frac{T_{ave}(A)}{T_{div}(A)} \qquad (1.2\text{-}4)$$

where $A_{ave}(T)$ is the average of the single terminal fade depth exceeded for the percentage time, T, and $T_{ave}(A)$ is the average of single terminal percentages of time exceeded at the fade level A.

1.3 DIVERSITY EXPERIMENTS

1.3.1 Experimental Methods

Four methods have been used to experimentally determine the performance of earth-space path diversity systems. The first, of course, is the direct measurement of path attenuation on actual earth-space paths using synchronous satellite beacons. This method is the most direct method but is expensive and relies on the availability of appropriate satellite beacons. The second method simulates path attenuation from measurements of radiometric noise emission. This radiometric technique is based on the simple relationship between radiometric sky temperature and path attenuation which is applicable when scattering is not significant, i.e., in rainfall at frequencies below

about 30 GHz. This method is generally less expensive than direct satellite beacons. However, as the path attenuation increases, the sky temperature asymptotically approaches the mean absorption temperature of the path, about 270°K; this limits the useful dynamic range of the inferred attenuation levels to approximately 10-12 db.

The third technique uses conventional meteorological radar measurements of backscatter from rainfall to estimate in turn the reflectivity, rain rate, and specific attenuation associated with each resolution cell. Path attenuations may then be found by summing the specific attenuation along the paths of interest. This approach is subject to uncertainties resulting from variations in the drop size distribution and the presence of ice, hail, and snow on the path. Nevertheless, the number of possible diversity configurations and paths that can be synthesized from digitally recorded reflectivity data makes this technique extremely attractive. It appears to be the only practical method for the study of spatial anisotropy, local climatological, and baseline orientation questions.

The fourth method utilizes radiometric measurements of solar emission to determine the atmospheric path attenuation. This method does not suffer from the dynamic range limitation of the radiometric method mentioned above. However, by virtue of the suntracking, the measurement paths are limited to a unique relationship between the path azimuth, path elevation, and local time of day. This makes the separation of dependences on these variables virtually impossible. Therefore, this latter technique will not be considered in detail in the following.

1.3.2 Experimental Results

The experimental diversity results available in the literature are summarized in Table 1.3.2-1. This table includes the results reported for each of the four methods described in the preceding section. In each case the reference is cited along with the location of the experiment, the frequency, separation distance, baseline orientation, path azimuth, and path elevation. In cases where multiple measurements are reported, the range of the appropriate parameters is indicated.

TABLE 1.3.2-1 SUMMARY OF DIVERSITY EXPERIMENTS

I. SATELLITE EXPERIMENTS

REFERENCE	LOCATION	FREQ.	SEPARATION	BASELINE	Az	EL
Hodge (1974)	Columbus, Ohio	15.3 GHz	4.0-8.3 km	159-164°	210°	38°
Hodge (1976b)	Columbus, Ohio	20-30	13.2-14.0	33-151°	197°	40°
Vogel, et al (1976)	Austin, Texas	30	11.0	0°	172°	55°
Hyde (1976)	Boston, Mass.	18	6.7-35.2	74-93°	212°	36°
	Columbus, Ohio	18	5.1-38.9	91-95°	196°	42°
	Starkville, Miss.	18	8.3-40.0	105°-113°	190°	51°

II. RADIOMETER EXPERIMENTS

Wilson (1970)	Crawford Hill, N.J.	16	3.2-14.4	135°	226°	32°
Wilson & Mammel (1973)	Crawford Hill, N.J.	16	11.2-30.4	135°	226°	32°
Gray (1973)	Crawford Hill, N.J.	16	19.0-33.0	45-135°	226°	32°
Funakawa & Otsu (1974)	Kokubunji, Japan	35	15.0	---	180°	45°
Hall & Allnutt (1975)	Slough, England	11.6	1.7-23.6°	20-106°	198°	30°
Allnutt (1976)	Slough, England	11.6	1.7-23.6°	20-106°	198°	30°
Strickland (1977)	Quebec, Canada	13	18.0	11°	122°	19°
	Ontario, Canada	13	21.6	1°	116°	16°
Bergmann (1977)	Atlanta, Georgia	17.8	15.8-46.9	141-146°	228°	38°
	Denver, Colorado	17.8	33.1	86°	197°	43°

III. RADAR EXPERIMENTS

Goldhirsh & Robison (1975)	Wallops Island, Va.	13-18	2-20	0-180°	0-360°	45°
Goldhirsh (1975)	Wallops Island, Va.	13-100	2-20	0-180°	0-360°	45°
Goldhirsh (1976)	Wallops Island, Va.	18	2-20	0-180°	0-360°	45°
Hodge (1978)	Montreal, Quebec	13	4-42	0-180°	122-240°	19-40°

IV. SUNTRACKER EXPERIMENTS

Wulfsburg (1973)	Boston, Mass.	35	11.2	158°	---	---
Funakawa & Otsu (1974)	Kokubunji, Japan	35	15.0	---	---	---
Davies & Croom (1974)	Slough, England	37	10.3	67°	---	---
Davies (1976)	Slough, England	37	10.3-18.0	67-110°	---	---

1.4 PATH DIVERSITY DESIGN FACTORS

1.4.1 Separation Distance

Diversity gain depends strongly upon the earth terminal separation distance, d. The diversity gain increases rapidly as d is increased over a small separation distance, i.e., up to about 10 km; thereafter the gain increases more slowly until a maximum value is reached, usually between about 10 and 30 km (Fig. 1.4.1-1). This maximum value is generally quite close to that value associated with uncorrelated fading at the individual earth terminals. The maximum value has been referred to in the literature as an optimum value in the sense that it is the largest observed value. It may be argued that negatively correlated rainfall along the separated paths could produce higher values of gain; however, no cases of this occurrence have been reported.

The uncorrelated diversity gain may be calculated from the single terminal attenuation distribution in the following manner. First, the conditional single terminal attenuation distribution, $P_c(A)$, is formed given that fading is occurring on the path. This is necessitated by virtue of the fact that the absence of fading on separated paths is well correlated during clear weather (Goldhirsh-1976). The joint conditional probability of uncorrelated attenuation on separated paths, $P_{div_c}(A)$, is then simply the square of the single path conditional probability, i.e.,

$$P_{div_c}(A) = \left[P_c(A)\right]^2 \qquad (1.4.1\text{-}1)$$

or

$$T_{div_c}(A) = \left[T_c(A)\right]^2/100 \qquad (1.4.1\text{-}2)$$

where the relationship between probability and percentage time is as described above. The relationships between the absolute and conditional quantities are

$$P(A) = P_R P_c(A) \qquad (1.4.1\text{-}3)$$

or

$$T(A) = T_R T_c(A)/100 \qquad (1.4.1\text{-}4)$$

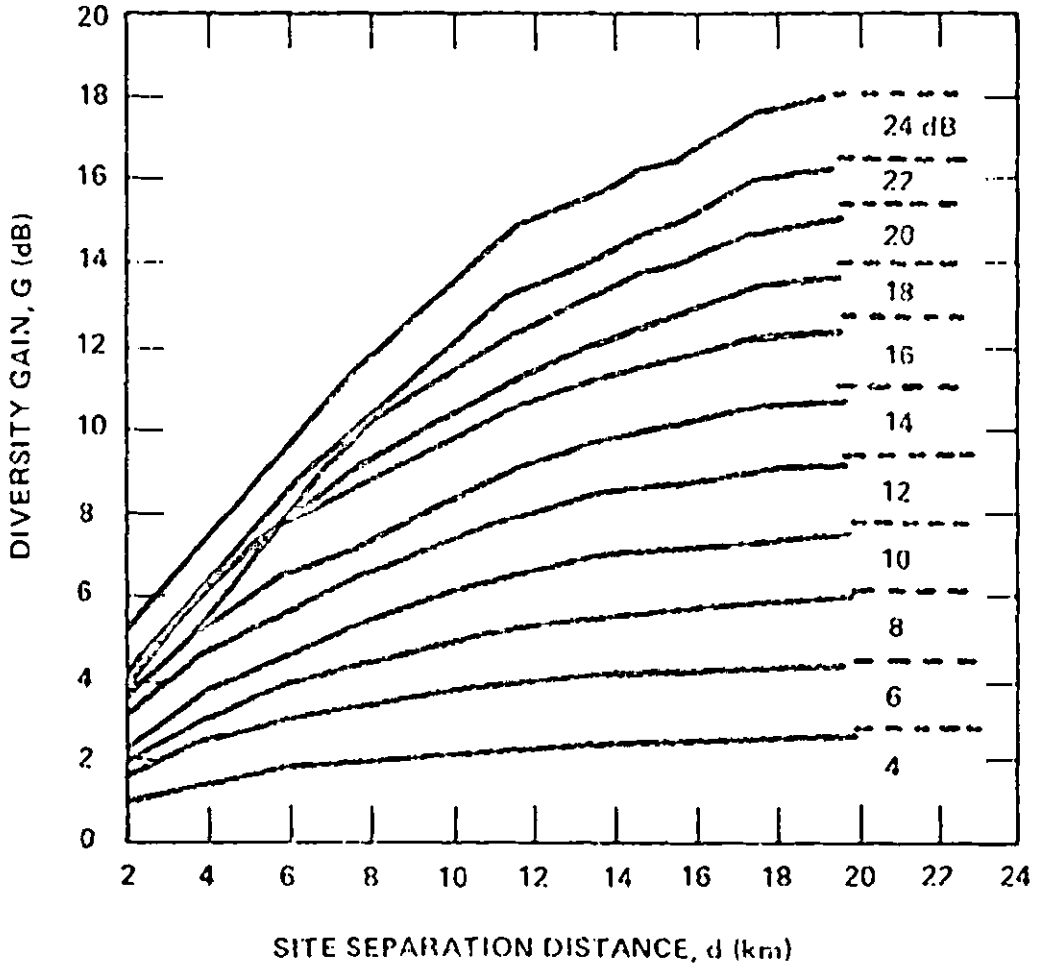

Figure 1.4.1-1 Diversity Gain, G, versus Separation Distance, d, f = 18 GHz. (Horizontal Dashed Lines Represent Optimum Labels) [Goldhirsh and Robison - 1975]

where the subscript R is associated with the probability or percentage time that rainfall attenuation is occurring on a single path.

A practical difficulty is associated with the determination of P_R and T_R. Namely, as a result of clear air and/or cloud induced scintillations on the received signal it is usually not possible to clearly distinguish between small rain induced fades and clear air scintillation. Therefore, it has been customary to establish a threshold of attenuation beyond which the fading is assumed to be due to rain. This level has been typically taken to be-tween 0.5 and 3.0 dB.

In contrast to the uncorrelated case, one may argue that correlated fading may occur for paths separated by distances associated with typical rain cell separation distances. This would tend to decrease the diversity gain over some range of separation distances. Such an effect may be inferred from the rainfall statistics of Freeny and Gabbe (1969); however, these statistics are associated with point rainfall rates rather than path average rainfall rates. Again, no definitive report of this effect has been published to date.

1.4.2 Baseline Orientation

The perpendicular separation between parallel paths is greatest when the earth terminals are located on a baseline perpendicular to the pro-jections of the paths on the earth's surface. This arrangement minimizes the possibility of both paths passing through the same rain cell. Nevertheless, the dependence of diversity gain on baseline orientation is quite weak except, possibly, for very short separation distances (Fig. 1.4.2-1).

The baseline orientation problem is further complicated if spatial anisotropy of the rain cells, i.e., a preferred direction of rain cell elongation, is known to exist in the region of interest. In this case, a baseline orientation perpendicular to the preferred axis of rain cell orientation would be desirable if the direction of the propagation path were ignored.

Considering both factors together, it appears that the most desirable baseline orientation is that which bisects the larger of the two angles between the projection of the propagation path and the preferred axis of rain cell orientation.

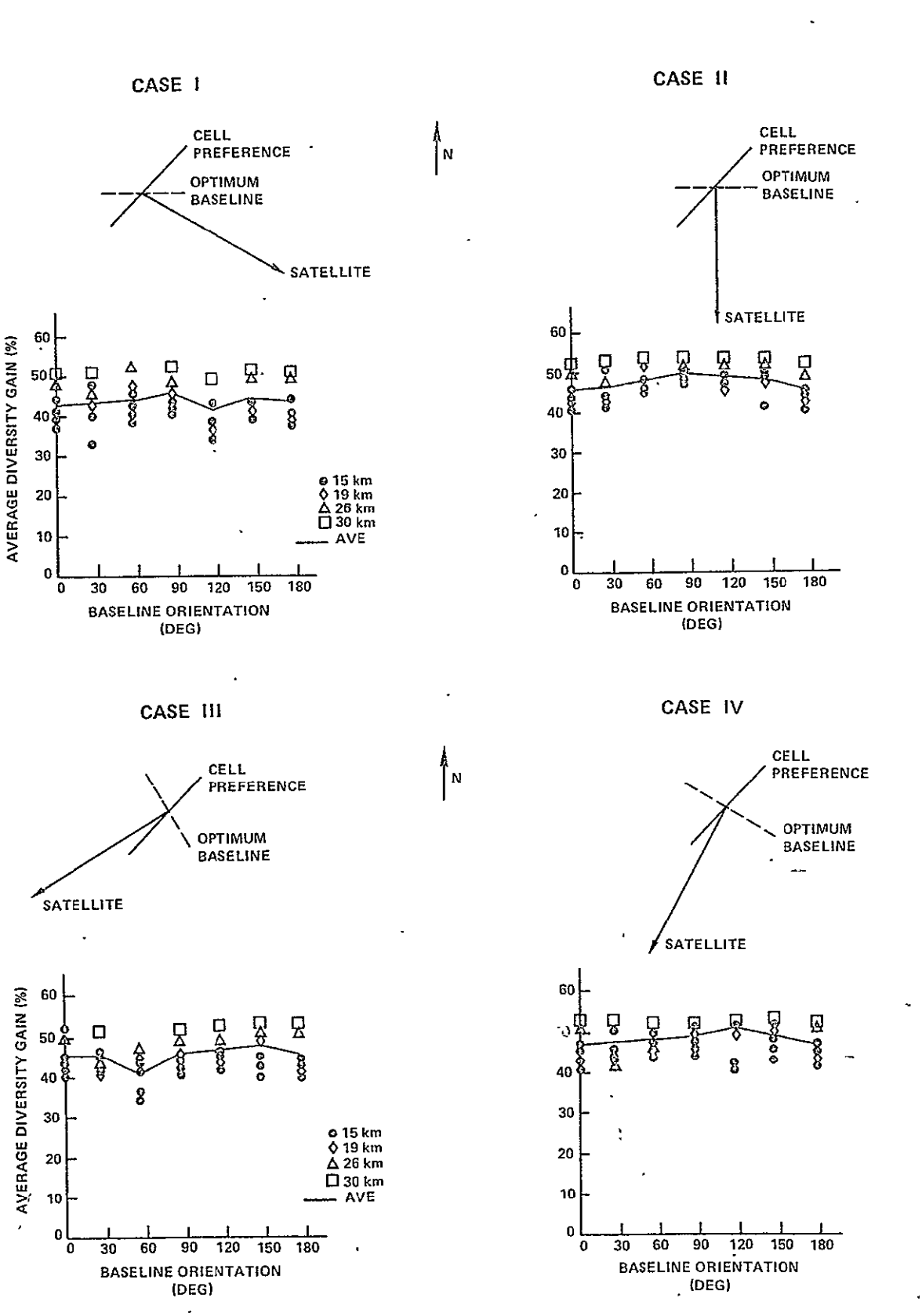

Figure 1.4.2-1 Average Diversity Gain versus Baseline Orientation (Hodge-1978)

1.4.3 Path Elevation Angle

The separation distance required to achieve a given level of diversity gain increases as the path elevation angle decreases (Hodge-1978). This is due to the increased likelihood of path intersections with rain cells at lower elevation angles. This effect is coupled to the problem of rain cell anisotropy and path azimuth as noted below.

1.4.4 Path Azimuth Angle

For synchronous satellites the path azimuth and elevation angles are not independent, and, thus, the dependence of diversity performance on these variables cannot be fully separated. If all rain cells were isotropic, one would expect no variation in diversity performance with azimuth angle other than that associated with the elevation angles. However, when rain cell anisotropy is considered, there appears to be a weak improvement in diversity performance for path azimuths in the quadrant not containing the preferred axis of rain cell orientation.

1.4.5 Link Frequency

Experimental measurements to data have shown no significant dependency of diversity gain on the link frequency (Goldhirsh and Robinson-1975) over the 10-30 GHz frequency. Certainly the probability of a given attenuation level being exceeded on a single path is strongly frequency dependent. However, diversity gain is a conditional statistic based upon the difference between single terminal and diversity attenuation levels. However, for link frequencies above 30 GHz, attenuation on both paths simultaneously can be sufficient to create an outage. Therefore, extrapolation beyond 30 GHz is not recommended.

1.4.6 Anisotropy of Rain Cells Along a Front

There is a tendency for convective rain cells associated with frontal activity to occur in bands nearly perpendicular to the direction of movement of the front. The direction of motion of the cells within such a band tends to be along or slightly ahead of the direction of the front, and, furthermore, the more intense cells tend to elongate in their direction of motion (Harrold and Austin-1974). Thus, two types of anisotropy are evident.

The first is associated with the elongation of individual cells and is related to the probability of parallel paths passing through the same cells. The second is associated with the statistics of the vector separation between rain cells and is associated with the probability of parallel paths simultaneously intersecting two different rain cells.

Fortunately, for simplicity's sake, these two preferred orientations are nearly parallel, and thus the same corrective action is required in each case. Namely, the baseline orientation should be nearly perpendicular to these preferred directions.

It should be noted at this point that diversity gain is not directly dependent upon either the speed or direction of rain cell motion; it is dependent only on motion through the relationship between motion and spatial anisotropy. On the other hand, fade duration statistics will be quite dependent upon the speed and direction of rain cell motion.

1.4.7 Local Climatology

To a first order of approximation it is commonly assumed that the probabilities of rain cell occurrence are uniformly distributed over rather large regions of the earth's surface. This assumption may be invalidated by the presence of any one of the following features: mountains, large valleys, large bodies of water, or urban heat "islands". These features can give rise to nonuniform spatial distributions of rain cell probabilities.

Spatial distributions of rainfall accumulation are readily available in the meteorological literature; however, it is not currently known whether the use of these data is applicable to the question of earth terminal siting. For example, it may be argued that these rainfall accumulations are dominated by low rainfall rates and thus do not reflect the spatial distributions of intense rain cells which dominate the occurrence of high attenuation levels on earth-space paths.

1.4.8 Switching Rates

The fading rate on a single path is relatively slow. The highest rates reported are on the order of 0.1 dB/sec. at 15 GHz (Hodge-1974a, Strickland-1977). This implies that the decision and switching process for diversity paths may be quite slow and should pose no significant problem in the system design.

1.4.9 Connecting Link

The implementation of a path diversity system must incorporate a connecting link between the two earth terminals. If this link is closed, i.e., waveguide, coax, etc., its performances will be independent of meteorological variables and will not directly influence the reliability improvement provided by the use of path diversity. If, however, the connecting link operates above 10 GHz in the atmosphere, the joint fading statistics of the connecting link with the earth-space paths must be considered. This degrading effect appears to be small except for cases of very long baselines or baseline orientations parallel to the earth-space propagation paths. (Ferguson and Rogers-1978)

1.4.10 Multiple Earth Terminals

Substantial link reliability improvements result from the use of two earth-space propagation paths. Thus one may conjecture that further improvement might result from the addition of additional diversity paths. Cost considerations generally make this approach unattractive. Furthermore, the resulting additional improvement is generally quite small. This can be observed by considering the uncorrelated fading case discussed earlier. The conditional probability of joint fading on N paths, given that fading occurs on a single path, is

$$P_{\substack{div \\ c_N}} = P_c^N(A) \qquad (1.4.10\text{-}1)$$

Determination of diversity gain for N diversity terminals shows that most of the gain is realized for two terminals with very little further increase in gain for additional terminals (Hodge-1974b).

2.0 PATH DIVERSITY DESIGN INFORMATION

2.1 EMPIRICAL MODEL

The data available from early diversity experiments in New Jersey and Ohio (Hodge-1974a, Wilson-1970, Wilson and Mammel-1973, Gray-1973) were used to develop an empirical model for the dependence of diversity gain on separation distance, d, and single site attenuation, A. (Hodge-1976a). The resulting model was of the form

$$G = a(1-e^{-bd}) \qquad (2.1\text{-}1)$$

where the coefficients a and b depended upon the single site attenuation according to

$$a = A - 3.6\ (1-e^{-0.24A}) \qquad (2.1\text{-}2)$$

$$b = 0.46\ (1-e^{-0.26A}) \qquad (2.1\text{-}3)$$

These results were nominally applicable to baseline orientations of 135°, i.e., NW-SE, elevation angles of 35°, azimuth angles of 220°, and link frequencies of 15 GHz. The model reproduced all of the available data at the time within 0.75 dB as shown in Fig. 2.1-1. The variation of the coefficients a and b are shown in Fig. 2.1-2.

The coefficient a represents the diversity gain achieved for large separation distances according to Eq. 2.1-1. From Eq. 2.1-2, it is seen that this achieved diversity gain is simply A-3.6 dB for large fade depths. In addition, referring to Eq. 2.1-1, the quantity 3/b is the separation distance required to achieve 95% of the maximum diversity gain for large fade depths; from the equation for b this model yielded a value of 6.5 km.

*The empirical relation should not be utilized for attenuation in excess of 15 or 20 dB, since it appears to reach an unphysical limit for large attenuation values such as those associated with frequencies above 30 GHz.

---

*This and the following paragraph were written by R. Kaul, ORI, Inc.

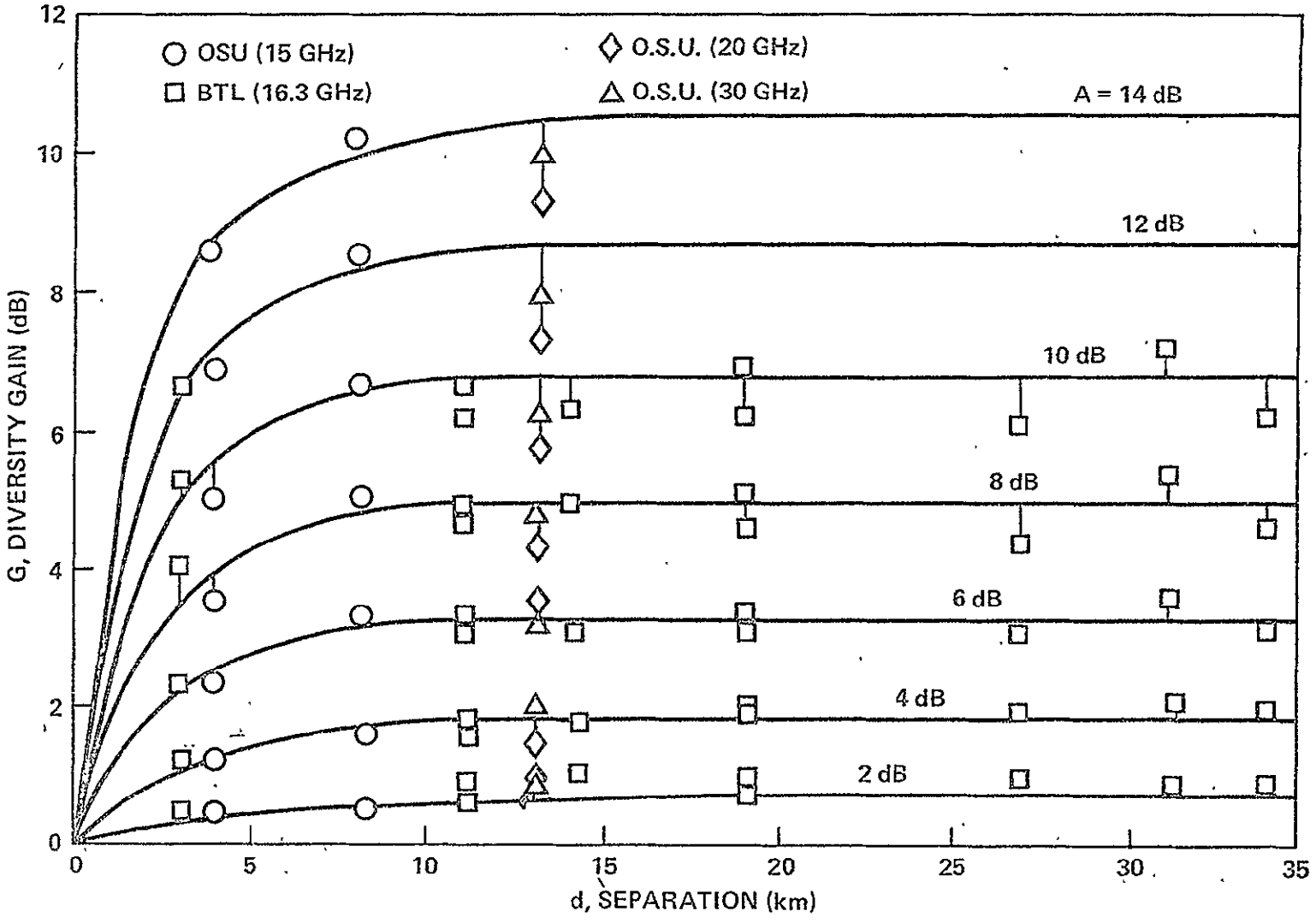

Figure 2.1-1 Diversity Gain versus Separation Distance

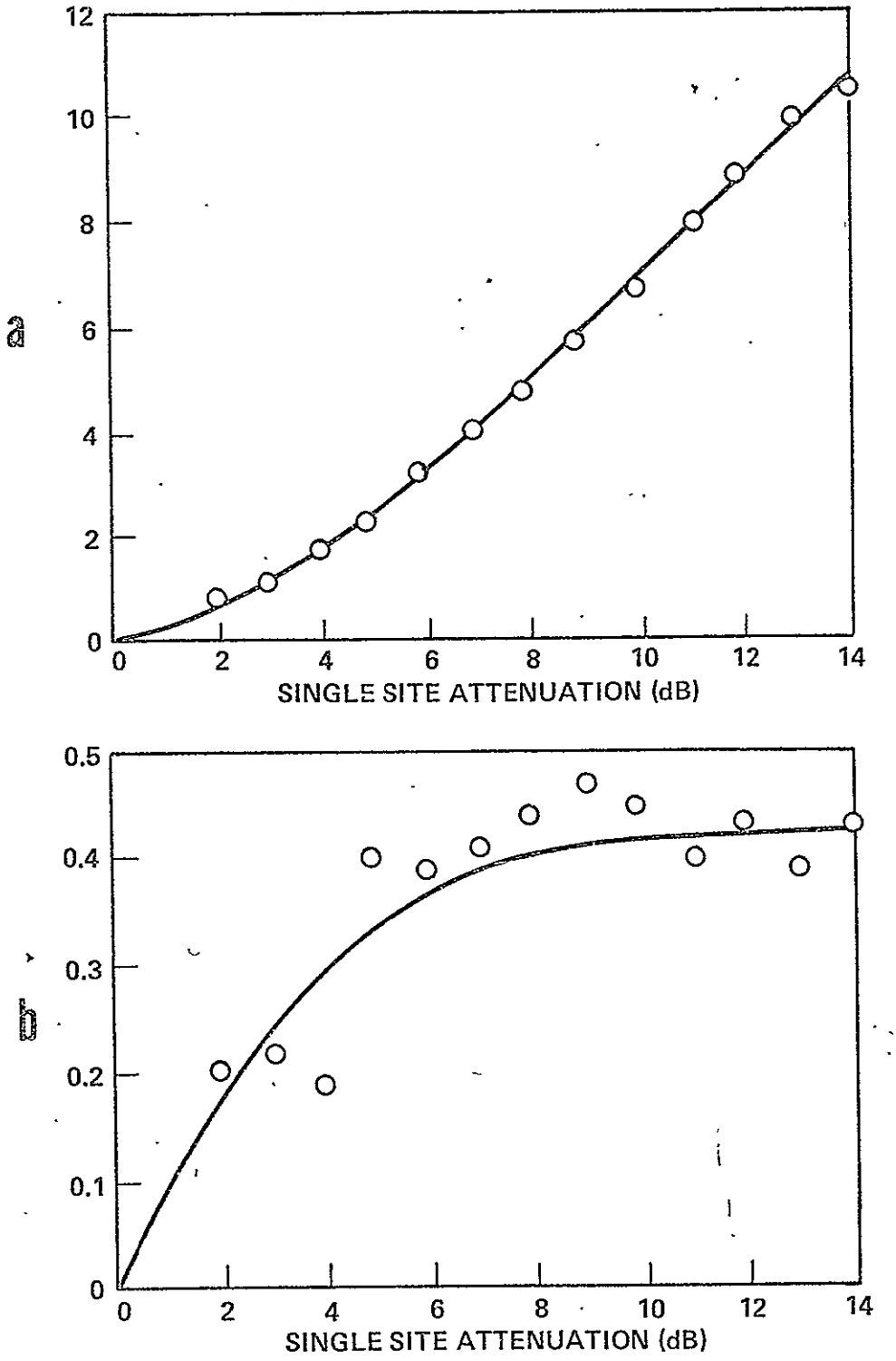

Figure 2.1-2 Variation of Empirical Model Coefficients with Fade Depth (Hodge-1976)

Consider the following relation for the link margin:

$$M' = M - A + G \qquad (2.1\text{-}4)$$

where M' is the link margin at any time and M is the zero-rain link margin. In the limit where A becomes large

$$M' \approx M - 3.6 - (A-3.6)e^{-0.46d} \qquad (2.1\text{-}5)$$

neglecting terms similar to $e^{-0.24A}$, etc. Thus for even moderate separation distances, $d \geq 10$ km

$$M' \approx M - 3.6 \qquad (2.1\text{-}6)$$

which says that the link only degrades 3.6 dB for any level af attenuation.

Rewriting Eq. 2.1-5 for A yields the amount of attenuation on the reference link allowable for a given M and M',

$$A = 3.6 + (M-M'-3.6)e^{+0.46d} \qquad (2.1\text{-}7)$$

Solving this for M = 20 dB, M'_{min} = 10dB for a low error rate and d = 10 km, yields

$$A_{max} = 3.6 + (20-10-3.6)e^{0.46d} \qquad (2.1\text{-}8)$$
$$\approx 640 \text{ dB!}$$

Clearly this is a physically unrealizable number. A term must be added to Eq. 2.1-7 and then into 2.1-1 to avoid this situation. The form of this term is now under study.

A more recent analysis of radar data near Montreal, Quebec, (Hodge-1978) has yielded considerably larger values of 3/b; they range from 13.8 to 31.3 km depending on the path azimuth and elevation angles. It is believed that these larger values are a result of the averaging method used to obtain the diversity gain in this case. The average percentage diversity gain was defined in this work to be

$$G_{ave} = \frac{1}{N} \sum_{i=1}^{N} \frac{G(A_i)}{A_i} \times 100 \qquad (2.1\text{-}9)$$

and the coefficient resulting from the modeling of $G_{ave} = a(1-e^{-bd})$ are given in Table 2.1-1.

TABLE 2.1-1 COEFFICIENTS FOR EMPIRICAL MODEL BASED ON MONTREAL DATA
(f = 13 GHz, Hodge-1978)

CASE	Az	El	a	b	3/b
I	121.5°	18.5°	53.0%	0.096 km^{-1}	31.3 km
II	181.5	37.7	51.2	0.155	19.4
III	240.1	17.9	50.5	0.126	23.8
IV	210.0	40.0	51.6	0.156	19.2

2.2 USE OF THE EMPIRICAL MODEL

The experimental results in Figure 2.1-1 do demonstrate that the diversity gain does appear to apply up to the 8 to 10 dB level in the 10 to 30 GHz frequency range. Using this fact, the cumulative attenuation statistics for a hypothetical ground station system of two identical stations separated by 10 to 15 km at Rosman, N.C., would yield statistics significantly better than one station. These are shown in Figure 2.2-1 based on the attenuation data obtained by the distribution extension technique in Section II. The diversity gain is the difference in attenuation levels for a given percentage of exceedance. For example, at A = 10 dB the diversity gain is approximately 6.7 dB (see Figure 2.1-1). The diversity advantage (defined in Figure 1.2-1) would be about 4.8 at A = 3.3 dB.

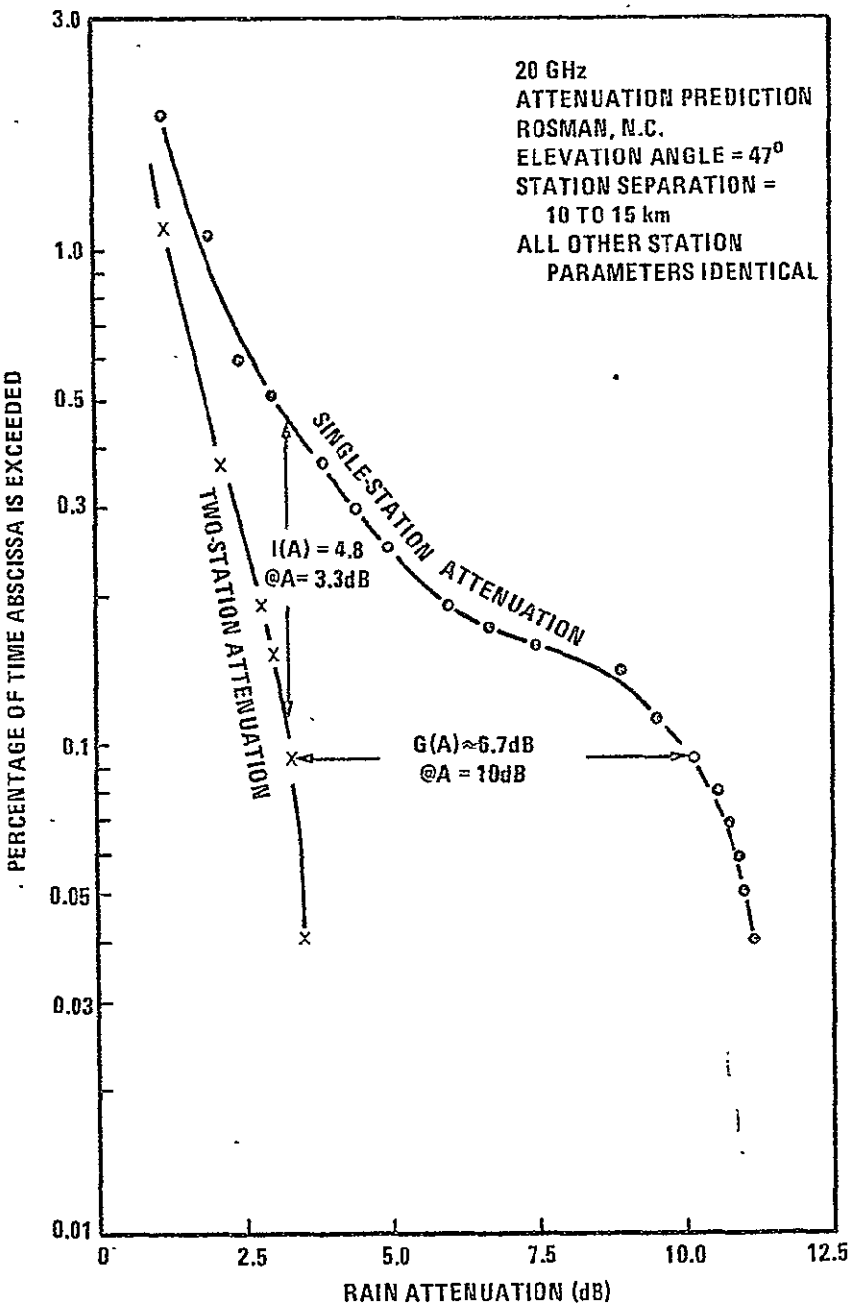

FIGURE 2.2-1. PATH DIVERSITY GAIN STATISTICS FOR ROSMAN, N.C.

REFERENCES

Allnutt, J.E., and J.E. Hall (1974), "Site Diversity Advantage for Satellite Communication at 11.6 GHz," Electronics Letters, V. 10, p. 527.

Allnutt, J.E. (1976), "Slant Path Attenuation and Space Diversity Results using 11.6 GHz Radiometers," Proceedings IEE, V. 123, p. 1197.

Bergmann, H.J. (1977), "Satellite Site Diversity: Results of a Radiometer Experiment at 13 and 18 GHz," IEEE Trans. Ant. Prop. V. AP-25, p. 483.

Brandinger, P. (1978), "Propagation Requirements for 30/20 GHz System Design," 1978 Spring URSI Meeting, Washington, D.C.

Davies, P.G., and D.L. Croom (1974), "Diversity Measurements of Attenuation at 37 GHz with Solar-Tracking Radiometers," Electronics Letters, V. 10, p. 482.

Davies, P.G. (1976), "Diversity Measurements of Attenuation at 37 GHz with Sun-Tracking Radiometers in a 3-site Network," Proceedings IEE, V. 123, p. 765.

Ferguson, A., and R.R. Rogers (1978), "Joint Statistics of Rain Attenuation on Terrestrial and Earth-Space Propagation Paths," Radio Science V. 13, p. 471.

Freeny, A.E., and J.D. Gabbe (1969), "A Statistical Description of Intense Rainfall," Bell System Technical Journal, V. 48, p. 1789.

Funakawa, K., and Y. Otsu (1974), "Characteristics of Slant Path Rain Attenuation at 35 GHz Obtained by Solar Radiation and Atmospheric Emission Observations," Journal de Recherches Atmospherique, V. 8, p. 339.

Goldhirsh, J., and F. Robison (1975), "Attenuation and Space Diversity Statistics Calculated from Radar Reflectivity Data of Rain," IEEE Trans. Ant. Prop. V. AP-23, p. 221.

Goldhirsh, J. (1975), "Prediction Methods for Rain Attenuation Statistics at Variable Path Angles and Carrier Frequencies Between 13 and 100 GHz," IEEE Trans. Ant. Pro., V. AP-23, p. 786.

Goldhirsh, J. (1976), "Path Attenuation Statistics Influenced by Orientation of Rain Cells (1976)," IEEE Trans. Ant. Prop., V. AP-24, p. 792.

Gray, D.A. (1973), "Earth-Space Path Diversity: Dependence on Base Line Orientation," 1973 G-AP/URSI Meeting, Boulder, Colorado, 1973.

Hall, J.E., and J.E. Allnutt (1975), "Results of Site Diversity Tests Applicable to 12 GHz Satellite Communications," IEE Conference Publication No. 126, "Satellite Communication Systems Technology," London.

Harrold, T.W., and P.M. Austin (1974), "The Structure of Precipitation Systems - A Review," Journal de Recherches Atmospherique, V 8, p. 41.

Hodge, D.B. (1974a), "Path Diversity for Reception of Satellite Signals," Journal de Recherches Atmospherique, V. 9, p. 443.

Hodge, D.B. (1974b), "A 15.3 GHz Satellite-to-Ground Path Diversity Experiment Utilizing the ATS-5 Satellite," Radio Science, V. 9, p. 1.

Hodge, D.B. (1976a), "An Empirical Relationship for Path Diversity Gain," IEEE Trans. Ant. Prop., V. AP-24, p. 250.

Hodge, D.B., D.M. Theobold, and R.C. Taylor (1976b), "ATS-6 Millimeter Wavelength Propagation Experiment," Ohio State University, ElectroScience Laboratory, Rept. 3863-6.

Hodge, D.B. (1978), "Path Diversity for Earth-Space Communication Links," Radio Science, V. 13, p. 481.

Hogg, D.C. (1968), "Millimeter Wave Communication through the Atmosphere," Science V. 159, p. 39.

Hyde, G. (1976), "Data Analysis Report - ATS-F Comsat Millimeter Wave Propagation Experiment," Comsat Laboratories, Clarksburg, Maryland.

Strickland, J.I. (1974), "Radar Measurements of Site Diversity Improvement During Precipitation," Journal de Recherches Atmospherique, V 8, p. 451.

Strickland, J.I. (1977), "Radiometric Measurements of Site Diversity Improvement at Two Canadian Locations," URSI Commission F Symposium, LaBaule, France.

Vogel, W.J., A.W. Straiton, B.M. Fannin, and N.K. Wagner (1976), "Attenuation Diversity Measurements at 20 and 30 GHz," Radio Science, V. 11, p. 167.

Wilson, R.W. (1970), "A Three-Radiometer Path Diversity Experiment," Bell System Technical Journal, V. 49, p. 1239.

Wilson, R.W., and W.L. Mammel (1973), "Results from a Three Radiometer Path Diversity Experiment," Processings of Conference on Propagation of Radio Waves at Frequencies above 10 GHz, London, p. 23.

Wulfsburg, K.N. (1973), "Path Diversity for mm-wave Earth-to-Satellite Links," Radio Science, V. 8, p. 1.

SECTION IV

ORI
Silver Spring, Maryland 20910

PREDICTION OF SIGNAL FLUCTUATIONS AND LOW ANGLE FADING ON EARTH-SPACE PATHS

DR. D.M. THEOBOLD
OHIO STATE UNIVERSITY

AND

DR. ROGER KAUL
ORI, INC.

NOVEMBER 1978

TABLE OF CONTENTS

LIST OF FIGURES

TABLE 1

1.0 INTRODUCTION

1.1 MECHANISMS FOR SIGNAL FLUCTUATIONS AND LOW ANGLE FADING

The amplitude, phase, and angle-of-arrival of a microwave signal passing through the troposphere vary due to inhomogeneities in the refractivity (clear air), clouds and rain. The effects occur on time scales shorter than a minute and on spatial scales shorter than a kilometer.

1.2 ANTENNA APERTURE EFFECTS

The effects of the tropospheric turbulences and the antenna can not be totally decoupled because, of course, the measurements and operating systems utilize antennas. The antenna aperture processes the incident wavefront with its spatial and temporal fluctuations into a received signal with only temporal variations.

Wavefront tilt due to inhomogeneities and gradients in the refractivity appear to the antenna as an angle-of-arrival variation. Average elevation angle ray bending is usually 10 times more pronounced than azimuthal ray bending. However wave tilt fluctuations tend to be randomly distributed in angle relative to the slant path porpagation direction, at least when the majority of the path is above the regime of surface effects (surface effects extend upwards several hundred meters).

Fluctuations occurring on spatial scales smaller than the size of the aperture are often referred to as wavefront ripple. This phase incoherence results in an instantaneous gain loss or degradation.

The fluctuations described herein apply to the ground station downlink because its antenna is in close proximity to the turbulent medium. An uplink satellite path will suffer fluctuation gain degradation only due to scattering of energy out of the path. Because of the large distance traversed by the wave since leaving the troposphere, the wave arrives at the satellite antenna as a plane wave (no ripple) and with only minute angle-of-arrival effects.

2.0 AMPLITUDE FLUCTUATIONS BASED UPON THE COMBINED EFFECTS OF AMPLITUDE AND ANGLE-OF-ARRIVAL FLUCTUATIONS -- MODEL AND EXPERIMENTAL RESULTS

2.1 OVERVIEW

The phenomena of amplitude and angle-of-arrival fluctuations combine to form received signal amplitude fluctuations. For many cases of propagation one or more of these effects may often be neglected. For example, a receiving system which employs an antenna with a wide beamwidth will not experience angle-of-arrival-induced amplitude fluctuations for most elevation angles. However, such simplification is not always possible. The theory of wave propagation and scattering in random media allows a combination of the turbulence-induced effects to be performed in the context of weak fluctuation along a line-of-sight path. The work of Ishimaru (1978), which defines coherent and incoherent field components as a plane wave propagates through a random medium, provides a method of combining amplitude and angle-of-arrival effects into a model of received signal amplitude fluctuation. A model utilizing the concept of incident plane wave decomposition (see Figure 1) has been proposed by Theobold and Hodge (1978).

2.2 VARIANCE OF RECEIVED SIGNAL AMPLITUDE

The assumption of weak turbulence, i.e., log-amplitude variance $\sigma_\chi^2 < 0.5$, is invoked for a plane wave incident on a region of turbulence, propagating a distance L(km) and impinging on a circular aperture of diameter

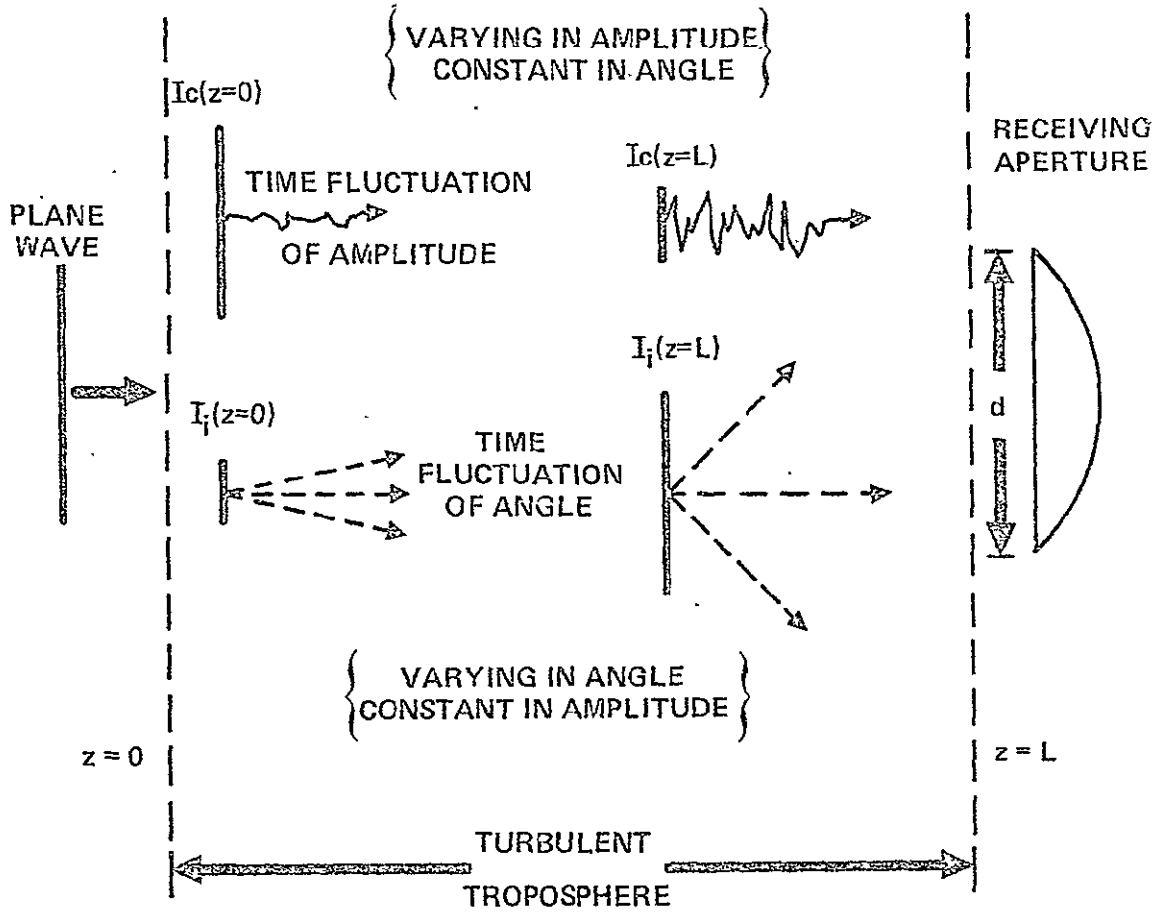

Figure 1. Decomposition into Coherent and Incoherent Components

d (meters). The antenna is assumed to have a Gaussian pattern function with half-power beamwidth B (degrees). If v is the received signal amplitude, an expression for signal variance relative to average power is

$$S^2 = 10 \log_{10} \frac{\langle v^2 \rangle - \langle v \rangle^2}{\langle v \rangle^2}$$

$$= 10 \log_{10} \frac{I_c \sigma_1^2 + \dfrac{I_i B^2}{8 \sigma_2^2 \ln(2) + B^2} - I_i \left(\dfrac{B^2}{4 \sigma_2^2 \ln(2) + B^2} \right)^2}{I_c + I_i \left(\dfrac{B^2}{4 \sigma_2^2 \ln(2) + B^2} \right)^2}$$

where

$I_i = 1 - \exp\left[-L/L_0\right]$

$I_c = (1 - I_i) / (1 + \sigma_1^2)$

σ_1^2 = amplitude variance $\approx \sigma_x^2$

σ_2^2 = angle-of-arrival variance (deg^2)

L = path length

L_0 = a function of density and cross-section of scattering along the path

Measurements at The Ohio State University of the ATS-6 2, 20 and 30 GHz beacons as the satellite underwent synchronous orbit transition were used to derive empirical constants for this model with an effective turbulence height, h, of 6 km (typical), r_e = mean earth radius = 6377 km, θ = elevation angle, and L = path length.

$$L = \left[h^2 + 2r_e h + (r_e \sin\theta)^2\right]^{\frac{1}{2}} - r_e \sin\theta.$$

The constants were

$L_0 = 180$ km

$\sigma_1^2 = 2.6 \times 10^{-7} f(\text{GHz})^{7/12} L(\text{km})^{11/6}$

$\sigma_2^2 = 5.67 \times 10^{-6} L(\text{km})^{1.56} d(\text{m})^{-1/3}$

A plot of the variance measurement, S^2, expressed in dB, is shown in Figure 2 for four representative frequencies for a 4.6 m diameter aperture. S^2 is plotted as a function of elevation angle and equivalent path length for a 6 km high region of turbulence.

Figure 2 represents the average S^2 as derived from the O.S.U. empirical constants. However, since both σ_1^2, and σ_2^2 may be represented in closed form as a function of C_n^2 (Tatarski-1961), instantaneous, diurnal, or seasonal values for S^2 may be found from this model given an estimate of the appropriate C_n^2.

2.2.1 Applicability of the Model

The empirical constants which were found from observed data are applicable for the prediction of average turbulence-induced propagation effects in a temperate climate, during the warmer seasons of the year, and under non-precipitating clear-air conditions. It is necessary to derive local estimates of C_n^2 for the model if these conditions are not the same.

2.2.2 Distribution of Amplitude Variance

It is known that peak-to-peak variations of 30 N-units in the refractive index are expected on a time scale of days and hours (Theobold-1978). Corresponding fluctuations in received signal amplitude variance expressed in dB would be expected to be about 20 dB peak-to-peak for a fluctuation of 30 N-units out of an average of 345. Figure 3 shows a representative case of average amplitude variance at 30 GHz for a 4.6 m diameter aperture as a function of elevation angle. Curves for plus or minus 10 dB variation in C_n^2 about the average are shown for comparison.

A more exact representation of the expected distribution of amplitude variance may be obtained given measured statistics of variance variability about the average. Figures 4 and 5 present probability distribution functions of variance differences for 2 and 30 GHz earth-space signals measured over a period of 26 days. The satellite was undergoing transition in elevation from 0.38^0 to 45^0 and the mean variance was removed as a function of elevation angle. The 90% confidence limits of 14.6 and 14.7 dB, respectively, are in good agreement with the statistics of expected refractive index variation.

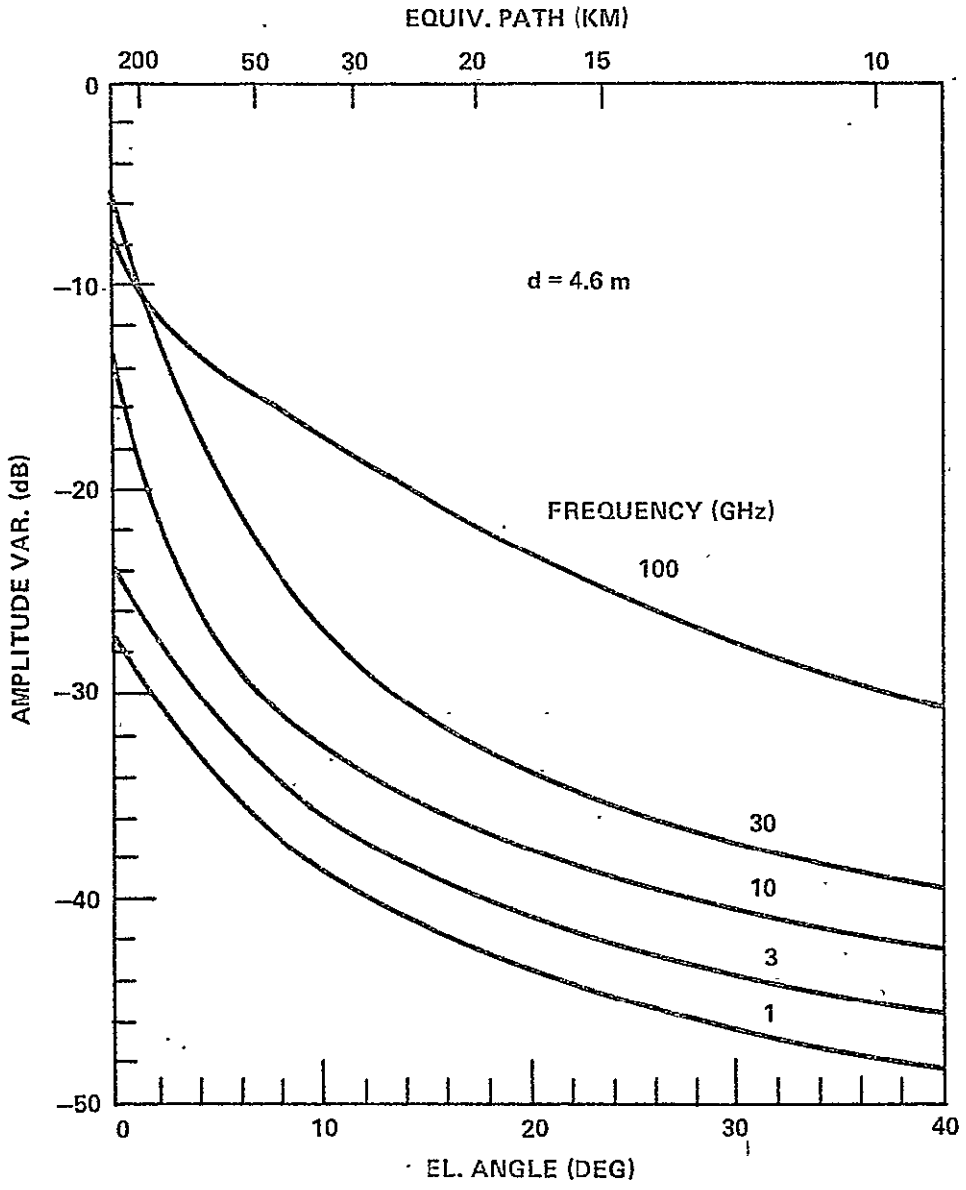

Figure 2. Amplitude Variance for a 4.6m Diameter Aperture for 1 to 100 GHz

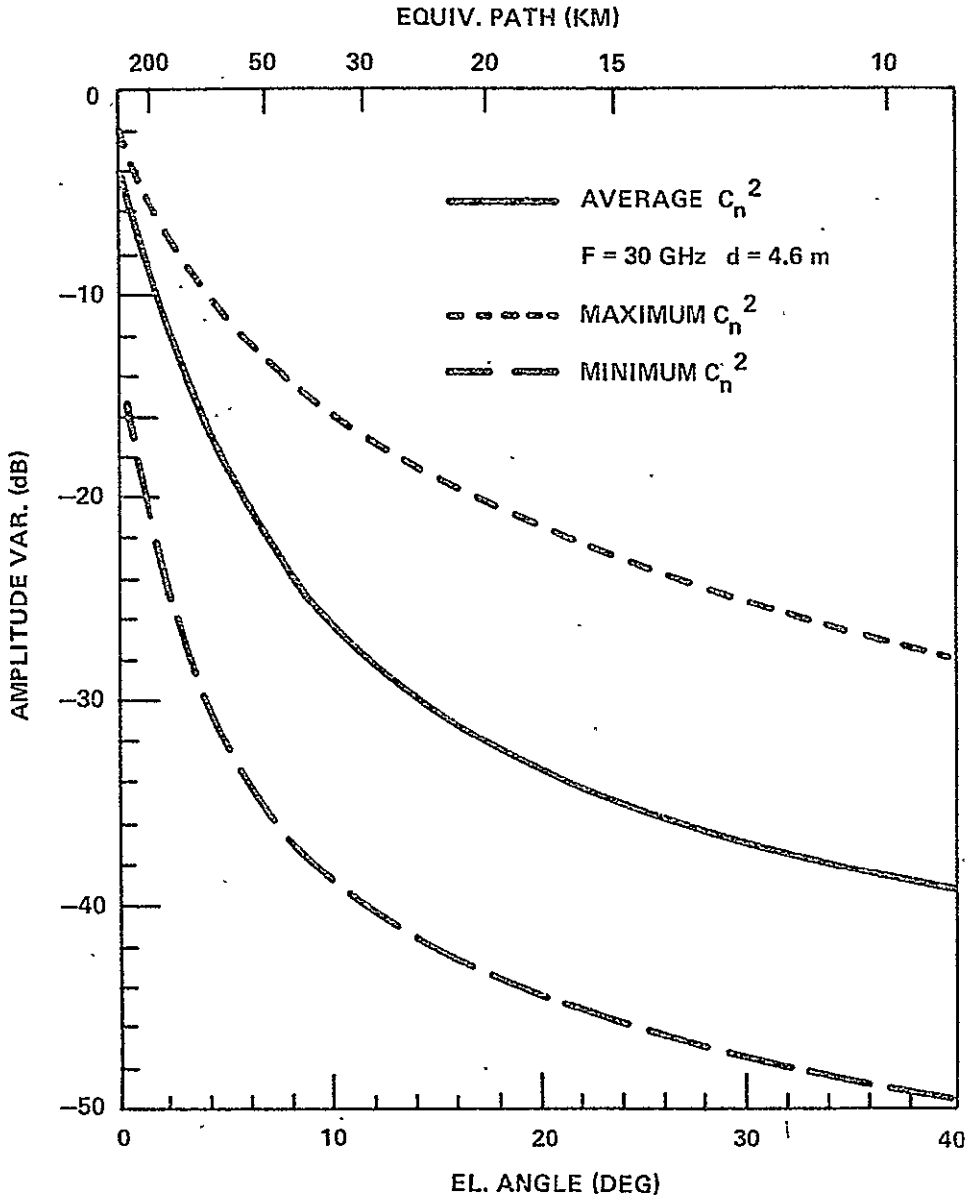

Figure 3. Effect of 20 dB Peak-to-Peak Variation of C_n^2 on Amplitude Variance

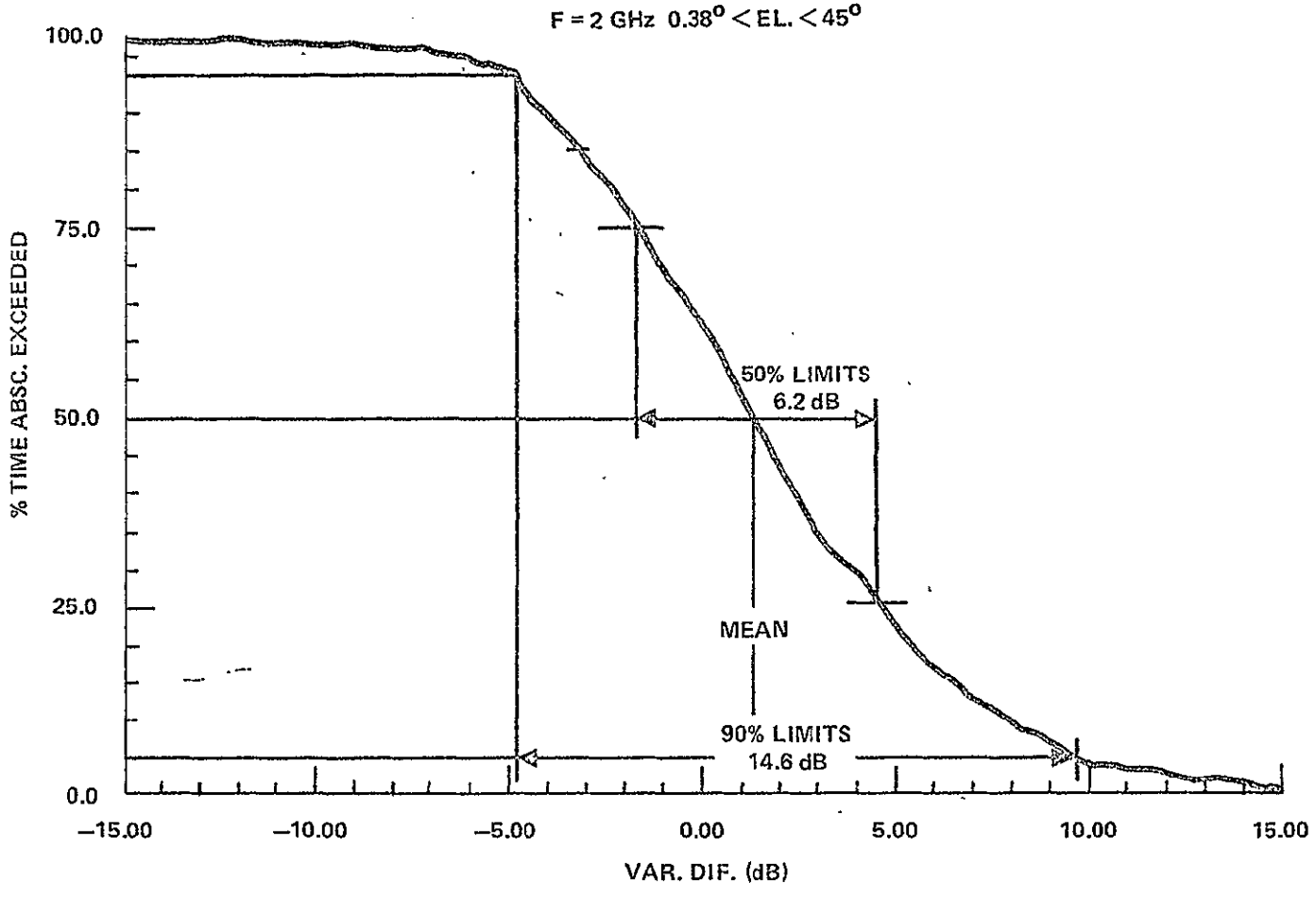

Figure 4. Distribution of Amplitude Variance from that Predicted from Average Turbulence-Induced Fluctuation Theory

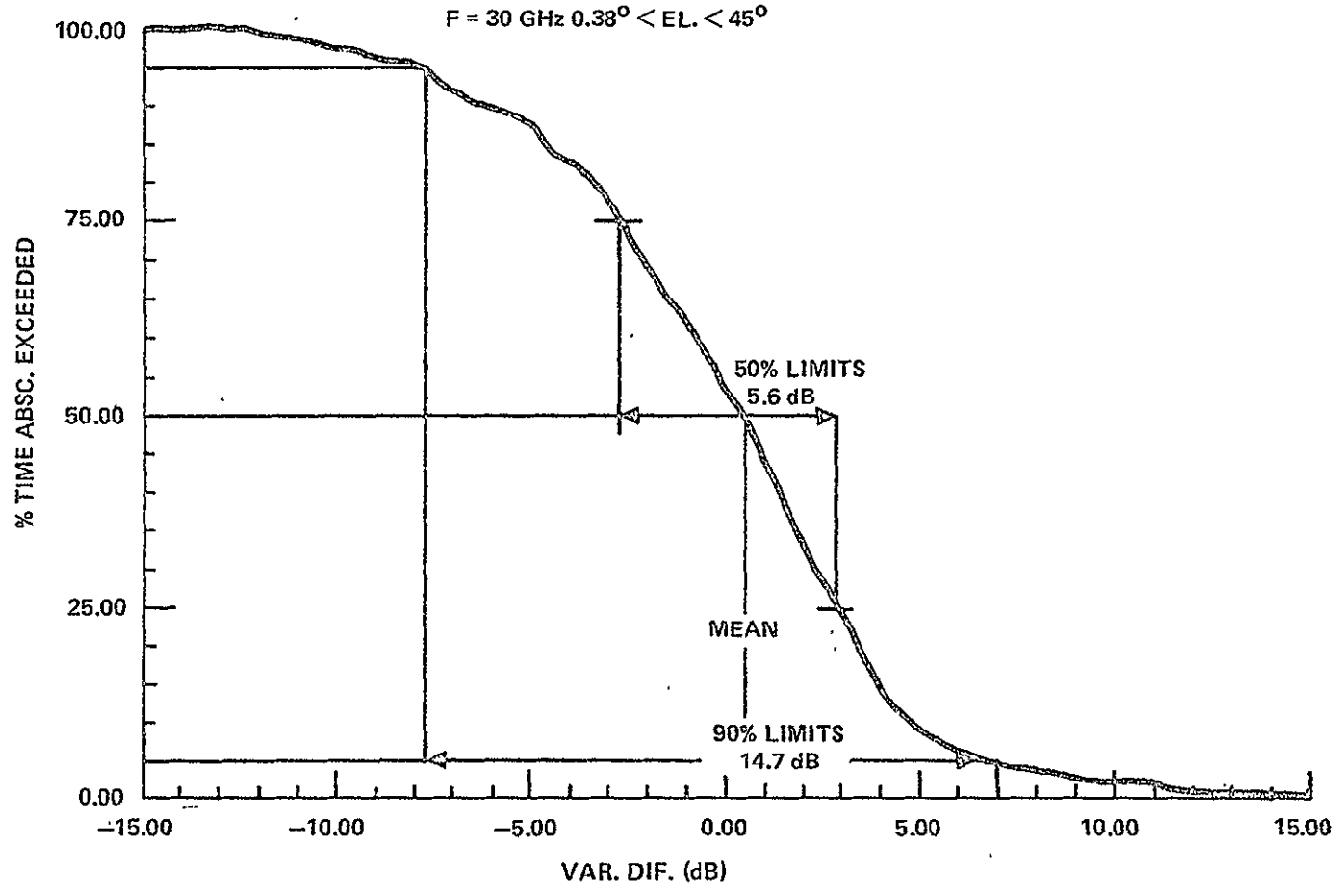

Figure 5. Distribution of Amplitude Variance from that Predicted from Average Turbulence-Induced Fluctuation Theory

2.2.3 Power Spectral Density

The formulation of the structure of the power spectral density of turbulence-induced amplitude fluctuations has been derived from classical turbulence theory (Tatarski-1961). The theoretical spectrum of amplitude fluctuations in a medium characterized by a real refractive index is found to roll off as $f^{-8/3}$, or -26.6 dB/decade, in frequency f. This behavior is not a function of operating frequency, as long as the wavelength is small or on the order of the smallest refractive inhomogeneities. Deviation from this slope will occur due to non-stationarity of the scintillation process.

The spectral slope was calculated for time records of 102.4 seconds at 2 and 30 GHz on the ATS-6 CW beacons as the satellite moved in elevation angle from 0.38 to 25 degrees (Baxter and Hodge -- 1978). Spectral slope was found to be essentially independent of equivalent path length and measured statistics were well centered about the theoretical value of -26 dB/decade. Figures 6 and 7 present the probability distribution functions of the 2 and 30 GHz spectral slopes, respectively. Figure 8 presents the worst-case confidence limits of distribution of spectral slope from an average -26.6 dB/decade, for 50% and 90% of total time. Such an estimate may be used to directly find the expected fading rates and spectral components due to turbulence-induced amplitude scintillation. The data represents clear air statistics over a period of 26 days.

2.3 LOW ANGLE SCINTILLATIONS/FADING

Measurement of low elevation angle scintillations or fading have been made while ATS-6 was descending and ascending for US observers. In addition, measurements of non-synchronous satellites have been made as their path sweeps through the atmosphere (Crane - 1977). These latter measurements are not reported here.

As ATS-6 was being moved to 35^{o} E longitude, experimenters at the Virginia Polytechnic Institute and State University measured the 20 GHz carrier amplitude during clear and rainy tropospheric conditions from 9^{o} elevation angle down (Stutzman, et al - 1975). During clear weather the average signal decreased due to clear air attenuation, but 2-3 dB scintillations with a period of 4 minutes were observed at 9^{o} elevation angle. As the

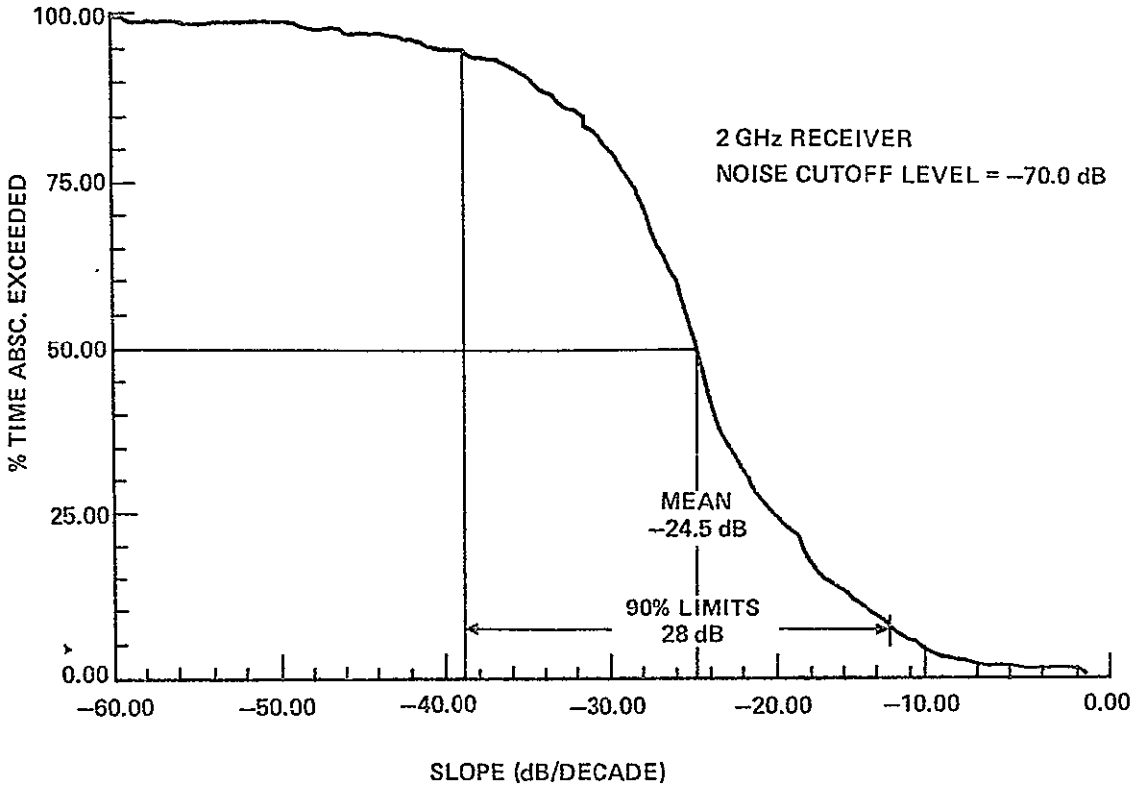

Figure 6. Probability Density Function of Spectral Slope (2GHz).

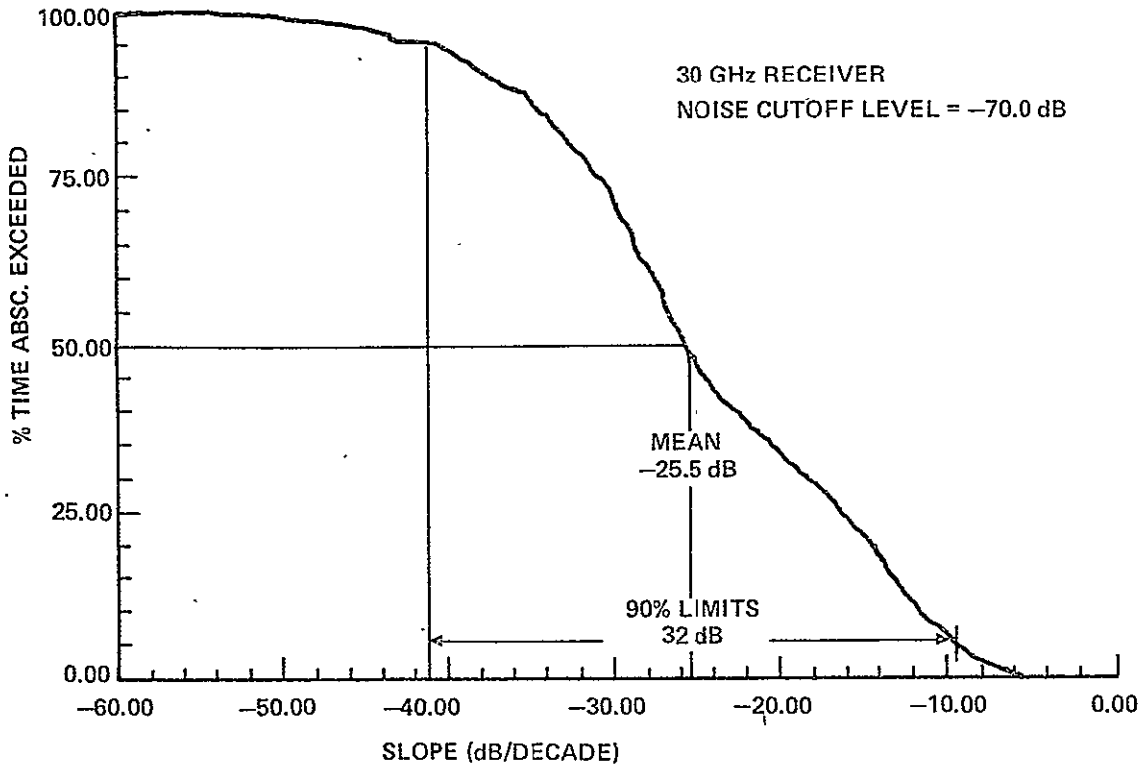

Figure 7. Probability Density Function of Spectral Slope (30GHz).

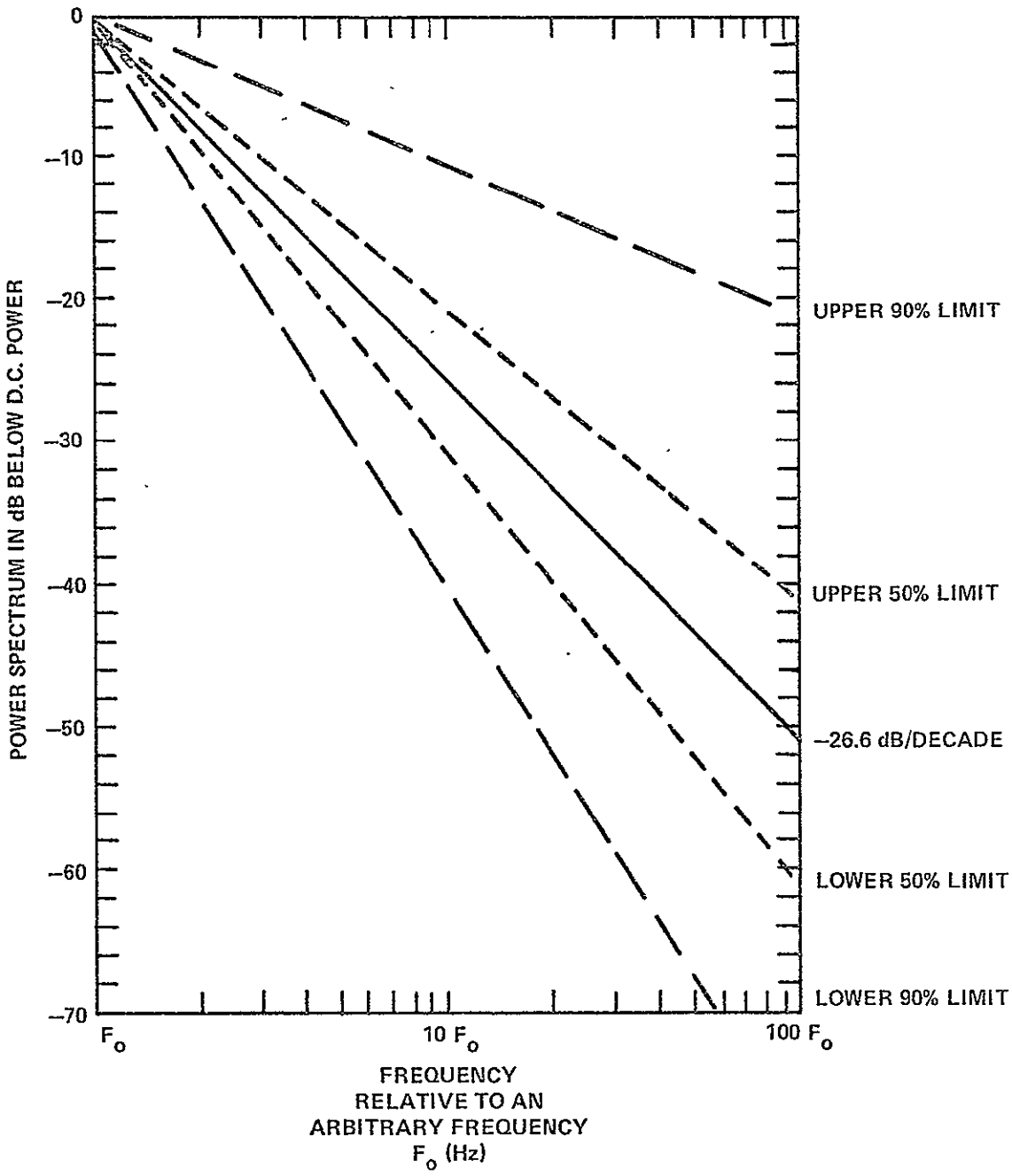

Figure 8. Confidence Limits of Distribution of Spectral Slope from Average -26dB/decade.

weather became hazier, the amplitude of the scintillations remained near 2 dB but the period decreased to 6 seconds. As the elevation angle decreased to 4 degrees, signal fluctuations averaged 7 dB. During rainy conditions, fades of 15 to 20 dB were observed for 10 mm/hr rain rates. These high values are assumed due to the long path length at low elevation angles.

Ohio State University also observed the descent of ATS-6 (Hodge and Theobold - 1976) from 42 to 2^{o} elevation angle. The variances of the scintillations as a function of elevation angle are given in Figure 9 (compare with Figure 2). Because the distribution suggested a cosecant behavior, a minimum mean-square-error curve was fit to the data as noted in Figure 9.

During the return of ATS-6 to 140^{o} W longitude (ascending for U.S. observers) Ohio State and COMSAT conducted elevation-angle measurements over land, while the University of Texas observed over water. The ascending OSU data (Hodge, et al, - 1977) was taken at 2.075 and 30 GHz from -0.7 to 43.9^{o} elevation angles (not corrected for refraction) with no discernable precipitation along the path. The resulting variance is similar to Figure 9 except that the 2 GHz variance is about 10 dB below the 30 GHz data. OSU also observed that the received power level was significantly below that predicted by simple atmospheric path loss calculations. The power spectra of the scintillations, other than the general reduction of amplitude of all components, was similar for all elevation angles and for the presence or lack of cumulus clouds.

COMSAT Laboratories (INTELSAT memo) conducted 13.2 GHz measurements at COMSAT and Westinghouse's Facility at Friendship Airport near Baltimore as the elevation angle increased from 3.6 to 14 degrees. The results from the Clarksburg site are given in Figure 10. The crosses denote the median signal levels and the minimum and maximum signal levels recorded during each 45-minute period are indicated by the vertical solid lines. The median signal strength was on the order of 3 dB lower than the predicted clear sky signal strengths. Typical fluctuation periods were 2 seconds with up to 15 db amplitude fluctuations.

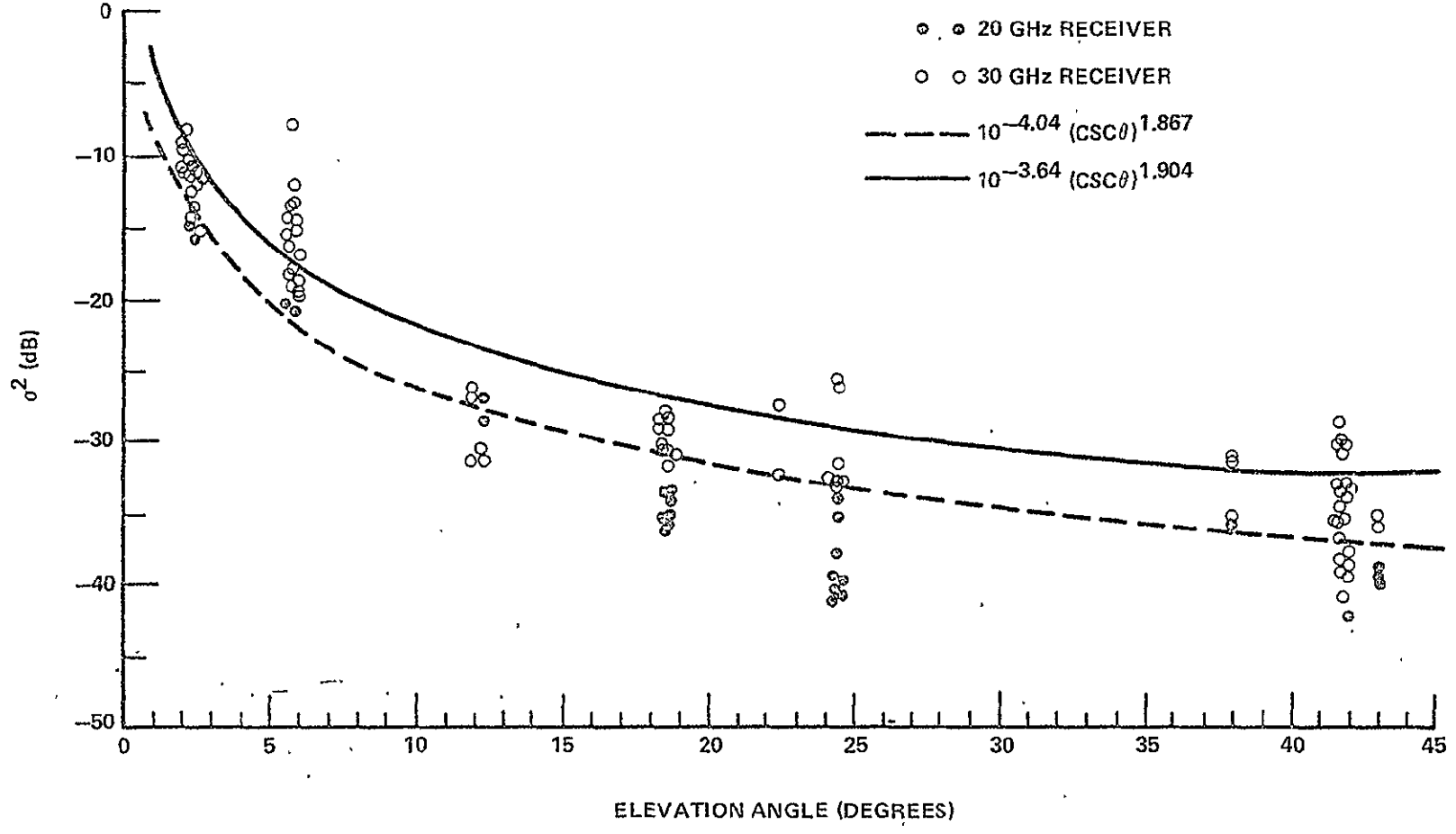

Figure 9. Measured Amplitude Variance Versus Elevation Angle (Columbus, Ohio).

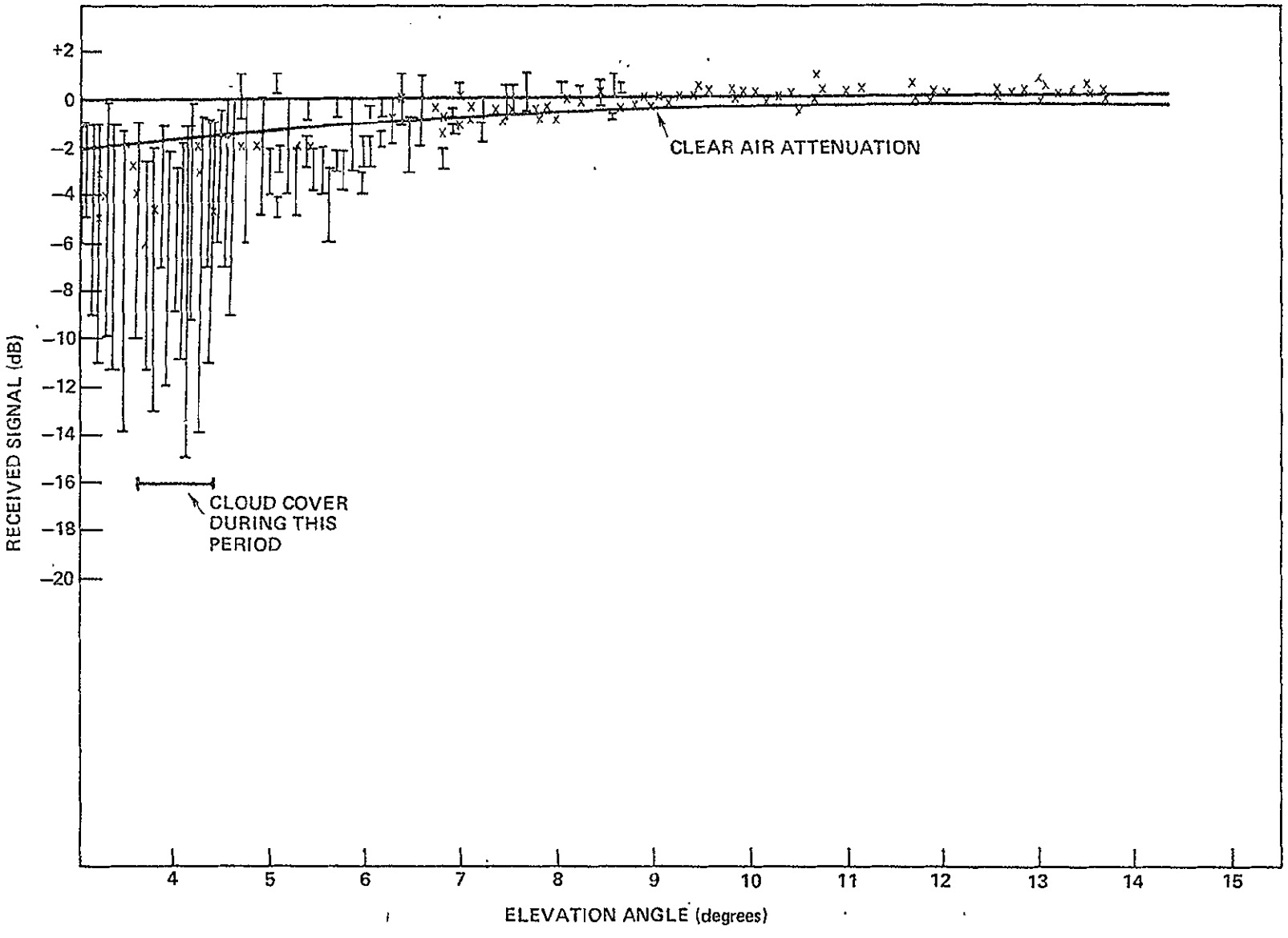

Figure 10. Median Signal Level (X) and Fluctuation (I) Versus Elevation Angle (Clarksburg, MD).

The University of Texas (Vogel, et al - 1977) installed a 30 GHz receiver at Port Aransas, Texas, to obtain a propagation path entirely over water. The beacon was monitored for at least one hour each day for 16 days in September 1976 while the elevation angle varied from 1.5 to 17.3°. The results presented here are based on 3.36 hours of data (15% of the data base). The cumulative distributions of the log attenuation relative to the day's mean attenuation for an arbitrarily chosen record per elevation angle are shown in Figure 11. Negative values of the ordinate represent signal levels above the mean. A rain event was observed while the satellite was near 8.5° elevation angle. Because the rain was over water, no rate was measured. However, the mean attenuation increased by 16 dB and the standard deviation increased to 2.7 dB during the rain.

Measurements made at low elevation angles in the Canadian artic at 4 and 6 GHz also demonstrate the magnitude of the effect at elevation angles near 1 degree (Strickland, et al - 1977) including the effects of refraction. The effects would be greater in a temperate region because of the higher values of refractivity, although the measurements were made during July when the water vapor in the atmosphere is greatest. The cumulative statistics for low angle fading are shown in Figure 12. The 4GHz data was nearly identical to the 5 GHz results. Table 1 demonstrates the 6 GHz link margins for low angle fading at 1 degree elevation angle.

The fade durations at 6 GHz for link margins from 0 to 21 dB below the long term medium are shown in Figure 13.

The cumulative distribution for the rate of change of signal amplitude between 0.4 second samples was found to be identical for positive and negative-going signals. The distribution is shown in Figure 14, where the signal exceeded 1 dB/sec for 1% of the time and 4 dB/sec for 0.1% of the time.

Scintillations of ± 1 dB have been recorded as a cloud passes through the ATS-6 20-GHz beam (Ippolito - 1975). The fluctuation rate was fairly constant at about 16 cycles per minute. The scintillations lasted for about 200 seconds. In addition, short bursts of scintillations have been observed for 10 to 20 second intervals on clear days. Their amplitude reaches 3 dB pk-pk with a fluctuation rate of 20 Hz.

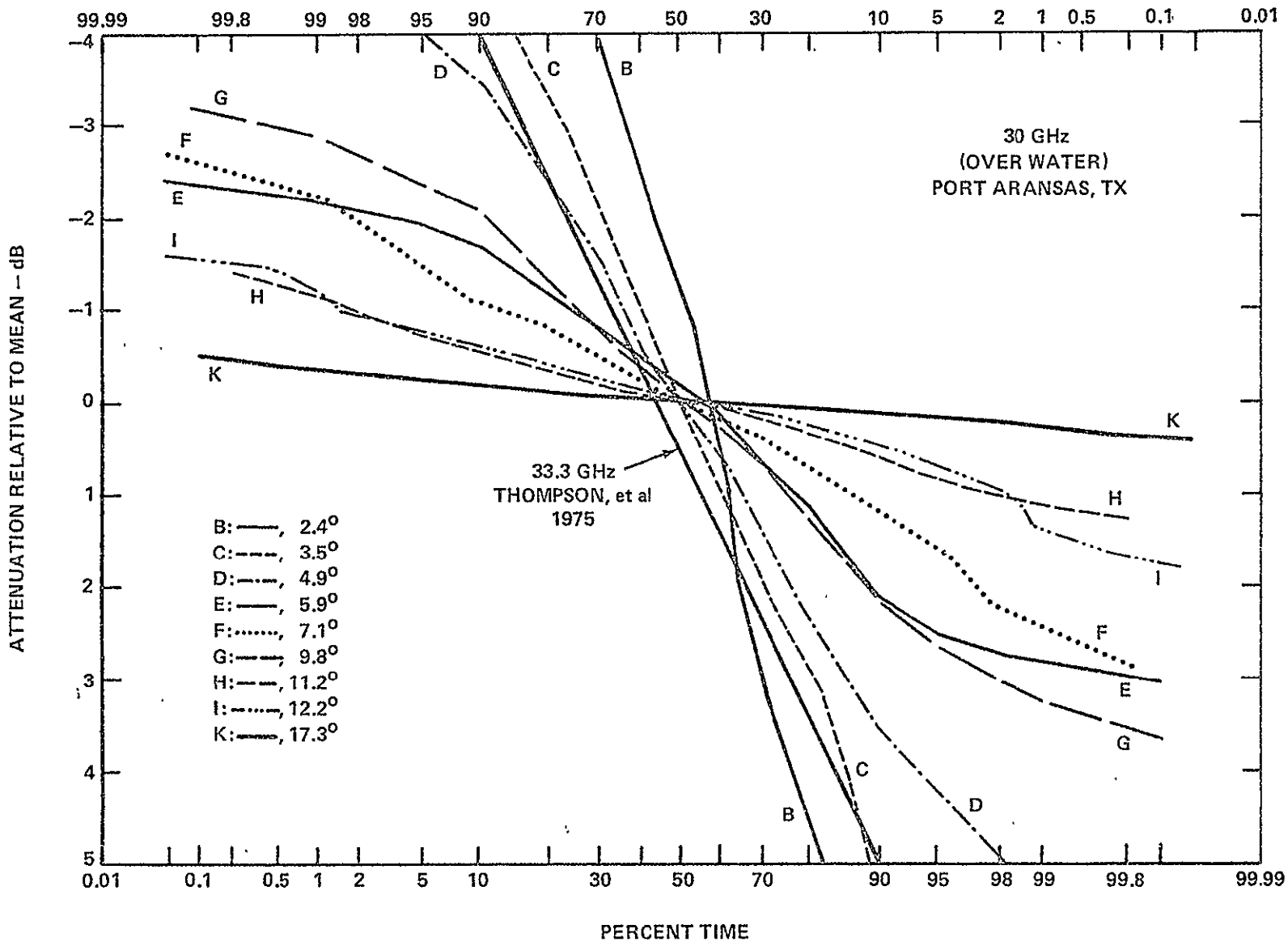

Figure 11. Cumulative Distribution of Signal Attenuation.

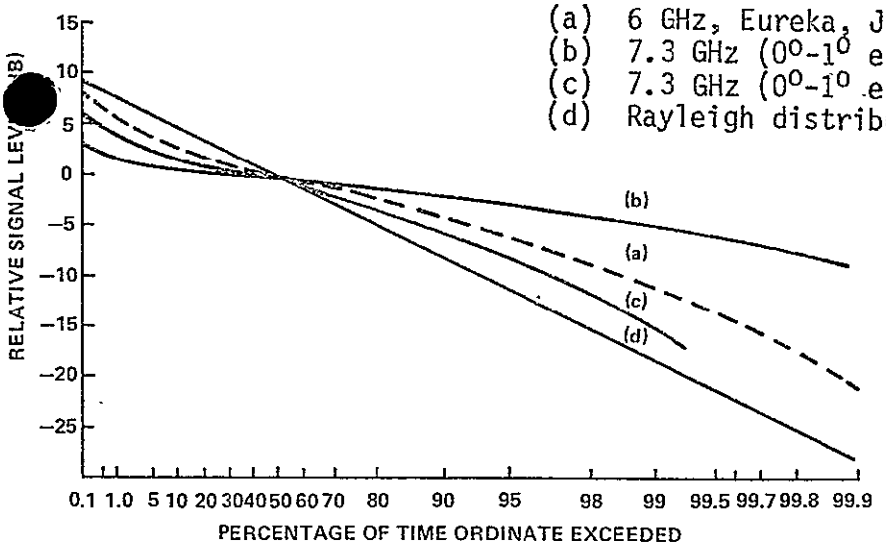

Figure 12. Cumulative Distributions of Low Angle Fading.

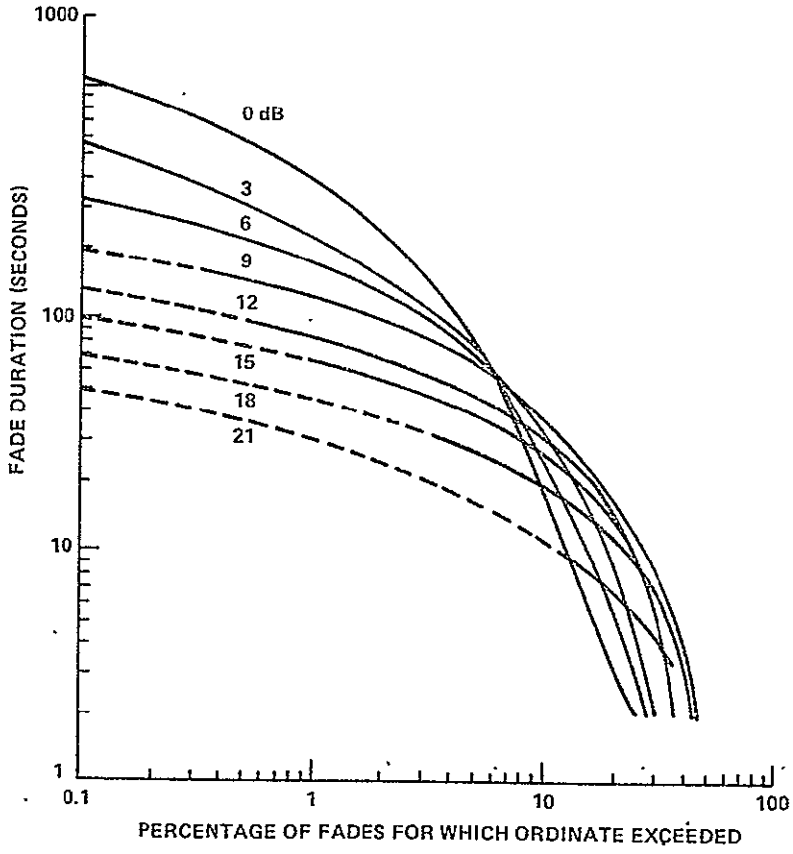

Figure 13. Cumulative Distributions of 6 GHz Fade Durations at Eureka for Various Fade Margins Relative to the Long Term Median Signal Level, July 1974.

TABLE I

6 GHz LINK MARGINS FOR TROPOSPHERIC FADING AT EUREKA, CANADA
ELEVATION ANGLE ≃ 1 DEGREE

Time Duration	Reliability		
	90 %	99 %	99.9 %
Worst two-hours	8.0 dB	18.0 dB	28.0 dB (Rayleigh)
Worst summer day	6.8 dB	15.5 dB	24.5 dB
Worst summer week (5 days) . . .	5.4 dB	13.0 dB	22.0 dB
Worst month, July (15 days). . .	3.8 dB	10.8 dB	20.3 dB

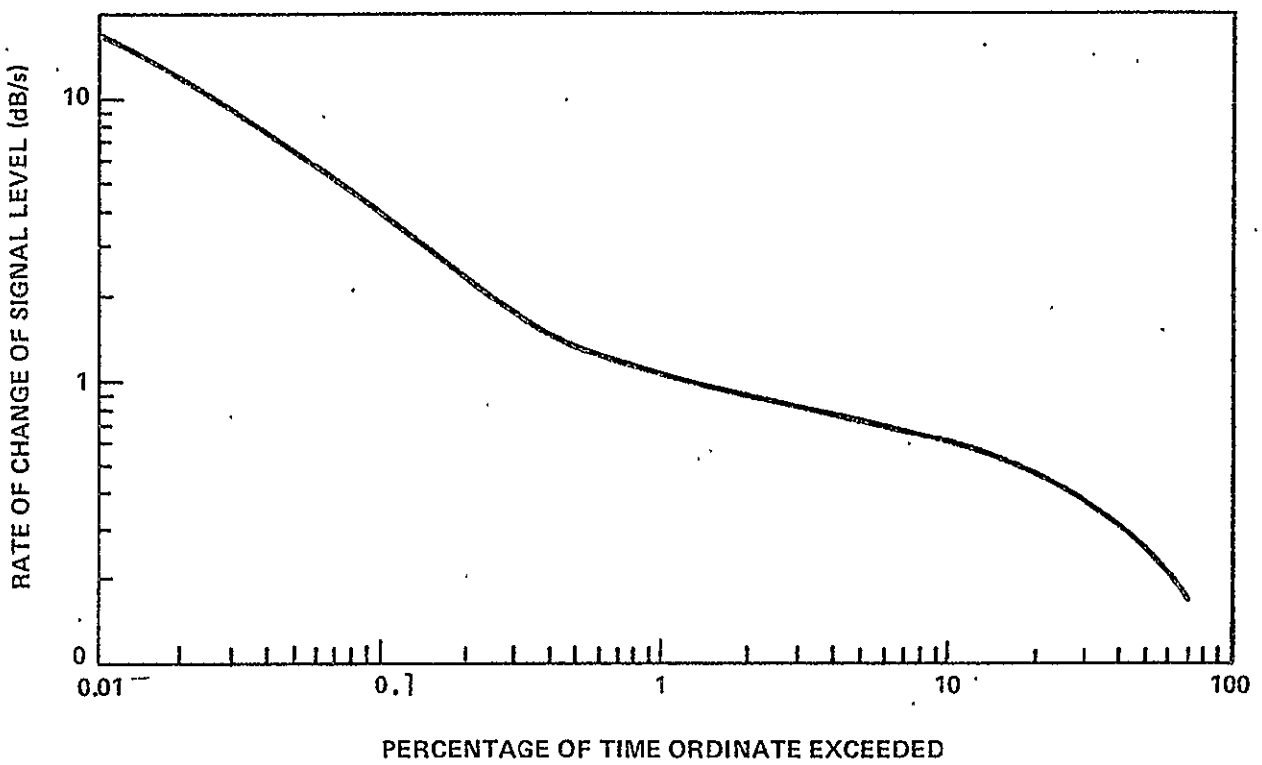

Figure 14. Cumulative Distribution of Rate of Change of .6GHz Signal at Eureka, July 1974.

3.0 PHASE AND ANGLE-OF-ARRIVAL VARIATIONS

Phase variations arise due to the variable delay as the wave passes through a medium with variable refractivity and also due to wavefront ripple introduced by the "lumpy" medium. The former is termed phase fluctuations, while the latter effect is called phase scintillations.

3.1 ESTIMATION OF PHASE FLUCTUATIONS ON EARTH-SPACE PATHS

The model of Muchmore and Wheelon (1955) may be used to estimate the r.m.s. phase fluctuation of a wave propagating on an earth-space path if the equivalent path length L expression of the previous section is employed. Figure 15 is representative of such an estimate. It assumes that the turbulent medium is contained in a height of 5 km and presents r.m.s. phase fluctuation for 3 and 10 GHz.

3.2 ESTIMATE OF PHASE SCINTILLATIONS ON EARTH-SPACE PATHS

Accompanying the amplitude scintillations of a plane wave propagating through tropospheric turbulence are phase variations. According to the theory of Tatarski (1961) the mean-square phase variation over a distance transverse to the propagation path is:

$$D_\phi(\rho) = K_\phi \, C_{no}^2 \left(\frac{2\pi}{\lambda}\right)^2 L\rho^{5/3}$$

where λ is wavelength, L is the propagation path length through the region of turbulence, and C_{no} is the surface structure constant. The constant K_ϕ is equal to 2.91 for the exponential C_n^2 model (Tatarski - 1961) and equal to

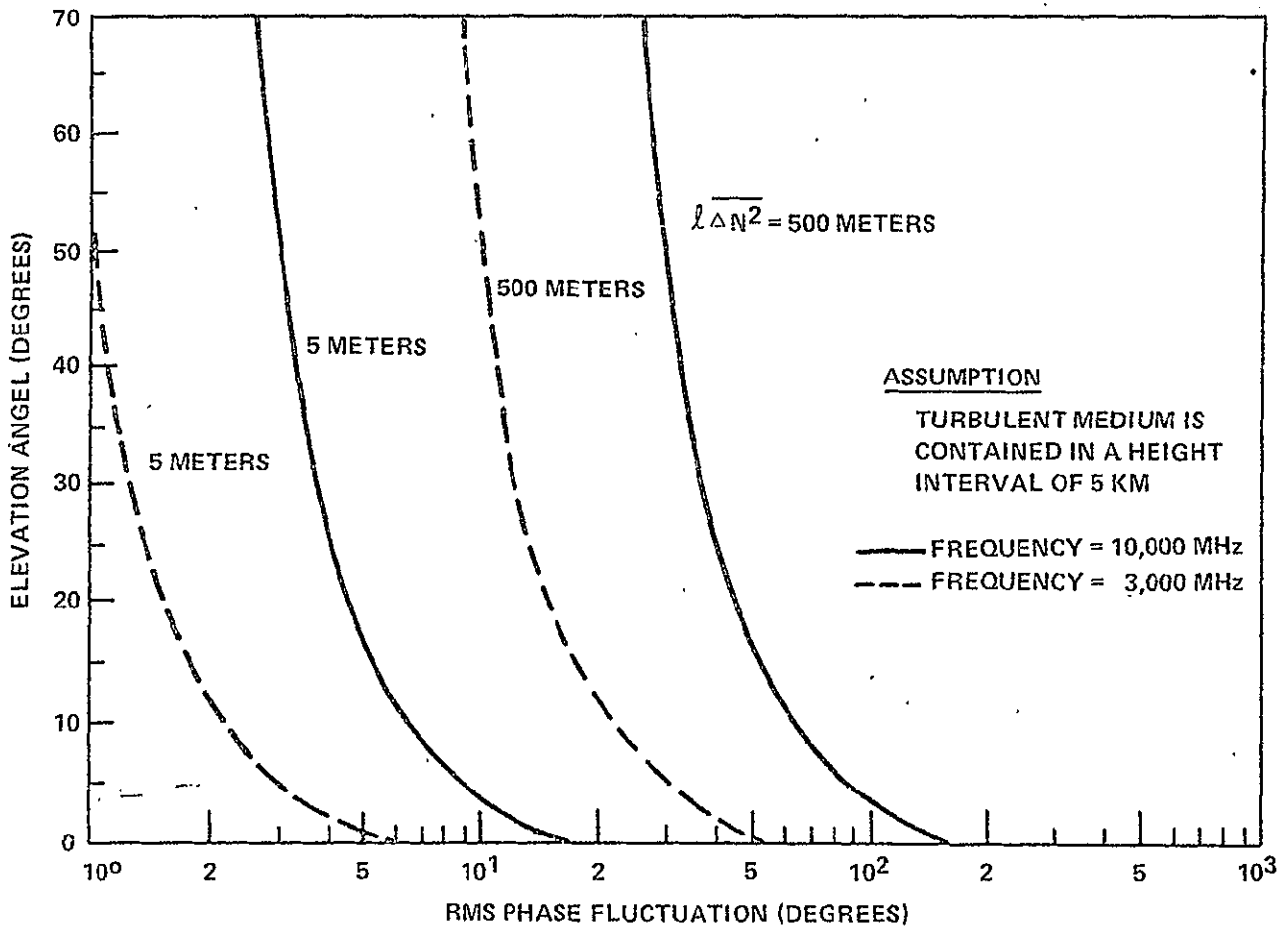

Figure 15. R.M.S. Phase Fluctuations for an Earth-Space Path.

4.57 from Ohio data (Theobold and Hodge-1978). This expression may be used to estimate the expected mean-square phase variation between two points, given an estimate of C_{no}.

An expression for the rms phase fluctuation for a finite circular aperture antenna of diameter d,

$$\sigma_\phi = \left[1 - \frac{d^2}{4\ell^2}\right] \left[2L\ \ell\ \overline{\Delta N^2}\right]^{\frac{1}{2}} \frac{2\pi \times 10^{-6}}{\lambda}$$

has been presented by Muchmore and Wheelon (1955). The derivation employs a ray theory approach and assumes an exponental spatial correlation for the turbulence scale. σ_ϕ is in radians, ℓ is the scale length of the turbulent eddy, L is the path length through the turbulence, λ is wavelength, and $\overline{\Delta N^2}$ is the mean-square fluctuation in the refractivity N. When using this expression, one should only assume values of ℓ and $\overline{\Delta N^2}$ such that

$$5m \leq \ell\ \overline{\Delta N^2} \leq 500m.$$

3.3 ESTIMATES OF ANGLE-OF-ARRIVAL VARIATIONS ON EARTH-SPACE PATHS

The same ray theory approach may be used to estimate angle-of-arrival fluctuation. The expression for r.m.s. angle-of-arrival fluctuation in radians is

$$\sigma_\theta = \left[\frac{2\sqrt{\pi}\ L\ \overline{\Delta N^2}}{\ell}\right]^{\frac{1}{2}} \times 10^{-6}$$

where all parameters are as previously defined. A Gaussian correlation function for the scale of turbulence was assumed and one should impose the limits

$$2 \times 10^{-4}/m \leq \overline{\Delta N^2}/\ell \leq 2 \times 10^{-2}/m$$

Figure 16 is an example for this expression, within the stated range of $\Delta N^2/\ell$, for a earth-space propagation path through a turbulent region of height 5 km. Note that σ_θ^2 is directly proportional to path length and independent of operating frequency. Also, σ_θ decreases with increasing eddy size, ℓ, while phase fluctuation σ_ϕ increases with increasing eddy size.

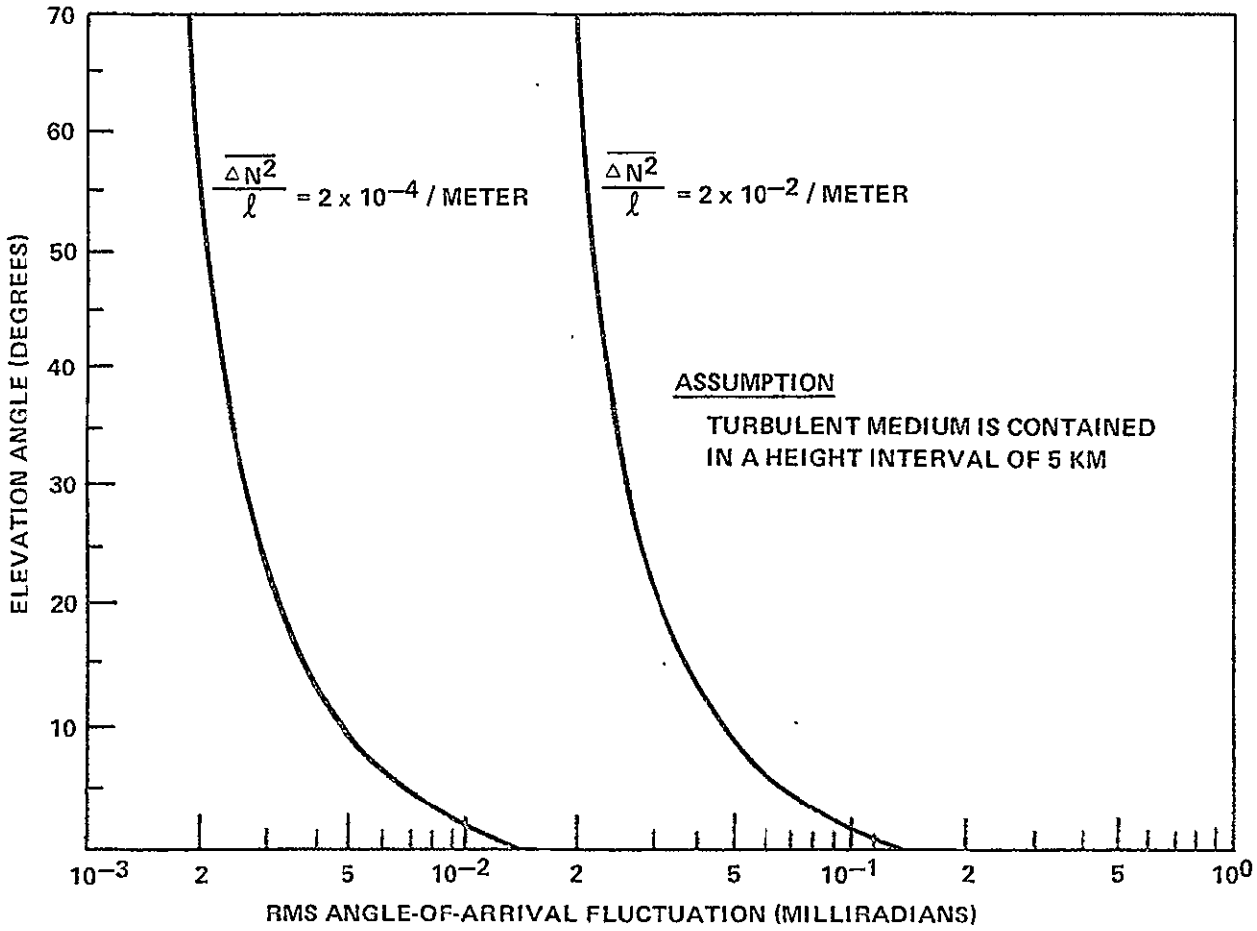

Figure 16. R.M.S. Angle-of-Arrival Fluctuations for an Earth-Space Path.

4.0 PREDICTION OF RECEIVED SIGNAL GAIN DEGRADATION

4.1 GENERAL

Wavefront tilt or angle-of-arrival variation results in time-averaged gain degradation; and phase incoherence results in instantaneous gain loss, excluding the atmospheric gas loss.

4.2 ESTIMATION OF GAIN DEGRADATION

The model of Section 2.2 for received signal amplitude veriance has also been used to derive an expression for gain reduction, R, defined by (Theobold and Hodge - 1978)

$$R = 10 \log_{10} \frac{\langle v \rangle^2}{\langle v \rangle^2 \Big|_{\text{no angle fluctuations}}}$$

$$R = 10 \log_{10} \frac{I_c + I_i \left(\frac{B^2}{4 \sigma_2^2 \ln(2) + B^2} \right)^2}{I_c + I_i}$$

where the constants are the same as those defined for the variance expression, S^2. This value for R may then be combined with atmospheric gas loss in order to obtain an estimate of average received signal level for an earth-space

path. Figure 17 presents an example of predicted signal levels for 2, 7.3, and 30 GHz for antenna beamwidths of 1.8^{o}, 0.3^{o}, and 0.15^{o} respectively. Also included are measured signal levels, relative to zenith, from the ATS-6 2 and 30 GHz (Devasirvatham and Hodge-1977) transmissions and TACSATCOM 7.3 GHz (McCormick and Maynard-1972) beacons as the satellites were moving in elevation angle.

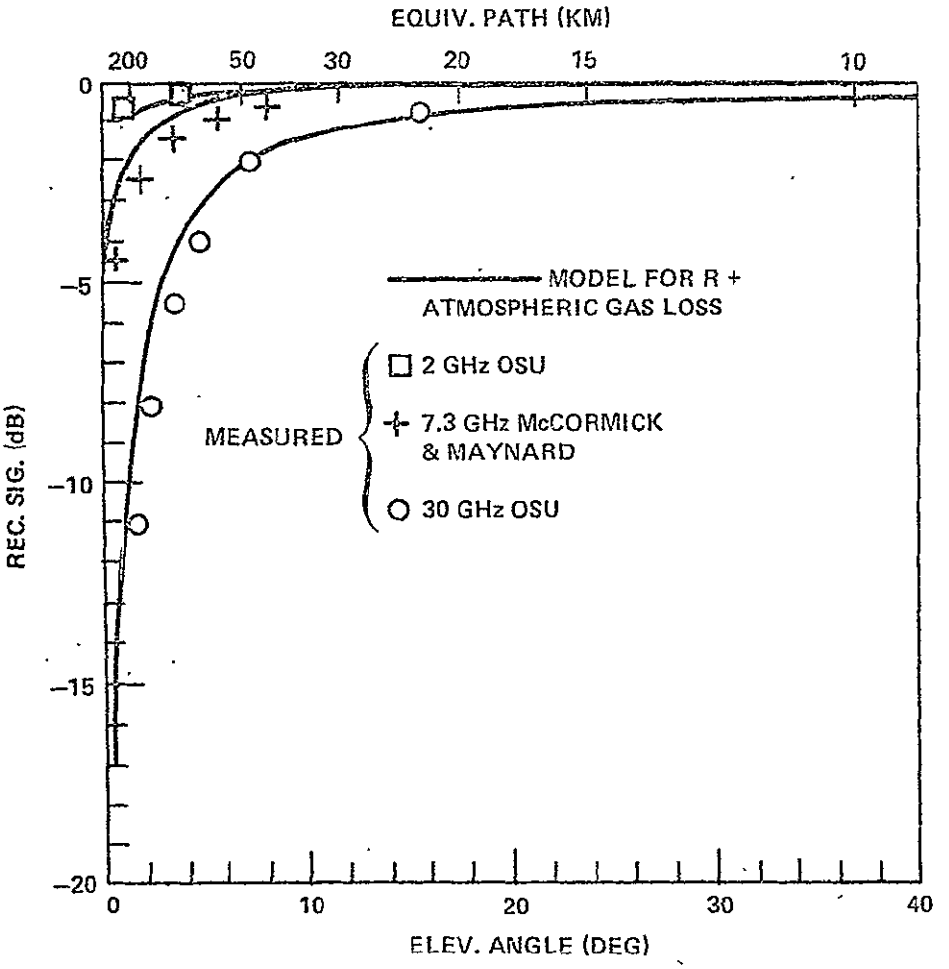

Figure 17. Predicted and Measured Signal Level as a Function of Elevation Angle

5.0 SCINTILLATION FADING AND GAIN DEGRADATION DESIGN INFORMATION

5.1 FADE DISTRIBUTION FUNCTION ESTIMATION

The estimates of gain reduction and signal variance parameters, R and S^2, have been presented. These quantities may be incorporated into distribution functions which are of the form used in link design. They represent the long term average fade statistics due to clear air amplitude and angle-of-arrival fluctuations. The estimates of R and S^2 may be more closely matched to local and seasonal conditions if a local estimate of C_n^2 is available. A hypothetical low elevation angle fade distribution is presented in Figure 18. The abscissa is referenced to the signal level received in the absence of turbulence, i.e., including free space loss and gaseous absorption. The point at which the signal level is R dB is also the mean of the received signal; thus, one point on the fade distribution is established. The fade distribution for turbulence induced fluctuations is assumed to be log-normal, with mean and median being equal. The fade distributions resulting from the Ohio State University ATS-6 30 GHz beacon measurements (Devasirvatham and Hodge-1977) indicate that this log-normal assumption is valid for elevation angles above approximately 2^o. A similar observation was made concerning the 7.3 GHz fade distribution above 4^o elevation angle observed by McCormick and Maynard (1972).

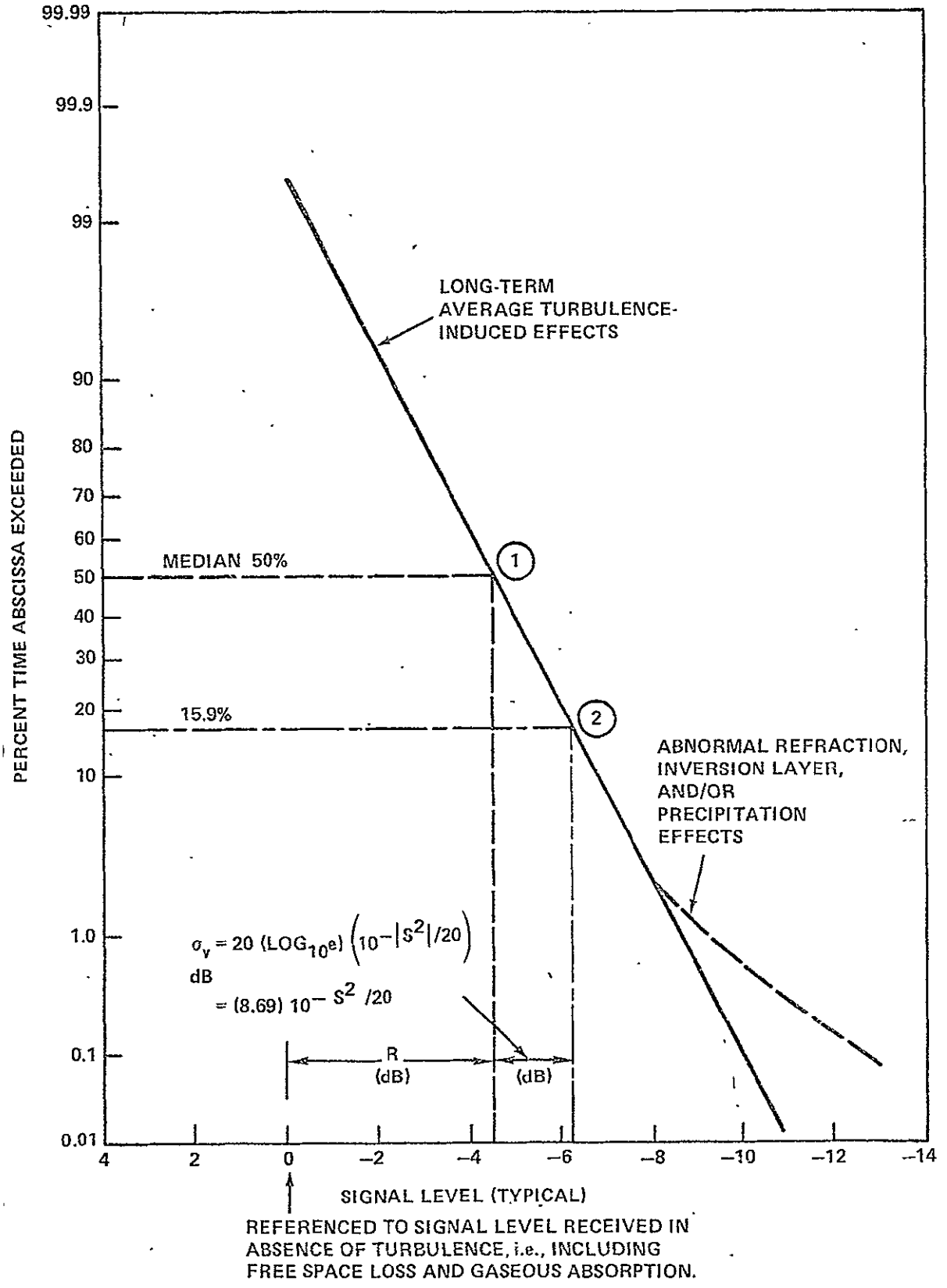

Figure 18. Hypothetical Fade Distribution Function

A fade distribution may now be produced using this assumption of linearity. Referring to Figure 18, it was noted that the point at which the received signal level is R dB represents the mean signal level. For a normal distribution, the mean is plotted at the 50% time abscissa exceeded point, indicated by (1) in the figure. One standard deviation to the right of the mean on a normal distribution occurs at the 15.9% time abscissa exceeded level. It may be easily shown that the standard deviation of received signal level, expressed in dB and denoted $\sigma_{V_{dB}}$, may be written in terms of the signal variances S^2. This point, $\sigma_{V_{dB}}$, to the right of R is denoted by (2) in the figure. A straight line drawn between points (1) and (2) now approximately represents the fade distribution, referenced to the mean signal level in the absence of turbulence induced fluctuations. This distribution was based on small fluctuation arguments and should be employed as a lower bound when estimating a particular fade distribution.

Deviation of this fade distribution from the expected linear form will occur at small time percentages. Additional fading due to precipitation, abnormal refraction, or inversions in the atmosphere will cause greater fade depths for the small time percentages. However, the turbulence effects, which are always present, are still dominant for larger time percentages. For high elevation angles, i.e., short path lengths, S^2 will be very small and the line drawn through points (1) and (2) will be virtually vertical.

However, the precipitation effects at the lower percentages will still be present for short path length cases and will become the dominant feature of the fade distribution.

5.2 DOMAINS IN WHICH GAIN DEGRADATION SHOULD BE CONSIDERED

5.2.1 Estimation of Domains

The effects of amplitude and angle-of-arrival fluctuation are, of course, most prominent for very long path lengths and/or very narrow beamwidths. One may estimate whether or not gain degradation need be considered in a path design if elevation angle (or equivalent path length) and antenna beamwidth are known. Figure 19 presents regimes of average gain degradation between 0.5 and 3 dB and where they must be considered as a function of elevation angle and antenna beamwidth.

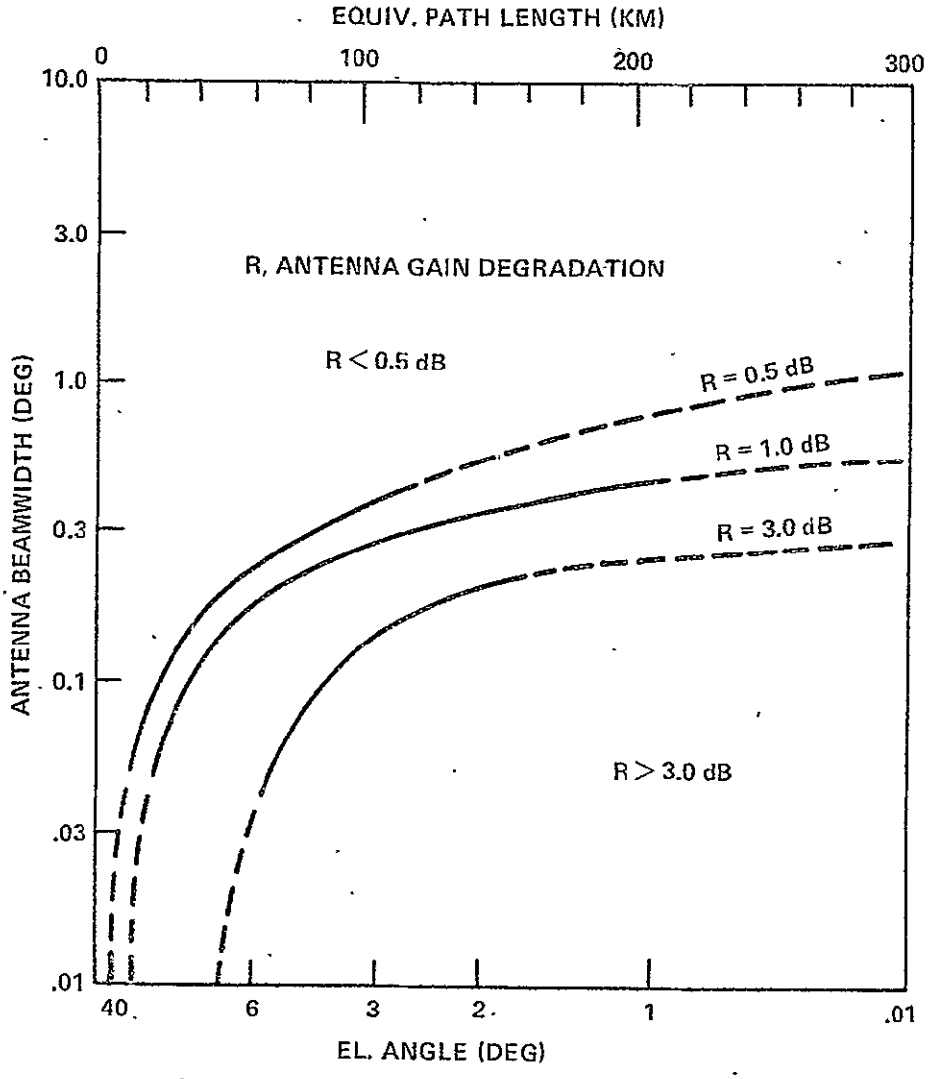

Figure 19. Gain Degradation Regimes as a Function of Beamwidth and Elevation Angle

Realized gain, that is, expected gain less gain degradation, is plotted as a function of antenna beamwidth (for any frequency) or equivalent aperture diameter at 30 GHz in Figure 20. All equivalent aperture diameters are presented for an antenna aperture efficiency of 0.6. The curve representing zero path length L is simply the common gain approximation $G = 41253/B^2$, where B is in degrees. Realized gain curves for path lengths of 50 to 300 km are plotted using the model of Section 4. Equivalent earth-space path elevation angles assuming a 6 km high homogeneous atmosphere are presented in parentheses.

Notice that gain degradation due to turbulence-induced fluctuation is negligible for beamwidths wider than about 0.7° for all path lengths. Degradation effects then gradually increase as beamwidth narrows from 0.7° to 0.05° and at any particular beamwidth are approximately directly proportional, in dB, to path length. As beamwidth narrows beyond 0.05°, a saturation effect occurs and the degradation becomes constant for any one path length.

All design figures of Section 5 represent estimates for clear air effects in a temperate climate during daytime and in the warmer months of the year. If a local value of C_n^2 is known, more accurate values of R and S^2 may be obtained. If local statistics of C_n^2 are known, statistics of R and S^2 may be obtained.

5.2.2 Spatial Diversity

Paths operating at very low elevation angles with narrow beamwidth antennas may experience unacceptable fading due to scintillation and multipath effects. The required reliability may be regained by the use of spaced site diversity. A site separation greater than 300 m transverse to the propagation path has been suggested (CCIR Doc. 5/25, 1974-78) as necessary to alleviate severe turbulence-induced effects. In effect, separation on the order of or larger than the scale size of the largest inhomogeneities in refractive index along the propagation path, and especially near the surface where refraction is greatest, results in decorrelation of the instantaneous signal fluctuations and hence improved performance.

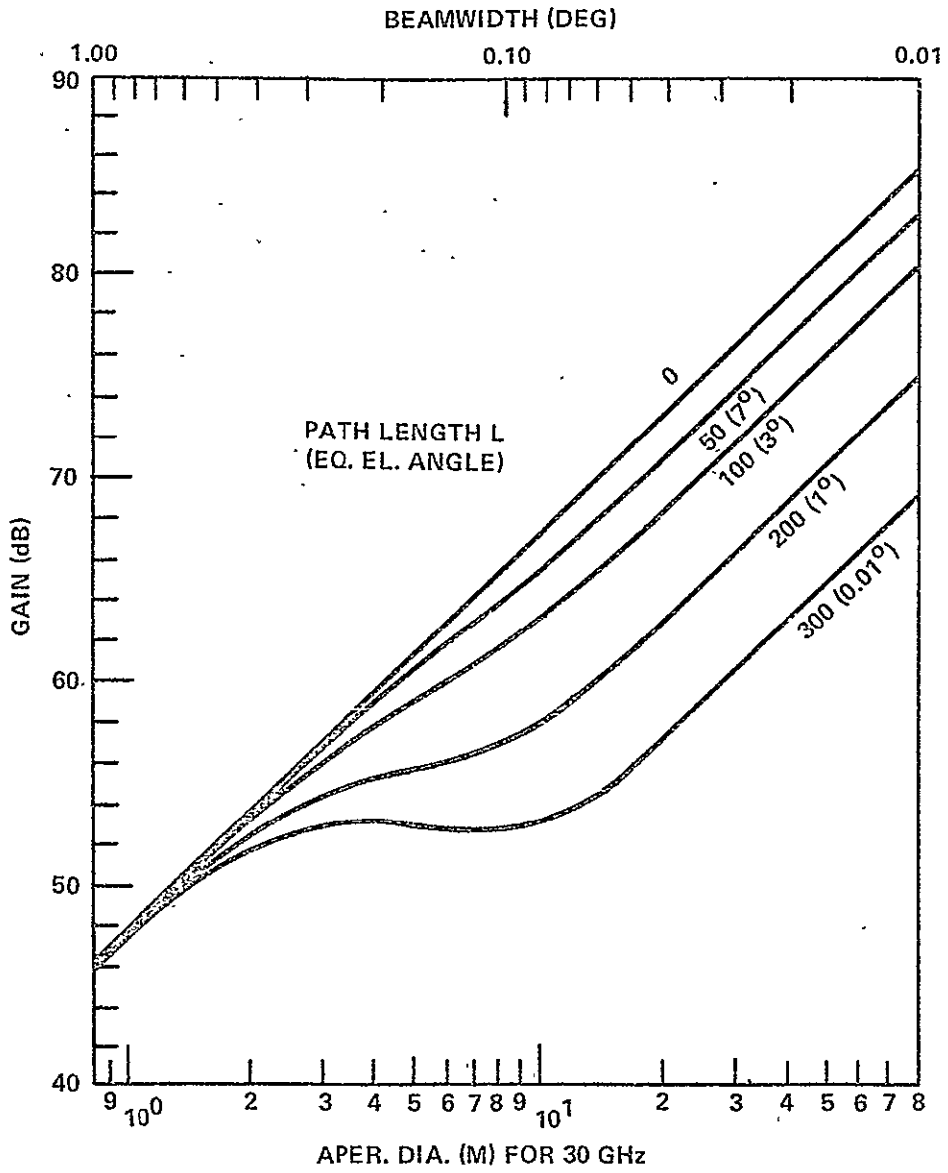

Figure 20. Realized Gain.

The aperture effects of large antennas may be circumvented if several phase-locked antennas, each with relatively wide beamwidth, are employed in an array to achieve the desired system gain. Of course, overall fade margins will be on the order of that for a single element, but angle-of-arrival effects are eliminated. In addition, such an array alleviates the need to mechanically track a geosynchronous satellite, as is necessary with large aperture, narrow beamwidth antennas.

6.0 EXAMPLE COMPUTATIONS OF SIGNAL FLUCTUATIONS AND LOW-ANGLE FADING ON EARTH-SPACE PATHS

In this section examples of the parameters described in this report are worked out for a hypothetical ground station located at Columbus, Ohio with a 4.6m (15 ft) diameter parabolic antenna observing a 28.56 GHz COMSTAR beacon at 10 degrees elevation angle. Actually, the COMSTAR satellites are not at that low an angle, but in order to demonstrate the effects of gain reduction this value has been arbitrarily selected.

6.1 AMPLITUDE FLUCTUATIONS

The variance of the received signal amplitude is calculated using the expression in Section 2.2. The full half-power beamwidth B in degrees is $70\ \lambda/d = 70\ c/fd = (70)(3\times10^{8}\text{m/sec})/(28.56\times10^{9}\text{sec}^{-1})(4.6\text{m}) = 0.16$ degrees. The path length of the turbulence L is computed from h = 6km, r_e = 6377 km and θ= 10 degrees using the equation

$$L = \left[h^2 + 2r_e h + (r_e \sin\theta)^2\right]^{\frac{1}{2}} - r_e \sin\theta$$

$$= 34 \text{ km}$$

The other constants are:

L_o = 180 km

$\sigma_1^2 = 1.18 \times 10^{-3}$

$$\sigma_2^2 = 8.35 \times 10^{-4}$$

$$I_i = 0.17$$

$$I_c = 0.83$$

and the signal variance relative to the average power is

$$S^2 = 10 \log_{10}\left(\frac{9.79 \times 10^{-4} + 0.14396 - 0.14297}{0.83 + 0.14}\right)$$

$$= 10 \log_{10} (2.03 \times 10^{-3})$$

$$\cong -27 \text{ dB}$$

Note that this agrees well with the results in Figure 2. Reference to Tatarski (1961) would have allowed evaluation in terms of C_n^2 rather then the formulation by Theobold and Hodge (1978) utilized here.

Reference to Figure 5 indicates that 50% of the time the S^2 would be between -24 and -30 dB, while 90% of the time S^2 would be between -20 and -34 dB.

The power spectrum density of the fluctuations decreases at 26.5 dB/decade (see Figure 8). That is if one considers some lower frequency cutoff for the amplitude fluctuations (say 0.1 Hz) the fluctuation power at 1 Hz is on the average 26.5 dB below the value of 0.1 Hz. Only 10% of the time will the 1 Hz fluctuation power be only 10 dB below the 0.1 Hz fluctuation power. Clearly most of the fluctuation power for clear air fluctuations is at the low frequencies (less than 1 Hz).

6.2 PHASE AND ANGLE-OF-ARRIVAL VARIATIONS

Phase fluctuations are estimated from the model of Muchmore and Wheelon (1955) presented in Section 3.1. Data quoted in Muchmore and Wheelon indicate typical values for $\ell \approx 60\text{m} = 200$ feet and $\overline{\Delta N^2} = \frac{1}{2}$. Thus $\overline{\ell \Delta N^2} = 30$ meters.

For a finite circular antenna (see Section 3.2) of 4.6 m diameter, the rms phase fluctuation is 0.85 radians = 48 degrees.

The estimate of the angle-of-arrival fluctuations in radians (see Section 3.3) is calculated to be 3.2×10^{-5} radians = 1.8×10^{-3} degrees. This is a small number compared to 0.16 degree half-power beamwidth of the antenna. Also note that the limits on $\overline{\Delta N^2}/\ell = 8.3 \times 10^{-3}$ m^{-1} are not exceeded.

6.3 PREDICTION OF THE AVERAGE RECEIVED SIGNAL GAIN REDUCTION

The average received signal reduction is calculated using the same parameters required for calculation of the amplitude fluctuations. Using the relation in Section 4.2

$$R = 10 \log_{10} \frac{(0.83 + 0.17(0.84))}{1.0}$$

$$= -0.12 \text{ dB}$$

Thus during clear weather this COMSTAR beacon will on the average be 0.12 dB below the value calculated considering clear air attenuation only. This same value could be estimated from Figure 20.

The long-term average distribution in Figure 18 is now constructed from R and S^2. The point 2 (15.9% point) is found to be $2Q(\log_{10} e)\left(10^{-|S^2|/20}\right) = 0.39$ dB which is the standard deviation of the receiver voltage taken from a square law detector.

7.0 REFERENCES

1. Baxter, R. A. and D. B. Hodge (1978), "Spectral Characteristics of Earth-Space Paths at 2 and 30 GHz," The Ohio State University, ElectroScience Lab. Tech. Rpt. 784299-7.

2. CCIR (1974-78), Doc 5/28.

3. Crane, R. K. (1977), "Tropospheric Scintillation at Microwave Frequencies on an Earth-Space Path," Proc. URSI Meeting, La Baule, France, pgs 415-9 (28 April - 6 May 1977).

4. Devasirvatham, D., and D. B. Hodge (1977), "Amplitude Scintillations on Earth-Space Propagation Paths at 2 and 30 GHz," The Ohio State University ElectroScience Lab., Tech. Rpt. 4299-4.

5. Hodge, D. B., and D. M. Theobold (1976), "Scintillations Observed on the ATS-6 20 and 30 GHz Downlinks," URSI/USNC Meeting, Boulder, CO, October, 1975 and D. B. Hodge, D. M. Theobold and R. C. Taylor, "ATS-6 Millimeter Wavelength Propagation Experiment," Ohio State University ElectroScience Rpt 3863-6.

6. Hodge, D. B., D. M. Theobold and D. M. J. Devasirvatham (1977), "Amplitude Scintillation at 20 and 30 GHz on Earth-Space Paths," Proc. URSI Meeting, La Baule, France, pgs. 421-5 (28 April - 6 May 1977).

REFERENCES (CONT'D.)

7. Intelsat Memo (1977), "Measurements of SHF Tropospheric Fading at Low Elevation Angles Using the ATS-6 in Route West," INTELSAT Memo BG/T-22-25E, 7 November.

8. Ippolito, L. J. (1975), "ATS-6 Millimeter Wave Propagation and Communications Experiments at 20 and 30 GHz," IEEE Aerospace and Electronic Systems, Vol. AES-11, pgs. 1067-82.

9. Ishimaru, A. (1978), Wave Propagation and Scattering in Random Media, Single Scattering and Transport Theory, Vol. 1, Academic Press, New York, N.Y.

10. McCormick, K. S., and L. A. Maynard (1972), "Measurements of S. H. F. Tropospheric Fading Along Earth Paths at Low Elevation Angles," Electronics Letters, Vol. 8, No. 10.

11. Muchmore, R. B. and A. D. Wheelon (1955), "Line-of-Sight Propagation Phenomena - I. Ray Treatment," Proc. IRE, Vol. 43, pgs 1437-1449.

12. Strickland, J. I., R. I. Olsen and H. L. Werstiuk (1977), "Measurements of Low Angle Fading in the Canadian Arctic," Ann. Telecomm., Vol. 32, Nos. 11-12, pp 530-535.

13. Stutzman, W. L., C. W. Bostian, E. A. Manus, R. E. Marshall and P. H. Wiley (1975), "ATS-6 Satelitte 20 GHz Propagation Measurement at Low Elevation Angles," Electronics Letters Vol 11, Nos. 25/26, pp 635-6 (11 December).

14. Tatarski, V. I. (1961), Wave Propagation in a Turbulent Medium, McGraw-Hill Book Co., New York, N.Y.

15. Theobold, D. M. (1978), "Tropospheric Refraction," report prepared for ORI, Inc. under NASA Contract NAS5-23438.

16. Theobold, D. M., and D. B. Hodge (1978), "Gain Degradation and Amplitude Scintillation Due to Tropospheric Turbulence," The Ohio State Univeristy Electro-Science Lab., Tech. Rpt. 784229-6, Revision 1.

17. Thompson, M. C., Jr., L. E. Woods, H. B. Janes and D. Smith (1975), "Phase and Amplitude Scintillations in the 10 to 40 GHz Band," IEEE Trans. Ant. Prop., Vol AP-23, pgs 792-797.

18. Vogel, W. J., A. W. Straiton, and B. M. Fannin (1977), "ATS-6 Ascending: Near Horizon Measurements Over Water at 30 GHz," Radio Science, Vol. 12, pgs 757-765, September-October.

SECTION V

ORI
Silver Spring, Maryland 20910

PREDICTION OF DEPOLARIZATION ON EARTH-SPACE PATHS

DR. ROGER KAUL

OCTOBER 1978

ORI, INC.
SILVER SPRING, MARYLAND 20910
CONTRACT NAS5-23438, MOD. 68

1.0 DEFINITIONS

Depolarization refers to that effect wherein an earth-space link wave's polarization is altered in the troposphere. For linear polarized waves a vertically (horizontally) polarized wave will, after passing through a media, have a horizontally (vertically) polarized component in addition to the initial wave. For circularly polarized waves a RHCP (LHCP) wave will develop into a elliptical wave. For frequency reuse systems based on polarization isolation this coupling reduces isolation and increases "cross-talk."

The measurement of depolarization by propagation researchers usually has been done utilizing orthogonally-polarized feeds on a single antenna while observing singly-polarized satellite signals.* This parameter is called the cross-polarization discrimination (CPD) or cross-polarization ratio (CPR) defined as (Ref. 1)

$$\text{CPD} = \frac{\text{power output from the co-polarized port}}{\text{power output from the cross-polarized port}}$$

$$= (\text{CPR})^{-1}$$

For perfect transmitting and receiving antennas and a perfect medium this isolation could become infinite, but with practical components some leakage is always present. Definitions and example calculations of depolarization terms have been well documented in a tutorial report by Stutzman (Ref. 2).

Unfortunately, the system designer desires the cross-polarization isolation (CPI) term defined as

CPI (dB) = co-polarized signal power (dB) - cross-polarized signal power (dB) on the same channel

Fortunately, for most levels of attenuation observed, CPI $\approx$ CPD = $(\text{CPR})^{-1}$ (Ref. 3)

* Most experimental depolarization data has been obtained from the 11.7 GHz right-hand circularly polarized communications Technology Satellite (CTS) beacon and the 19.04 and 28.56 GHz linear polarized ATT COMSTAR satellite beacons.

2.0 SOURCES OF DEPOLARIZATION

Depolarization on earth-space paths has been observed due in the presence of

- rain
- ice
- snow
- multipath
- refractive effects

These hydrometeor and scattering effects generate depolarization because of their asymmetry. For example, as raindrop sizes increase their shape departs from spherical and becomes oblate spheroid with an increasingly pronounced flat bottom. For large drop sizes a concave depression develops (Ref. 4). Polarized microwave energy scattered from these particles can easily be converted into an orthogonal polarization.

2.1 RAIN DEPOLARIZATION

2.1.1 Depolarization Versus Attenuation

Correlation of depolarization with rain rate has not been too successful because of the many parameters required for these calculations. However, experimentally and analytically (Ref. 5) it has been observed that depolarization can be related to total attenuation by the formula

$$CPD = a - b \log_{10} (AL_e)$$

where CPD is the cross-polarization discrimination in dB and AL_e is the total attenuation in dB due to rain (not including the clear air attenuation).

At 11.7 GHz, the University of Texas at Austin (Ref. 6) has measured the cumulative attenuation and depolarization statistics for the CTS

operational periods from 18 October 1976 to 31 January 1978. Relating the statistics plots for equal probabilities of exceedance the results

$$CPD = 41 - 20.6 \log_{10} (AL_e)$$

were obtained with excellent accuracy. For example, for a 10 dB fade, the CPD is 20 dB. This may be related to the rain rate and rain rate statistics using the effective path length and specific attenuation described in Section II at 11.7 GHz.

In Ottawa, measurements during the July and August 1976 (Ref. 7) light rains with attenuation less than 3 dB tended to yield scattered results. Convective storms yielded a more consistent relation between CPD and AL_e, namely

$$CPD = 33.7 - 19.9 \log_{10} (AL_e)$$

For both Texas and Ottawa results, attenuations below 3 to 5 dB were believed partially related to ice clouds which resulted in significant depolarization without attenuation. This deploarization, sometimes referred to as "anomalous" depolarization, has frequently been observed synchronous satellites over the U.S. and Canada.

At Blacksburg, Virginia, preliminary measurements of the CTS beacon have yielded (obtained by curve fitting Figure 9 of Ref. 1)

$$CPD \simeq 40 - 20 \log_{10} (AL_e)$$

for four major storms during June and July 1977.

The CCIR has recommended the approximate relation

$$CPD = 30 - 20 \log_{10} (AL_e)$$

in CCIR Draft Report 215-3 (Rev. 76).

Depolarization models are currently under development at several organizations. These include:

- Virginia Polytechnic Institute and State University (Refs. 17 and 18)
- Bell Telephone Laboratories (Ref. 19)
- University of Texas at Austin (Ref. 6)
- Communications Research Centre (Ref. 5).

2.1.2 Frequency Scaling Depolarization Measurements

The Virginia Polytechnic Institute and State Univeristy (Ref. 8) has also made measurements of the depolarization at 19 GHz vertical and horizontal and 28.56 GHz using the Comstar beacons. Their preliminary results for August 1977 are given in Table 1.

TABLE 1

CROSS-POLARIZATION DISCRIMINATION VERSUS ATTENUATION
(Least-Mean-Square Fits)

Blacksburge, VA Elevation Angle = θ

Frequency/Polarization	CPD = a - b $\log_{10}$ (AL_e)
11 GHz, RHCP (CTS, $\theta = 33^o$)	CPD = 44.7 - 22.6 $\log_{10}$ (AL_e)
19 GHz, vertical (COMSTAR, $\theta = 44^o$)	CPD = 47 - 24.5 $\log_{10}$ (AL_e)
19 GHz, horizontal* (COMSTAR)	CPD = 37.1 - 20.0 $\log_{10}$ (AL_e)
28 GHz, vertical (COMSTAR)	CPD = 39.4 - 15.4 $\log_{10}$ (AL_e)
* Note: The 19 GHz horizontal data was taken in the month of September 1977. All other data is in August 1977.	

The analysis of Nowland, et al (Ref. 5) may be utilized to show the expected frequency dependence of the coefficients a and b in CPD = a - b $\log_{10}(AL_e)$. Using Equations 11 and 12 of Ref. 5 and many of the constants in the paper, the solid curve was derived in Figure 1. The dashed curve was derived using the effective path length $L_e = 12.82R^{-0.3}$ and the specific attenuation in Section II. Several experimental data points are shown, but these do not correlate well with the theory (possibly because of the polarization dependence of "a"). The important results of these figures are that "a" increases with increasing frequency, while "b" appears to be relatively constant. In the relation CPD = a - b $\log_{10}(AL_e)$ this would imply that the CPD increases with increasing frequency, but because of the rapid increase in AL_e with frequency, CPD will decrease for increasing frequency for moderate rain rates.

The revised CCIR values for "a" and "b" are (CCIR Doc. 5/276-E, 21 Sept 1977)

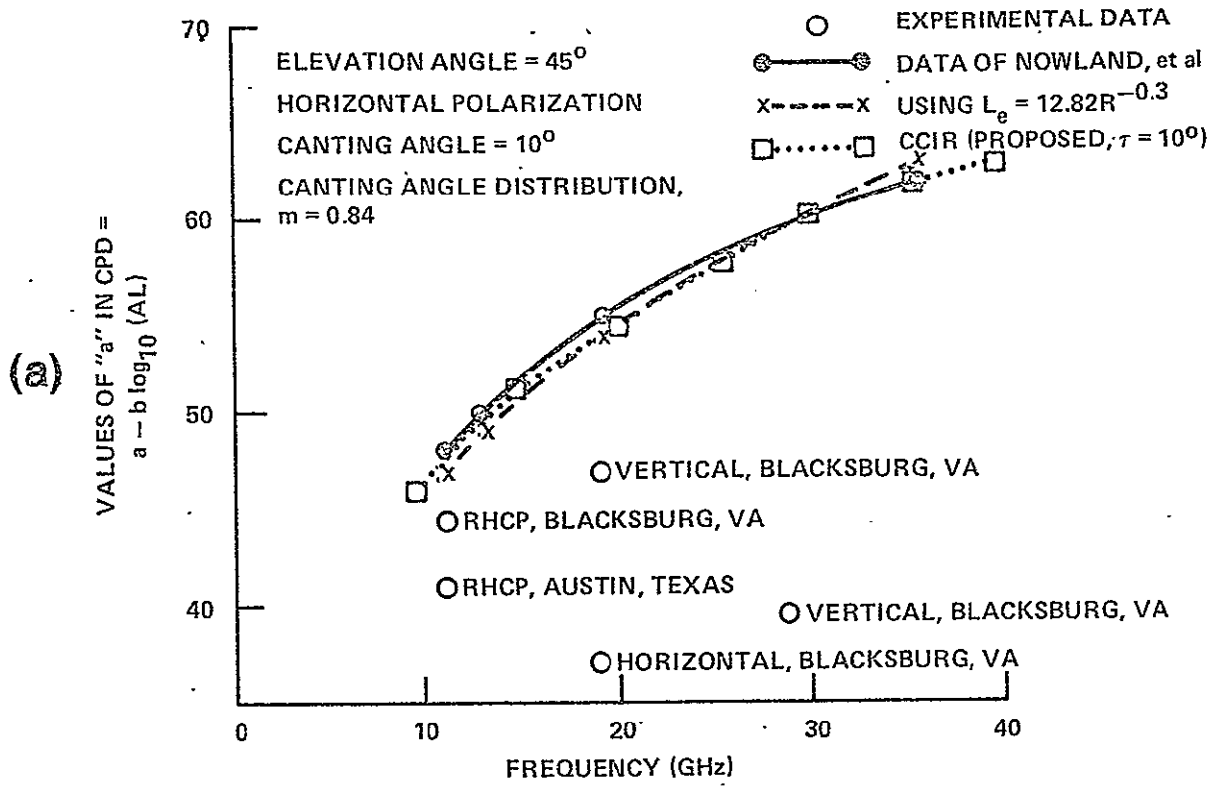

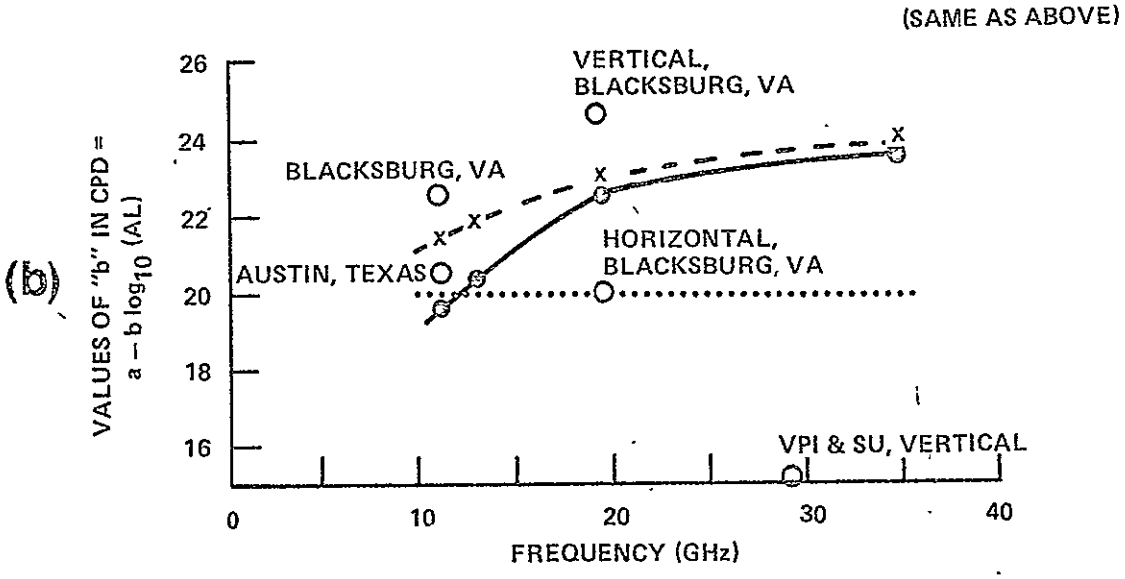

FIGURE 1. Frequency Dependence of the Coefficients in the Cross-Polarization Discrimination Relation

$$a = 30 \log_{10} (f) - 40 \log_{10} (\cos\theta) - 20 \log (\sin 2\tau)$$

$$b = 20$$

where f = frequency in GHz, θ = elevation angle and τ = polarization tilt angle with respect to horizontal ($\tau = 45^0$ for circular polarization). This approximation is believed valid for: 1 dB $\leq AL_e \leq$ 15 dB, 10 dB $\leq$ CPD $\leq$ 40 dB, 8 GHz $\leq f \leq$ 40 GHz, 10 deg. $\leq \tau \leq$ 45 deg. and 10 deg. $\leq \theta \leq$ 60 deg. This estimate is provisional and should be used with caution.

2.1.3 Elevation Angle Dependence of Depolarization

The depolarization measurements presented earlier were obtained at elevation angles from 24.6 degrees in Ottawa (Ref. 7) to 49^0 at Austin, Texas (Ref. 6). The general dependence of CPD versus AL_e on elevation angle θ can be obtained from the theoretical results of Ref. 5. Note that both the coefficient a and the total attenuation AL_e depend on elevation angle.

The elevation angle dependent results of Ref. 5 for 11.0 and 11.7 GHz (experimental data) are shown in Figure 2. Clearly the "a" coefficient is elevation angle dependent, however the experimental data does not confirm this fact. The "b" coefficient appears to be nearly independent of elevation angle and does appear to agree with the limited data base.

2.1.4 Phase Variations During Depolarization Events

The Blacksburg group (Ref. 1) has also made measurements of the phase difference between the co-polarized and cross-polarized signal components. The phase has been observed to both decrease and increase by about 150 degrees for 3 dB fades and then does not change significantly for higher attenuations. The differential phase has also been observed to increase and then decrease in the same storm. The mechanism for this plateau at 150 degrees and why the sign changes remains unexplained.

More recent theoretical results and comparison to data from the Communication Technology Satellite and the Comstar beacons are presented in Ref. 20. An inexpensive self-adaptive cancellation system is also proposed and its predicted performance is presented in Ref. 20.

2.2 ICE DEPOLARIZATION

Ice particles well above the height of the melting layer may have significant cross-polarization effects even for small values of attenuation (typically below 3 to 5 dB at 11.7 GHz). This effect is believed to contribute to the poor correlation between the excess attenuation and the cross-polarization discrimination at these low values of attenuation.

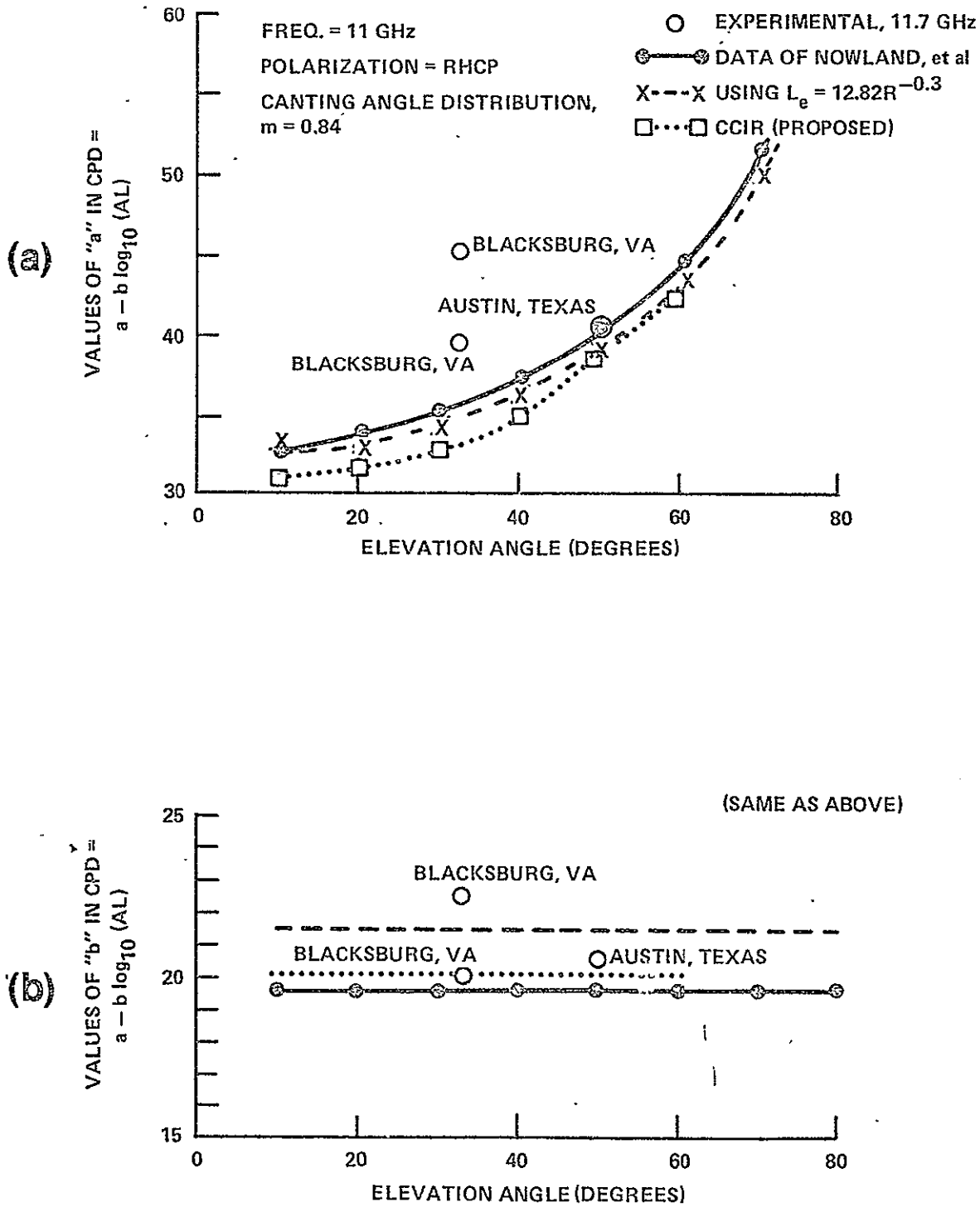

FIGURE 2. Elevation Angle Dependence of the Coefficients in the Cross-Polarization Discrimination Relation

In Austin (Ref. 6) ice depolarization was associated with either thunderstorms during the summer months or with clouds in the presence of polar air masses during the winter. An example of the percentage of time that CPD was less than or equal to the abscissa given that the excess attenuation was less than or equal to 1 dB is shown for the 18 month period from 12 June 1976 to 31 January 1978 in Figure 3. This curve shows that 45 per cent of the time that the CPD was less than or equal to 35 dB, there was less than 1 dB of attenuation; 24 per cent of the time that the CPD $\leq$ 30 dB the $AL_e \leq 1$ dB and 12 per cent of the time that CPD $\leq$ 25 dB the $AL_e \leq 1$ dB. In contrast, using the rain depolarization relation; for 1 dB yields a CPD $\simeq$ 40 dB. Therefore systems requiring 30 dB or more CPD should expect a significant number of depolarization events due to ice.

In England, simultaneous measurements of the 20-and 30-GHz ATS-6 satellite signals at elevation angles of 22-23 degrees and 9.4 radar signatures have demonstrated that the bright band ($0^{\circ}C$ isotherm) does not contribute significantly to the depolarization because of its limited extent (Ref. 8).

Also, it has been observed (Ref. 9) that at 30 GHz ice crystals yield a constant value (typically 90 degrees) of the relative phase angle between the crosspolar and copolar signals as a function of CPD as shown in Figure 4. The corresponding polar plot for a heavy rain event is shown in Figure 5. In this case the CPD was reduced by signal attenuation and the signal to noise ratio of the relative phase measurement decreased as the CPD decreased. This effect appears to increase the scatter of the phase angle with decrease in CPD.

English investigators have also noted that rapid changes in relative phase and CPD are observed in thunderstorms and are associated with realignment of the ice crystal orientation by the electrostatic fields. In electrically-active thunderstorms, these electrostatic fields discharge rapidly resulting in rapid relative phase shifts of 180° and rapid decreases in CPD of 27 dB in 20 seconds (Ref. 10) have been observed at the occurrence of a lightning flash. An example of this is shown in Figure 6 where the spikes in the relative phase occur for increasing CPD and result in large phase changes.

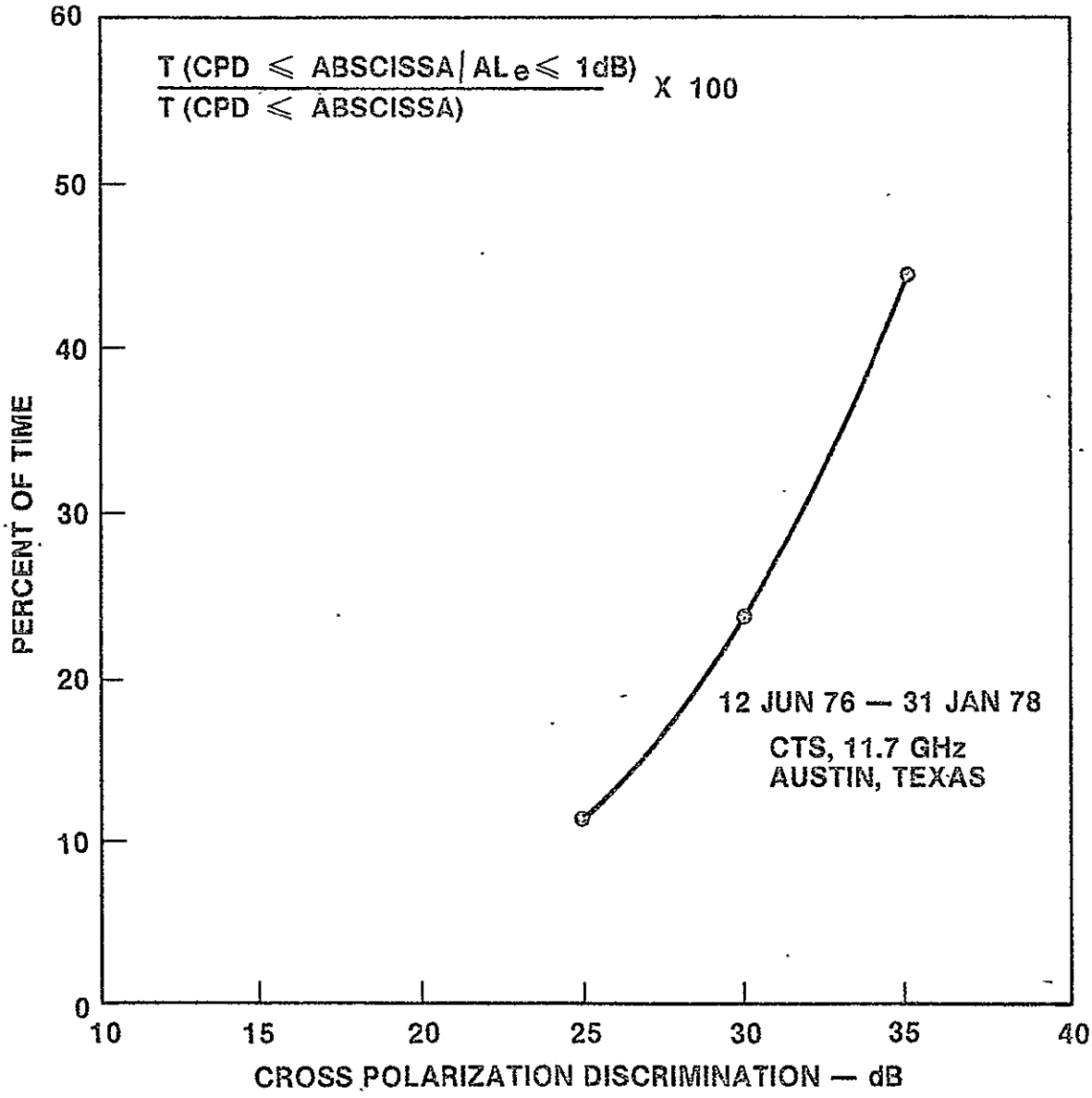

FIGURE 3. THE PERCENTAGE WITH WHICH ICE DEPOLARIZATION CONTRIBUTED TO THE TOTAL DEPOLARIZATION EVENTS

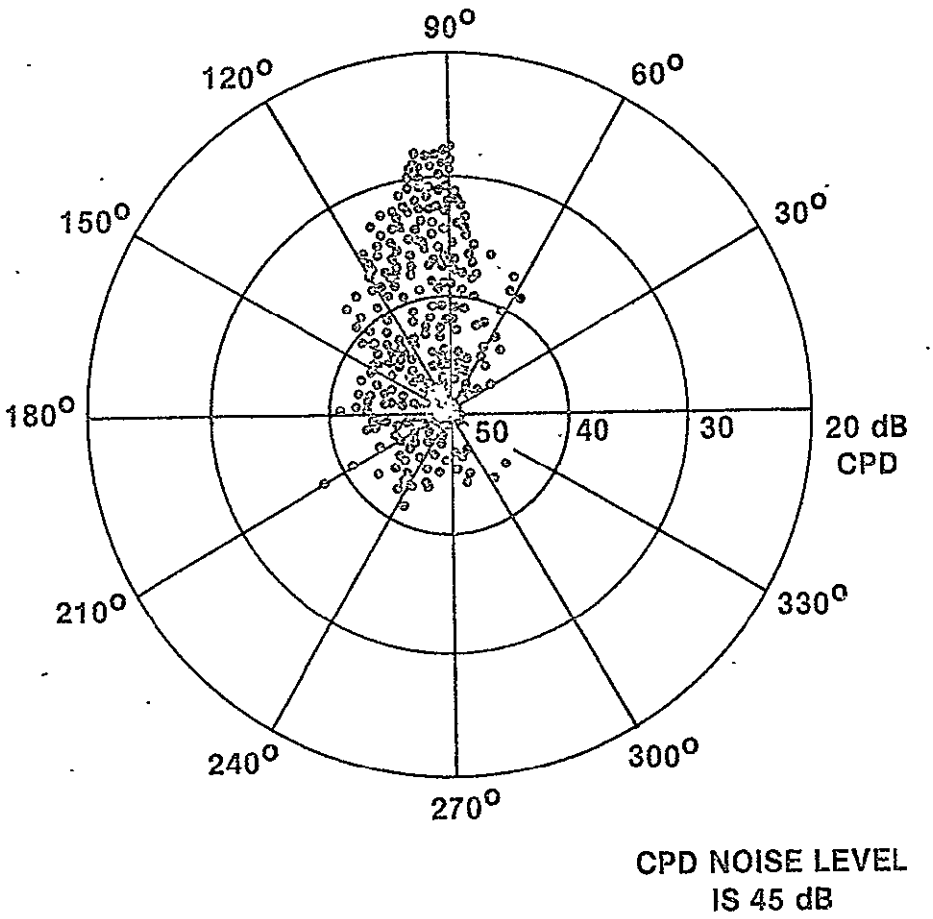

FIGURE 4. POLAR PLOT OF THE CROSS POLARIZATION DISCRIMINATION ARISING FROM AN ICE CLOUD

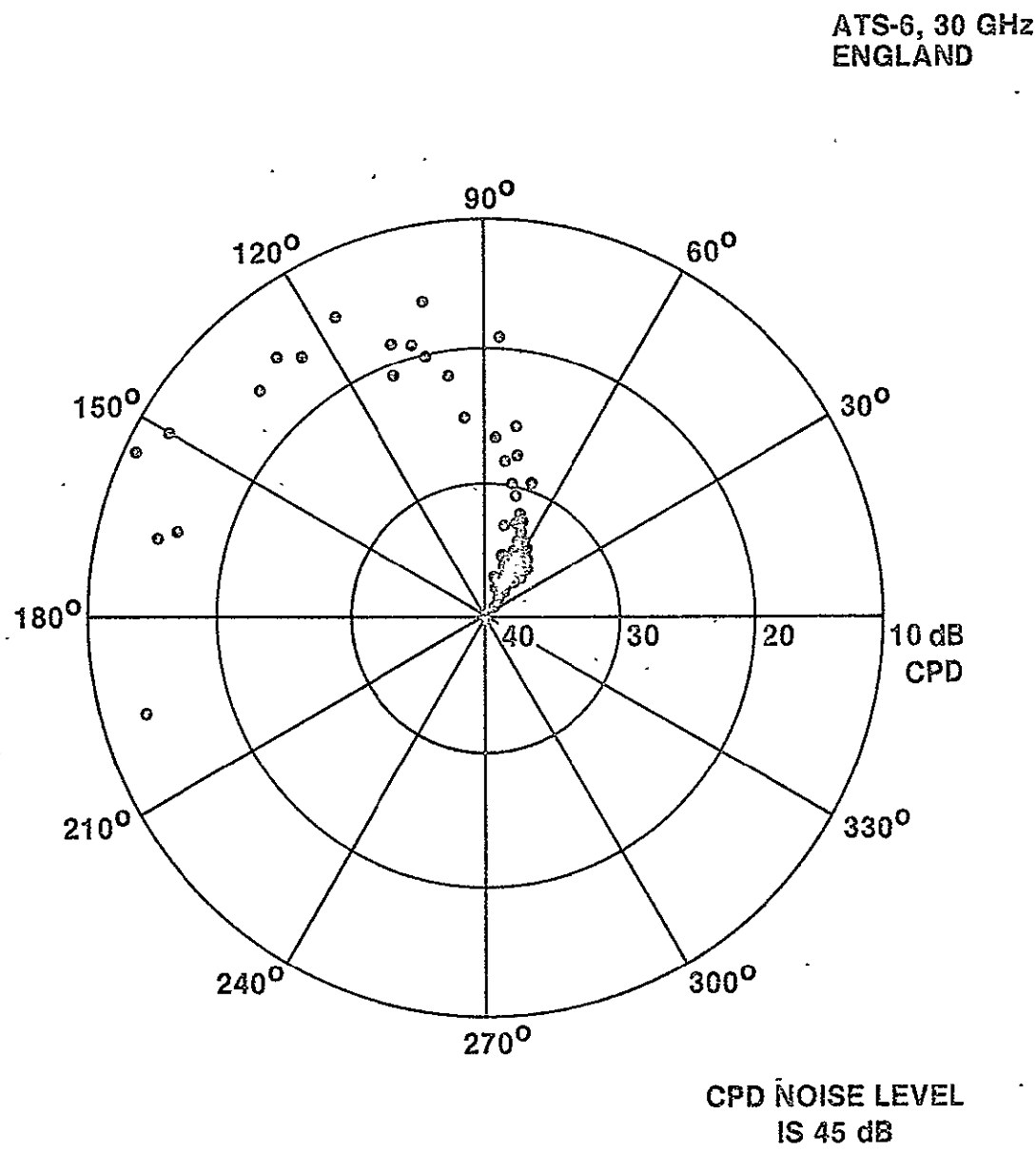

FIGURE 5. POLAR PLOT OF THE CROSS POLARIZATION DISCRIMINATION ARISING FROM A HEAVY RAIN EVENT

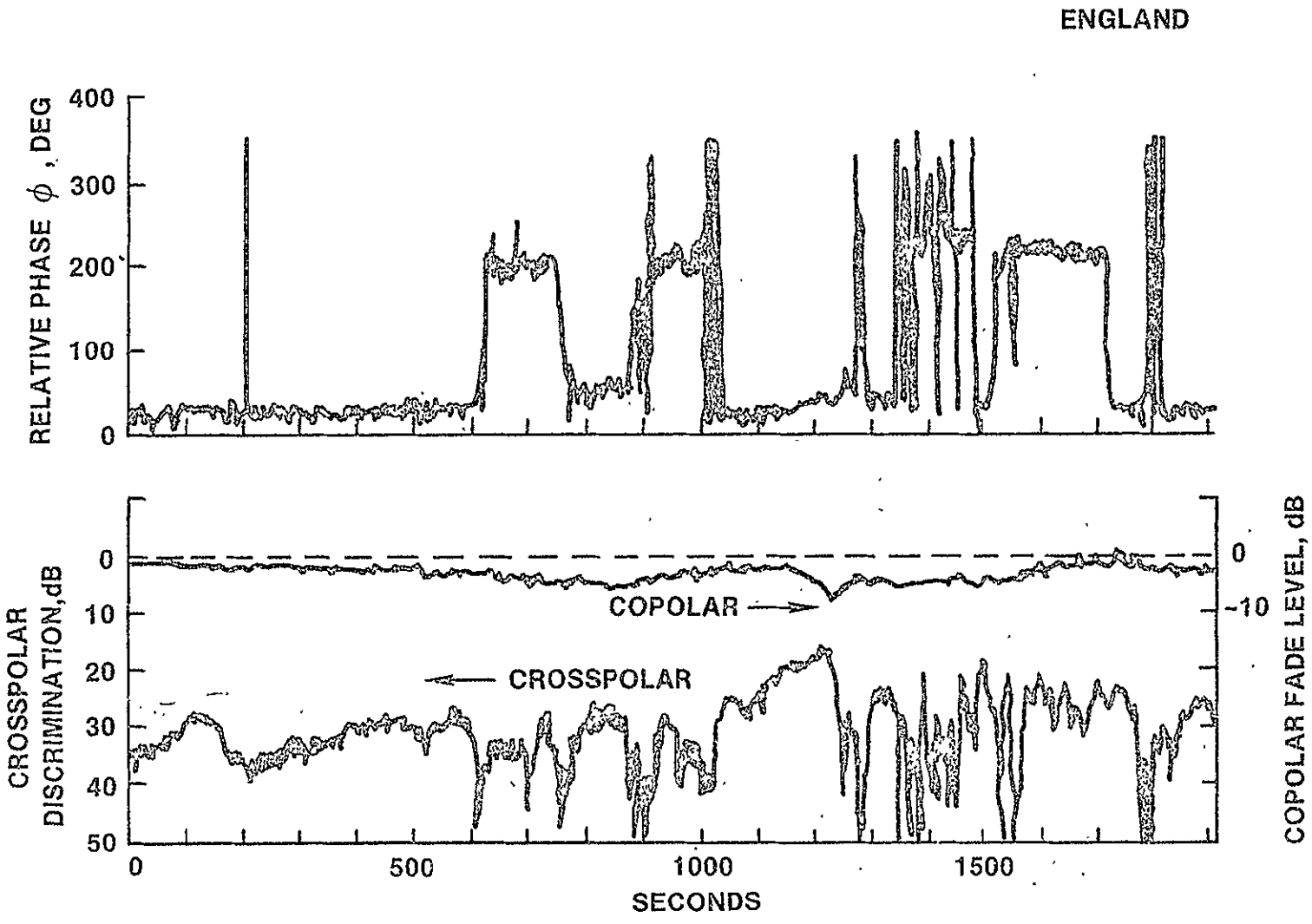

FIGURE 6. PHASE, COPOLAR FADE AND CROSSPOLAR DISCRIMINATION FOR AN ELECTRICALLY ACTIVE THUNDERSTORM (15th July 1976)

2.3 SNOW DEPOLARIZATION

Snow depolarization occurs during both the winter and summer months. During the summer months snow exists above the $0^{o}C$ isotherm. During winter as the isotherm lowers the thickness of the snow increases and the depolarization due to rain decreases.

In Canada (Ref. 11) tests using circularly polarized diversity radars at frequencies near 2.9 GHz (10.4 cm wavelength) and 16.7 GHz (1.8 cm wavelength) at an elevation angle of 3.2 degrees have diagnosed storms during both summer and winter. During June snow occurred during a storm from 2.6 to 8.2 km altitude and yielded a differential phase shift of 0.36 deg/km at 2.9 GHz. Winter data taken at 16.7 GHz gave more variable results 0.16 to 1.17 deg/km for moderate to heavy snowstorms ranging in altitude from 70 m to 2.6 km. The mean value of differential phase shift was 0.69 deg/km at 16.7 GHz.

2.4 MULTIPATH DEPOLARIZATION

A sharp antenna cross-polarization diagram can allow an oblique indirect ray to produce a significant cross-polar component. This condition is usually associated with low elevation angle events where the sidelobes are receiving energy from the oblique ray. Measurements have been made on terrestrial links at 11 GHz (Ref. 12) and 22 GHz (Ref. 13).

The magnitude of the indirect signal reflected from the earth can be roughly estimated from the data in Refs. 14 and 15 (data taken near 3 GHz). Generally the ground-scattered wave amplitude is at least 20 dB below the direct wave.

2.5 REFRACTIVE EFFECTS

Variations in the radio refractivity (dielectric constant of tropospheric layers can cause rotation of the polarization plane of the rays refracting through the layers. This condition will occur for layers which are not perpendicular to the vertical plane containing the transmitter and receiver as described in Ref. 16 (in French).

3.0 DEPOLARIZATION STATISTICS - AN EXAMPLE

In most cases depolarization arises due to two sources: rain and ice. The statistics of depolarization events can be estimated using the methodology shown in Figure 7. For rain depolarization the starting point is the cumulative rain attenuation statistics computed or measured via techniques described in Section II. For example, the cumulative attenuation statistics for Rosman, NC while observing the 20GHz ATS-6 satellite beacon are shown in Figure 8. This data was obtained by the distribution extension technique described in Section II.

Since the ATS-6 was nearly vertically polarized (within 20 degrees of vertical) the formula

$$CPD = 47 - 24.5 \log_{10}(AL_e)$$

is selected from Table 1. At this point, two techniques exist for correcting this formula for frequency and elevation angle. If a large frequency or elevation angle scaling were required, the best approach would be to use the equations of Nowland, et. al. (Ref. 5). However, since no frequency scaling is required and since the elevation angle to ATS-6 from Rosman is 47 degrees compared to the Blacksburg, VA elevation angle to COMSTAR of 44 degrees, no scaling is needed. If the effects of polarization need to be considered, the equations of Ref. 5 or CCIR Doc. 5/276-E must be used.

Within the accuracy of the required statistics the relation

$$CPD\ (dB) = 47 - 25 \log_{10}(AL_e)$$

will be utilized. Substituting the attenuation values for a given percentage of the year (from Figure 8) into this relation yields the CPD statistics for

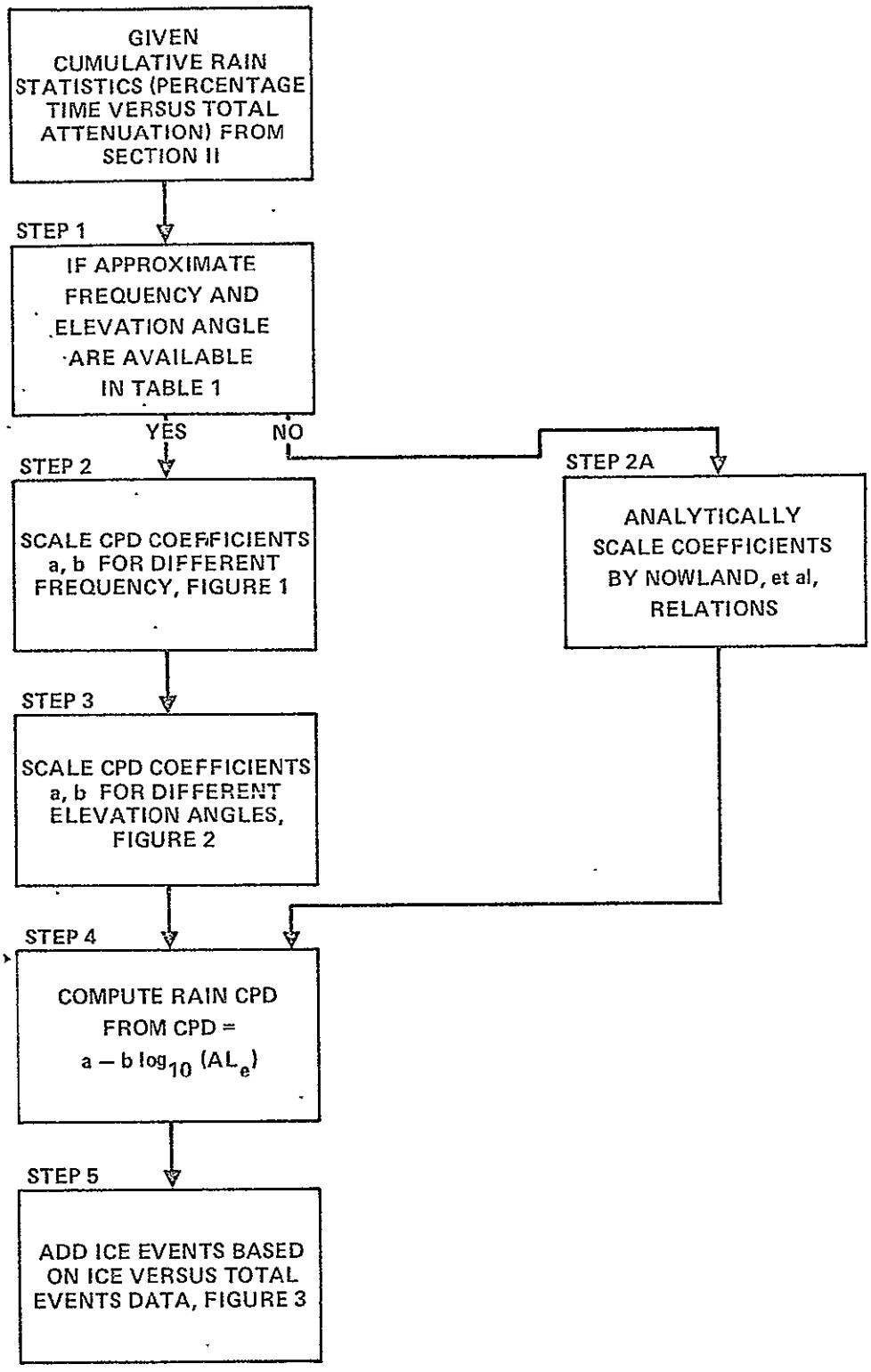

FIGURE 7. TECHNIQUE FOR PREDICTION OF DEPOLARIZATION STATISTICS

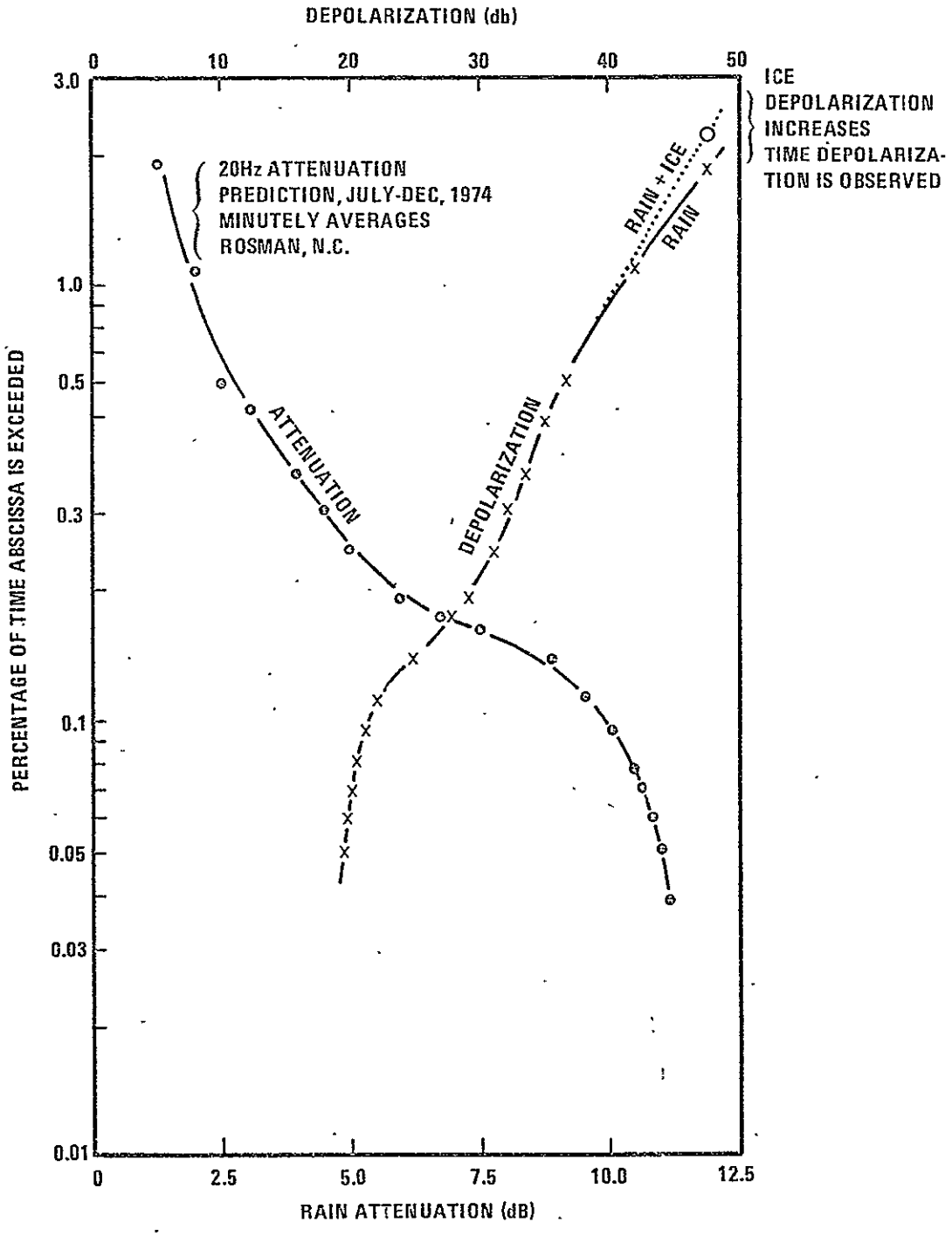

FIGURE 8. ATTENUATION AND DEPOLARIZATION STATISTICS FOR ROSMAN, N.C.

rain shown in Figure 8. Based on these results the CPD will exceed 20 dB during 99.9% of the year.

However, for low attenuation levels (high CPD's), ice will introduce depolarization. A crude estimate of this effect can be made based on the data in Figure 3. Namely, when $AL_e \leq 1$ dB about 30% more CPD events occur due to ice and rain, than just rain alone. This translates the data point in Figure 8 corresponding to $AL_e = 1$ dB from about 0.18 percent of the year to (1.3)(0.18%) = 0.23% of the year (indicated by an O in Figure 8). Thus the CPD curve is raised up for low values of attenuation. For attenuations above 3 dB the rain plus ice depolarization plots are essentially all rain effects.

Note that one could have added in the effect of ice depolarization by translating the corresponding rain and ice CPD's. This is probably less accurate because high values of CPD are equipment dependent. Therefore an average value of 30% ice contribution was selected rather than converting each value of CPD using data shown in Figure 3. This correction is based on very preliminary results from a single geographic location and should be added only to show a trend, since the absolute value is probably in error.

4.0 REFERENCES

1. C.W. Bostian, S.B. Holt, Jr., S.R. Kauffman, E.A. Manus, R.E. Marshall, W.L. Stutzman and P.H. Wiley, "Rain Depolarization and Attenuation Measurements at 11.7, 19.04 and 28.56 GHz: A Description of the Experiment and Some Preliminary Results," URSI Comm. F Proc., La Baule, France, 28 April - 6 May 1977, pp 403-408.

2. W.L. Stutzman, "Mathematical Formulations and Definitions for Dual Polarized Reception of a Wave Passing Through a Depolarizing Medium (A Polarization Primer)," Virginia Polytechnic & State Univ. Report, NASA Contract NAS5-22577, June 1977.

3. P.A. Watson and M. Arbabi, "Cross-polarization Isolation and Discrimination," Electronics Letters, Vol. 9, No. 22, pp 516-517, November 1973.

4. H.R. Pruppacher and R.L. Pitter, "A Semi-empirical Determination of the Shape of Cloud and Rain Drops," J. Atmos. Science, Vol. 28, pp 86-94.

5. W.L. Nowland, R.L. Olsen and I.P. Shkarofsky, "Theoretical Relationship Between Rain Depolarization and Attenuation," Electronics Letters, Vol. 13, No. 22, pp 676-677, 27 October 1977.

6. W.J. Vogel, "CTS Attenuation and Cross-Polarization Measurements at 11.7 GHz," Final Report, Elect. Eng. Res. Lab., Univ. Texas at Austin, NASA Contract NAS5-22576, September 1978.

7. W.L. Nowland, I.I. Strickland, J. Schlesak and R.L. Olsen, "Measurements of Depolarization and Attenuation at 11.7 GHz by Using the Communications Technology Satellite," Electronics Letters, Vol. 13, No. 24, pp 750-751, 24 November 1977.

8. N.J. McEwan, P.A. Watson, A.W. Dissanayake, D.P. Haworth and V.T. Vakili, "Crosspolarization from High Altitude Hydrometeors on a 20 GHz Satellite Radio Path," Electronics Letters, Vol. 13, pp 13-14, 1977.

9. P.F. Shutie, E.C. MacKenzie and J.E. Allnutt, "Relative Phase Measurements at 30 GHz Between Copolar and Induced Crosspolar Signals Produced by Ice Particles on a Satellite-to-Ground Link," Electronics Letters, Vol. 14, No. 4, pp 105-107, 16 February 1978.

10. P.F. Shutie, J.E. Allnutt and E.C. MacKenzie, "Depolarization Results at 30 GHz Using Transmisssions from the ATS-6 Satellite," Proc. URSI, Symposium on Propagation in Non-Ionized Media, La Baule, France, 28 April - 6 May 1977, pp 367-369.

11. A. Hendry, G.C. McCormick and B.L. Barge, "Ku-Band and S-Band Observations of the Differential Propagation Constant in Snow," I.E.E.E Trans. Ant. Prop., Vol. AP-24, No. 4, pp 521-525, July 1976.

12. P.A. Watson, et al., "Linear Cross-Polarization and Attenuation Measurements at 11 and 36 GHz," IEE Conf. Proc. No. 98, 1973.

13. D.J.W. Turner, "Measurements of Cross-Polar Discrimination at 22 and 37 GHz," IEE Conf. Proc. No. 98, 1973.

14. Peter Beckman and Andre Spzzichino, The Scatteirng of Electromagnetic Waves from Rough Surfaces, Pergamon Process., MacMillan Co., New York, N.Y., 1963.

15. L.H. Lord and R. Oliver, "An Experimental Investigation of the Reflection and Absorption of Radiation of 9-cm Wavelength," Proc. Phys. Soc., Vol. 58, pp 265-280, 1946.

16. G. LeFrancois, L. Martin and M. Rooryck, "Influence de la Propagation Sur la Valeur de Decouplage de Deux Polarisations Orthogonales, " Ann. des Telecomm., Vol. 28, July-August, 1973.

17. C.W. Bostian, et al, "A Depolarization and Attenuation Experiment Using the Comstar and CTS Satellites," Virg. Poly, Inst.and State Univ., Final Report, February 9, 1978.

18. C.W. Bostian, et al., "Data Report for December 1976 through March 1978," Virg. Poly. Inst.and State Univ., April 28, 1978.

19. T.S. Chu, "Rain - Induced Cross-Polarization at Centimeter and Millimeter Wavelengths," Bell Syst. Tech. Jrnl., Vol. 58, No. 8, October 1974, pp 1557-1579.

20. W.P. Overstreet and C.W. Bostian, "The Phase of the Crosspolarized Signal Generated by Millimeter Wave Propagation Through Rain," Virg. Poly. Inst. and State Univ., Report 1978-2, June 1978.

SECTION VI

ORI
Silver Spring, Maryland 20910

PREDICTION OF BANDWIDTH COHERENCE ON EARTH-SPACE PATHS

DR. ROGER KAUL
ORI, INC.

FOR
NASA/GSFC
CONTRACT NAS5-23438

NOVEMBER 1978

TABLE OF CONTENTS

LIST OF FIGURES

1.0 INTRODUCTION

If the dispersion of the propagating medium is sufficiently high, the phase and/or amplitude of wide bandwidth trnasmissions may be selectively altered. The tropospheric effects ahve been predicted and measured to be small, however the ionospheric dispersion may be significant. Therefore, in this section of the report the ionospheric effects on the path are considered.

Measurements are underway with the COMSTAR satellite at 28.56 $\pm$ 0.264 GHz by Bell Laboratories. However results of these measurements have not been published to date. The first available data was obtained from the ATS-6 satellite and is presented here.

2.0 TROPOSPHERIC EFFECTS

2.1 AMPLITUDE VARIATIONS

2.1.1 Theoretical Results

Theoretical estimates of the degradation of pulse shapes through rain have indicated that only minor effects are observed. The calculations (Ref.1) indicated that pulse distortion does not become significant until total rain attenuations of the order of 100 dB are encountered. Since current link margins do not allow such high attenuations, the link will fail due to signal attenuation before the pulse shape affects transmission.

However, if required, calculations of the amplitude dispersion are possible for both clear air and rain attenuation based on the data and formulas in Section II of this report.

For rain the frequency dependence of the specific attenuation A (db/km) is

$$\frac{\partial A}{\partial f} = \frac{\partial (aR^b)}{\partial f} = A\left[\frac{1}{a}\frac{\partial a}{\partial f} + (\ln R)\frac{\partial b}{\partial f}\right]$$

where, for example, for the frequency range from 8.5 to 25 GHz

$$\frac{\partial a}{\partial f} = 1.02 \times 10^{-4} f^{1.42}$$

$$\frac{\partial b}{\partial f} = -0.11\ f.^{-1.0779}$$

For example, at 20 GHz and R = 25 mm/hr,

$$a = 5.93\times10^{-2}$$

$$b = 1.12$$

$$\frac{\partial a}{\partial f} = 7.18\times10^{-3}$$

$$\frac{\partial b}{\partial f} = -4.36\times10^{-3}$$

$$A = 2.18 \text{ dB/km}$$

so

$$\frac{\partial A}{\partial f} = 0.23 \text{ dB/(km-GHz)}$$

For a typical effective path length $L_e = 12.82R^{-0.3}$ at 45 degree elevation angle

$$\frac{\partial(AL_e)}{\partial f} = L_e \frac{\partial A}{\partial f} = 1.14 \text{ dB/GHz}$$

2.1.2 Experimental Results

The ATS-6 beacons at 20 and 30 GHz were both capable of being modulated with ±180, ±360, ±540 and ±720 MHz sidetone signals. Typical selective fading events across the 1.44 GHz bands are shown in Figures 1 and 2, respectively (Ref.2). These are four-second averages taken on day 270 of 1974 just before the onset of a fade event (232000Z), at the beginning of the fade event (232352Z), and before receiver lock was lost during the fade event (232428Z). Except for fade depths in excess of 20 dB, the accuracy of the attenuation measurements is ±1 dB. These rain fade results, while representative of those taken at Rosman, do not appear to be sufficiently accurate for deep fades because the signal levels approach the noise floor of the receiver. For one-minute averages, no measureable selective fading was observed (Ref. 2).

The cross-correlation of 4 and 6 GHz signals due to low angle fading in the Canadian arctic was found to be low (Ref. 3). During a 2.5 hour period on the day when the fading was most severe the correlation coefficient was 0.34 since the 6 GHz signal experienced 55% more fades than the 4 GHz signal.

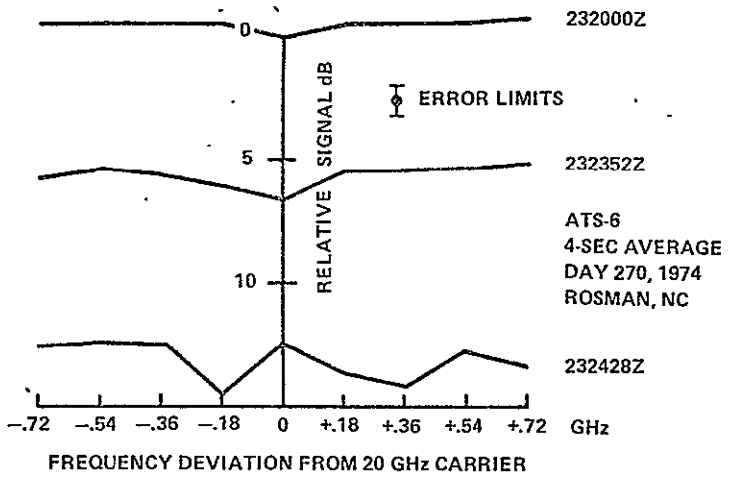

FIGURE 1. SELECTIVE FADING NEAR 20 GHz

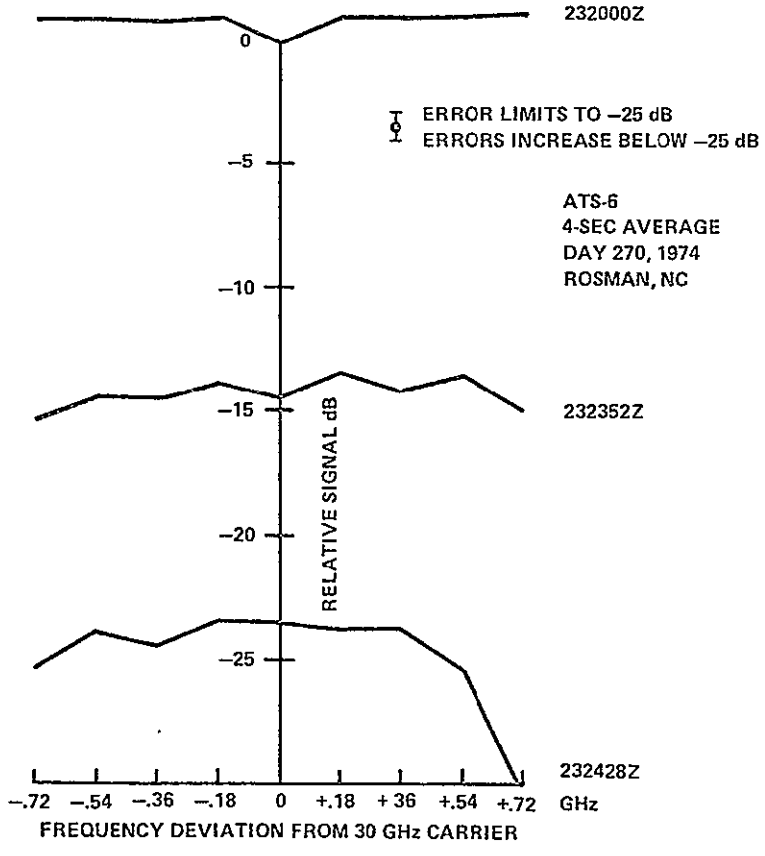

FIGURE 2. SELECTIVE FADING NEAR 30 GHz

2.2 PHASE VARIATIONS

Phase measurements have not yielded significant results above 10 GHz. The phase coherent sidetone signals on ATS-6 showed only minor variations across the 1.44 GHz bandwidths. These variations were most evident for the shorter (one and four second) averaging periods compared to the one-minute period (Ref. 2).

Phase measurements have been attempted for the one degree elevation angle satellites observed from the arctic (Ref. 3). Unfortunately, no significant fade events occurred and no differential phase variations were recorded.

3.0 IONOSPHERIC EFFECTS

3.1 AMPLITUDE VARIATIONS

Ionospheric attenuation is inversely proportional to the frequency squared (Ref. 4) and is generally less than 0.001 dB at 15 GHz and an elevation angle $\Theta = 90^{\circ}$. The variation is approximately related to cosecant θ.

3.2 PHASE VARIATIONS

The group delay due to the free electrons in the ionosphere is (Ref. 5)

$$\Delta\tau = 40.3 \frac{N_e}{cf^2}$$

where N_e is the total electron content in electrons/m^2, $c = 3\times10^8$ m/sec and f is in Hertz. This delay is equivalent to a phase delay (in radians)

$$\Delta\tau = \frac{\Delta\phi}{2\pi f}$$

so that

$$\Delta\phi = (2\pi)(40.3)N_e/(cf).$$

For a typical value of $N_e = 10^{17}\ m^{-2}$, the total phase delay at 11.7 GHz is only 7.21 radians. The frequency dependence of this is only

$$\frac{\partial(\Delta\phi)}{\partial f} = -\frac{2\pi(40.3)N_e}{cf^2}$$

$$= -\ 6.2\times10^{-10}\ \text{radian/Hertz}$$

= 0.62 radian/GHz

= 35 degrees/GHz.

Of course for higher frequencies, the rate of change of phase with frequency decreases.

REFERENCES

1. R. K. Crane, "Coherent Pulse Transmission through Rain," IEEE Trans. Ant. Prop., Vol. AP-15, p 252, March 1967.

2. "ATS-6 Millimeter Wave Propagation Experiment, Final Data Analysis Report," prepared for NASA/GSFC by Westinghouse Electric Corp., Baltimore, MD, September 1975.

3. J. I. Strickland, R. L. Olsen and H. L. Werstiuk, "Measurements of Low Angle Fading in the Canadian Arctic," Ann. Telecommunic., Vol. 32, Nos. 11-12, pp 530-535, 1977.

4. G. H. Millman, "Atmospheric Effects on VHF and UHF Propagation," Proc. IRE, Vol. 46, p 1492, August 1958.

5. "Total Electron Content Studies of the Ionosphere," ed. by J. A. Klobuchar, Air Force Cambridge Research Laboratories Technical Report AFCRL-TR-73-0098, Bedford, Mass., February 1973.

SECTION VII

ORI
Silver Spring, Maryland 20910

PREDICTION OF SKY NOISE

DR. ROGER KAUL

NOVEMBER 1978

ORI, INC.
1400 SPRING STREET
SILVER SPRING, MD. 20910

CONTRACT NO. NAS5-23438, MOD. 68

TABLE OF CONTENTS

LIST OF ILLUSTRATIONS

1.0 OVERVIEW AND SOURCES

The absorbing gases and hydrometeors in the troposphere are a source of broadband incoherent noise. This is normally expressed as a sky temperature T_S observed by the receiving system, such that the noise power is $P_{NOISE} = kT_SB_n$ where k = Boltzmann's constant = 1.38×10^{-23} joule/degree and B_n is the noise bandwidth (equivalent to the bandwidth of a rectangular filter whose noise output is the same as the receivers actual bandwidth limiting filter). The other sources of noise are extra-terrestrial sources (primarily the sun) and noise entering the antenna sidelobes at low elevation angles.

The above noise sources are observed by ground station antennas. Satellite antennas pointed at a ground station observe noise radiated by the earth and cloud tops.

Hence precipitation in the path will both reduce the system carrier strength and raise the background noise level, resulting in a reduced carrier-to-noise ratio. The increase in noise level (noise temperature) is particularly significant in low-noise receiver front ends (4 dB or less), where the resultant noise figure during a precipitation event could be increased by 2 dB or more.

2.0 SKY NOISE OBSERVED BY GROUND STATIONS

2.1 TROPOSPHERIC CONTRIBUTION TO SKY NOISE

The effective sky noise due to the troposphere is primarily dependent on the attenuation at the frequency of observation. For sky radiometers an empirical equation has been derived (Ref. 1):

$$AL_e(dB) = -10 \log_{10} \left(\frac{T_m - T_s}{T_m} \right)$$

where T_m is the mean absorption temperature in degrees Kelvin of the attenuating medium and AL_e is the specific attenuation times the effective path length. The value (Ref. 1)

$$T_m = 1.12\,(\text{surface temperature in } {}^0K) - 50^0K$$

has been empirically determined. For a typical $\bar{T}_m = 275^0K$ and as T_S increases toward T_m, the radiometer tends to saturate. For typical radiometer $(\Delta\bar{T})_{rms}$ values, the radiometer can only accurately measure to 15 or 20 dB attenuation levels.

Inverting this relation, yields the resulting sky temperature for a given path attenuation AL_e (in dB) of

$$T_S = T_m \left\{ 1 - 10^{(AL_e/-10)} \right\}$$

This relation may now be utilized for estimation of the sky temperatures using the data in Section II of this report for $AL_e(dB)$.

2.1.1 Clear Air Sky Noise

The sky noise contributed by water vapor and oxygen may be computed from the clear air attenuation. A typical set of curves (Ref. 2) as a function of elevation angle θ are shown in Figure 1. Here the ground station is assumed to be at sea level, one atmosphere (1013.6 millibars), surface temperature is 20°C and water vapor density is 10gm/m^3 (R.H. = 58%).

As an example, for a 20 GHz downlink at 10 degrees elevation angle, T_S = 150°K. In a 1000 MHz noise bandwidth the noise power would be 2×10^{-7} watts.

2.1.2 Sky Noise Due to Rain

The value of sky noise increases significantly during rain events. When the total attenuation approaches 10 to 20 dB the sky noise temperature is nearly T_m.

Actual values of T_S may be obtained using the specific attenuation and effective path length techniques in Section II.

Cumulative statistics of sky noise temperature versus climate region are now given for the Global model observing the ATS-6 20 GHz beacon from Rosman, N.C. The elevation angle is 47 degrees. The station elevation = 880 meters, the 0°C isotherm $\approx$ 3700 m above the station and so the path length $D \cong 3$ km. For this path length the rain rate average parameter $r = 1.6R^{-0.13}$ so the average rain rate along the path is

$$R_{ave} = 1.6\ R^{0.87}$$

where R is the one minute average surface rain rate in mm/hr. Referring to Table 3.5 of Section II and the sky noise temperature relation, the values in Table 1 are developed. These are plotted in Figure 2 along with the rain rate distribution.

The sky noise temperature (see last column of Table 1) will degrade the overall system noise figure of the link. For example, for a receiver with 4 dB noise figure, the resultant noise figure for the rain rate corresponding to 0.01% of the year will be 5.4 dB, i.e., an increase of 1.4 dB.

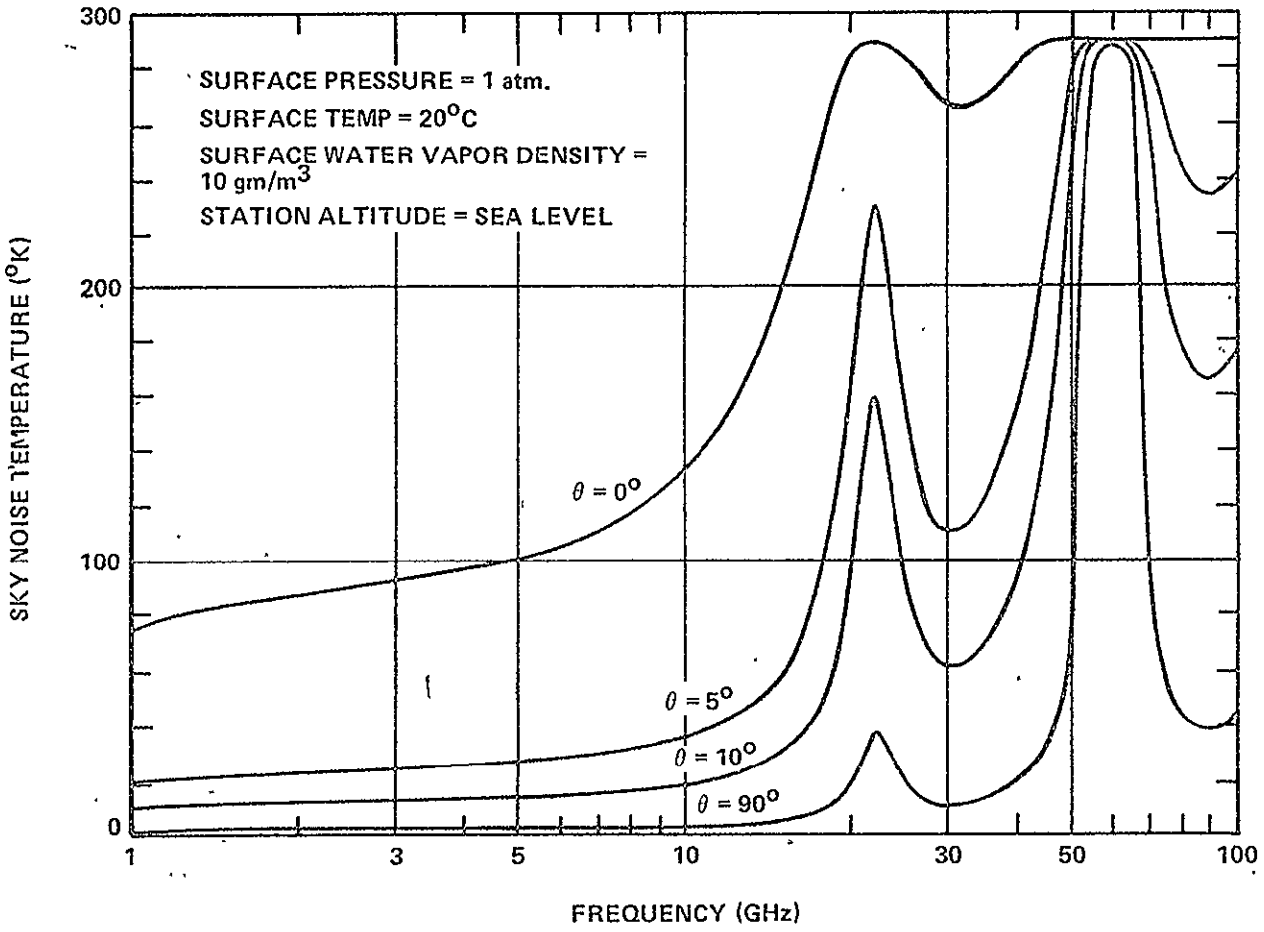

FIGURE 1. SKY NOISE TEMPERATURE DUE TO CLEAR AIR

TABLE 1

CUMULATIVE STATISTICS OF SKY TEMPERATURE

DUE TO RAIN FOR ROSMAN, N.C. AT 20 GHz

$T_m = 275^0K$

PERCENT OF YEAR	POINT RAIN RATE VALUES	AVERAGE RAIN RATE	TOTAL RAIN ATTENUATION*	SKY NOISE TEMPERATURE†
0.001	102 mm/hr	89 mm/hr	47 dB	275°K
0.002	86	77	40	275
0.005	64	60	30	275
0.01	49	47	23	274
0.02	35	35	16	269
0.05	22	24	11	252
0.1	15	17	7	224
0.2	9.5	11.3	4.6	180
0.5	5.2	6.7	2.6	123
1.0	3.0	4.2	1.5	82
2.0	1.8	2.7	0.93	53

NOTES:

* At 20 GHz the specific attenuation $A = 0.06\ R_{ave}^{1.12}$ dB/km and for Rosman, N.C. the effective path length is 5.1 km to ATS-6.

† For a ground temperature of 17°C = 63°F the $T_m = 275^0K$.

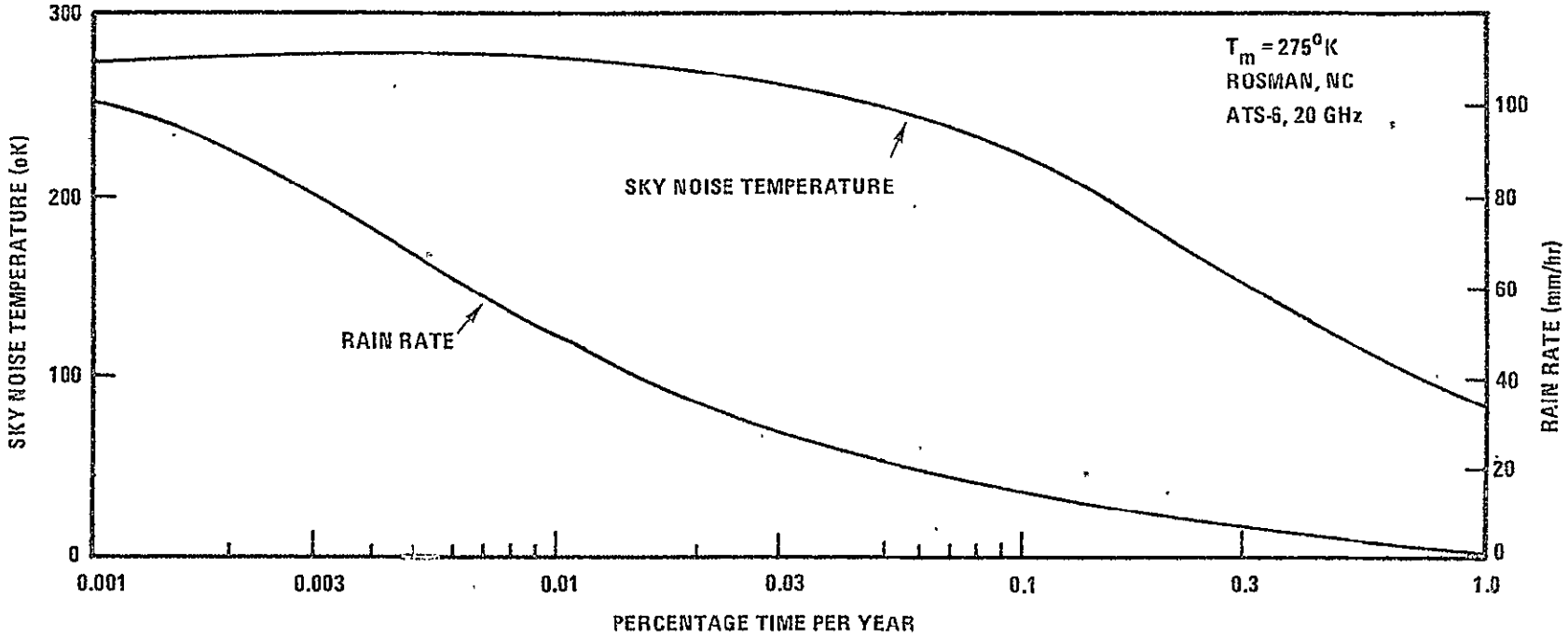

FIGURE 2. CUMULATIVE STATISTICS FOR SKY NOISE TEMPERATURE DUE TO RAIN

2.1.3 Sky Noise Due to Clouds, Fog, Sand and Dust

The major contributor to the sky noise temperature is the medium with the highest attenuation. Generally, clouds will present the highest attenuations. For example, for cumulus clouds with no precipitation the water density will be approximately 0.5 gm/m^3. For the Rosman example described earlier, (20GHz)

$$AL_e = K_c \rho_w t_c \csc \theta$$

where t_c is the thickness of the clouds (typically 2 kilometers). Using typical numbers

$$AL_e = (0.4 \text{ dB m}^3/\text{gm km})(0.5 \text{ gm/m}^3)(2\text{km}) \csc (47^0)$$
$$= 0.55 \text{ dB}$$

The corresponding sky noise contribution is then

$$T_s = T_{mc} \left\{1-10^{(0.55/-10)}\right\}.$$

The value to select for T_{mc} is unknown, but letting T_{mc} equal the temperature of the cloud should be conservative (i.e., T_{mc} = 0°C = 273°K). The result is only 32°K. Clearly, rain represents a much more significant contributor to the sky noise temperature.

2.1.4 Total Sky Noise Temperature Arising From Several Contributors

The sky noise temperature from several sources do not add linearly. Rather, the attenuation from each contributor must be added and the total result substituted into the sky noise versus attenuation relation. For example, for the Rosman ground station observing the ATS-6, the clear air attenuation is 1.2 dB yielding a T_s (clear air) = 66°K. From Table 1 for 0.2% of the year (105 minutes) the rain induced sky temperature is 180°K. The actual sky temperature due to clear air and rain is 203°K which is significantly less than the sum of each contributor (246°K). During rain conditions the cloud contributions should also be added, but these will generally be even a smaller contribution than the clear air attenuation.

2.2 EXTRATERRESTRIAL SOURCES OF SKY NOISE

2.2.1 Solar Noise

The sun is the major source of sky noise when collinear with the ground station - satellite path. For geosynchronous satellites this occurs during the equinox periods each year for a short period each day. The sky noise as a function of frequency has been measured (Ref. 3). The noise level appears to level off at -183 dBW/Hz (active sun) and -188 dBW/Hz (quiet sun) above 20 GHz (see Figure 3).

Another approach is to model the sun as a 7000°K blackbody in the microwave region (Ref. 4). The power per unit area and Hertz is then

$$W_f = \frac{2\pi h f^3}{c^2(e^{hf/kT_s}-1)} \simeq \frac{2\pi f^2 k T_S}{c^2} \left(\frac{W}{m^2 Hz}\right)$$

where T_S = 7000°K = apparent solar temperature

k = Boltzmann's constant
= 1.38×10^{-23} Watt sec/degree

h = 6.626×10^{-34} Watt sec^2

c = 3×10^8 m/sec.

The effective sky noise temperature observed by the ground station is then proportional to the integral of the solid angle subtended by the sun over the antenna field pattern. The sun subtends approximately a ½ degree arc when observed from the earth. Also the sun power density is attenuated by the troposphere, so that during rain periods the power density is reduced. This is the mechanism for suntracker propagation measurements.

2.2.2 Lunar Noise

The moon reflects solar radio energy back to earth. It also subtends approximately a ½ degree arc from the earth with an apparent temperature of 205 to 215°K depending on frequency. However, because of the phases of the moon and the ellipticity of its orbit, the solid angle of the moon in a propagation path varies throughout the month. Reference 5 has calculated the necessary parameters, but as a worst case a temperature of 215°K is typical.

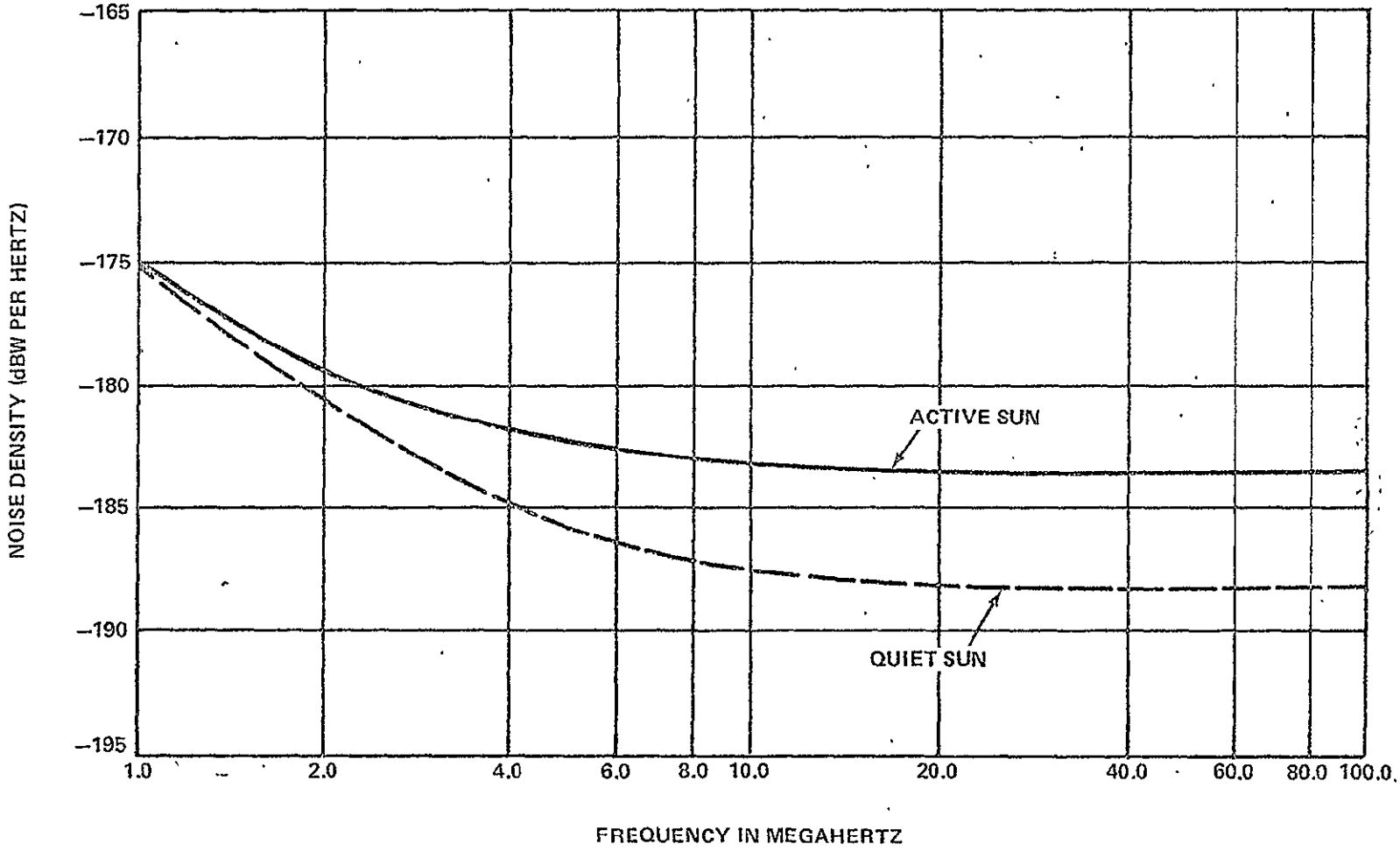

FIGURE 3. VALUES OF NOISE FROM QUIET AND ACTIVE SUN.
SUN FILLS ENTIRE BEAM (REF. 3).

2.2.3 Radio Stars

The strongest radio stars are ten times weaker than the lunar emission. The strongest stars (Ref. 6) emit typically 10^{-23} W/m^2·Hz in the 10 to 100 GHz frequency range. Three of these strong sources are Cassiopeia A, Taurus A and Orion A. These sources are sometimes utilized for calibration of the ground station G/T. During the calibrations the attenuation due to the troposphere is usually cancelled out by comparing the sky noise on the star and subtracting the adjacent (dark) sky noise. Thus the attenuation-induced sky noise cancels out.

3.0 NOISE OBSERVED BY SATELLITE-BORNE RECEIVERS

Receiving (uplink) antennas aboard spacecraft observe the warm earth or the earth's cloud cover. This represents a noise source competing with the uplink signal from the ground station.

Measurements of the brightness temperature of the earth measured with the electrically scanned microwave radiometer aboard Nimbus-5 at 19.35 GHz have demonstrated brightness temperature differences of 160°K when comparing water (130°K) and land (290°K) (Ref. 7). Clouds appear to have a temperature near 270°K (0°C). Because of the high percentage of clouds and ocean areas on the earth, a full earth coverage antenna will observe approximately 270°K. However, when observing a ground based temperate zone ground station a 300°K brightness temperature is not uncommon. The power density is then calculated from the relation kT_sB_n.

REFERENCES

1. K.N. Wulfsberg, "Apparent Sky Temperatures at Millimeter-Wave Frequencies," Phys. Science Res. Paper No. 38, Air Force Cambridge Res. Lab., No. 64-590, July 1964.

2. CCIR Working Group 5-2, Doc. No. 5-269-E, 16 Sept. 1977.

3. S. Perlman, W.J. Russel, Jr., and F.H. Dickson, "Concerning Optimum Frequencies for Space Vehicle Communications," IRE Trans. Mil. Elect., Vol. MIL-4, Nos. 2-3, 1960, pp. 184-192.

4. G.R. Welti, "Intersatellite Link for Multiple-Access Telephone," EASCON '78 Record, IEEE Electronics and Aerosp. Syst. Conv., Arlington, VA., Sept. 25-27, 1978, pp. 432-440.

5. K.G. Johannsen and A. Koury, "The Moon as a Source for G/T Measurements," IEEE Trans. Aerosp. Elect. Syst., Vol. AES-10, No. 5, Sept. 1974, pp 718-727.

6. D.F. Wart, W.C. Daywitt, M. Kanda and C.K.S. Miller, "A Study of the Measurement of G/T Using Casseopeia A," Natl. Bur. of Standards, Rept. No. NBSIR 74-382, June 1974.

7. W.J. Webster, Jr., T.T. Wilheit, T.C. Chang, P. Gloersen and T.J. Schmugge, "A Radio Picture of the Earth," Sky and Telescope, Vol. 49, No. 1, January 1975, pp 14-16.

CONCLUSION

This report represents an ongoing effort to compile in one place a concise, readily useable handbook for satellite system engineers. This report is the initial effort and will be updated and expanded in FY 1979.

People utilizing this report are encouraged to contact the authors with their suggestions and criticisms of both format and content. These comments, where appropriate, will be incorporated in later editions of the handbook.